UNIVERSITY OF BIRMINGHAM

Development and Application of a Novel High-Throughput Technique for Screening Neutrophil Extracellular Traps

by

Ilaria Jessica Chicca

A thesis submitted to the University of Birmingham for the degree of

DOCTOR OF PHILOSOPHY

School of Dentistry

College of Medical and Dental Sciences

The University of Birmingham

December 2016

UNIVERSITY OF
BIRMINGHAM

University of Birmingham Research Archive

e-theses repository

This unpublished thesis/dissertation is copyright of the author and/or third parties. The intellectual property rights of the author or third parties in respect of this work are as defined by The Copyright Designs and Patents Act 1988 or as modified by any successor legislation.

Any use made of information contained in this thesis/dissertation must be in accordance with that legislation and must be properly acknowledged. Further distribution or reproduction in any format is prohibited without the permission of the copyright holder.

Abstract

Neutrophil extracellular traps (NETs) are antimicrobial web-like structures whose release is mediated by reactive oxygen species (ROS) and purpose is to combat infections. Unbalanced NET production and clearance is, however, associated with auto-antibody production and disease. This thesis aimed to develop a High-Content-Analysis (HCA) approach to study human NETosis and its modulation. Initially, NET-related disease-relevant conditions were studied. Individual periodontal-bacteria generated substantial NET production compared with bacterial biofilms. Calcium or magnesium ions and increases in cell density enhanced NET responses. As part of this study the use of fixation and cell adherence procedures were explored and data indicated that addition of paraformaldehyde prior to centrifugation and the absence of poly-L-lysine provided appropriate conditions for downstream cytological analysis. 'Compartmental Analysis' and 'Tube Formation' algorithms were initially assessed for HCA, however, it was determined that bespoke 'NET Detection' and 'Nuclear Decondensation' algorithms provided more accurate analysis of NETosis and peptidyl-arginine-deiminase-4 translocation. The optimised protocol employed for the high-content-screening of a 56-compound library identified 8 NETosis modulators. Further characterisation of compounds' abilities to modulate ROS and NET production, identified roles for glutathione reductase, Src, molecular-target-of-Rapamycin and mitogen-activated-protein-kinase signalling. These pathways may provide new therapeutic targets for treatment of NET-related inflammatory disorders including periodontitis.

Dedication

I dedicate this thesis to my family who have always believed in me and supported my decisions throughout my academic journey. To my future husband Fabio, who has remained by my side and has embarked on this challenge in a foreign country with me; to my sister Barbara, my mum Mirella and my dad Vincenzo who have encouraged me to achieve my doctoral studies in their loving and irreplaceable way.

Acknowledgment

Firstly, I would like to thank Professor Paul Cooper, Dr Mike Milward and Professor Iain Chapple for their continued guidance and constructive feedback provided throughput the PhD; for teaching me to look at the 'glass half full' and for their endless patience demonstrated in understanding my reoccurring episodes of 'ital-english'. A special thanks to Dr Gareth Griffiths, Dr Rod Benson and Dr Joanna Dutkogwozdz at Imagen Therapeutics for sharing their knowledge and equipment which aided completion of this research. Additionally, I would like to thank the technical staff at the School of Dentistry for their continuous support and training provided from day one.

I would also like to thank the Immunity Research Group at the University of Glasgow for providing the bacterial biofilms and the murine models which were used in this study. A special mention goes to Ana Adrados Planell who turned out to be the best collaborator I could ever hope for, a dear friend and the perfect companion to share a glass of red wine with.

I would like to acknowledge the European Union 7th Framework Program for their financial support and the RAPID project for the invaluable training provided. A special thanks to the 'RAPIDers' who have turned every workshop in an interesting and amusing social occasion.

I wish to thank every person who kindly volunteered to donate blood as this helped to make my research possible. My friends and colleagues of the postgraduate office with whom I shared numerous meals, teas and lots of chocolate! I would like to dedicate a special thanks to Carla Alandia Román and Cleo White, two beautiful people who I have been lucky enough to encounter along my PhD path and have became valuable and irreplaceable friends.

Lastly, I would also like to thank the Balduccis who have supported me throughout the PhD and are warmly welcoming me into their club.

Table of Contents

List of figures

List of tables

Abbreviations

2D	Two dimensional
ACPA	Anticitrullinated protein antibodies
ADC	Air-droplet control
AFU	Arbitrary fluorescence units
ALK	Anaplastic lymphoma kinase
AMP	Antimicrobial peptide
ANCA	Antineutrophilic cytoplasmic antibody
BF	Brightfield
BSA	Bovine serum albumin
CD	Cluster of differentiation
CF	Cystic fibrosis
CGD	Chronic granulomatous disease
CXCR2	C-X-C motif receptor 2
CXCR4	C-X-C motif receptor 4
Cyto	Cytosolic
DAB	Diaminobenzidene
DAG	Diacylglycerol
DMEM	Dulbecco's modified Eagle's medium
DMSO	Dimethyl sulfoxide
DNA	Deoxyribonucleic acid
DNase	Deoxyribonuclease
DPI	Diphenylene iodonium
DVT	Deep vein thrombosis
eDNA	Extracellular deoxyribonucleic acid
EDTA	Ethylenediaminetetraacetic acid
EGFR	Epithelial growth factor receptor
ELISA	Enzyme-linked immunosorbent assay
Ep	Epithelial
ERK	Extracellular signal regulated kinase
ET	Extracellular trap
FACS	Fluorescent-activated cell sorting
FcγR	Fc-gamma receptor
FGFR	Fibroblast growth factor receptor
fMLP	*N*-formyl-methionyl-leucyl-phenyalanine
Fn	*Fusobacterium nucleatum*
G-CSF	Granulocyte colony stimulating factor
GCF	Gingival crevicular fluid
GCPR	G-coupled protein receptor
GM-CSF	Granulocyte-macrophage colony-stimulating factor
gPBS	Glucose-phosphate buffer saline

GSH	Glutathione
GSSG	Disulphide glutathione
H_2O	Water
H_2O_2	Hydrogen peroxide
HCA	High-content analysis
HCS	High-content screening
HER	Human epidermal growth factor receptor
HIF-1α	Hypoxia-inducible factor-1α
HO·	Hydroxyl radicals
HOCl	Hypochlorous acid
ICAM	Intercellular adhesion molecule
ICC	Immunocytochemistry
IgG	Immunolgobulin
IL	Interleukin
KO	Knockout
LBP	Lipopolysaccharide binding protein
LDH	Lactate dehydrogenase
LPS	Lipopolysaccharide
MAPK	Mitogen-activated protein kinase
MNase	Micrococcal nuclease
MOI	Multiplicity of infection
MPO	Myeloperoxidase
mTOR	Molecular target of Rapamycin
NADPH	Nicotinamide adenine dinucleotide phosphate
NE	Neutrophil elastase
NET	Neutrophil extracellular trap
NF-κB	Nuclear factor kappa B
NO	Nitric oxide
NOX	NADPH-oxidase
Nuc	Nuclear staining
O_2	Oxygen
$O_2^{\bullet-}$	Superoxide anion
OD	Optical density
OEC	Oral epithelial cell
PAD4	Peptidylarginine deiminase 4
PAMP	Pathogen-associated molecular pattern
PBS	Phosphate buffer saline
PDGFR	Platelet-derived growth factor receptor
PFA	Paraformaldehyde
Pg	*Porphyromonas gingivalis*
PKC	Protein kinase C
PMA	Phorbol 12-myristate 13-acetate

PRR	Pattern recognition receptor
PSGL1	P-selectin glycoprotein ligand-1
PVP	Polyvinylpyrrolidone
RA	Rheumatoid arthritis
Rcf	Relative centrifugal force
RLU	Relative light unit
ROS	Reactive oxygen species
ROS1	Proto-oncogene 1 receptor
RPMI	Roswell Park Memorial Institute
RT	Room temperature
SEM	Scanning electron microscopy
SEM	Standard error of the mean
siRNA	Small inhibitory ribonucleic acid
SLE	Systemic lupus erythematosus
SOD	Superoxidase dismutase
Sp	Species
SSC	Side-scatter
Sup	Supernatant
T-EDTA	Trypsin-ethylenediaminetetraacetic acid
TADM	Total aspiration and dispensing monitoring
TEM	Transmission electron microscopy
TK	Tyrosine kinase
TLR	Toll-like receptor
TNFα	Tumour necrosis factor
VCAM	Vascular cell-adhesion molecule
VEGFR	Vascular endothelial growth factor receptor
WT	Wild type

CHAPTER 1: INTRODUCTION

2.1 The innate immune response and neutrophils

The innate immune system provides immediate defence against pathogens through the activity of leukocytes, macrophages and dendritic cells. Neutrophils are the most abundant cells of the innate immune system, they circulate in the blood stream and, subsequently, represent the first effectors at the site of infection, providing defence against invading microorganisms (Amulic *et al.*, 2012). They were first described and termed neutrophilic polymorphonuclear leukocytes (PMNLs) by Paul Ehrlich and Elie Metchnikoff in the late nineteenth century (as reviewed in Kaufmann, 2008). They are characterised by a unique lobulated and segmented nucleus and by the presence of numerous storage organelles and granules which carry a range of antimicrobial proteins and signalling molecules (Figure 1.1) (Borregaard & Cowland, 1997). Neutrophils are terminally differentiated leukocytes which patrol the peripheral vascular circulation and can act as primary effectors or can collaborate with other cells of the innate and adaptive immune systems to clear infection (Jaillon *et al.*, 2013). During inflammation in response to infection, local tissue resident cells including epithelial cells, fibroblasts and dendritic cells secrete pro-inflammatory cytokines, such as interleukin-8 and tumour-necrosis factor α (TNFα), which recruit neutrophils from the circulation to the site of infection where they become activated to enable pathogen clearance (Kolaczkowska & Kubes, 2013; Sadik *et al.*, 2011). Pathogen detection occurs in a less specific manner compared with the adaptive immune response, with neutrophils identifying highly conserved foreign molecular patterns associated with pathogens *via* a diverse array of surface pattern recognition receptors ([PRRs]; Akira, 2011). Neutrophils, subsequently, coordinate the maturation and activities of other leukocytes and lymphocytes through cell-cell interaction and cytokine signalling (Jaillon *et al.*, 2013). The neutrophil's migratory activity and functionality are a fundamental pre-requisite for defending the human body against infections as demonstrated in both leukocyte adhesion diseases and chronic

granulomatous disease (CGD), where defective neutrophil functionality results in severe immunodeficiency (Bunting *et al.*, 2002; Holland, 2010).

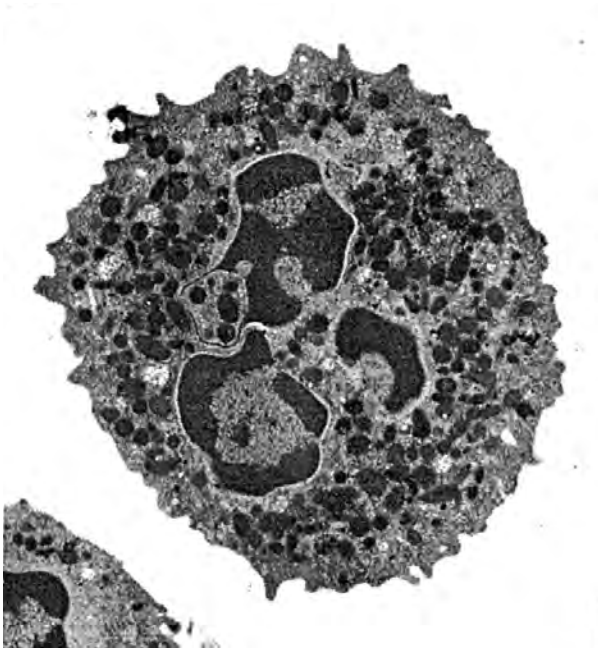

Figure 1.1: Micrographic image of a neutrophil.
Image obtained by transmission electron microscopy. The multilobulated nucleus is visible in dark colouration in the central region of the cell surrounded by numerous granules visible in shades of grey (Fernandez *et al.*, 2013).

2.1.1 From the bone marrow to the circulation

Neutrophils are produced abundantly in the bone marrow at an estimated rate of $1\text{-}2x10^{11}$ cells/day in a healthy adult human (Borregaard, 2010). Neutrophils originate from myeloid precursors in a process regulated by the cytokine granulocyte colony stimulating factor (G-CSF) in order to compensate for the number of mature cells eliminated in the circulation and in tissues (Lieschke *et al.*, 1994). Only fully mature neutrophils possess the characteristic granules and PRRs required for antimicrobial functions (Borregaard, 2010). Neutrophils mature in the bone marrow and are released into the circulation at a rate which in the presence of infection and inflammation, can increase up to 10-fold in only a few hours (Furze & Rankin, 2008). The

egress from the bone marrow is regulated by the expression of antagonist chemokine receptors, C-X-C motif receptor 4 (CXCR4) and C-X-C motif receptor 2 (CXCR2), which respond to the signals of retention and release (Strydom & Rankin, 2013). Neutrophil production and release is regulated by their rate of clearance and apoptosis in tissues. Tissue-resident macrophages and dendritic cells identify and phagocytose apoptotic neutrophils and can subsequently signal the recruitment of more neutrophils by down-regulation of interleukin 23 expression (IL-23) (Stark *et al.*, 2005). Once in the circulation mature neutrophils patrol the human body in search of microbial invasion, however, ageing neutrophils are believed to be redirected for clearance back into the bone marrow by up-regulation of CXCR4 receptor expression at their surfaces (Eash *et al.*, 2009).

2.1.2 Neutrophil activation, extravasation and chemotaxis

The neutrophil mechanism of extravasation includes several strategies depending on the systemic organ in which the infection occurs (Nauseef & Borregaard, 2014). Migration from the vasculature to infected peripheral tissues largely takes place at post-capillary venules which have relatively thin vessel walls but are large enough for neutrophils to arrest and accumulate in without the risk of occlusion (Borregaard, 2010). In the transmigration process (Figure 1.2) the neutrophil functional state is re-programmed from a circulating cell to a tissue phagocyte capable of oxidative activity and pro-inflammatory cytokine production (Nauseef & Borregaard, 2014).

2.1.2.1 Activation of endothelial cells and neutrophil tethering

When infection occurs, resident tissue cells detect invading pathogens and release a range of pro-inflammatory mediators including TNFα, IL-8, -1β (IL-1β) and -17 (IL-17), which create, along with bacterial-derived components, a chemotactic gradient in the host tissues. This

gradient of inflammatory stimuli also activates blood vessel endothelial cells by inducing the expression of specific adhesion molecules including P-selectin, E-selectin and members of the immunoglobulin superfamily (Amulic *et al.*, 2012). During circulation neutrophils randomly probe the endothelial wall and once P-selectin glycoprotein ligand-1 (PSGL1) and L-selectin (which are constitutively expressed on the neutrophil cell surface) interact with the P-selectin and E-selectin molecules on endothelial cells, the free-flowing neutrophils become tethered on the vessel wall (Kolaczkowska & Kubes, 2013). Following this interaction neutrophils roll along the endothelial wall by dynamic formation and dissociation of ligand binding adhesion molecules (Ramachandran *et al.*, 2004).

2.1.2.2 Neutrophil activation and extravasation

The binding of PSGL1 and L-selectin triggers an intracellular cascade of kinases, including Src and Syk, which ultimately lead to neutrophil activation and commitment for pathogen killing (Ley *et al.*, 2007). These intracellular signals, in turn, trigger the activation and clustering of integrin family protein members on the neutrophil surface, which interact with immunoglobulin superfamily members on the endothelial cells, namely intercellular adhesion molecules (ICAMs) and vascular cell-adhesion molecules (VCAMs), causing the arrest and firm adhesion of neutrophils to the vessel wall (Campbell *et al.*, 1998). In this phase, cytoskeleton rearrangements define cellular reorganisation which polarise surface receptors for chemokines and phagocytosis at the forefront of the cell (Borregaard, 2010; Sperandio *et al.*, 2012). Two pathways have been described for leukocyte extravasation: paracellular or transcellular (Phillipson *et al.*, 2006). In the paracellular pathway neutrophils ‘squeeze’ between junctions of adjacent endothelial cells by interaction with integrins and their respective immunoglobulin ligands (Ley *et al.*, 2007). For the transcellular pathway, neutrophils pass through the lumen of endothelial cells which form protrusions or transmigratory cups to cover and seal the leukocyte

away from the blood flow (Feng *et al.*, 1998; Kolaczkowska & Kubes, 2013). Once past the endothelial wall neutrophil migration must occur through the pericyte sheath and the venular basal membrane before reaching infected tissues, however little is understood about these processes (Woodfin *et al.*, 2010).

2.1.2.3 Chemotaxis

The directional migration of neutrophils towards, or opposite to, a chemotactic gradient is known as chemotaxis (Insall, 2010). Potentially, an initial chemotactic gradient produced by endothelial cells drives neutrophils from the circulation to the subluminal area while a second gradient, which overrides the first, directs neutrophils through the tissue to the infected site (Kolaczkowska & Kubes, 2013). The movement itself, and its orientation, are determined by cytoskeletal rearrangements which result in the formation of a pseudopod at the leading edge of the cell while retracting the rear (Friedl *et al.*, 2001). Chemotaxis follows the concentration of endogenous or exogenous soluble mediators which act as chemoattractants including complement components, chemokines such as IL-8 and bacterial-derived *N*-formyl-methionyl-leucyl-phenyalanine (fMLP) (Amulic *et al.*, 2012; Sadik *et al.*, 2011). The migration to the infected site, as represented in Figure 1.2, is coordinated by combinations of chemoattractants sensed by G-protein coupled receptors (GPCRs) on the neutrophil surface. Upon interaction, GPCRs trigger the activation of intracellular signalling pathways including those mediated by protein kinase C (PKC) and mitogen-activated protein kinases (MAPKs) (Selvatici *et al.*, 2006). Downstream, these kinases activate the pathways responsible for neutrophil defence, including the oxidative burst and degranulation (Amulic *et al.*, 2012).

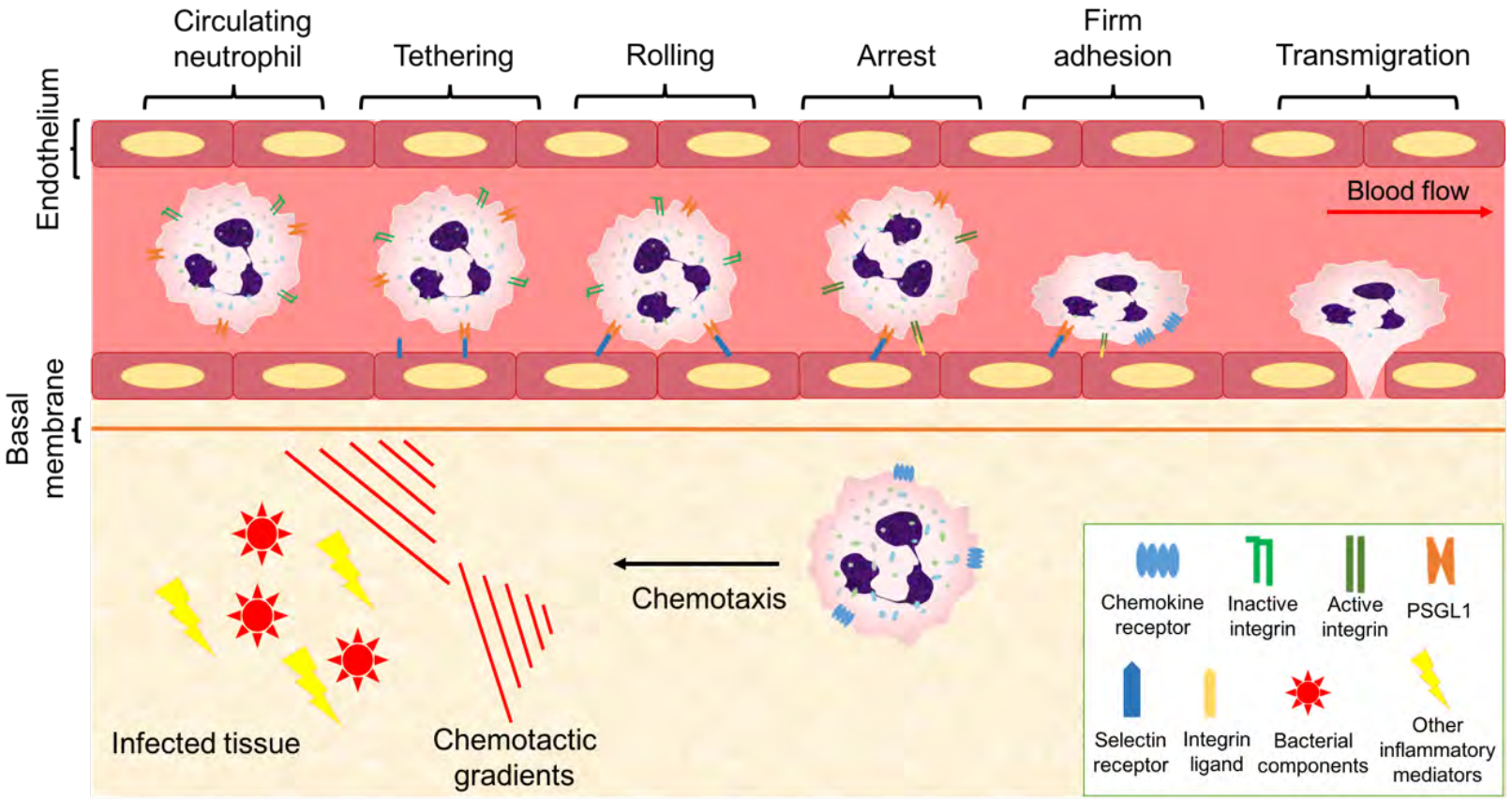

Figure 1.2: Schematic representation of neutrophil extravasation and chemotaxis.
Mature circulating neutrophils constitutively express on their surface PSGL1 and inactive integrin receptors. Once infection occurs in the peripheral tissue, bacterial and other pro-inflammatory signals induce the expression of selectin receptors on the endothelial cell surface. The interaction between selectin receptors and PSGL1 results in the tethering and slow rolling of the neutrophil along the endothelial wall. Integrin receptors become activated and interact with their respective ligands on endothelial cells resulting in the arrest and firm adhesion of neutrophils. Following adhesion, neutrophils cross the endothelial wall and transmigrate into the tissue (here represented by the paracellular pathway) where they migrate towards the infected site following chemoattractant gradients (image produced by I. J. Chicca).

2.1.3 The neutrophil killing arsenal

With the aim of killing or neutralising foreign microorganisms, neutrophils exhibit a range of microbicidal mechanisms at their disposal comprising phagocytosis, oxidative damage, release of antimicrobial peptides (AMPs) and extracellular killing (Amulic *et al.*, 2012). The neutrophil cytoplasm is packed with granular organelles containing a wide range of AMPs which can cause damage and death to pathogens. In neutrophils three types of granules have been identified and categorised for their content (Branzk & Papayannopoulos, 2013) and these comprise: i) primary or azurophilic granules, which carry the serine protease neutrophil elastase (NE) and myeloperoxidase (MPO) amongst others, ii) secondary or specific granules, and iii) tertiary or gelatinase granules which store the majority of flavocytochrome b_{558} on their membranes (Amulic *et al.*, 2012). Although the neutrophils primary function is to remove microorganisms and protect the human body, their antimicrobial strategies can also cause significant collateral host tissue damage as described in section 2.4 (Kruger *et al.*, 2015).

2.1.3.1 Reactive oxygen species and the oxidative burst

The dominant mechanism neutrophils adopt for infection resolution is by causing oxidative damage to pathogens through the production of reactive oxygen species (ROS). The process, also called “the respiratory burst” (Figure 1.3), is initiated by the intracellular enzyme complex nicotinamide adenine dinucleotide phosphate (NADPH)-oxidase which converts molecular oxygen (O_2) into superoxide anions ([$O_2^{\bullet-}$] Babior *et al.*, 1973). The NADPH-oxidase (NOX) machinery is comprised of numerous components which are partially located in the cytoplasm and partially bound to granule membranes. Flavocytochrome b_{558} is the central enzyme required for the electron transfer activity and is composed of two membrane-bound subunits. Upon cellular activation the expression of flavocytochrome b_{558} increases and NOX-complex component assembly is induced (El-Benna *et al.*, 2008). The electron transfer activity catalysed

by activated NOX-complexes produces $O_2^{\bullet -}$ which is transformed into hydrogen peroxide (H_2O_2) either spontaneously in the phagosome lumen or by the catalytic activity of superoxidase dismutases (SODs). The H_2O_2 produced at this stage can be converted by the enzyme MPO into hypochlorous acid (HOCl) which, in turn, is converted into hydroxyl radicals ([$HO^{-}\cdot$]; Chapple, 1996). The production of ROS is fundamental for the neutrophils' bactericidal activity as shown in the immunodeficiency syndrome CGD, in which patients with mutations in genes responsible for the NOX-complex compontents cannot generate ROS (Holland, 2010). The antimicrobial activity mediated by ROS operates following two paths: i) direct oxidation of pathogen membranes, proteins and nucleic acids, and ii) induction of membrane depolarisation and consequential mobilisation of cationic species, including potassium and calcium, which contribute to electrophysiological alterations and microbial killing (Hampton *et al.*, 1998; Rada *et al.*, 2004).

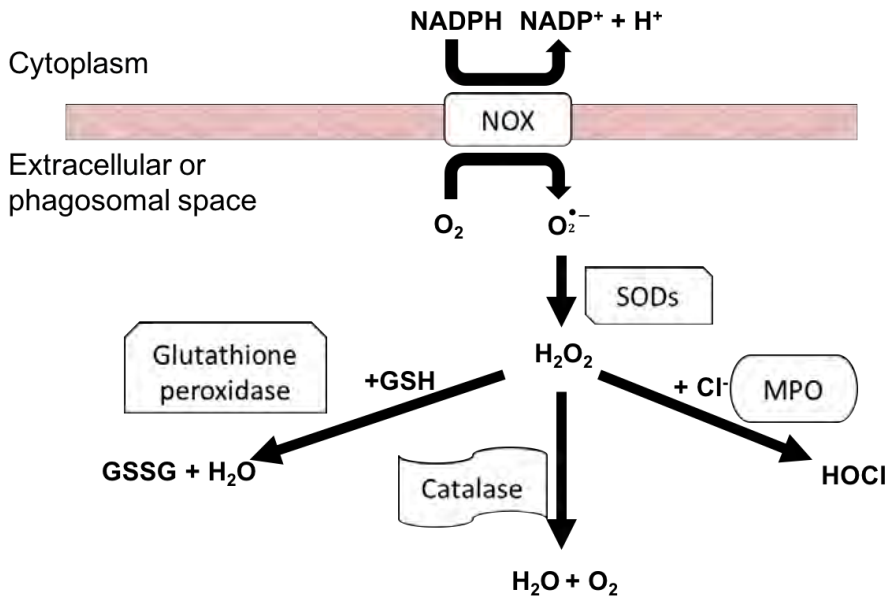

Figure 1.3: Schematic representation of the respiratory burst.
NOX complexes on the plasma or phagosomal membranes catalyse the conversion of NADPH into NADP+ and concomitantly convert O_2 into $O_2^{\bullet -}$, which in turn is converted into H_2O_2 by SOD. H_2O_2 acts as substrate for downstream reactions including i) the formation of HOCl by MPO; ii) the conversion into water (H_2O) by catalase; iii) the oxidation of glutathione (GSH) to form its disulphide form (GSSG) by the enzyme glutathione peroxidase (schematic produced by I. J. Chicca).

2.1.3.2 Phagocytosis and intracellular killing

Neutrophils are instructed to phagocytose bacteria encountered by host tissues and compartmentalise invading organisms. The process is mediated by specialised surface receptors which recognise highly conserved pathogen-associated molecular patterns (PAMPs) or opsonised pathogens coated with host-derived immunological proteins, such as immunoglobulins (IgGs) or complement components (Lee *et al.*, 2003). Fc-gamma receptors (FcγR) or activated integrins can also trigger diverse phagocytic strategies. Bacterial components, including lipopolysaccharide (LPS) and peptidoglycans, are detected through PRRs, such as Toll-like receptors (TLRs) to clear pathogens and initiate the inflammatory response (Underhill & Ozinsky, 2002). This receptor-ligand binding activates an intracellular process leading to cytoskeletal rearrangements, plasma membrane extension and, finally, engulfment of the pathogen into phagocytic vacuoles (Lee *et al.*, 2003). Once the phagosome is assembled the cytoplasmic granules fuse with its membrane and release their toxic materials into the intracellular compartment. Along with the granule contents the phagosome acquires flavocytochrome b_{558}, which provides an anchor for NOX assembly and activation (Jesaitis *et al.*, 1990). Once phagosomes are equipped with granules and the oxidative burst machinery, they are considered fully mature and can undertake microbial killing (Nunes *et al.*, 2013). Some pathogens, however, have evolved strategies to interfere with phagosome assembly or its maturation and can escape this killing mechanism as described in section 2.2.4.1 (Amulic *et al.*, 2012).

2.1.3.3 Degranulation and extracellular killing

An alternative employ of granules is their release outside the cell which occurs when granules fuse with the outer plasma membrane rather than internally with the phagosome. This fusion results in the release of antimicrobial molecules into the extracellular space as well as the

assembly of NOX complexes on the plasma membrane and, therefore, creates a hostile environment for pathogens (Amulic *et al.*, 2012). Release of granule proteins with non-specific proteolytic activity such as NE and the extracellular production of ROS can also cause damage to the surrounding tissue and lead to development of chronic inflammatory diseases such as periodontitis (Cooper *et al.*, 2013; Matthews *et al.*, 2007a). This degranulation, however, may provide a signalling gradient for the recruitment of other leukocytes or provide a signal for induction of alternative killing mechanisms such as the release of neutrophil extracellular traps (NETs) (Lacy, 2006; Soehnlein *et al.*, 2009).

2.2 Neutrophil extracellular traps

Among the many strategies neutrophils utilise for clearing infections in tissues is the release of neutrophil extracellular traps (NETs). The formation and physiological function of NETs were only first reported in 2004 and were described as a neutrophil strategy targeted against both Gram positive and Gram negative bacteria (Brinkmann *et al.*, 2004). NETs comprise extracellular deoxyribonucleic acid (DNA)-fibres which form a web-like structure with the function of immobilising pathogens, arresting their spread within the tissue and, eventually, facilitating their death (Figure 1.4). Notably, NET components, which are mainly relaxed chromatin and granule proteins, have direct antimicrobial affects (Brinkmann & Zychlinsky, 2007). Since their discovery more than 10 years ago, NETs have been the subject of intense research which has attempted to unravel the molecular pathways responsible for their production, release and functionality. Numerous microorganisms, chemical compounds and host-derived proteins, which are reviewed in more details in section 2.3, have been shown to activate NET release. The production of NETs is believed by some researchers to represent an ultimate sacrifice which neutrophils undergo as an alternative to phagocytosis, however, this cell death mechanism is distinct from necrosis and apoptosis (Fuchs *et al.*, 2007). Conversely,

others maintain that neutrophils utilise their mitochondrial DNA to form NETs and remain viable in order to preserve their other antimicrobial strategies (Yousefi *et al.*, 2009). Nucleic acid based extracellular traps (ETs) are not exclusive to neutrophils and they have been identified in other leukocytes including mast cells, macrophages, eosinophils and basophils (Boe *et al.*, 2015; Möllerherm *et al.*, 2016; Yousefi *et al.*, 2015; Yousefi *et al.*, 2012). Although molecular mechanisms leading to activation and formation of ETs differs between leukocytes (Goldmann & Medina, 2012), evidence suggests it represents an evolutionary conserved mechanism of anti-microbial and anti-fungal defence. Indeed, the formation of ET-like structures has been shown to act as defence mechanism in other mammals, birds, fish, invertebrates and also in plants (Brinkmann & Zychlinsky, 2012). Although NET release has been shown to be necessary for host immune defence, dysregulation of the process has been shown to play a pivotal role in the pathogenesis of auto-inflammatory and auto-immune diseases as is described in section 2.4.2 (Branzk & Papayannopoulos, 2013).

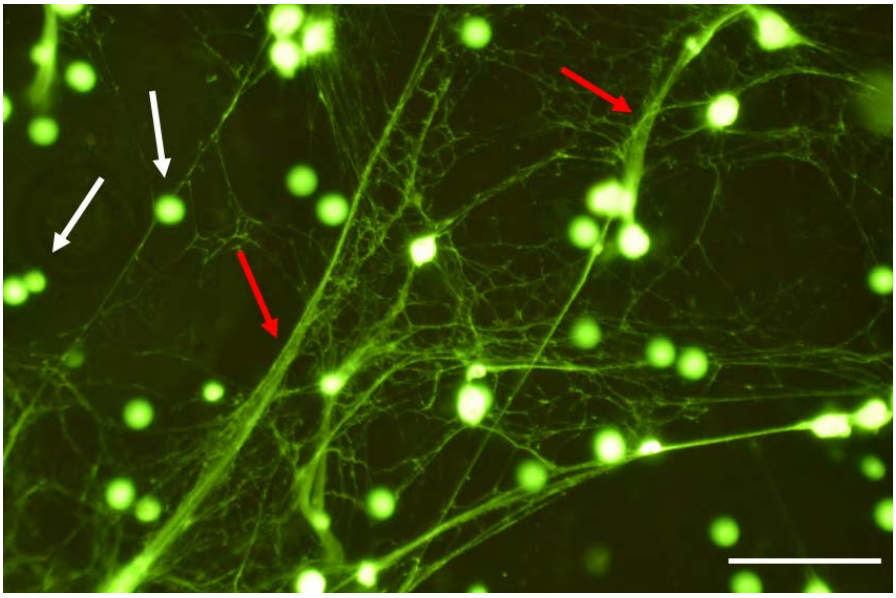

Figure 1.4: Image of neutrophils and their NETs.
Fluorescence visualisation of NETs (red arrows) following neutrophil (white arrows) stimulation with phorbol 12-myristate 13-acetate (PMA) and DNA staining with Sytox green®. Images were visualised using 20X magnification and the scale bar represents 100μm (image produced by I. J. Chicca).

2.2.1 Requirements for NET formation

NETosis is a complex process triggered by diverse signals and involving multiple transduction pathways including NOX activation, peptidylarginine deiminase 4 (PAD4) and NE esterase activities. Martinelli *et al.* (2004) demonstrated that the majority of molecular components required for signal transduction and neutrophil activation, in particular for NET release, are only generated in the late phase of neutrophil maturation, indicating that only mature circulating neutrophils are able to perform NET-mediated defence.

2.2.1.1 The respiratory burst

Neutrophils from CGD patients, which have mutations in the genes for NOX subunits (Seger, 2008), are unable to initiate the respiratory burst cascade and have been shown to exhibit poor NET responses (Fuchs *et al.*, 2007). Furthermore, patients with mutations in genes responsible for MPO activity, which can cause complete depletion of the enzyme, are more susceptible to infections compared with healthy individuals, partially due to defective NET formation (Metzler *et al.*, 2011). These and other studies have identified the key role of the oxidative burst in NET production, and this has also been confirmed by our own research which demonstrated that HOCl, one of the final products of the ROS production cascade, can efficiently and directly induce NET release (Palmer *et al.*, 2012a).

2.2.1.2 Deimination and esterase activities

The deimination activity of PAD enzymes has been shown to be important in chromatin decondensation, and is regarded as one of the early stages of NET formation (Neeli *et al.*, 2008). PAD4 knockout mice have been generated and analysed for NET-mediated immune defence (Li *et al.*, 2010), and data demonstrated that depletion of PAD4 activity is associated with increased susceptibility to bacterial infection, partially due to absent NET response. Similarly,

immunodeficiency has been shown in NE knockout mice as they were unable to produce NETs (Papayannopoulos *et al.*, 2010). Although several publications have described a role for PAD4 in NET formation, its involvement remains controversial as it has been suggested there is insufficient evidence for attributing the deimination activity to the PAD4 enzyme (Branzk & Papayannopoulos, 2013; Yousefi & Simon, 2016).

2.2.1.3 Calcium influx

Calcium flux has been reported to be involved in several stages of neutrophil activation (Tintinger *et al.*, 2005). Firstly, treatment of neutrophils with calcium ionophores, which increase intracellular calcium influx in intact cells, induces rapid NET formation via a NOX-independent pathway (Parker *et al.*, 2012a; Douda *et al.*, 2015). The effect of calcium on neutrophil function has been widely reported in the literature, showing a significant involvement in phagocytosis and migration (Alteraifi & Zhelev, 1997; Dewitt *et al.*, 2003). Furthermore, calcium mobilisation has been linked to NET-inducing stimuli, such as IL-8 (Gupta *et al.*, 2014), and to the activation of processes involved in NETosis, including superoxide generation and histone citrullination (Vossenaar *et al.*, 2003; Bréchard & Tschirhart, 2008).

2.2.2 NET structure and content

Since the early publications, NETs have been described as being highly orchestrated structures with a multifactorial composition. By atomic force microscopy, NETs appear as branching 2D meshworks organised in porous structures (Figure 1.5) (Pires *et al.*, 2016). The scaffold of this intricate web is comprised of smooth filaments of double-stranded DNA which have been demonstrated to be sensitive to degradation by deoxyribonuclease (DNase) enzymatic activity (Brinkmann *et al.*, 2004). Decorating the DNA strands are numerous neutrophilic proteins,

including histones and granule proteins, distributed and organised in globular domains of 30-50nm (Brinkmann & Zychlinsky, 2012), a fundamental property which distinguishes NETs from DNA released due to necrosis (Cooper *et al.*, 2013). Although proteolytic activity *in vitro* is not sufficient to eliminate NETs (Brinkmann *et al.*, 2004), protein degradation does, however, significantly alter the structural organisation and spatial distribution of NETs (Pires *et al.*, 2016).

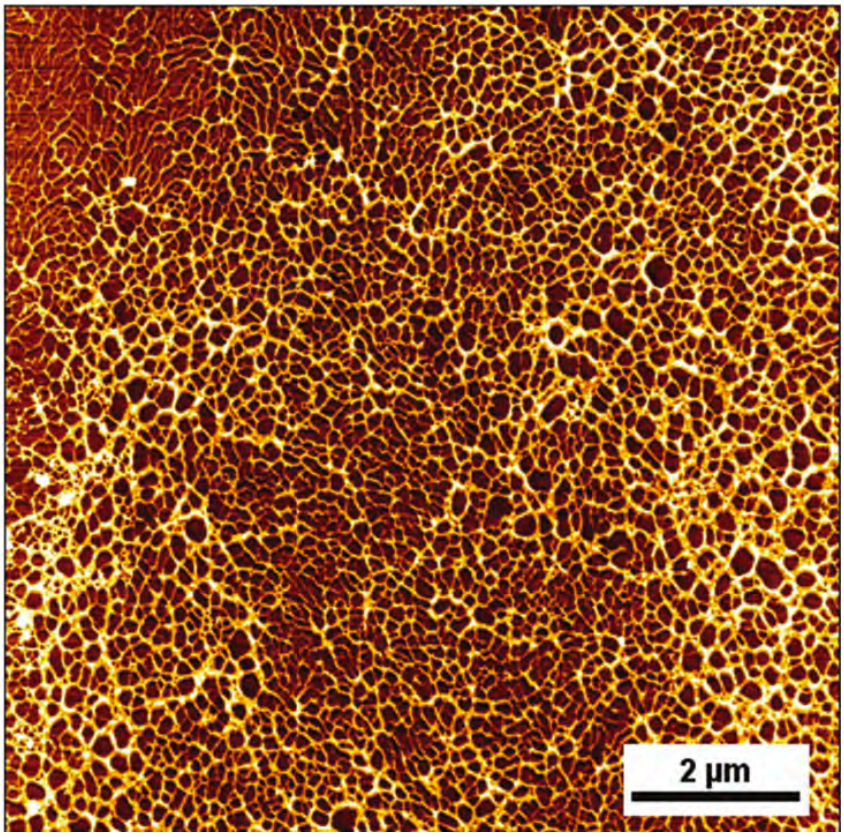

Figure 1.5: Atomic force microscopy images of NETs.
PMA-induced NET structures visualised using atomic force microscopy. NETs appear as a web-like structure composed of variable sized pores (Pires *et al.*, 2016).

2.2.2.1 DNA backbone and histones

Although it is universally accepted that the main component of NETs is DNA, the source of the nucleic acid remains controversial (Yousefi & Simon, 2016). While nuclear DNA has been described as being released as NETs in Fuchs *et al.*, (2007), Yousefi *et al.*, (2009) identified

mitochondrial rather than genomic DNA in NETs. In general the two hypothesis are accepted by the scientific community as alternative pathways for NET release elicited by neutrophils following different inflammatory and infectious stimuli (Branzk & Papayannopoulos, 2013). Other key components of NETs are the histones which have been found to be associated as granular domains within the filaments and are the most abundant proteins present in NETs (Urban *et al.*, 2009). As histones are known to form nucleosomes and to control the DNA condensation state in the nucleus, researchers have suggested they may operate the same function in NET assemblies (Pires *et al.*, 2016). Indeed all four types of histones which form the nucleosome core, H2A, H2B, H3 and H4, together with the histone linker H1, have been identified within NETs (Brinkmann *et al.*, 2004). However, their distribution, composition and post-translational modifications differ significantly from those found in the nuclear chromatin (Urban *et al.*, 2009). In addition to a structural role, the presence of histones is believed to partially account for the antimicrobial function of NETs (Palmer, 2010).

2.2.2.2 Granule proteins

Numerous proteins that are usually found in neutrophil granules have also been associated with NETs (Urban *et al.*, 2009). Among these is MPO, which has been shown to be released into the extracellular space and to actively produce ROS while bound to NET structures, an association which has been proposed to occur in the cytoplasm following neutrophil stimulation with PMA. MPO peroxidase activity is understood to represent another strategy NETs employ for creating a hostile environment for invading pathogens (Parker, *et al.*, 2012b) along with the protease activity of other granule enzymes such as NE, which has also been associated with NETs (Brinkmann *et al.*, 2004; Yousefi *et al.*, 2009). NE, like other neutrophil proteases, has antimicrobial properties and causes damage to the outer membranes of bacteria and can degrade their virulence factors (Korkmaz *et al.*, 2008).

Another class of granule proteins identified on NETs are the AMPs. LL-37 is part of the cathelicidin family which offers a wide range of host defence roles including regulation of the inflammatory response, immune cell chemoattraction and neutralisation of bacterial LPS (Dürr *et al.*, 2006). LL-37 in NET structures is associated with two important functions: antibacterial activity and protection of the NET-DNA from nuclease digestion (Neumann *et al.*, 2014). Its presence within NET-DNA complexes is also believed to propagate the auto-inflammatory activity which has been described for NETs (Kaplan & Radic, 2012).

2.2.2.3 Cytoplasmic enzymes

A wide range of neutrophilic proteins are non-granule-derived and have been identified in association with NETs. The majority of these have been described in Urban *et al.*, (2009), who first demonstrated the presence of calprotectin in NETs. Calprotectin is a cytosolic protein with a strong antimicrobial activity generated by the chelation of metal ions which are fundamental for microbial growth (Weinberg, 1975). This mechanism was confirmed for the antifungal activity of NET-associated calprotectin on *Candida albicans* growth, which was restored with the enrichment of zinc and manganese in the media (Urban *et al.*, 2009). Other cytosolic proteins reported by Urban *et al.* (2009) include cytoskeleton and glycolytic proteins, however, their function in NETs has not yet been described.

2.2.3 Events leading to NET formation

The release of NETs as an antimicrobial strategy is a highly orchestrated process which has been shown to involve several neutrophilic proteins. To date, three main mechanisms have been described for the production of NETs and these are described below.

i) Fuchs *et al.* (2007) described NET formation as a process dependent on NOX activity which leads to cell death following nuclear decondensation and rupture of nuclear and plasma

membranes. This mechanism has been supported by many other publications demonstrating that nuclear decondensation is regulated by the enzymatic activity of NE and MPO following their nuclear translocation (Metzler *et al.*, 2011; Papayannopoulos *et al.*, 2010).

ii) An alternative oxidant-independent mechanism has been proposed whereby neutrophils release NETs in vesicles and remain vital upon stimulation with *Staphylococcus aureus* whilst losing their nuclei (Pilsczek *et al.*, 2010).

iii) A further mechanism of vital NET formation has been described as being ROS-dependent which does not result in cell death. This form of ETosis has been described in eosinophils, basophils and neutrophils and the NETs generated are composed of mitochondrial rather than nuclear DNA (Yousefi *et al.*, 2015; Yousefi *et al.*, 2009; Yousefi *et al.*, 2008). Notably, only the nuclear-NET process has been extensively described and, subsequently, is schematically represented in Figure 1.6.

Upon stimulation, the first upstream process required for NET assembly is the activation of NOX complexes and the consequential production of ROS. The cascade of oxidative events, described in section 2.1.3.1, has been identified as a major trigger for NET production. Notably, treatment of neutrophils with diphenylene iodonium (DPI), a potent inhibitor of NOX, was able to inhibit NET production following chemical and bacterial stimulation (Fuchs *et al.*, 2007; Palmer *et al.*, 2012a). Following ROS production, nuclear chromatin decondensation occurs as a result of the activity of two enzymes which operate in sequence. First, a deiminase enzyme catalyses the conversion of arginine amino acid residues into citrulline on histone tails (Wang *et al.*, 2009). This conversion removes the positive charges on the arginine residues on histones which lose their interaction with the negatively charged DNA. The loss of electrostatic interactions relaxes the chromatin sufficiently for NE to then operate (Rohrbach *et al.*, 2012).

NE is understood to translocate from its cytoplasmic granule location to the nucleus upon activation. The proteolytic activity of NE degrades the bond between the histones of the nucleosome and further relaxes the chromatin structure. At this stage, MPO, which follows NE into the nucleus, is believed to associate with the DNA (Papayannopoulos *et al.*, 2010). The resulting relaxed chromatin is first released into the cytoplasm, following nuclear membrane dissociation, where it combines with a wide range of proteins deriving, for the most part, from disaggregated granules (Fuchs *et al.*, 2007). The extracellular release of DNA/protein complexes in the extracellular space is understood to be, then, actively mediated by the cytoskeleton of the cell. In fact, treatment with cytochalasin D, an inhibitor of actin polymerisation, impedes the release of NETs but not their assembly (Cooper *et al.*, 2013).

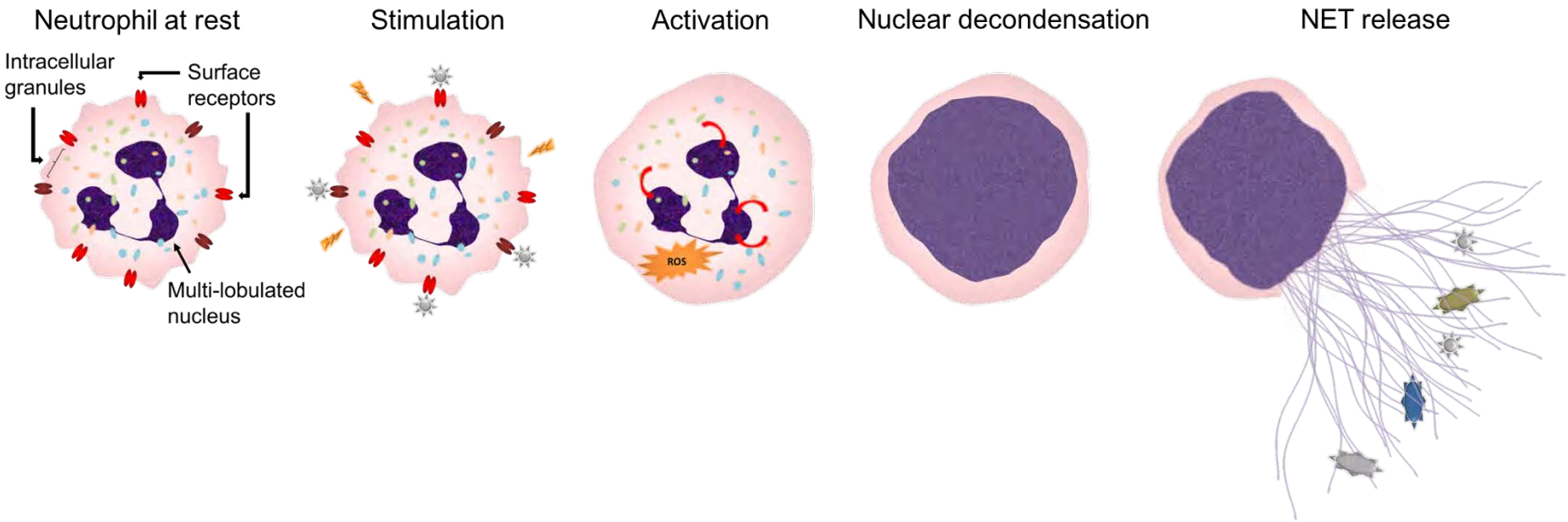

Figure 1.6: Schematic representation of neutrophil activation.
Mature neutrophils are characterised by a multi-lobulated nucleus, intracellular granules and PRRs expressed on their surface. Stimulation occurs *via* receptor recognition for physiological stimuli, such as microorganisms, or intracellularly for non-physiological stimuli, such as PMA. Upon stimulation, intracellular signal transduction leads to ROS production and granule protein translocation to the nucleus where enzymatic activities mediate nuclear decondensation and loss of the multi-lobulated shape. At this stage the nuclear membrane disintegrates and the DNA mixes intracellularly with cytoplasmic and granule contents. DNA/protein complexes are then actively released into the extracellular space as NETs which can target, trap and kill microorganisms (image produced by I. J. Chicca).

2.2.4 NET physiological functions

Although the existence of NETs and their role in the immune system have been extensively described in the literature, their exact function and mechanism of action requires further investigation (Yipp & Kubes, 2013). The release of extracellular DNA has been widely identified in the animal and plant kingdom as a protection mechanism against bacterial and fungal infections. Since this defence strategy appears to be highly conserved in other more primitive species, it is likely that NETs accomplish the same function in humans (Cooper *et al.*, 2013). NET antimicrobial mechanisms can be categorised into two main roles: i) direct trapping/killing of microorganisms, and ii) clearing infections *via* cross-talk with other cells of the immune system.

2.2.4.1 NET ensnaring and killing of microorganisms

Considering their intricate mesh-like structure, the most obvious function of NETs is to physically interact with, and capture microorganisms. The direct adhesion to NET-DNA has been identified with a number of bacterial and fungal species (Abdallah *et al.*, 2012; Brinkmann *et al.*, 2004; Urban *et al.*, 2009). Furthermore, NET entrapment functions by containing microorganism spread within the tissue and this may provide a strategy for their immobilisation while other antimicrobial effectors operate. A mechanism which has been proposed for the containment and killing of periodontal disease-associated bacteria (White, 2015). Subsequently, microorganisms have evolved virulence strategies which enable them to escape and survive NET killing. One of these mechanisms is the modification of the bacterial surface or structure, such as mimicking the expression of the host sialic acid on the external capsule in order to escape neutrophil recognition (Carlin *et al.*, 2009). Another strategy employed by microorganisms is the production of degradative enzymes. DNase production in bacteria was previously reported by Hirsch, (1958), however, its degrading function has only been re-

interpreted relatively recently since the discovery of NETs. Indeed, the bacterial production of DNase has been shown to degrade NETs and has also been related to increased virulence and disease severity (Beiter *et al.*, 2006; Berends *et al.*, 2010; Buchanan *et al.*, 2006). A further component of NETs, however, can also be targeted by bacterial evasion strategies. Proteases from microorganisms may also enable their escape by disrupting NET architecture, altering NET mechanical strength and its binding abilities (Pires *et al.*, 2016).

2.2.4.2 NET interactions in the host response

Besides their direct antimicrobial activity, NETs are believed to interact with other cells of the immune system. NETs have been proposed to collaborate with the phagocytic function of other 'non-NETosing' neutrophils (Brinkmann *et al.*, 2004). NET structures have been shown to bind complement component C1q which, in turn, initiates the host's complement cascade and enhances infection clearance (Leffler *et al.*, 2012). The interaction between platelets and NETs has also been proposed to play a role in disease pathogenesis. Platelets are able to induce NET production in their activated state and can be activated by NETs themselves (Cooper *et al.*, 2013). Numerous studies have proposed that NETs are also able to activate different types of lymphocytes and enable connections between the innate and adaptive immune response (Puga *et al.*, 2011; Tillack *et al.*, 2012).

2.3 Stimulation and regulation of NET release

NET production has been reported in response to various stimuli which include host-immune system mediators, whole bacteria, their components and products, as well as chemical compounds. In the descriptions below, stimuli have been categorised into physiological and non-physiological in order to distinguish between their functions under *in vivo* and in *in vitro* conditions. Neutrophil responses to such stimuli, however, can be modulated for lesser or

greater NET production. In the past, the identification of modulatory compounds has led to the unravelling of NET regulatory intracellular pathways and has opened new perspectives for developing therapeutic approaches for NET-related diseases. Several compounds have been found to inhibit NETosis while others have the ability to priming neutrophils to increase their responsiveness for NET production.

2.3.1 Physiological stimulation

Physiological stimuli are considered those related to the pathogenesis of diseases, including periodontitis, and are known to activate neutrophils through receptor-binding. These include foreign stimuli, such as bacteria, oral biofilms and LPS, and host-derived compounds, such as cytokines, AMPs and platelets (Cooper *et al.*, 2013). Neutrophils utilise their surface receptors for the identification of foreign or host-derived molecules, which activate intracellular cascades, usually mediated by kinases, and ultimately lead to ROS and NET production.

2.3.1.1 Microorganisms and microbial products

A variety of Gram positive and Gram negative bacteria are known to induce NET production during *in vitro* and in *in vivo* models of diseases (Branzk & Papayannopoulos, 2013). Among these are periodontal disease-associated bacteria including *Fusobacterium nucleatum* (Figure 1.7) and *Porphyromonas gingivalis*, which are two Gram negative bacteria (Delbosc *et al.*, 2011; Palmer *et al.*, 2012a). These bacteria reportedly activate neutrophils through TLR-binding (Kikkert *et al.*, 2007) which, in turn, triggers intracellular cascades leading to ROS production and NET release (Prince *et al.*, 2011).

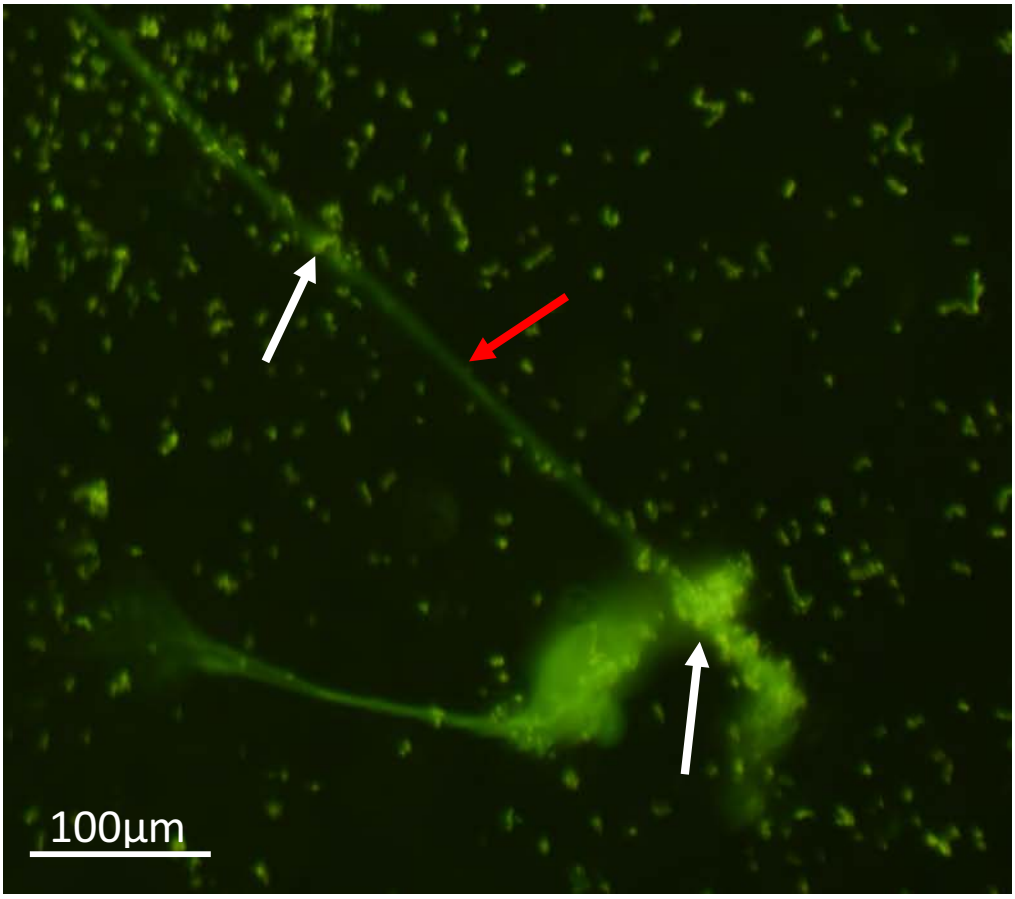

Figure 1.7: Bacteria entrapped in NETs.
Fluorescence micrographic image of *F. nucleatum* trapped (white arrows) in a NET filament (red arrow). Magnification of an image acquired with a 10X lens and scale bar is shown (image produced by I. J. Chicca).

Although whole bacteria are reportedly more efficient in stimulating NETs, their components can also activate neutrophils (Fuchs *et al.*, 2007). LPS is derived from the outer wall of Gram-negative bacteria, and during infection it is released as a soluble particle which is recognised by the immune system. CD14 on the neutrophil surface binds LPS and acts as co-receptor for TLR4 activation. Previous studies indicate LPS-binding improves when the molecule forms complexes with the lipopolysaccharide-binding protein (LBP) abundant in human plasma (Luchi & Munford, 1993). Notably LPS is reported to induce NET formation in neutrophils following neutrophil priming with cytokines, such as granulocyte-macrophage colony-stimulating factor (GM-CSF) (Yousefi *et al.*, 2009) or *via* platelet-activation (Clark *et al.*, 2007).

A relatively unexplored area in NET biology is that of the anti-fungal functions of NETs, which is proposed to be similar to the activity identified in other mammals and plants. Fungal infection spreads systemically when the fungal organism switches to its hyphal growth phase, which generates a highly proliferative form with pathogenic filaments too large to be phagocytosed (Urban *et al.*, 2006). Whole fungi and fungal hyphae, including *Candida albicans* and *Aspergillus fumigatus*, have been shown to induce the release of NETs, which then neutralise the microorganisms by employing the antifungal calprotectin (Bruns *et al.*, 2010; Urban *et al.*, 2009).

Relatively few studies have examined the role of NET formation in parasite and viral infections. Interestingly the promastigote, which is the parasitic component mediating the pathogenicity from *Leishmania amazonensis*, can also stimulate the formation of NETs (Descoteaux *et al.*, 2010; Guimarães-Costa *et al.*, 2009). Furthermore, among viruses, the influenza A and human immunodeficiency virus-1 (HIV-1) have been shown to trigger neutrophil activation through TLR7 and TLR8 recognition and this has been associated with the production of NETs, which can capture and inactivate the virus by MPO and defensin activities (Narasaraju *et al.*, 2011; Saitoh *et al.*, 2012).

2.3.1.2 Host-derived molecules

Neutrophils are able to cross-talk with other cells of the immune system through the release of cytokines and other inflammatory mediators. NET production has been proposed to play a key role in mediating interactions between cells of the immune system, indeed, several host-immune mediators have been found to induce NET release. Pro-inflammatory cytokines including TNF-α, IL-1β and IL-8, which are released by tissue structural cells and other leukocytes in response to invading microorganisms, have been reported to enhance ROS production and NET formation in neutrophils (Keshari *et al.*, 2012a). A further inflammatory

mediator, nitric oxide (NO), has also been shown to be involved in the activation of NET pathways. Keshari *et al.* (2012b) utilised NONOates, a specific NO donor, in order to investigate NO-mediated NET release and found a high neutrophilic response following treatment in terms of ROS and NET production. Furthermore, LPS-activated platelets have been shown to interact *in vivo* with circulating neutrophils and mediate bacteria killing through NET formation (Clark *et al.*, 2007).

2.3.2 Non-physiological/chemical stimulation

Chemical stimuli frequently utilised in NET studies include HOCl, phorbol 12-myristate 13-acetate (PMA) and ionomycin (Ermert *et al.*, 2009; Gupta *et al.*, 2014, 2005; Palmer *et al.*, 2012a). These molecules activate neutrophils by bypassing the interaction with surface receptors and, therefore, function relatively rapidly.

HOCl, one of the key products of MPO activity and of the neutrophil ROS cascade, is required for efficient NET formation. In fact, chemical inhibition of MPO catalytic activity using 4-aminobenzoic acid hydrazide resulted in decreased NET production, while treatment with exogenous HOCl was able to restore NET formation in CGD patients' neutrophils. Moreover, suppression of HOCl by taurine was able to prevent NET formation and preserved neutrophil viability (Palmer *et al.*, 2012a).

PMA is extensively used by researchers to induce ROS and NET production. Its chemical structure resembles that of the host-derived diacylglycerol (DAG) which is a physiological lipid second messenger activator of the PKC pathway. PMA stimulation and its resulting intracellular kinase activity ultimately lead to NOX activation, ROS formation and NET release (Neeli & Radic, 2013). PMA stimulation *in vitro* has been reported by Fuchs *et al.* (2007) to stimulate NETs in approximately one-third of neutrophils that were assayed. Similar data were

provided by the research conducted by the Periodontal Research Group at the University of Birmingham (Palmer, 2010).

Treatment with ionomycin, a lipid-soluble ionophore which transports calcium across the membrane, has also been shown to mediate NET production in an oxidant-independent pathway and this demonstrated calcium influx was required for NETosis (Gupta *et al.*, 2014; Parker *et al.*, 2012a).

2.3.3 Increased response in primed neutrophils

Some agents have the effect of modulating neutrophil responsiveness to stimuli and have been used in studies of ROS and NET stimulation. The effect of cytokine priming on ROS production has been extensively described in neutrophils (El-Benna *et al.* 2008) and similar mechanisms have been proposed to enhance the response of neutrophils in terms of NET production (Kaplan & Radic, 2013). GM-CSF is an inflammatory cytokine which can function in recruiting neutrophils from the circulation as well as activating them at the site of infection (Sullivan, 1992). Exposing neutrophils to GM-CSF prior to stimulation with LPS or complement molecules resulted in viable neutrophils releasing NETs comprised of mitochondrial DNA (Yousefi *et al.*, 2009). Subsequently it has been proposed that different combinations of stimuli with cytokine priming affect the response and the fate of neutrophils (Dias *et al.*, 2013; Kaplan & Radic, 2013).

2.3.4 Compound-mediated inhibition

Several compounds which pharmacologically inhibit NET release have so far been identified. Most researchers focus on the inhibition of the ROS cascade utilising DPI, which blocks the activity of NOX complexes, or use specific MPO inhibitors to decrease NET formation (Palmer *et al.*, 2012a). Recently, a potent inhibitor of NETosis has been described as a potential

treatment for NET-related auto-inflammatory diseases (Yu *et al.*, 2015). Celastrol, also known as tripterine, is one of the active components in root extracts derived from *Tripterygium wilfordii,* or Thunder god vine, utilised in Chinese medicine. Celastrol treatment has been shown to down-regulate cytokine expression and to exhibit anti-inflammatory properties in several animal models of disease (Kannaiyan *et al.*, 2011). Notably exposing neutrophils to celastrol prior to stimulation with TNF-α drastically reduced the percentage of cells undergoing NETosis (Yu *et al.*, 2015).

2.4 NETs in the pathogenesis of disease

Besides the beneficial antimicrobial function of NETs and the additional roles they exert upon the immune system in fighting infections, the presence of DNA/protein complexes in extracellular tissue has been associated with certain pathologies. Indeed, excessive production and/or delayed or defective removal of NETs are believed to play a role in the pathogenesis of several inflammatory diseases such as cystic fibrosis (CF) and systemic lupus erythematosus (SLE) (Brinkmann & Zychlinsky, 2012; Hakkim *et al.*, 2010; Manzenreiter *et al.*, 2012). Furthermore, NET structures have been implicated in thrombus formation in deep vein thrombosis (DVT) (Fuchs *et al.*, 2012), in cancer development (Demers & Wagner, 2014) and, also, NETs may provide a source of auto-antigens in rheumatoid arthritis (RA) patients (Khandpur *et al.*, 2013). Due to their contradictory functions in human biology, NETs have been described as being a “double-edged sword” and their homeostatic control may determine the difference between health and disease (Cooper *et al.*, 2013).

2.4.1 Murine models of disease

Over the past decades mice have been extensively used as model organisms in human disease research. Indeed, murine models have been developed for studying the immune-system and

immune-related diseases, in particular, they have been employed in studies focused on linking neutrophils with auto-inflammatory diseases (Németh *et al.*, 2016). NET production has been successfully suppressed in PAD4 knockout mice, generated by deletion of exon II of the gene responsible for PAD4 transcription, resulting in the expression of a non-functional form of the enzyme (Li *et al.*, 2010). Together with the increasing evidence recognising NETs as major source of auto-antigens, murine models have been developed for targeting NET cascade events in SLE, autoimmune arthritis, anti-neutrophilic cytoplasmic antibody-(ANCA)-associated vasculitis and gout. The subsequent data generated has supported a role for NETs in human disease pathogenesis (Knight *et al.*, 2015; Willis *et al.*, 2011; Kessenbrock *et al.*, 2009; Schauer *et al.*, 2014).

2.4.2 Aberrant NET formation & clearance

Following efficient microbial entrapment in host tissue, NET removal is understood to comprise two steps. Initially, NETs are processed by either DNases, which can degrade the DNA backbone, or NETs are opsonised by C1q complement molecules. Subsequently, NETs are cleared by macrophage engulfment, a process known as efferocytosis in which NETs and other neutrophil remnants are degraded in intracellular lysosomal vacuoles (Farrera & Fadeel, 2013). Notably the efferocytosis process must be efficient in order to prevent NET-derived cytotoxic components persisting in the host tissues and causing tissue injury or the induction of autoimmunity. Indeed ineffective macrophage-dependent efferocytosis, identified in the alveoli of patients with chronic lung diseases, has been proposed to contribute to persistent inflammation in CF (McCubbrey & Curtis, 2013). In CF patients with impaired antimicrobial neutrophil function excessive NET formation was identified and attributed to elevated levels of host-inflammatory molecules within the circulation. The extracellular filaments of DNA released as NETs are believed to accumulate in the mucus in the airways of CF patients and to

contribute to its viscosity (Cheng & Palaniyar, 2013). Another chronic condition in which impaired NET clearance has been identified is the autoimmune disease SLE. Patients affected by SLE present elevated serum levels of ANCA targeted against the major components of NETs including chromatin and granular proteins (Hakkim *et al.*, 2010). Impaired NET clearance has been proposed as a primary source of auto-antigens (Munoz *et al.*, 2005) and a subset of patients identified by Hakkim *et al.* (2010) presented defective DNase degradation of NET structures. Taken together, these findings suggest imbalanced NET formation and clearance processes represent suitable targets for the treatment of several diseases (White *et al.*, 2016a).

2.4.3 NETs as a scaffold

NETs are potentially a major source of extracellular DNA in fluid and tissues which may function as a scaffold for bacterial colonisation and biofilm development (Thornton *et al.*, 2013). Indeed, extracellular DNA (eDNA) has been shown to provide a functional structure for bacterial adhesion and biofilm formation, subsequently enabling antimicrobial resistance (Okshevsky & Meyer, 2015). Bacterial and host-derived eDNA are employed as scaffolds for forming and stabilising a pathogenic biofilm in the middle ear of children affected with otitis. One of the sources of host-derived eDNA, interestingly, was suggested to be the local production of NETs (Thornton *et al.*, 2013). The structural function of NETs as a scaffold for bacterial colonisation was also suggested for chronic infections identified in CF patients (Cheng & Palaniyar, 2013). This structural function is not limited to bacterial colonisation, indeed NETs can also provide a scaffold for the development of thrombi as well as activating their formation in an experimental model of DVT (Fuchs *et al.*, 2012). In sepsis, NET release occurs inside the vasculature and can activate platelets with the DNA/protein structures being associated with platelet adhesion (shown in Figure 1.8). Their aggregation with red blood cells

and other coagulation factors subsequently results in the formation of clots and thrombotic complications (Kaplan & Radic, 2012).

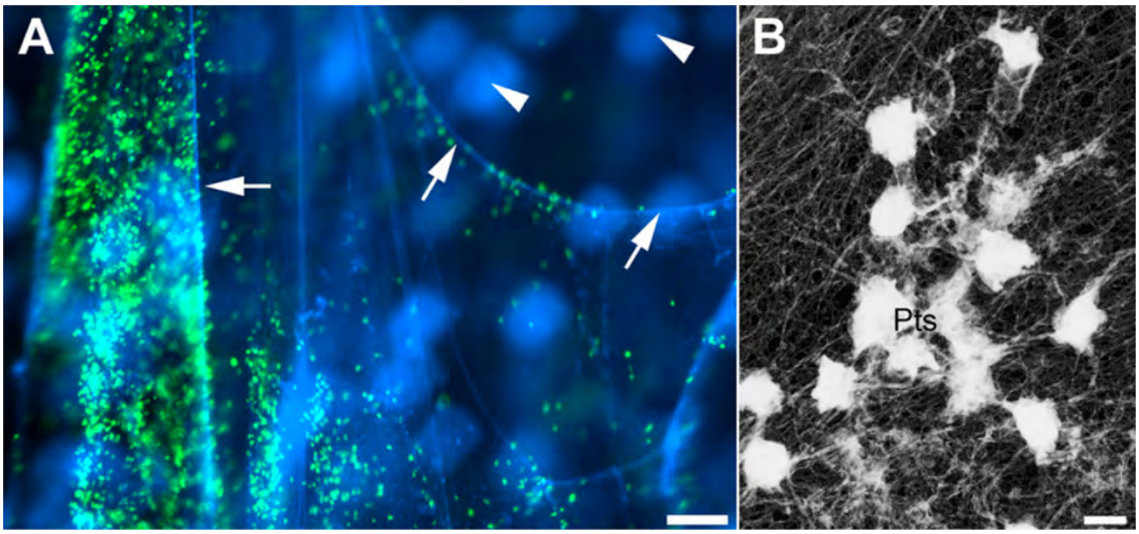

Figure 1.8: Micrograph images of platelets adhering to NET structures.
a) Fluorescence images of platelets, visible in green, attached to NET structures, visible in blue and indicated by arrows, while no interactions are identified with neutrophils, out of focus and indicated by arrowheads. b) Electron micrograph of platelets (Pts) aggregated with NET filaments (Fuchs *et al.*, 2010).

2.4.4 NETs as a source of auto-antigens

RA is a chronic disease characterised by the production of antibodies against self-antigens, leading to joint inflammation and swelling (Koch, 2007). Similar to SLE patients, RA patients produce elevated levels of autoantibodies directed against NET components, in this specific case against citrullinated proteins, which are known as anticitrullinated protein antibodies (ACPAs). Indeed, serum and synovial fluid from inflamed joints of RA patients have been shown to trigger NET production in neutrophils from healthy individuals (Branzk & Papayannopoulos, 2013). Subsequently, aberrant NETosis has been demonstrated in the synovial fluid of RA patients providing a source of autoantigens and enhancing the inflammation; a positive feedback mechanism has also been described to perpetuate this

pathogenicity in RA (Khandpur *et al.*, 2013). Recently, citrullination and PAD4 activity have been identified in the synovial fluid associated with the release of NETs, and this has been linked to the elevated production of ACPAs in serum from the same patients and to disease progression in RA pathogenesis (Spengler *et al.*, 2015).

2.4.5 NET function in cancer

Over recent years NET pathogenicity has also been associated with cancer progression, with extracellular release of neutrophil chromatin being shown to contribute to tumour development, angiogenesis and metastasis (Demers & Wagner, 2014). NET-like structures have been identified in sections of tumours by two independent studies (Berger-Achituv *et al.*, 2013; Ho-Tin-Noé *et al.*, 2009), and recently Cools-Lartigue *et al.* (2013) demonstrated *in vitro* and in an *in vivo* murine model that NET release can result in the capture of circulating tumour cells, promoting their adhesion in distant organs and thereby mediating metastatic disease. Subsequently, the presence of NETs in tumours and in the blood of patients affected by cancer has provided new information on the potential use of NET-associated biomarkers for diagnostic and therapeutic approaches (Demers & Wagner, 2014).

2.5 Neutrophils and NETs in the pathogenesis of Periodontitis

The interaction between oral bacteria and the host immune response has been extensively investigated. While oral commensal bacteria, usually colonising the tooth surface, are known to positively balance the recruitment and the activity of immune cells in healthy periodontal tissue, when this homeostasis is lost, inflammation can occur (Devine *et al.*, 2015). Periodontitis is a well characterised chronic inflammatory disease affecting the supporting tissues of the tooth and its progression can be modulated by many factors, such as smoking and stress. Moreover it has been demonstrated that diabetes and genetic predisposition also represent significant risk

factors for periodontal diseases (Figure 1.9). The chronic, non-resolving inflammation in response to the bacterial plaque biofilm, if left untreated, results in damage to the tooth's supporting tissues, identified in patients as loss of bone and connective tissues, and ultimately disease progression can lead to tooth loss (White *et al.*, 2016a). Salivary calcium has also been shown to play a major role in sub-gingival plaque accumulation and contributes to calculus formation (Miller *et al.*, 2006). The level of calcium in saliva from periodontitis patients has been analysed in several studies and this has demonstrated levels to be elevated in patients compared with healthy individuals. Subsequently calcium saliva levels have been reported as a biomarker for periodontal disease (Sewón *et al.*, 1995; Sewón *et al.*, 1998; Kambalyal *et al.*, 2015). Notably, increased levels of salivary calcium mirrors the fluctuations occurring at a systemic level following disease progression (Greabu *et al.*, 2009) and, interestingly, extracellular calcium flux is involved in several stages of NETosis, as previously described in section 2.2.1.3. Neutrophils are known to play a significant role in the inflammatory process in periodontal disease and previous studies have shown the presence of NETs in purulent exudates from inflamed gingiva. It is therefore, reasonable to speculate that NETs may be important in periodontitis pathogenesis, as previously reported for other chronic inflammatory diseases (Cooper *et al.*, 2013). Notably, chronic periodontitis is associated with systemic diseases including RA. Interestingly, the periodontal disease-associated bacteria, *P. gingivalis*, which is the only bacteria expressing its own PAD enzyme, is reportedly involved in the production of citrullinated host-peptides which may act as auto-antigens in RA pathogenesis (de Pablo *et al.*, 2009).

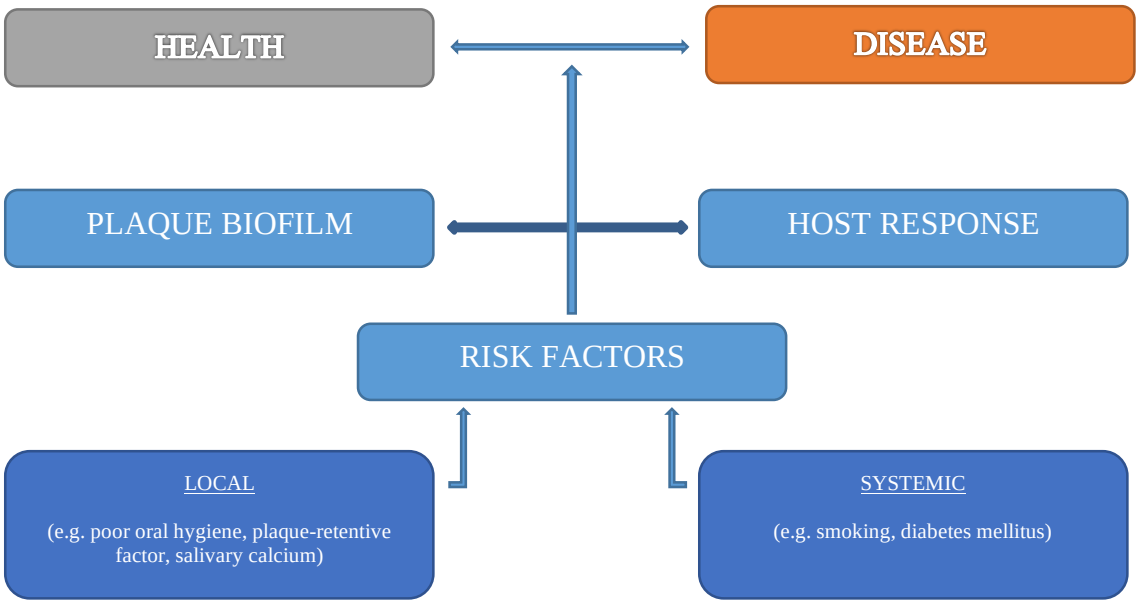

Figure 1.9: Diagram of key factors involved in the aetiology of periodontitis.
Periodontitis occurs due to a dysbiosis between the plaque biofilm at the gingival margin and the host immune response. Several risk factors, such as poor oral hygiene, plaque retention, increased salivary calcium levels, smoking or systemic conditions, can influence disease progression and lead to chronicity (image produced by I. J. Chicca).

2.5.1 Characteristic phenotype of neutrophils from periodontitis patients

The immune response plays a fundamental role in the pathogenesis of chronic periodontitis, indeed, disease development is understood to occur in predisposed individuals which present an exaggerated inflammatory response (Matthews *et al.*, 2007a). Recently, neutrophils from periodontitis patients have been shown to exhibit chemotactic anomalies in response to certain chemoattractants, such as fMLP, and in particular they move relatively slower and with compromised directionality compared with healthy neutrophils (Roberts *et al.*, 2015). This prolonged tissue transit time has been hypothesised to contribute to collateral host tissue damage and is associated with the neutrophil's tissue extravasation process and their release of an arsenal of cytotoxic molecules (Roberts *et al.*, 2015). Indeed, neutrophils isolated from chronic periodontitis patients have been shown to exhibit an abnormal phenotype in respect to pathogen interaction and ROS production. In response to bacterial stimulation, periodontitis

patients' neutrophils have been shown to generate increased levels of extracellular oxygen radical release compared with neutrophils derived from healthy control individuals. The baseline ROS activity, in the absence of any exogenous stimulation, was also higher than in control neutrophils. Taken together these findings highlight the characteristic hyper-responsiveness and -reactivity of neutrophils derived from chronic periodontitis patients (Ling *et al.*, 2015; Matthews *et al.*, 2007b). Notably however, although ROS production directly correlates with NET formation, neutrophils from chronic periodontitis exhibit similar levels of NET release compared with healthy control (White *et al.*, 2016b).

2.5.2 Periodontal pathogens and NETs

Periodontitis is characterised by the accumulation of bacteria and biofilm formation at the gingival margin. A wide range and variety of bacterial species have been identified and categorised based on their association with disease stages. Key periodontal bacteria include *F. nucleatum* and *P. gingivalis* which are strongly associated with disease pathogenesis (Socransky *et al.*, 1998). Exposing neutrophils to these periodontal bacteria induces the release of tissue-degrading molecules and cytokines which may exacerbate local tissue inflammation (Scott & Krauss, 2012). Several periodontal pathogens have also been shown to differentially activate ROS and NET responses in neutrophils from healthy volunteers and this has indicated that, although NETs entrap bacteria, they are not necessarily capable of killing them (White, 2015). It is reasonable to speculate that the function of NETs at the periodontal site is to provide a source of extracellular DNA, which functions to provide a scaffold for biofilm formation, rather than acting antimicrobially, and subsequently this could contribute to disease development, as described in section 2.4.3. In addition, this may provide a source of, eDNA which has been shown to provide a suitable substrate for oral bacterial adhesion, protection

from antimicrobial agents and a source of nutrients which can enable oral biofilm progression and development (Jakubovics & Grant Burgess, 2015).

2.5.3 NETs in periodontal tissues

During periodontal inflammation neutrophils migrate to the infected gingival tissues where they undertake antimicrobial functions. Neutrophils are also constantly released through the gingival crevicular fluid (GCF) around the tooth to provide a tissue defence mechanism. Once GCF is enriched with neutrophils it is clinically considered a purulent exudate. Notably, exudates and biopsies of the gingival epithelium collected from chronic periodontitis patients have been shown to exhibit elevated levels of NETs which were identified by NE immunostaining (Vitkov *et al.*, 2009). Similar results were presented in Cooper *et al.* (2013) who reported for the first time increased MPO-positive NET structures in the gingival connective tissue following inflammation compared with healthy tissue (Figure 1.10).

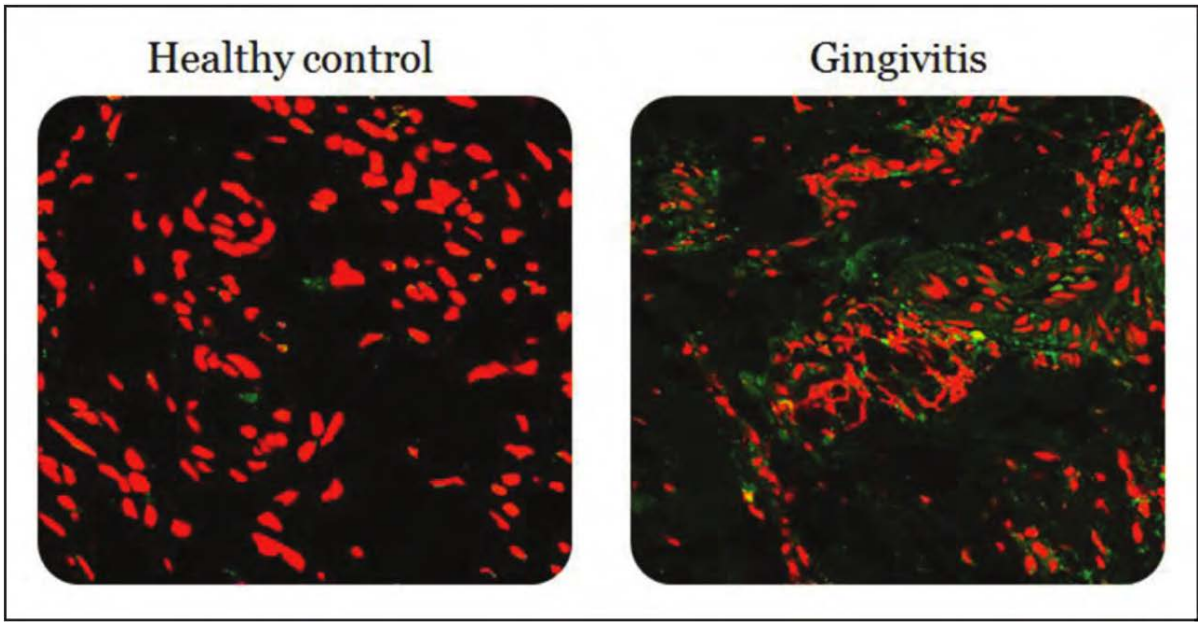

Figure 1.10: Evidence of NETs in inflamed periodontal tissue.
Confocal microscopy of MPO-stained NETs in healthy and diseased gingival tissues. An increased amount of DNA is visible in red and co-localising with extracellular MPO, visible in green, in the diseased tissue (Cooper *et al.*, 2013).

2.6 Current methods used for NET analysis

Following evidence demonstrating the association of NETs with several inflammatory diseases there is now a growing need to develop a better understanding of the NETosis process. Current approaches for the analysis of NETs in biological samples or tissues are based on the identification of their components and include DNA quantification, NET-related protein immunostaining and immunoblotting or enzyme-linked immunosorbent assays (ELISA) (Palmer *et al.*, 2012a; Urban *et al.*, 2009; Wang *et al.*, 2009). These methods can be relatively low-throughput, expensive and there has been lack of consistency between findings since different approaches are applied, and results can be prone to bias. Only relatively recently have efforts focused on improving the analytical method for NETs by developing objective semi-automated and high-throughput solutions (Brinkmann *et al.*, 2012; Zhao *et al.*, 2015).

2.6.1 Microscopy analysis

The most frequently published methods used for the analysis of NETs *in vitro* and in tissues utilise microscopic approaches. These approaches, in general, utilise fluorescence, such as in confocal laser microscopy, or electrons such as in transmission electron microscopy (TEM) and scanning electron microscopy (SEM) (de Buhr & von Köckritz-Blickwede, 2016). Although microscopic approaches are generally the preferred method utilised by many researchers, as NETs are fragile structures their careful handling and preparation is paramount to ensuring that artefacts are not introduced during their analysis (Brinkmann & Zychlinsky, 2012). Since the major component of NETs is DNA, visualisation by fluorescence microscopy is achieved by using cell impermeable DNA dyes which highlight the extracellular filaments (Brinkmann *et al.*, 2004; Urban *et al.*, 2009). DNA staining is often performed alongside immunostaining targeted at NET-related proteins such as histones, MPO or NE (Brinkmann *et al.*, 2004; Hakkim

et al., 2010; Metzler *et al.*, 2011). While fluorescence microscopy is employed for the analysis of NET components, electron microscopy allows structural investigations. Indeed, SEM and TEM were employed for the initial characterisation of the NETosis process (Brinkmann *et al.*, 2004; Fuchs *et al.*, 2007) as shown in Figure 1.11. SEM has demonstrated the structural properties of NET filaments and, TEM has been used to determine the characteristic cell morphology assumed by neutrophils during NETosis, such as nuclear decondensation and nuclear membrane disintegration. However, observation of NETs by microscopy has two main disadvantages: first, the detection of NET structures is prone to lack of objectivity and bias which is introduced by the operator who must search and identify DNA/protein complexes in the detection area; second, these techniques are performed on microscopy slides which allow only a limited number of cells and samples to be analysed over a relatively long time period (de Buhr & von Köckritz-Blickwede, 2016).

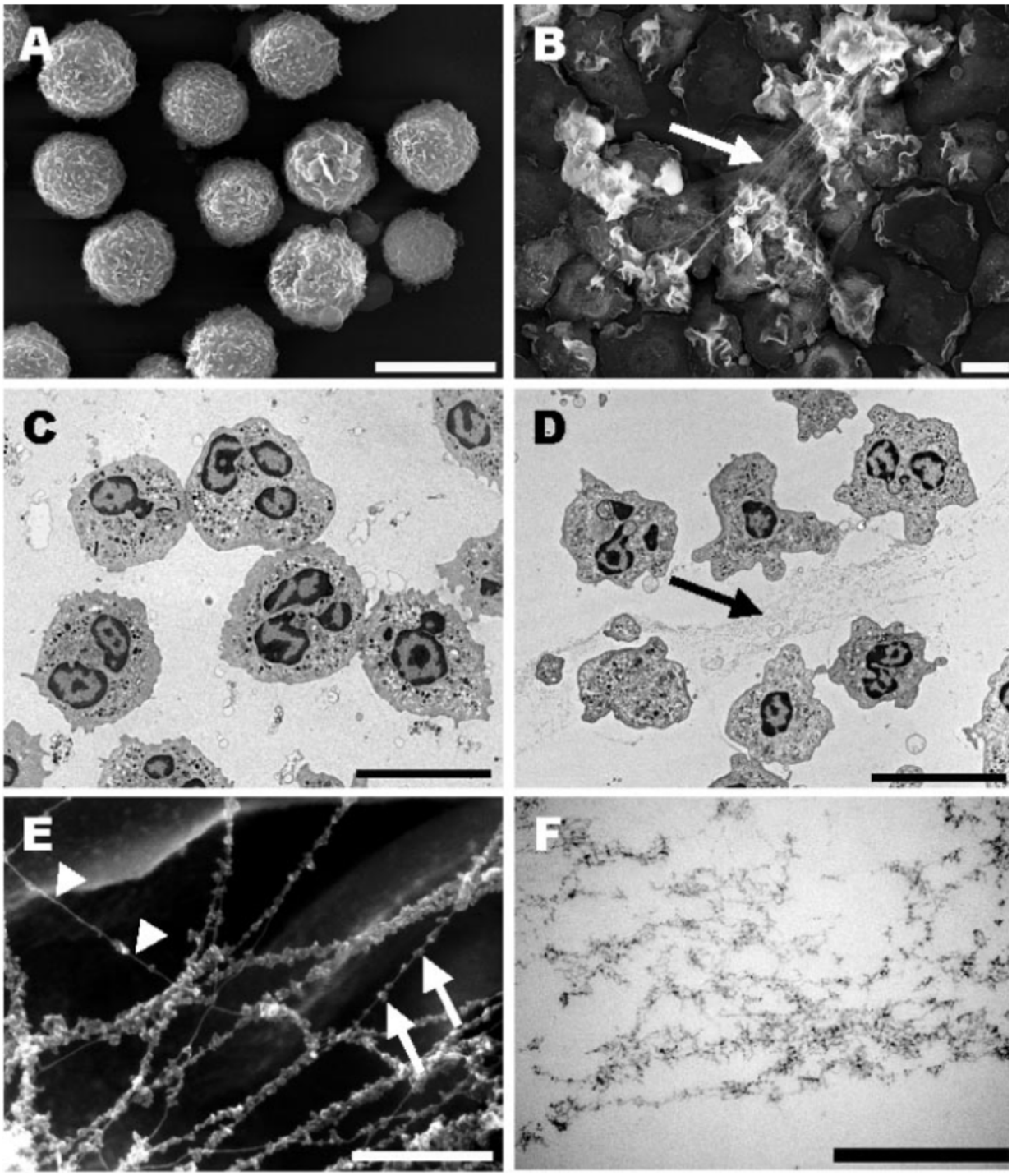

Figure 1.11: Electron micrographs of neutrophils and NETs.
SEM images of unstimulated neutrophils (a) and PMA-induced NETs (indicated by arrows in b & e). TEM images of unstimulated (c) and PMA stimulated (d) neutrophil morphology, and NET filaments (f). Scale bars represent 10μm in a) to d) and 500μm in e) and f) (from Brinkmann *et al.*, 2004).

2.6.2 NET-DNA analysis using fluorescence spectroscopy

Besides visualisation by microscopy, NETs can also be quantified based on the amount of extracellular DNA detected in samples *in vivo* and *in vitro* in culture media. This method routinely utilises the partial digestion of NET structures in order to isolate the DNA component from the rest of the cell, and is followed by its fluorometric quantification using a multiwell plate reader (Köckritz-Blickwede *et al.*, 2010; Palmer *et al.*, 2012a). The main advantage of this procedure is the possibility of analysing a greater number of samples compared with microscopy approaches (de Buhr & von Köckritz-Blickwede, 2016). Furthermore, this approach allows NET analysis without requiring sample processing, such as fixation and washing passages, which may affect outcomes. However, care is necessary when performing this procedure in order to avoid artefacts caused by DNA released due to other types of cell death (Brinkmann & Zychlinsky, 2012).

2.6.3 Immunoassays for NET-related protein detection

Although NET components can be observed by fluorescence microscopy following immunostaining, a more qualitative characterisation can be performed using other immunoassay approaches. For this purpose, NET structures are partially digested in order to isolate DNA/protein complexes from the samples and then antibodies specifically targeted for NETs are applied (Masuda *et al.*, 2016). The immuno-based assays developed for NETs include ELISA and western blotting (Keshari *et al.*, 2012b; Kessenbrock *et al.*, 2009; Papayannopoulos *et al.*, 2010). Immunoassay applications are not limited to NET components, but have been extended for the quantification of NET-bound enzyme activity. For instance, antibody-based immunoassays have been developed for quantifying the citrullination activity of PAD4 during the NETosis process (Spengler *et al.*, 2015). Although this approach offers the possibility of

quantifying NET-related proteins, accurate standardisation is required for relative data comparison in unstimulated neutrophils and only a limited number of parameters can by analysed for each readout.

2.6.4 High-throughput and automated methods for NET quantification

It is only recently that alternative approaches have been proposed for the high-throughput analysis of NETs. These solutions were developed for the quantification of NET-related features in a relatively short-time scale and with the aim of minimising operator bias. Two recent publications in the same year have proposed flow cytometry-based approaches for the detection of NETs. The method developed by Zhao *et al.* (2015) is based on the analysis and identification of nuclear decondensation in stimulated neutrophils, which has been shown to represent the initial stage of NETosis (as previously described in section 2.2.3). The method employs Multispectral Imaging Flow Cytometry which integrates the advantages of fluorescence microscopy with those of flow cytometry (Figure 1.12). The technique is morphologically-based and was developed to analyse nuclear shape, DNA staining intensity and co-localisation of the MPO signal in order to differentiate vital NETosis from non-vital NETosis. Conversely, the method proposed by Gavillet *et al.* (2015) aimed at directly quantifying NET levels in blood samples employing citrullinated-H3 and MPO biomarkers using a fluorescent-activated cell sorting (FACS)-mediated approach. The main disadvantage of this technique, however, was the limitation to the analysis of citrullinate-H3 positive NETotic events which, whilst being suggested to represent the majority of NETotic events, may not represent them all (de Buhr & von Köckritz-Blickwede, 2016; Li *et al.*, 2010). Following the need for automation of NET analysis, Brinkmann *et al.* (2012) developed a technique for automated image analysis of NETosing cells. This method was based on monitoring the fluorescent signal associated with H2a-H2b-DNA complexes, which become exposed during

chromatin relaxation, and utilised a computer algorithm for the automatic analysis of NETosing cells. The software quantified the NETosing rate based on the ratio between chromatin relaxation and DNA staining. However, in this approach neutrophils were prepared on a glass slide, processed for immunostaining and only 5 random images were selected for analysis, and this approach remains somewhat subjective. An additional semi-automated method was recently proposed for screening compound libraries of inhibitors in order to identify novel NET regulatory molecules and associated pathways. This method eliminated operator bias related to image acquisition by utilising automated microscopy for the identification of NETosing cells. Indeed using this approach the author identified that inhibition of the Raf-MEK-ERK pathway was sufficient to block NET formation (Hakkim *et al.*, 2011).

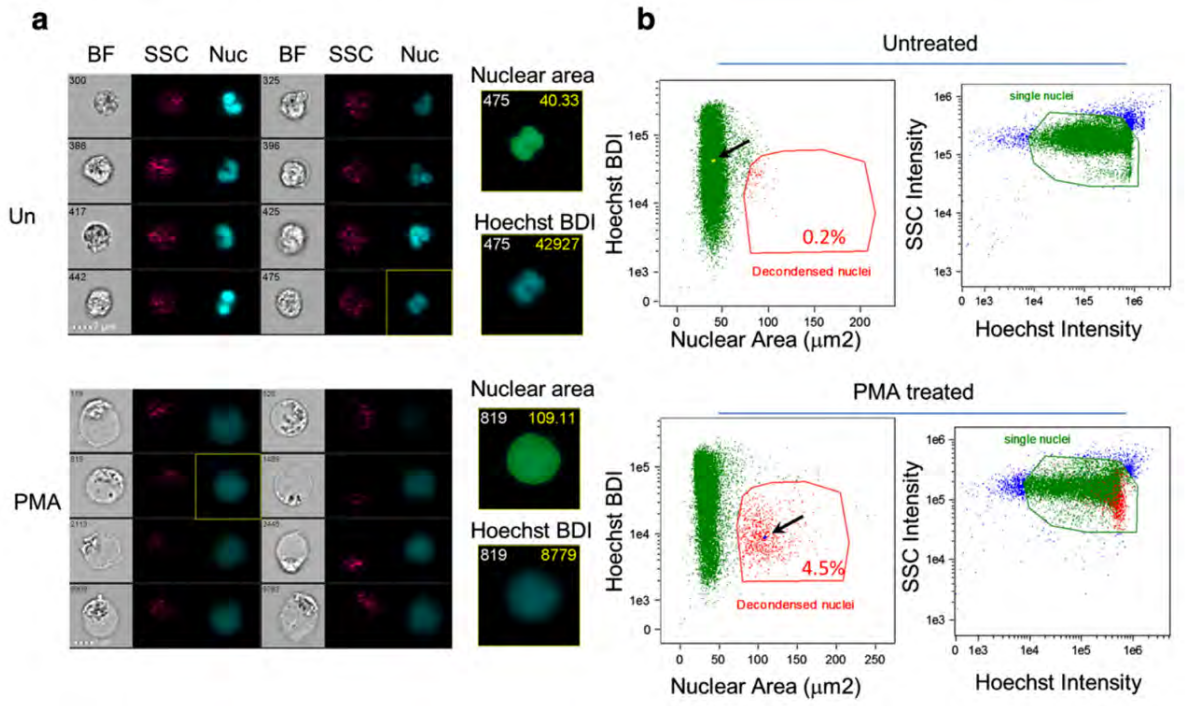

Figure 1.12: Flow-cytometry based high-throughput approach for the identification of neutrophils undergoing NETosis.
Nuclear features of unstimulated and stimulated neutrophils are analysed by flow-cytometry. a) Images obtained with brightfield (BF), side-scatter for granular content (SSC) and nuclear staining (Nuc) are shown. b) The portion of NETosing cells is quantified in scatterplots and gated in red (Zhao *et al.*, 2015).

2.7 High-Content Analysis

As described above, the majority of studies on neutrophils and NETs have allowed only relatively small scale analysis. Now, with the introduction of automated tools for image acquisition and data analysis, high-throughput analyses have become a reality for the study of biological samples (Abraham *et al.*, 2004). High-content analysis (HCA) is a high-throughput imaging approach which integrates automated cell image acquisition with automated data analysis. A comprehensive definition has been provided by Shariff *et al.* (2010) which described HCA as a combination of "*image processing, computer vision, and machine learning to provide fast and objective methods for analysing large amounts of bioimage data*". This technology has broad application in the pharmaceutical industry with an increasing number of biological assays now being performed with HCA. Using this automated imaging system major breakthroughs have been achieved in the field of neuroscience and in the screening of small-inhibitory ribonucleic-acid (siRNA) (Daub *et al.*, 2009; Dragunow, 2008; Drake *et al.*, 2009). The main advantages of HCA compared with low-throughput analyses are: i) quantification of protein staining intensity and molecular subcellular localisation, ii) obtaining independent cell information, and iii) rapid acquisition of multiparametric data, such as information on spatial and temporal variables (Drake *et al.*, 2009). The image analysis aspect is performed using bioinformatics software with built-in algorithms for diversified biological applications, with examples including cell death investigations, measurement of oxidative stress and analysis of protein-related parameters (Ghosh *et al.*; Mandavilli; Miller *et al.*). HCA is a completely automated platform for the investigation of biological features in high-resolution images captured by an automated fluorescence microscope capable of reading 96-, 384-, 1536-well plate formats, which dramatically increases the number of conditions which can be analysed simultaneously (Mayr & Bojanic, 2009). Furthermore, cell-based HCA has been extensively

employed for the screening of compound libraries, often referred to as high-content screening (HCS), which aims to identify novel therapeutic leads (Korn & Krausz, 2007).

2.7.1 From its early origins to today's HCA technology

Since its introduction to scientific research in the 17th century, the microscope has provided a powerful tool for studying cells. Its technological evolution has so far contributed to notable improvements in our research approach and the quality of results generated (Bardell, 2004). A major breakthrough leading to the development of HCA was the introduction of the fluorescence microscope in the 1950s which integrated the accuracy of fluorescence investigation with the specificity of targeted antibodies (Coons & Kaplan, 1950). Successively, the introduction in the early 1990s of optimised fluorescent dyes with different ranges of excitation and emission wavelengths made possible the simultaneous investigation of multiple parameters in the same cell, as is shown in Figure 1.13 (DeBiasio *et al.*, 1987). Inspired by the flow cytometry system and early forms of automated microscopy, the biotechnological company Cellomics introduced, in 1997, a high-throughput automated fluorescence platform for the analysis of large biological samples (Giuliano *et al.*, 1997; Taylor, 2007). This automated transition represented both time-saving as well as cost-saving improvements due to the reduced amount of reagents and personnel time required for the screening approach whilst maintaining high-sensitivity readouts (Drake *et al.*, 2008). Subsequently, HCA merged with confluent innovations in probe technology, automated image instrumentation, image analysis and bioinformatics.

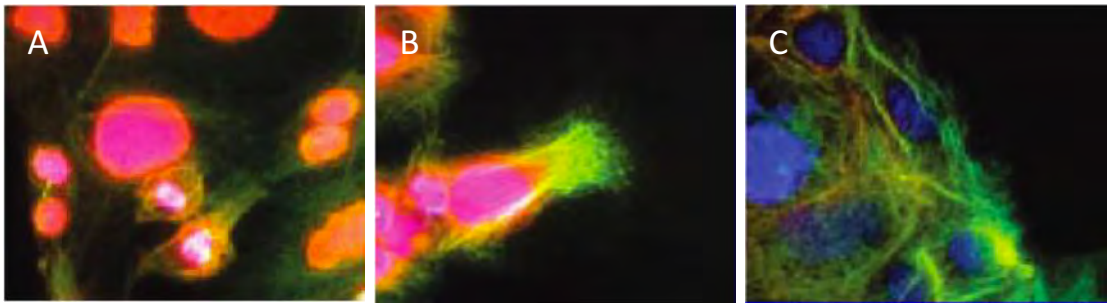

Figure 1.13: Multiple combined fluorescent staining for the analysis of acetylation modifications of the cytoskeleton provides powerful multi-parametric data.
Images of colorectal cells fixed and stained for nuclear DNA (blue), keratin proteins (green) and acetylation modifications (red). Different patterns of acetylation are shown for the different cytokeratin domains A) K10, B) K471 and C) 482 (Drake *et al.*, 2009).

2.7.2 Application of HCA for large-scale biology

With low-throughput imaging technologies, cell-based biology can only be investigated in relatively small sample sizes with the image produced as a relevant output. However, automated HCA has application for the study of thousands to millions of cells simultaneously and focuses on the translation of imaging data to digital output (Taylor, 2007). Low- and high-throughput imaging approaches are often integrated for accurate identification of functional parameters (Abraham *et al.*, 2004). In the past, HCA has been successfully applied for the identification of genes or cellular/molecular activities involved in a wide range of biological processes (Mattiazzi Usaj *et al.*, 2016). For example, using HCA researchers have screened RNA inhibitor libraries and have identified numerous genes involved in differentiation and proliferation processes of several organism systems including zebrafish and human embryonic stem cells (Chia *et al.*, 2010; Huang *et al.*, 2012). Other applications of HCA for large-scale biology have monitored the expression of sensitive reporters which lead to the identification of pathways involved in the pathogenesis of several neurological diseases including Huntington's and Alzheimer diseases (Honarnejad *et al.*, 2013; Schulte *et al.*, 2011). Furthermore, HCA has been applied for genome-wide screening and the analysis of protein suppression or amplification.

This approach has facilitated the identification of pathways and their temporal sequence enabling identification of molecular targets for possible therapeutic interventions (Abraham *et al.*, 2004).

2.7.3 High-Content Screening of compound libraries

Intracellular signal transduction pathways are often involved in the pathogenesis of diseases such as cancer, inflammatory disease and metabolic disorders. Frequent therapeutic approaches for such diseases are, therefore, targeted to regulate abnormalities in signalling including modulation of receptor activation and kinase activities. Indeed HCA has been applied for the screening of modulatory compound libraries targeting a wide range of intracellular processes (Korn & Krausz, 2007). With HCA, protein translocation and subcellular compartmentalisation can be monitored by fluorescently labelling the protein target and compound libraries can be screened for the identification of protein translocation inhibitors. Utilising this approach researchers have discovered inhibitors for the translocation of Akt1 and phosphoinositide-3-kinase, pathways involved in cell survival and cancer cell growth (Lundholt *et al.*, 2005; Wolff *et al.*, 2006). Fluorescent fusion proteins have also now been developed for investigating intracellular protein trafficking including receptor activation and internalisation mechanisms. More than 700,000 compounds have been screened using HCA to investigate the activation and internalisation of GPCRs in metabolic and obesity diseases (Garippa *et al.*, 2006). Numerous compound libraries are routinely screened in cell viability assays in order to determine the level of cytotoxicity of potential drug candidates and assess their potential clinical safety. With HCA, multiple cytotoxic parameters, including mitochondrial integrity, nuclear area and plasma membrane integrity can be evaluated simultaneously (O'Brien *et al.*, 2006).

NET formation is a complex process which is regulated by an intricate modulation of intracellular pathways. The numerous parameters associated with NETosis have the potential for being investigated by HCA. With the potential of monitoring multiple conditions simultaneously, HCA can be applied for screening compound libraries for regulating NETosis to enable: i) identification of the molecular mechanisms leading to NET formation, ii) understand the role of NETs in the pathogenesis of inflammatory disorders, and iii) identify modulators of NETosis with possible therapeutic application. However, a detailed protocol for the HCA of neutrophils and NETosis has yet to be proposed.

2.8 Aims and objectives

In the last decade, NETs have been extensively studied in order to identify the molecular pathways mediating their formation, to try to understand their involvement in disease pathogenesis and, ultimately, develop appropriate therapeutic approaches. However, the screening methods currently utilised for NET analysis are generally low-throughput, are subject to operator biases and often lack consistency and reproducibility. NETs have the potential for being investigated by high-throughput and automated methods, and several studies have begun to propose different techniques to do this (Brinkmann *et al.*, 2012; Gavillet *et al.*, 2015; Moussavi-Harami *et al.*, 2016; Zhao *et al.*, 2015).

- The initial aim of this study was to develop and optimise a protocol for the investigation of neutrophil activation and NET formation using the automated high-throughput platform of HCA. In order to address this aim three main objectives were considered:
  - The evaluation of suitable experimental conditions and stimuli which could be applied for the development of a HCA method for NETosis investigation.

- The development of an appropriate fixation protocol for preservation of neutrophil and NET sample integrity.
- The validation of HCA algorithms and the optimisation of algorithm parameters for the correct identification of neutrophils and NET-related features.

Maintaining the homeostasis between NET formation and clearance may determine the difference between health and disease conditions. Several studies are now focusing on the identification of compounds able to pharmacologically modulate NETosis and with possible application for the treatment of NET-related diseases (Lapponi *et al.*, 2013; Mcinturff *et al.*, 2013; Yu *et al.*, 2015). Screening modulatory compounds on NETosis activity has the potential for being investigated by HCA.

- The second aim of this study was to apply HCA for screening (HCS) a pharmaceutically-derived compound library and identify those with the ability to induce or inhibit the process of NETosis. In order to address this second aim two main objectives were considered:
  - Perform HCS using a 56 member compound library for the modulation of NETosis activity.
  - Characterise and validate the compound 'hits' selected by HCS for their effects on unstimulated and PMA-stimulated neutrophils in term of ROS and NET production using specific targeted approaches.

CHAPTER 2: MATERIALS & METHODS

2.1 Isolation of human peripheral blood neutrophils

For experiments using human peripheral blood neutrophils, cells were isolated from human venous whole blood from orally and systemically healthy volunteers using a discontinuous Percoll gradient, erythrocyte lysis and sedimentation processes as previously described (Matthews *et al.*, 2007a). On average ~2-million cells per ml of whole blood were obtained, purity was assayed by flow cytometry as described below in section 2.1.8.

2.1.1 Discontinuous Percoll gradient

Neutrophil isolation was performed using Percoll solutions as there is a low grade of toxicity associated with polyvinylpyrrolidone (PVP)-coated silica particles which constitute the Percoll solution (Pertoft *et al.*, 1978) and previous research performed at the School of Dentistry Laboratories has demonstrated the lowest levels of neutrophil activation using this method compared with Ficoll or Dextran (Chapter 3 of White, 2015). Two distinct densities were prepared combining Percoll (GE Healthcare 17-0891-01), distilled sterile water and sterile 1.5M NaCl (Sigma S7653) in distilled water (Table 2.1).

Gradient densities (g/ml) / **Components (ml)**	**1.079**	**1.098**
Percoll	19.708	24.823
Water	11.792	6.677
1.5M NaCl	3.5	3.5
Total volume (ml)	**35**	**35**

Table 2.1: Composition of Percoll density gradients.

Resulting solutions were stored at 4°C for no longer than 7 days prior to use. To create the discontinuous density gradient 8ml of 1.098 was slowly layered under 8ml of 1.079 Percoll solutions using a 3ml plastic Pasteur pipette in 25ml or 30ml centrifuge tubes (Fisher Scientific).

2.1.2 Venous blood collection

Peripheral venous blood was collected from healthy volunteers in 6ml Vacutainers (Greiner, Bio-One Ltd.) coated with lithium heparin, anticoagulant suitable for cell isolation purposes.

2.1.3 Erythrocyte lysis buffer

To remove erythrocyte contamination and increase the purity of isolated neutrophils, samples were treated with a buffer solution to generate osmotic disequilibrium and induce erythrocyte cell lysis. The buffer was prepared by dissolving 8.3g NH_4Cl (Sigma A9434), 1g $KHCO_3$ (Sigma P9144), 0.04g Na_2 EDTA $2H_2O$ (Sigma E5134), 2.5g bovine serum albumin ([BSA]; Sigma A7906) in 1L distilled water and stored at 4°C prior to use.

2.1.4 Phosphate Buffered Saline (PBS)

A buffer solution to maintain neutrophils in osmotic and pH conditions similar to that of the human body was generated by dissolving 7.75g NaCl (Sigma S7653), 0.2g KH_2PO_4 (Sigma P5655), 1.5g K_2HPO_4 (Sigma P3786) in 1L distilled water, autoclaved and stored at 4°C prior to use.

2.1.5 Neutrophil isolation method

Venous blood was carefully layered above the discontinuous Percoll density gradient using the 9ml volume of blood within each gradient tube, then centrifuged (Rotina 380R or Universal 320R, Hettich Zentrifugen) for 8 minutes at 150 relative centrifugal force (rcf) followed by 10

minutes at 1200 rcf. Sedimentation through the discontinuous gradient results in the stratification of blood as shown in Figure 2.1.

The upper layers containing plasma (see Figure 2.1), leukocytes and monocytes were removed from centrifuge tubes and discarded using a 3ml plastic Pasteur pipette. The neutrophil layer was carefully transferred in 30ml erythrocyte lysis buffer to a 50ml centrifuge tube and mixed by inversion. The cell suspension was incubated for 5 - 10 minutes at room temperature until the solution became clear and then centrifuged for 6 minutes at 500 rcf to pellet the neutrophils. The supernatant was discarded and the pellet suspended in an additional 3ml of erythrocyte lysis buffer. Following a further 5 minutes of incubation at room temperature, the cell suspension was re-centrifuged for 6 minutes at 500 rcf. The supernatant was discarded and the pellet was washed in 5ml of PBS, centrifuged once more for 6 minutes at 500 rcf and re-suspended in 5ml of PBS after the supernatant was discarded.

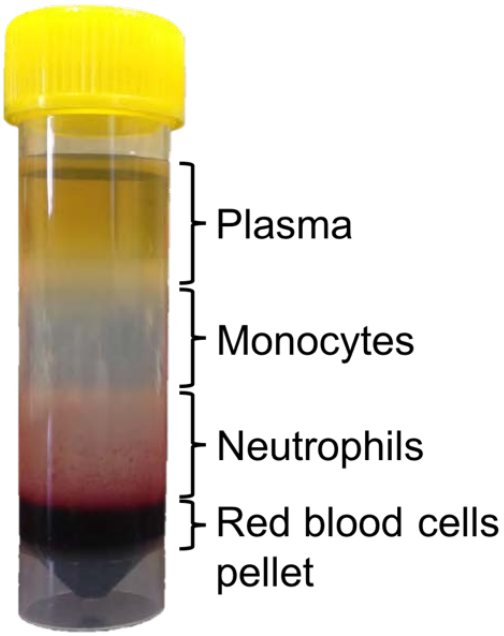

Figure 2.1: Venous blood layered in Percoll gradient.
Labelled layers of stratified blood through the Percoll gradient.

2.1.6 Neutrophil count

The haemocytometer chamber is divided into 9 squares, the central square area measures $1mm^2$ and is subdivided in 25 squares of $0.04mm^2$ surrounded by triple lines. The chamber depth is 0.1mm, therefore the volume of the central square is $0.1mm^3$ ($1mm^2$ x 0.1mm). Cells were counted in 9 of the 25 squares and those within the triple lines on the left margin and above the central square, but cells were not counted if they were on or beyond the the right margin and below the bottom margin as shown in Figure 2.2.

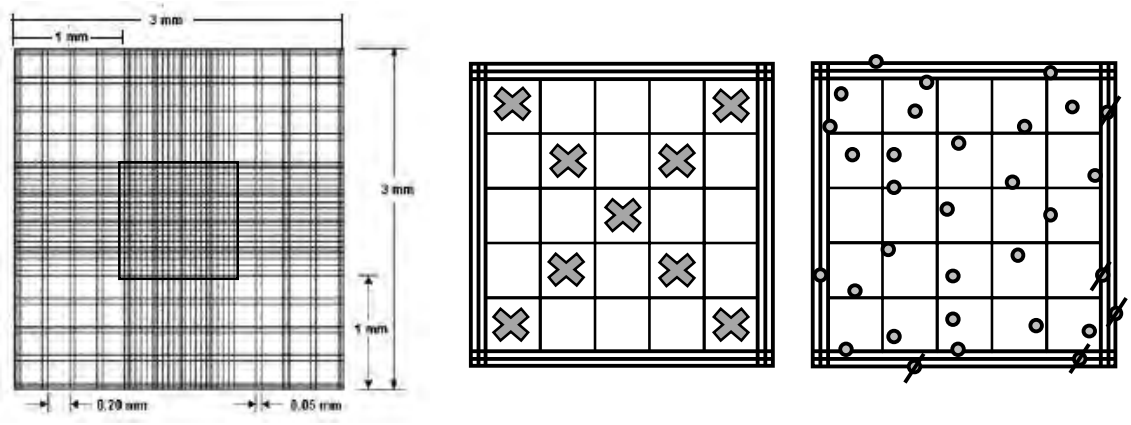

Figure 2.2: Representation of the haemocytometer chamber used for cell counting. Dimensions of a standard haemocytometer chamber are shown in the left image. Centre and right figures show a schematic representation used for cell counting. Barred circles represent cells excluded from the counting process (adapted from ProSciTech SV520-N product information sheet).

Number of neutrophils within cell suspension was calculated using the equation:

$$\frac{Count \times 25 \times 10000}{9} = Number\ of\ neutrophils\ in\ each\ ml\ of\ cell\ suspension$$

Where 25 refers to the number of small squares, 10,000 is the correction factor to convert $0.1mm^3$ into $1cm^3$ (equal in volume to 1ml) and 9 is the number of small squares used.

Following counting, the suspension was diluted with the appropriate amount of buffer to give a final concentration of $1x10^6$ neutrophils per ml of suspension.

2.1.7 Neutrophil viability assessment

Neutrophil viability was assessed using the Trypan Blue exclusion assay or, alternatively, compound-induced cytotoxicity was determined by measurement of lactate dehydrogenase (LDH) cell release where specified and as described below.

2.1.7.1 Trypan Blue exclusion

Neutrophil suspensions were routinely analysed for cell viability by light microscopy (Leitz Laborlux S) under 20X magnification. Ten-µl of cell suspension was combined with 10µl of Trypan Blue dye (Sigma T8154) and 10µl of the solution was loaded into a haemocytometer (Neubauer, Reichert) chamber. Viability was determined using the Trypan Blue exclusion assay which identifies the fraction of cells with an intact outer membrane not permeable to the blue dye as being viable. Cells stained blue were considered dead or dying due to outer membrane damage. Viable cells were counted as described in 2.1.6 and multiplied two fold in order to account for the dilution factor.

2.1.7.2 Lactate dehydrogenase (LDH) leakage assay

LDH is a cytosolic enzyme which catalyses the conversion of lactate to pyruvic acid and *vice versa*. Upon damages of the plasma membrane its enzymatic activity can be measured in the extracellular medium and is therefore used as a sensitive and precise indication of cytotoxicity (Korzeniewski & Callewaert, 1983). Compound-mediated cytotoxicity assays were performed using the Pierce LDH Cytotoxicity Assay Kit (Thermo Scientific 88953). A couple of enzymatic reactions are involved in the assay. Initially, the enzyme LDH catalyses the conversion of lactate to pyruvate and concomitantly the reduction of NAD^+ in NADH. Subsequently, the Diaphorase enzyme utilises the NADH to catalyse the conversion of a tetrazolium salt into a formazan product which can be measured by absorbance at 490nm (as

described in the manufacturer's instructions of Pierce LDH Cytotoxicity Assay Kit). All reagent preparations and storage instructions were provided by the manufacturer. The Reaction Mixture was prepared by combining 0.6ml of Assay Buffer with 11.4ml of Substrate Mix dissolved in ultrapure water. Besides compound-induced LDH, spontaneous LDH activity was determined by incubating neutrophils with 10µl sterile ultrapure water, while the maximum LDH activity was achieved by incubation with 10µl Lysis Buffer (provided in the Pierce LDH Cytotoxicity Assay Kit). The LDH Positive Control solution was used in triplicate in the 96-well plate in order to verify the assay effectiveness. Upon incubation, 50µl of the supernatant was transferred into a new clear 96-well plate and were gently mixed with 50µl of Reaction Mixture. After 30 minutes incubation at room temperature and protected from light, 50µl Stop Reaction were added to each well and gently mixed. Absorbance was measured at 490nm and 680nm using a microplate reader (BioTek ELx800). The absorbance measured at 680nm was subtracted by the readings at 490nm in order to correct values for the background. The percentage of compound-induced cytotoxicity was calculated using the formula:

$$\frac{(Compound-treated\ LDH\ activity) - (Spontaneous\ LDH\ activity)}{(Maximum\ LDH\ activity) - (Spontaneous\ LDH\ activity)} \times 100$$

2.1.8 Neutrophil purity determination by flow cytometry

Neutrophil purity was assessed in samples by Flow Cytometry targeting the cell marker cluster of differentiation 66b (CD66b) expressed on the human neutrophil surface (Schmidt *et al.*, 2012). Flow cytometry experiments were performed at the laboratories of the School of Life & Health Sciences at Aston University, unless differently specified. Once isolated as described above, cells were diluted to $1x10^6$ cells per ml of suspension, 100µl of sample were combined with 5µl anti-human CD66b with a phycoerythrin tag antibody (clone G10F5, eBioscience 12-

0666-41) for positive identification or with 1µl mouse IgG1 K isotype with a phycoerythrin tag immunoglobulin (clone P3.6.2.8.1, eBioscience 12-4714-42) for the negative control. For comparison, 50µl of whole blood were treated with 450µl OptiLyse C (Beckman Coulter) for 2 hours for erythrocyte lysis, then 100µl of this was analysed as a control. Samples were incubated on ice for 30 minutes with the antibodies and transferred to flow cytometry tubes (Sarstedt 55476005) for analysis on a Cytomics FC 500 flow cytometer (Beckman Coulter, CXP software, FL3 wavelength). Upon Percoll gradient isolation, neutrophil isolations were shown to contain greater than 95% neutrophils (Figure 2.3).

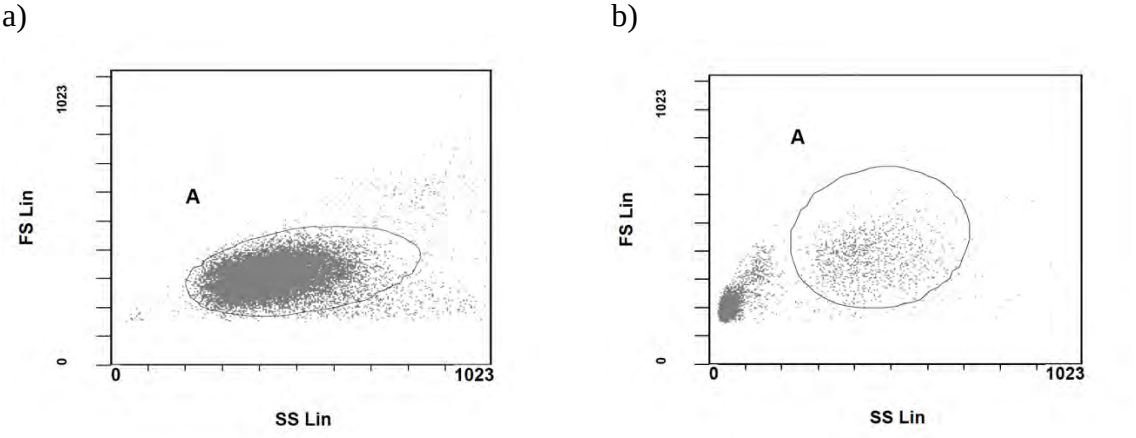

Figure 2.3: Representative scatter plots of neutrophil population.
Flow Cytometry scatter plots of CD66b positive events in a) isolated neutrophil samples and b) whole blood. The population of neutrophils in the gated area represents 97% in a) and 24% of the total cells in b), respectively.

2.2 Derivation of murine bone marrow neutrophils

Long bones obtained from C57 black 6 wild-type and PAD4 knockout (PADi4$^{-/-}$) mice were kindly donated by the Infection and Immunity Research Group at the University of Glasgow, UK. Murine bone marrow was extracted by flushing RPMI-1640 throughout tibias and femurs of wild-type and knockout mice and filtered through a 70µm mesh cell strainer (Fisher Scientific 22363548) to eliminate debris and cell aggregates. Neutrophil purification was

performed using the MACS® Cell Isolation kit for murine application (Miltenyi Biotec 130-097-658). Cell suspensions were treated as per manufacturer instructions. The bone marrow suspension was centrifuged at 300 rcf for 10 minutes at 20°C, the supernatant was carefully removed and the cell pellet was re-suspended in 200µl (per $5x10^7$ total cells) of MACS buffer (solution 1:20 of MACS BSA Stock Solution [130-091-376] with autoMACS® Rinsing Solution [130-091-222]), following addition of 50µl (per $5x10^7$ total cells) of biotin-conjugated monoclonal antibody cocktail against non-neutrophil antigens. After 10 minutes incubation at 4°C cells were washed with 10ml (per $5x10^7$ total cells) of MACS buffer and centrifuged at 300 rcf for 10 minutes at 20°C. The supernatant was carefully removed and the pellet was re-suspended in 400µl (per $5x10^7$ total cells) of MACS buffer. Cells were incubated with 100µl (per $5x10^7$ total cells) of anti-biotin MicroBeads for 15 minutes at 4°C and then washed with 10ml (per $5x10^7$ total cells) of MACS buffer. The solution was centrifuged as before and up to $1x10^8$ cells were re-suspended with 500µl of MACS buffer. Magnetic separation was performed with a MidiMACS™ Separator (Miltenyi Biotec 130-042-302). The LS column (Miltenyi Biotec 130-041-306) was rinsed with 3ml of MACS buffer before use, subsequently, the cell suspension was loaded into the column and topped with 9ml of MACS buffer. The flushed unlabeled neutrophils were collected in a fresh 15ml conical tube (Fisher Scientific 14-959-53A). The cell count was determined as in section 2.1.6 and bone marrow neutrophils were re-suspended in RPMI (Roswell Park Memorial Institute)-1640 (Sigma R7509) at the desired concentration. Sample purity and neutrophil viability were assessed by flow cytometry as described in section 2.1.8 upon staining for Ly6G (GR-1) (eBioscience 12-5931-81), CD11b (eBioscience 17-0112-81) and Fixable Viability Dye eFluor® 450 (eBioscience 65-0863-14). Flow cytometry demonstrated more than 97% of cells were CD11b and Ly6G (GR-1) positive (Figure 2.4).

a) b)

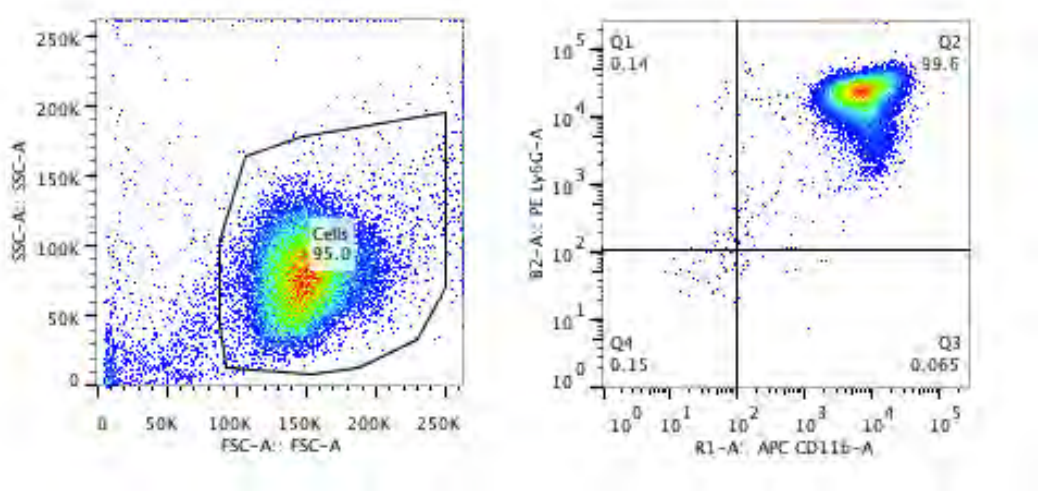

Figure 2.4: Representative scatter plots of murine neutrophils.
Flow cytometry scatter plot of murine bone marrow neutrophils indicating the population of neutrophils in the gated area represent a) the 95% of isolated cells and b) >99% of the population is comprised of viable cells.

2.3 Culture of Oral Epithelial Cells

Experiments were performed with cultured human oral epithelial cells (OECs). The OEC line was a kind donation of Prof S. Prime at Bristol University, UK. The immortal cell line was derived from oral squamous cells isolated from a carcinoma of the alveolar process at stage 2 from a 55 year old female patient. Cultured cell biological behaviour and similarity to oral epithelial cells were previously determined and published by (Prime *et al.*, 1990). H400 cells have previously been identified as a suitable model for *in vitro* studies in OEC inflammatory processes (Milward *et al.*, 2007; Milward *et al.*, 2013).

2.3.1 Culture media and reagents

Media and reagents for H400 cell culture were maintained in sterile conditions and pre-warmed at 37°C in a water bath prior to use. Aliquots were regularly tested for infections at 37°C and 5% CO_2 for 24h and observed for changes in turbidity.

2.3.1.1 Storage medium

For long term storage at -80°C, cells were suspended in Dulbecco's modified Eagle's medium and Ham's F-12 (DMEM/F-12) 1:1 solution (Invitrogen 21331-020) supplemented with 20% foetal calf serum (Labtech FB-1001T/500) and 10% dimethyl sulfoxide (DMSO) (Sigma D8418).

2.3.1.2 Growth medium

For H400 culture, DMEM/F-12 was supplemented with 2% L-glutamine (Sigma G7513), 0.005% hydrocortisone (Sigma H0888) and 10% foetal calf serum (Labtech FB-1001T/500) prior to use. Supplemented media were stored at 4°C until use.

2.3.1.3 Trypsin-Ethylenediaminetetraacetic Acid (T-EDTA) solution

In order to disaggregate the H400 cell monolayer and therefore release cells into suspensions, cell cultures required treatment with a solution of 0.0025% trypsin and 0.01% Ethylenediaminetetraacetic Acid (EDTA) in Hank's balanced salt buffer (Invitrogen R-001-100). Aliquots of this solution were stored at -20°C until needed.

2.3.2 H400 cell storage and recovery

H400 cells were preserved in 1ml storage medium (section 2.3.1.1) and archived in liquid nitrogen until needed. For recovery, cells were defrosted in a water bath at 37°C and diluted in 9ml growth medium (section 2.3.1.2). Following 10 minutes centrifugation at 150 rcf, the cell pellet was re-suspended in 10ml growth medium (section 2.3.1.2), seeded in 75cm^2 cell culture flask (Thermo Scientific 174952) and incubated at 37°C 5% CO_2 for 3-4 days (Galaxy S CO_2 Incubator, New Brunswick). Cell growth was monitored by microscopy (Light microscope, Leitz Laborlux s) and 10ml media was replaced every 2-3 days of incubation. Once the

monolayer reached approximately 90-100% confluence, cells were passaged as described below.

2.3.3 H400 cell passage and culture

To maintain H400 cultures, cells were re-seeded in new culture flasks with fresh media once the monolayer reached 90-100% confluence. The exhausted growth media was removed and cell cultures were washed with 10ml Dulbecco's PBS (Invitrogen 14190). Adherent cells were then treated with 4ml T-EDTA (section 2.3.1.3) at 37°C, 5% CO_2 until the dissolution of the monolayer was microscopically confirmed. The cell suspension was then diluted with 6ml growth medium (section 2.3.1.2) and cells were collected and pelleted by centrifugation for 10 minutes at 150 rcf. Cells were re-suspended in fresh growth medium (section 2.3.1.2) and the concentration (cells per ml of solution) was determined by counting cells within 4x1cm^2 quadrants of a haemocytometer (described in section 2.1.6). Cells were suspended in fresh growth medium (section 2.3.1.2) and seeded at 5x10^5 cells/10ml per 75cm^2 culture flask, 1x10^5 cells/1ml per well of a 24-well plate or 1x10^3 cells/100µl per well of a 96-well plate. For immunocytochemistry analysis H400 cells were cultured on heat-sterilised (100°C overnight) multi-well glass slides (Hendley-Essex PH005). Glass slides were placed in petri dishes (Appleton Woods AB260) and seeded with 4x10^5 cells in 14ml growth medium (section 2.3.1.2).

2.4 Neutrophil stimulation

The following section describes all types of stimuli employed for *in vitro* induction of ROS and NETs. Stimuli were categorised as physiological or non-physiological for their different interactions with neutrophils and the different intracellular pathways involved in cellular

activation as described in section 2.3. Neutrophil stimulation can also be chemically modulated by blocking the activation cascade or priming cells with cytokines for increased responsivity.

2.4.1 Physiological stimuli

Bacteria and related stimuli were considered physiological due to their *in vivo* relevance and association with inflammation. Bacterial stimulation usually occurs via surface receptor recognition as described in section 2.3.1 and are known to trigger a variety of neutrophil responses including ROS and NET production (Hayashi *et al.*, 2003; White, 2015).

2.4.1.1 Bacteria

F. nucleatum and *P. gingivalis* are two Gram negative anaerobic bacteria known to have pathogenic activity and to trigger inflammatory responses in immune-cells. They are both strongly associated with periodontitis pathogenesis (Socransky *et al.*, 1998) and interact with neutrophils via TLR-2 and -4 binding (Darveau *et al.*, 1997; Kikkert *et al.*, 2007).

2.4.1.1.1 Bacterial growth

F. nucleatum sp. Nucleatum (ATCC number 25586) was grown anaerobically on blood agar plates (Oxoid PB0114) followed by planktonic growth in Brain hearth infusion broth (Oxoid CM1135) prepared as per manufacturer's instructions. *P. gingivalis* (Strain W83) was grown anaerobically on neomycin supplemented blood agar plates (Oxoid PB0112) followed by planktonic growth in Fastidious anaerobe broth (Lab M LAB071) prepared as per manufacturer's instructions.

3.1.1.1.1 Strain validation by Gram staining

Bacterial species were identified by colony observation and Gram staining. Following appropriate staining procedures Gram positive bacteria appear blue or purple while Gram negative exhibit a red or pink coloration. A single representative colony was emulsified with

saline solution on a glass slide and heat fixed over a Bunsen burner. The bacterial sample was covered with few drops of Crystal violet (solution 1:1 of crystal violet [Sigma C0775] diluted in ethanol and 1% ammonium oxalate [Sigma A8545] water) for 30 seconds and rinsed with distilled water. Lugol's iodine (Sigma L6146) was, then, applied for 30 seconds followed by rinsing with distilled water and application of carbon fuchsin (BDH 351874U diluted 1:10 with water) for further 30 seconds. After rinsing and drying, colonies on glass slides were observed with a light microscope (Leitz Dialux 22) using an oil immersion objective X100 lens and images were captured with a digital camera (Nikon Coolpix 1990). Gram stained bacterial suspensions showed Gram negative rods consistent with the colonial morphology and suggestive of *P. gingivalis* and *F. nucleatum*.

2.4.1.1.2 Bacterial stock preparation

Planktonic bacterial growth was estimated by optical density measurements (Spectrophotometer Jenway 6300) at 600nm wavelength (OD_{600}) and sterile broth was used to correct values for media changes in absorbance. Values (*F. nucleatum* $1OD_{600}=1.62x10^9$; *P. gingivalis* $1OD_{600}=1.69x10^9$) used for calculating bacterial growth were pre-determined by the Forsyth Institute, Boston and are published in Roberts *et al.* (2002). Bacterial suspensions were centrifuged (Harrier 18/80) three times for 15 minutes at 1800 rcf and 4°C, followed by resuspension in sterile PBS. Bacterial concentrations were determined as before and solutions were diluted to obtain a final stock suspension of $4x10^9$ cells/ml. Bacteria were heat-killed by incubation in a Hot Air Oven (LTE OP30) at 80°C for 1 hour prior to solutions being aliquoted and stored at -20°C prior to use. To confirm bacterial death 1ml heat-killed stock solutions were plated on blood agar plates and incubated anaerobically for several days.

2.4.1.2 Multispecies biofilms

Three-, 7- and 10-species biofilms were developed on Termanox™ coverslips (13mm diameter; Fisher 174950) as described in Millhouse *et al*. (2014), and kindly donated by the Infection and Immunity Research Group at the University of Glasgow, UK. Fully mature biofilms, had compositions as described in Table 2.2, and were deprived of media and stored at -80°C until use. For biofilm regeneration, coverslips were placed in 24-well plate (Costar 3526) and incubated overnight in sterile artificial saliva (composition for 1l: 2.5g porcine stomach mucins, 3.5g NaCl, 0.2g KCl, 0.2g $CaCl_2 \bullet 2H_2O$, 2g yeast extract, 1g lab lemco powder, 5g proteose peptone, 1.25ml urea) in anaerobic conditions. After 24 hours incubation, the supernatant was carefully removed, aliquoted and stored at -20°C until use. Twenty-five-µl of each type of biofilm supernatant was used in 200µl microwells for ROS and NET experiments.

Biofilm type	Model/Disease status	Bacterial Species Composition
3-species	Health	*Streptococcus mitis* *Streptococcus intermedius* *Streptococcus oralis*
7-species	Gingivitis	*Streptococcus mitis* *Streptococcus intermedius* *Streptococcus oralis* *Veillonella dispar* *Actinomyces naeslundii* *Fusobacterium nucleatum* *Fusobacterium nucleatum spp. Vincentii*
10-species	Periodontitis	*Streptococcus mitis* *Streptococcus intermedius* *Streptococcus oralis* *Veillonella dispar* *Actinomyces naeslundii* *Fusobacterium nucleatum* *Fusobacterium nucleatum spp. Vincentii* *Aggregatibacter actinomycetemcomitans* *Porphyromonas gingivalis* *Prevotella intermedia*

Table 2.2: Multispecies biofilm composition and association with disease status.

2.4.1.3 Oral epithelial cell co-culture with multispecies biofilms

OECs were cultured as described in section 2.3 in 24-well plates. After 24 hours incubation at 37°C 5% CO_2, H400 cells reached 70-80% confluency, as assessed visually by optical microscopy (Leitz Laborlux s), subsequently growth media was removed and replaced with sterile pre-warmed media. Three-, 7- and 10-species biofilms on coverslips (section 2.4.1.2), after 24 hours incubation in artificial saliva, were removed from the plate, inverted and mounted with Vaseline® to hanging cell culture inserts for 24-well plates (Greiner Bio-one ThinCert™ 662630). Inserts with attached biofilms were placed in H400 cell cultures in 24-well plates leaving a space between the biofilm and cell culture layer of ~0.5mm (Figure 2.5) and placed in a humidified incubator (Galaxy S, New Brunswick). After 24 hours incubation, biofilms were carefully removed, culture media was collected, aliquoted and stored at -20°C until use.

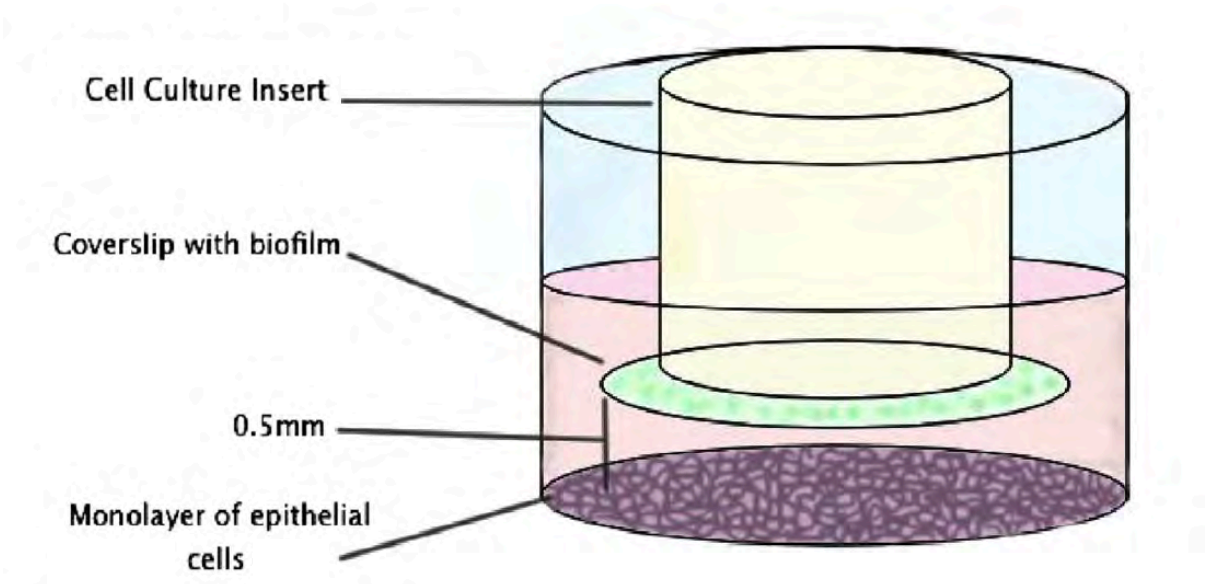

Figure 2.5: Schematic representation of H400 cell co-culture with biofilms.
Multispecies biofilms grown on coverslip were mounted on a cell culture insert and placed in incubation with H400 cells (Millhouse *et al.*, 2014).

2.4.1.4 Lipopolysaccharide

One-mg/ml *Escherichia coli* O26:B6 LPS solution (Sigma L8274) was diluted in desired buffer or media supplemented with 10% and 20% sterile human plasma (Sigma H4522) or 10% BSA (Sigma A4503) to generate solutions of 8μg/ml and 20μg/ml. LPS solutions were aspirated with siliconised tips, aliquoted in siliconised centrifuge tubes and stored at -20°C until used.

2.4.2 Non-physiological stimuli

Those stimuli which activate neutrophils by bypassing the interaction with surface receptors and are not bacterial components were classified as being non-physiological. PMA is a well characterised neutrophil activator and mimics the role of the physiological mediator DAG in activating the PKC pathway (Fuchs *et al.*, 2007), and HOCl, is a downstream product of the ROS cascade and has been established to induce rapid formation of NETs (L. J. Palmer, Cooper, *et al.*, 2012).

2.4.2.1 Phorbol 12-myristate, 13-acetate

One-mg PMA powder (Sigma P8139) was dissolved in DMSO to prepare a stock solution of 1.62mM equivalent to 1mg/ml. Further dilutions were prepared with PBS to obtain a range of concentrations of between 5.6nM and 400nM working solutions. PMA solutions were aliquoted, stored at -20°C and protected from light by wrapping in aluminium foil.

2.4.2.2 Hypochlorous acid

HOCl was obtained by diluting sodium hypochlorite solution (Sigma 425044) with PBS. Hypochlorite ions in solution were previously estimated by Palmer *et al.* (2012a) by measuring the OD at 290nm of pH 12 solutions with an extinction coefficient of 350M/cm. Solutions used in neutrophil experiments had an equivalent pH and acid dissociation constant (pKa) of 7.5, therefore assuming that hypochlorite ions in solutions exist as HOCl and as OCl^- in a 1:1 ratio.

HOCl solutions were diluted to a 0.75mM final concentration (which is physiologically relevant) for neutrophil experiments and prepared fresh when required.

2.4.3 Modulators of neutrophil response

GM-CSF has been previously used in neutrophil assays to prime the cells before LPS exposure and, therefore, increase their stimulation (Matthews *et al.*, 2007a). Celastrol is a triterpenoid compound extracted from the Chinese Thunder of God Vine (*Tripterygium wilfordii*) and has been used for the treatment of inflammatory disorders due to its antioxidant properties. Celastrol acts as inhibitor of the inflammatory response and has multiple targets, such as nuclear factor-κB (NF-κB), the molecular-target-of-Rapamycin (mTOR) pathway and the MAPK cascade (Kannaiyan *et al.*, 2011). The compound has also been shown to block NET formation upon neutrophil stimulation and was used in experiments as a control for neutrophil inhibition (Yu *et al.*, 2015).

2.4.3.1 Granulocyte-macrophage colony stimulating factor

A total of 20 μg of GM-CSF powder (Sigma SRP3050) were dissolved in sterile water to obtain an initial 100μg/ml solution and further diluted in PBS 0.1% BSA (Sigma A4503) to prepare 1.25ng/ml working solutions. Once aliquoted, GM-CSF solution was stored at -20°C until used.

2.4.3.2 Celastrol

Celastrol 5mg powder (Cayman 70950) was dissolved in DMSO to obtain a 1mg/ml stock solution (2.219mM), aliquoted and stored at -20°C protected from light. Working solutions were prepared immediately before use by diluting the 2.219mM stock with PBS to a 74μM solution and used at 10μM final concentration.

2.5 H400 stimulation

H400 cells were cultured in black, clear bottom 96-well plates (Greiner Bio-one 655096) or on multi-well glass slides (section 2.3.3) for 2 to 4 days until the monolayer reached 90-100% confluence. NF-κB translocation from the cytoplasm to the nucleus was induced by incubation with 20µl/ml LPS (section 2.4.1.4) for 1 hour at 37°C and 5% CO_2. H400 were pre-treated with 10µM celastrol (section 2.4.3.2) for 30 minutes before LPS stimulation as a negative control and left unstimulated as a media control in order to ensure staining specificity of NF-κB and its LPS-induced nuclear translocation.

2.6 Neutrophil assays

Neutrophil metabolism and activity can be measured using a wide range of assays, including the quantification of ROS produced by the oxidative burst cascade and the analysis of NET release. ROS were quantified using a well characterised chemiluminescence assay, a technique established within the Periodontal Research Group (Matthews *et al.*, 2007a). NET analysis was performed by fluorometric quantification of extracellular NET-DNA, qualitative observation by fluorescence microscopy (Palmer *et al.*, 2012a), and high-throughput investigation by HCA. All experiments were performed in triplicate and repeated using neutrophils from 3 different healthy donors.

2.6.1 Pre-treatment of cultureware with blocking buffer

To prevent cell adhesion or non-specific activation, cultureware used for neutrophil incubation were pre-treated with PBS 1% BSA or “blocking buffer”. The solution was made by dissolving 10g BSA (Sigma A4503) in 1l standard PBS, filter sterilised (pore size 0.22µm) and stored at -20°C in 20ml aliquots. Each well was filled with 200µl blocking buffer and incubated overnight

at 4°C. Subsequently plates were washed 5 times with standard PBS before being used in neutrophil assays.

2.6.2 Pre-treatment of cultureware with poly-L-lysine

To facilitate cell adhesion on cultureware, multiwell plates were pre-treated with an adhesive agent. A thin layer of 0.1% of poly-L-lysine in water (Sigma P8920) was aliquoted to cover the bottom surface of each well. After 10 minutes incubation at room temperature, wells were decanted using a vacuum pump and washed with PBS to remove excess adhesive agent.

2.6.3 Chemiluminescent quantification of ROS

For the quantification of intra- and extra-cellular ROS, neutrophils were exposed to the chemiluminescent substrate luminol, a substrate able to cross the cell membrane and to detect the presence of ROS. Luminol reacts with ROS generated by MPO catalytic activity and the interaction changes the oxidative status of luminol molecules which emit a light signal once excited (Lundqvist *et al.*, 1995). Light output is monitored by a microplate luminometer and translated in relative light units (RLU) which are used as a measure of ROS generation (Bergström & Asman, 1993; Matthews *et al.*, 2007a).

2.6.3.1 Glucose-supplemented PBS

Standard PBS buffer was supplemented with glucose for optimal superoxide production in neutrophils (Tan *et al.*, 1998). Glucose-PBS (gPBS) was prepared by mixing 1.8g glucose (Sigma G8270), 0.15g $CaCl_2$ (BDH 10070) and 1.5ml $MgCl_2$ (BDH 22093) in 1l sterile PBS (section 2.1.4). The solution was filter-sterilised (pore size 0.22μm), aliquoted and stored at -20°C until used.

2.6.3.2 Luminol

A 30mM stock solution was prepared by dissolving 0.5g luminol (Sigma A8511) in 94.05ml of 1mM NaOH and stored at 4°C for 6 months protected from light. To prepare the working solution, 1ml of stock solution was diluted with 9ml PBS and the pH was adjusted when necessary to 7.3 with the addition of HCl or NaOH.

2.6.3.3 ROS assay

Neutrophils were diluted in gPBS (section 2.6.3.1) and seeded at $1x10^5$ cells/well in white 96-well plates (Costar 3912), pre-treated overnight with blocking buffer (section 2.6.1) unless otherwise specified. To analyse the production of total ROS, cells were incubated with 30µl luminol (section 2.6.3.2) in the luminometer (Berthold Tristar^2 LB942) for an initial 30 minutes to obtain a baseline reading, prior to addiction of modulators to selected wells and obtaining readings for a further 30 minutes. Subsequently, neutrophils were incubated with 25µl of selected stimuli in the luminometer for the required incubation time. All readings were obtained at 37°C, recorded by MikroWin2000 software (Mikrotek version 4) and expressed in RLU. The maximum production of ROS, or peak ROS, was identified using Excel software (Microsoft, US) as the highest RLU value registered within the stimulation time.

2.6.4 Induction of NETosis

Neutrophils were diluted in RPMI-1640 and seeded as indicated in Table 2.3 in multi-well plates pre-treated overnight with blocking buffer (section 2.6.1), unless otherwise specified. After an initial 30 minutes incubation period at 37°C and 5% CO_2, modulators were added to selected wells followed by further incubation for 30 minutes. Subsequently, 25µl stimuli were added to each well and neutrophils were incubated for the appropriate stimulation time.

NET assay	Multi-well plate formats	Cell seeding (cells/well)
Fluorometric Quantification	Clear 96-well plate (Costar 3370)	$1x10^5$
Visualisation	Clear 24-well plate (Costar 3524)	$1x10^5$
	Clear 48-well plate (Costar 3548)	$1x10^5$
	Clear 96-well plate (Costar 3370)	$1x10^5$
High-Content Analysis	Black, clear bottom 96-well plate (Greiner Bio-one 655096)	$1x10^5$
	Black, clear bottom 384-well plate (Greiner Bio-one 781096)	$5x10^3$

Table 2.3: Neutrophil seeding details for assays and plate format.

2.6.5 Fluorometric quantification of NETs

During the NETosis process, NET filaments are released in the extracellular space as a result of pro-inflammatory stimulation. NET filaments are predominantly made of DNA that can be easily isolated from intact cells and quantified following appropriate staining. A quantitative method for the analysis of NETs was developed in the School of Dentistry Laboratories (Palmer *et al.*, 2012a). For reliable quantification, samples were initially treated with micrococcal nuclease to detach NET structures from cells and, subsequently a fluorescent DNA dye, Sytox green®, was added to the supernatant. Cell free NET-DNA was quantified using a multiplate fluorescence reader (Berthold Twinkle^2 LB970) and data recorded as arbitrary fluorescence units (AFU).

2.6.5.1 Micrococcal nuclease

A stock solution of 2136.3U/ml was prepared by dissolving micrococcal nuclease powder ([MNase]; Worthington 4789) in 10ml sterile water. The 311.3µl stock solution was diluted in

50ml sterile PBS to obtain a working solution of 13.3U/ml. This solution was divided into 1ml aliquots and stored at -20°C until used.

2.6.5.2 Sytox green®

Syotx green® stock solution was supplied by Invitrogen (S7020) and 10µl was diluted in 5 ml RPMI-1640 to generate a working solution of 10µM. The working solution was foil-covered and stored at -20°C.

2.6.5.3 Method for NET quantification

Neutrophils were isolated as described in sections 2.1.5 and NETs were induced as per section 2.6.4. Post-incubation, samples were treated with 15µl of MNase (section 2.6.5.1) for 15 minutes at room temperature. Afterwards, plates were centrifuged for 10 minutes at 1800rcf (Hettich Universal 320R) and 150µl of supernatant was carefully transferred from each well to a black 96-well plate (Costar 3915). The supernatant was stained with 15µl of Sytox green® (section 2.6.5.2) and the fluorescence emission was read 5 times using a multiplate fluorometer (Berthold Twinkle^2 LB970) with an excitation wavelength of 485nm and emission wavelength 525nm. All readings were obtained at 37°C, recorded using MikroWin2000 software and expressed in AFU.

2.6.6 NET visualisation

Neutrophils were isolated as described in sections 2.1.5 and NETs were induced as for section 2.6.4. Since DNA is the major component of NETs their structures can be visualised following DNA staining. NET visualisation was, therefore, performed following fluorescence staining of DNA and using a fluorescence microscope (CoolLed pE excitation system).

2.6.6.1 Paraformaldehyde solution

Paraformaldehyde (PFA) powder was supplied by Sigma (P6148) and stored at 4°C until use. A 20% PFA stock solution was prepared by dissolving 4g powder in 20ml PBS with gentle agitation and heating to 60°C. After cooling at room temperature for several minutes the solution was filter sterilised and stored at 4°C until used. The 20% PFA solution was further diluted with PBS to obtain a working solution of 4%.

2.6.6.2 PFA fixation

The 20% PFA solution was added to neutrophil culture medium to give a final concentration of 4% and samples were incubated at room temperature for 10 minutes. Unless otherwise specified, plates were then centrifuged for 10 minutes at 1800rcf (Hettich Universal 320R), media was carefully removed from each well and samples were washed twice with PBS.

2.6.6.3 Visualisation using epifluorescence microscopy

Post-incubation samples were fixed with PFA (section 2.6.6.2) when specified. Sytox green® (section 2.6.5.2) was added and neutrophils were visualised using an epifluorescence microscope (Nikon Eclipse TE300) with excitation wavelength of 472nm and emission wavelength 520nm (CoolLed pE excitation system). Images were captured with a Nikon D5100 camera and adjusted for brightness and colour using Fiji software (Image J version 2; Schindelin *et al.*, 2012).

2.7 Immunocytochemical analysis of NF-κB translocation in H400 cells

Immunocytochemistry (ICC) is a histological technique based on antibody-recognition of specific intracellular or extracellular antigens of interest, the visualization is then achieved using a secondary labelling system which comprises enzymatic colorimetric reaction or fluorophore conjugation (Ordronneau *et al.*, 1981).

The translocation of NF-κB from the cytoplasm to nuclei in H400 cells was qualitatively assessed using an indirect biotin-streptavidin amplification system (Milward *et al.*, 2013). The intracellular NF-κB bound to primary antibody is targeted by a secondary antibody conjugated with biotin which has strong affinity for the labelling streptavidin, which is in turn conjugated with peroxidase. NF-κB location sites assume a brown colouration due to a change in the oxidative state of diaminobenzidene (DAB) activated by the peroxidase.

2.7.1 Staining technique

H400 cells were cultured and stimulated on multi-well glass slides as described in sections 2.3.3 and 2.5. Upon stimulation the glass slides were washed 3 times in PBS followed by fixation in dry acetone for 15 minutes. Samples were then air dried for a further 15 minutes. All the following staining procedures were performed with the Super Sensitive™ Link-Label IHC Detection System kit (BioGenex QD470-60K) and incubation were performed in a dark humidifier box set at room temperature. Each well of the glass slide was covered with 100µl solution of the anti-NF-κB primary antibody (described in section 2.8.2.2) 1:100 solution in PBS 1% BSA (as prepare in section 2.6.1) and washed 3 times in PBS after 1 hour incubation. Subsequently each well was covered with Link, a pre-diluted biotinylated anti-mouse IgG secondary antibody solution in PBS, and incubated for 20 minutes. Slides were washed 3 times in PBS and the Label component (horseradish peroxidase-conjugated streptavidin solution in PBS) was applied for further 20 minutes. After washing 3 times with PBS, slides were overlaid with DAB reagent previously prepared by diluting 38µl of 3,3'-DAB chromogen solution in 1 vial of Substrate Buffer. After 5 minutes incubation slides were washed under running water and Mayer's Haematoxylin (BioGenex HK100-5K) was applied for a further 5 minutes. Slides were rinsed with deionised water and dehydrated in graded alcohols passages (90%, 100%,

100%), cleared in xylene and mounted in XAM neutral medium (BDH Laboratory supplies 36119).

2.7.2 Image acquisition, processing and cell count

Images of stained H400 cells were visualised and acquired using a light microscope (Leitz Laborlux s) with 20X lens. Five randomly selected image areas for each experimental condition were analysed for NF-κB staining. An image with no cells was used for background correction and staining enhancement performed with Fiji software equipped with the "calculator plus" plug in (Landini, 2012). The number of cells positive or negative for NF-κB translocation to the nucleus were counted in the 5 images with the Fiji software plug in "Cell counter" (De Vos & Sheetz, 2007). The percentage of positive cells were determined using the formula:

$$\frac{Number\ of\ positive\ cells}{(Number\ of\ positive\ cells) + (Number\ of\ nugative\ cells)} \times 100$$

2.8 High-Content Analysis

The HCA technique utilises automated high-resolution fluorescence imaging to allow rapid qualitative and quantitative measurement of multiple parameters (Shariff *et al.*, 2010). Images are analysed through a bioinformatics software approach which translates biologically-related features in numbers, tables and graphs. The HCA platform has been designed for the analysis of biological samples in micro-well plate formats such as 96-, 384- and 1536-well plates, and for the simultaneous visualisation of multiple fluorescent staining (Mayr & Bojanic, 2009). Therefore, in order to perform HCA, neutrophils and H400 cells were processed for immunofluorescence staining in conjunction with a DNA fluorescent counterstaining application based on previously published protocols (Corfe *et al.*, 2013).

HCA was performed using the platform located at the laboratory of Imagen Therapeutics Ltd (Manchester, UK) as summarised in Figure 2.6 and as described below in more detail.

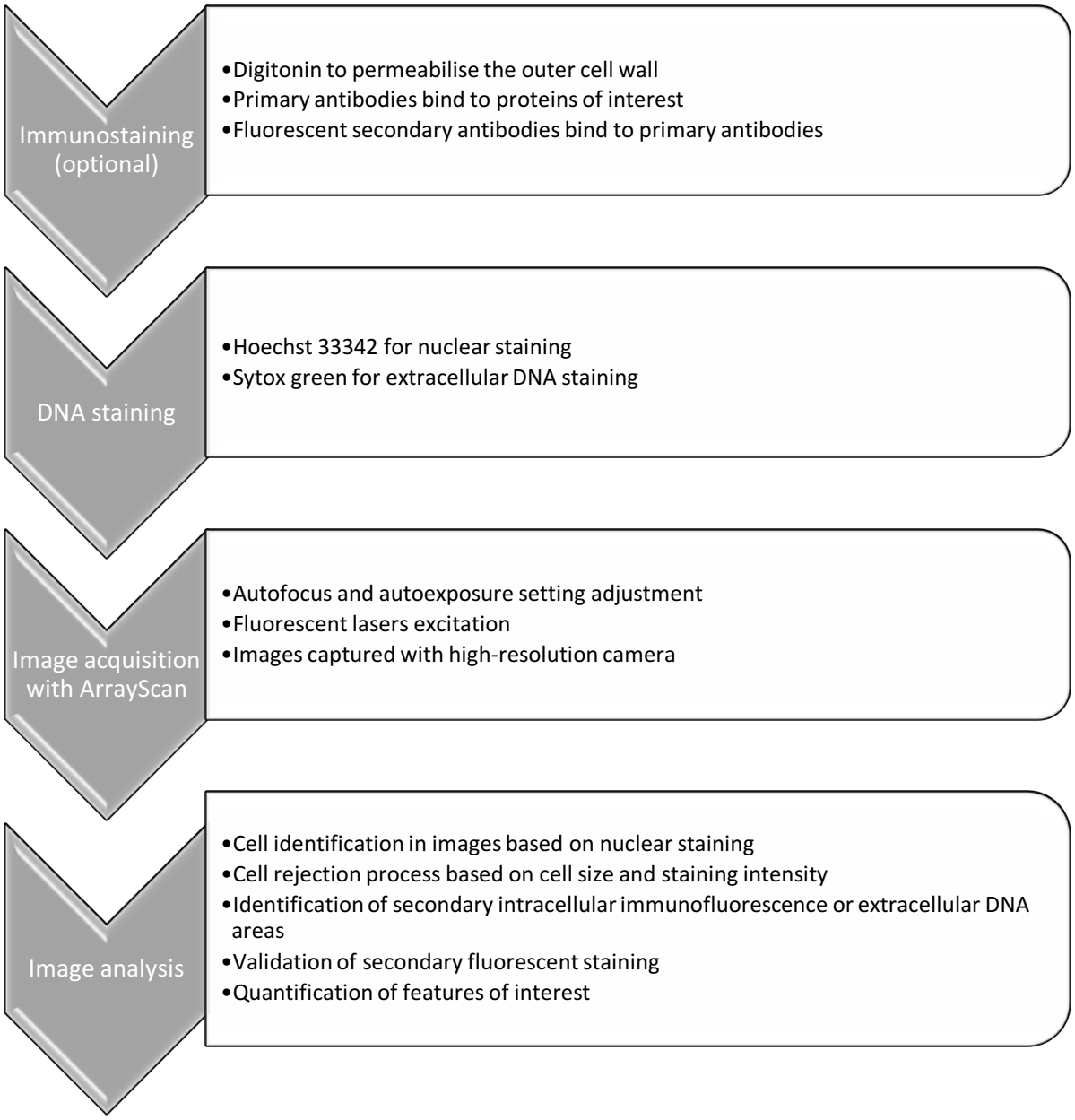

Figure 2.6: Flow diagram of the HCA process for neutrophil analysis.
Steps involved in sample preparation and HCA application are subdivided into 4 main categories and are described within the flow diagram.

2.8.1 Fluorescent DNA staining

To visualise neutrophil nuclei and NET structures, two DNA fluorescent dyes were used for sample staining. Syotx green® was used as the primary DNA-NET stain as reported in section 2.6.5.2, while a working solution 20µg/ml Hoechst 33342 (Sigma 14533) was prepared by diluting 10µl stock solution in 5ml of sterile PBS and used to highlight neutrophil nuclei.

2.8.2 Protein immunofluorescence staining

For the identification and the localisation of protein through the HCA technology, samples were processed to allow targeted antibodies, intracellular binding and their fluorescent identification.

2.8.2.1 0.05% Digitonin

A 500µg/ml solution (0.05%) of Digitonin was prepared by dissolving 15g of powder (Calbiochem, 300410) in 30ml PBS. The solution was heated and boiled in order to dissolve the powder for a maximum of 20 seconds and incubated at room temperature until cooled. The solution was prepared fresh before every application and stored at room temperature for a maximum of 2 hours.

2.8.2.2 Primary antibodies

Primary antibodies were carefully selected for specific protein targeting and stock solutions were stored at 4°C until used. For cell immunostaining, primary antibodies were diluted as indicated in Table 2.4 in 0.05% Digitonin (see section 2.8.2.1). Antibody solutions were prepared immediately before use and made fresh prior to application.

Target	Species	Manufacturer	Dilution
PAD4	Mouse	Abcam (ab128086)	1:150
Citrullinated histone 3	Rabbit	Abcam (ab5103)	1:150
MPO	Mouse	Abcam (ab25989)	1:150
NE	Rabbit	Abcam (ab131260)	1:150
NF-κB	Mouse	Abcam (ab13594)	1:200

Table 2.4: Targets and primary antibodies for immunostaining application.

2.8.2.3 Secondary antibodies

Combination of secondary antibodies were selected from Table 2.5 for simultaneous applications. Selected secondary antibodies were diluted 1:500 in Hoechst 33342 solution (section 2.1.1) immediately before use and prepared fresh prior to application.

Target	Species	Colour	Wavelength (Ex/Em)	Manufacturer
Rabbit IgG	Goat	Alexa Fluor® 594 (red)	590/617nm	ThermoFisher Scientific A-11037
Mouse IgG	Goat	Alexa Fluor® 488 (green)	495/519nm	ThermoFisher Scientific A-11001
Mouse IgG	Goat	Alexa Fluor® 594 (red)	590/617nm	ThermoFisher Scientific A-11005
Rabbit IgG	Goat	Alexa Fluor® 680 (far red)	679/702nm	ThermoFisher Scientific A-21109
Mouse IgG	Goat	Alexa Fluor® 680 (far red)	679/702nm	ThermoFisher Scientific A-21057

Table 2.5: Targets and secondary antibodies for immunostaining application.

2.8.2.4 Method for immunofluorescent staining

Cultures were incubated with 50µl primary antibodies in 0.05% Digitonin (section 2.8.2.2) at room temperature for 1 hour. Following the incubation time, cells were washed twice with PBS and further incubated at room temperature with secondary antibodies diluted in Hoechst 33342 solution (section 2.8.1) for 30 minutes. Subsequently, cells were washed twice with PBS, sealed with adhesive film (Greiner A5596-100EA) and stored in the dark prior to image acquisition.

2.8.3 High-Content Analysis of NETs

Neutrophils were isolated as described in sections 2.1.5 and NETs were induced as described in section 2.6.4 in a black, clear bottom 96-well plate (Greiner Bio-one 655096). Following PFA fixation (section 2.6.6.2), neutrophil samples were sealed with an adhesive film to avoid evaporation and were transported to the laboratory of Imagen Therapeutics Ltd (Manchester, UK) for staining procedures (sections 2.1.1 & 2.8.2) and analysis.

2.8.4 High-Content Analysis of NF-κB translocation in H400 cells

H400 cells were cultured and stimulated in a black, clear-bottomed 96-well plate as described in sections 2.3.3 and 2.5. Following PFA fixation (section 2.6.6.2), plates were washed 3 times with PBS and were sealed with an adhesive film to avoid evaporation during transport to the laboratory of Imagen Therapeutics Ltd. NF-κB immunostaining was performed as described in section 2.8.2 and H400 cell nuclei were stained with 20µg/ml Hoechst 33342 prepared as des cribed in section 2.1.1. HCA was employed to quantify NF-κB nuclear translocation in stimulated H400 cells and compared with unstimulated and celastrol treated cells.

2.8.5 High-throughput screening of NETosis modulation

A 56-compound library (Table 2.6.) pre-established by the team at Imagen Therapeutics Ltd for ovarian cancer treatment were screened for modulatory effects on neutrophils activation and NET release using the HCA technology. The HCS was performed in 384-well plates as is described below.

2.8.5.1 Robotic benchtop workstation

Compound library preparation and neutrophil handling in 384-well plate was performed with Microlab STAR Line robotic benchtop workstation (Hamilton Star) shown in Figure 2.7. The automatic seeding was performed with an air-based advanced pipetting Total Aspiration and Dispensing Monitoring (TADM) system for a real time supervising of any error that could occur during all pipetting steps. The Air-Droplet Control (ADC) system eliminated dripping by compensating the pressure changes in the channels. The system uses the CO-RE Technology to avoid build-up of aerosols due to forceless tip pick-up and ejection. The automatic workstation was programmed and controlled through the VENUS software (Hamilton).

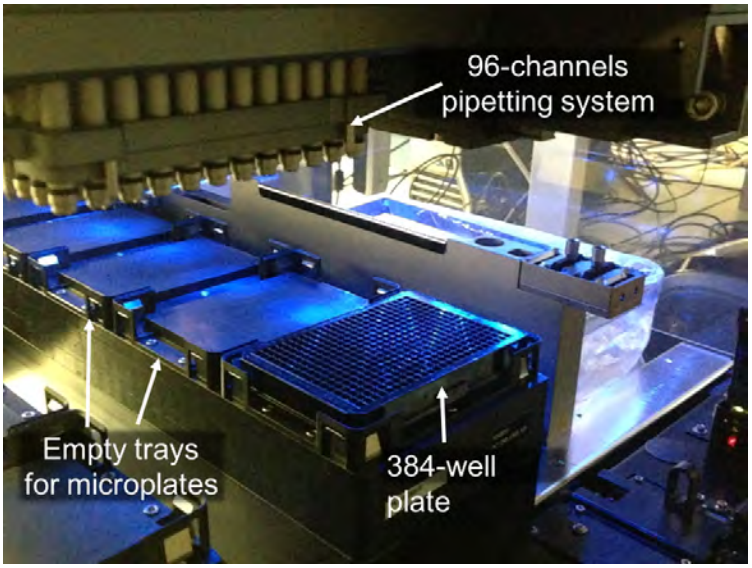

Figure 2.7: Hamilton Star robotic benchtop workstation.
Illustration of the Hamilton Star automatic benchtop operating on biological samples in a 384-well plate.

2.8.5.2 56-compound library preparation

All compounds were diluted in DMSO as per manufacturer instructions. Master plates with compounds 1000 times concentrated were prepared in advance, sealed with adhesive film and stored at -20° until application. Compounds were combined and diluted in PBS to obtain 5 concentrations ranging between 0.025nM and 250000nM. Twenty-µl of each concentration were then added to 30µl of neutrophils to obtain compound concentrations ranging between 0.01nM and 100000nM as recommended by the team of Imagen Therapeutics Ltd and as specified in Table 2.6.

Compound name	Dosage	Manufacturer
Benzethonium Chloride	100nM	Selleckchem S4162
Axitinib	1-10000nM	Selleckchem S1005
BEP (Bleomycin, Etoposide, Cisplatin)*	0.1-1000nM	
Bleomycin Sulfate	1-10000nM	Selleckchem S1214
Bortezomib (PS-341)	0.1-1000nM	Selleckchem S1013
Bosutinib (SKI-606)	1-10000nM	Selleckchem S1014
Cabozantinib (XL184, BMS-907351)	0.1-1000nM	Selleckchem S1119
Capecitabine	1-10000nM	Selleckchem S1156
Carboplatin	1-10000nM	Selleckchem S1215
Carboplatin & Gemcitabine*	0.1-1000nM	
Carboplatin & Taxol*	0.1-1000nM	
Carfilzomib (PR-171)	0.1-1000nM	Selleckchem S2853
Carmustine	1-10000nM	Sigma C0400
Cisplatin	1-10000nM	Selleckchem S1166
Cladribine	1-10000nM	Selleckchem S1199
Clofarabine	1-10000nM	Selleckchem S1218
Crizotinib (PF-02341066)	1-10000nM	Selleckchem S1068
Dabrafenib (GSK2118436)	1-10000nM	Selleckchem S2807
Dacarbazine	1-10000nM	Selleckchem S1221
Dasatinib	1-10000nM	Selleckchem S1021
Docetaxel	0.1-1000nM	Selleckchem S1148
Doxorubicin & Topotecan*	0.1-1000nM	
Doxorubicin (Adriamycin)	1-10000nM	Selleckchem S1208
Epothilone B (EPO906, Patupilone)	1-10000nM	Selleckchem S1364
Erlotinib HCl (OSI-744)	1-10000nM	Selleckchem S1023
Etoposide	1-10000nM	Selleckchem S1225
Everolimus (RAD001)	0.1-1000nM	Selleckchem S1120
Gefinitib (ZD-1839, Iressa)	1-10000nM	Selleckchem S1025
Gemcitabine & Cisplatin	0.1-1000nM	

Gemcitabine	0.1-1000nM	Selleckchem S1714
Imatinib (STI571, Gleevec)	1-10000nM	Selleckchem S2475
Irinotecan	0.1-1000nM	Selleckchem S1198
Lapatinib	1-10000nM	Selleckchem S2111
Lomustine	10-100000nM	Selleckchem S1840
Methotrexate	1-10000nM	Selleckchem S1210
Mitoxantrone	0.1-1000nM	Selleckchem S1889
Nilotinib (AMN-107)	1-10000nM	Selleckchem S1033
Olaparib (AZD2281, KU0059436)	1-10000nM	Selleckchem S1060
Oxaliplatin	1-10000nM	Selleckchem S1224
Paclitaxel (Taxol)	0.1-1000nM	Selleckchem S1150
Pazopanib	1-10000nM	Selleckchem S3012
Ponatinib (AP24534)	1-10000nM	Selleckchem S1490
Rapamycin (Sirolimus)	0.1-1000nM	Selleckchem S1039
Regorafenib (BAY 73-4506)	1-10000nM	Selleckchem S1178
Ruxolitinib (INCB018424)	1-10000nM	Selleckchem S1378
Sorafenib Tosylate	1-10000nM	Selleckchem S1040
Staurosporine	0.01-100nM	Selleckchem S1421
Sunitinib	1-10000nM	Selleckchem S7781
Teniposide	1-10000nM	Selleckchem S1787
Temozolomide (TMZ)	1-10000nM	Selleckchem S1237
Topotecan HCl	1-10000nM	Selleckchem S1231
Trametinib (GSK1120212)	1-10000nM	Selleckchem S2673
Vandetanib (ZD6474)	1-10000nM	Selleckchem S1046
Vemurafenib (PLX4032, RG7204)	1-10000nM	Selleckchem S1267
Vinorelbine Tartrate	1-10000nM	Selleckchem S4269
Vismodegib (GDC-0449)	1-10000nM	Selleckchem S1082
Vorinostat (SAHA, MK0683)	1-10000nM	Selleckchem S1047

Table 2.6: Compound library composition.
*Combination of equal proportions of specified compounds.

2.8.5.3 Application of the compound library for neutrophil analysis

Neutrophils were isolated as described in section 2.1.5 and seeded at 30µl/well in a black, clear bottom 384-well plate. The 56-compound library (described in section 2.8.5.2) was applied to neutrophils followed by 30 minutes incubation at 37°C and 5% CO_2. Subsequently, NETs were induced with PMA as for section 2.6.4, neutrophils were fixed with PFA (section 2.6.6.2) and plates were sealed with an adhesive film to minimise evaporation.

2.8.6 Image acquisition

Plates for HCA and HCS were sequentially loaded onto the Cellomics™ ArrayScan™ reader (ThermoFisher Scientific, VTI) using a computer driven Thermo Catalyst express robotic arm. Samples were visualised with the ArrayScan™ automated Observer Z1 inverted microscope (Zeiss) with transmitted light and fluorescence and high-resolution images of up to 30 fields per well were acquired and captured using a CCD camera (Hamamatsu Orca ER) equipped with 5X/0.25 Fluar, 10X/0.3 Plan Neofluar and 20X/0.4 Epi Plan objectives (Zeiss). Visualisation of fluorescence staining was achieved using an automated excitation filter wheel and automated dichroic/emission cube turret for efficient automated imaging of combinations of dyes covering blues, greens, reds, and long reds. All operations were driven by the HCS Studio™ 2.0 Client software (Cellomics, ThermoFisher Scientific) with features for autofocus, autoexposure and cell subpopulation settings.

2.8.7 Image analysis

Quantitative analysis of images obtained with the ArrayScan™ (section 2.8.6) were performed using the ArrayScan HCS Reader software (Cellomics, ThermoFisher) provided with built-in algorithms for biological analysis. Settings of pre-determined algorithms were modified and adjusted for the correct identification of individual cells or subdivision into sub-populations as

for features of interest. The software automatically identified cells in each image based on their nuclear size and staining intensity (Figure 2.8a). Rejection thresholds were adjusted as required to exclude objects exceeding a minimum or maximum size or intensity which did not relate to cellular features (Figure 2.8b). Afterwards, the software analysed pixels of any staining area associated with the previously identified nuclei (Figure 2.8c) and translated image outputs in numbers which, in turn, were statistically analysed. The algorithms employed in this thesis comprise built-in Compartmental Analysis and Tube Formation algorithms, and custom built NET Detection and Nuclear Decondensation algorithms.

a)

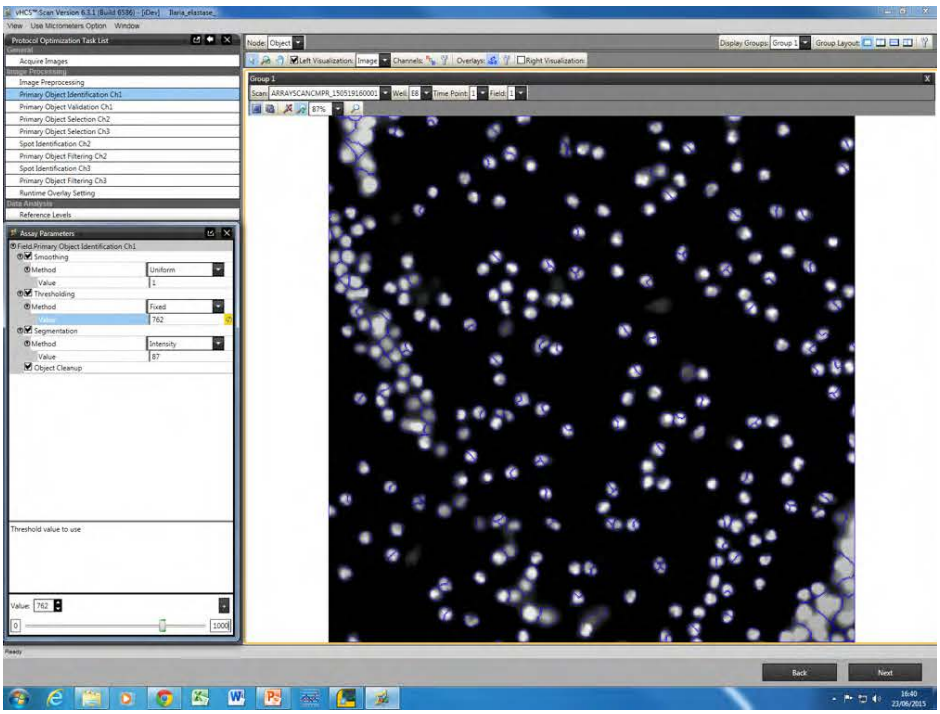

b)

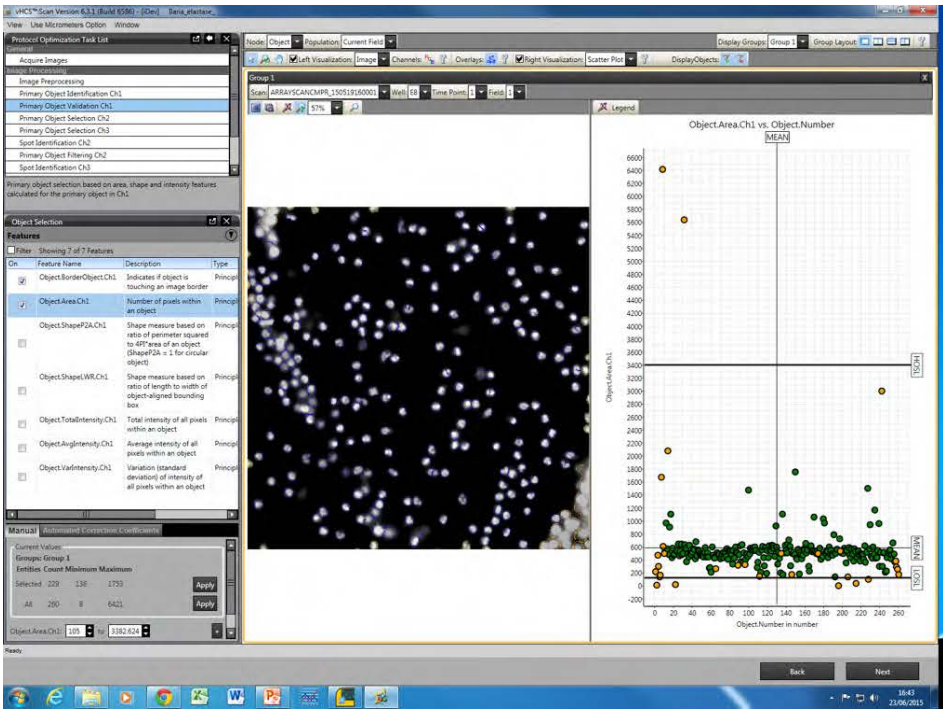

c)

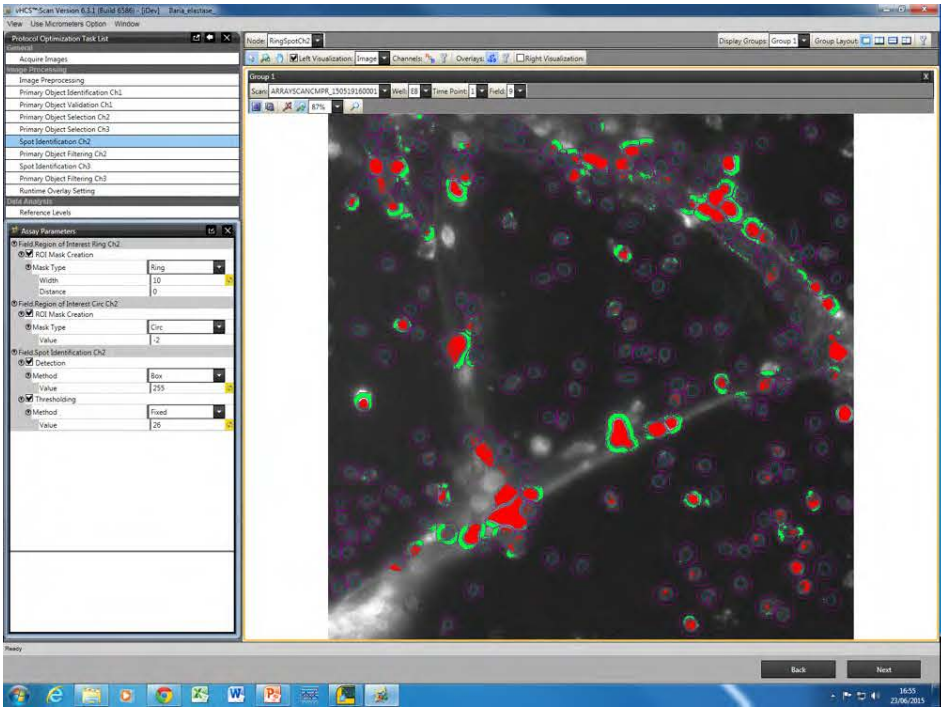

Figure 2.8: Images of screenshots of the operating ArrayScan HCS software.
Screenshot of the ArrayScan HCS software acquired during NET image processing using the Compartmental Algorithm. a) Setting adjustment for cell identification. b) Setting adjustment for the validation of cell recognition shown in a). c) Quantification of pixels of florescence staining within the area surrounding those cells selected in a) and b).

2.9 Statistical analysis

Statistical analysis and graph presentation of data was performed with Prism version 6 and 7 (GraphPad). Data are expressed as mean values and error bars indicate standard error of the mean (SEM). Analysis of normal distribution was run with the D'Agostino-Pearson omnibus normality test which determined whether the dataset followed a normal or non-normal distribution, therefore data were treated as appropriate. Statistical tests were considered valid exclusively with P values ≤ 0.05. N number, statistical tests and significance are expressed for each dataset.

CHAPTER 3: CHARACTERISATION OF CONDITIONS FOR NET ANALYSIS

5.1 Background

During microbial infections, neutrophils are recruited to diseased sites from the capillary circulation (Kolaczkowska & Kubes, 2013). Once neutrophils localize and reach the colonising microorganisms, they become activated and initiate their antimicrobial strategies (as described in section 2.1.3) (Chapple & Matthews, 2007). Periodontitis is a well characterised inflammatory disease and the events occurring at the site of infection, including neutrophils interacting with periodontal pathogens, can be modelled *in vitro* (Serhan *et al.*, 2008). In order to reproduce the *in vivo* conditions implicated in inflammation, human neutrophils were isolated from peripheral venous blood for *in vitro* analysis. Infectious conditions were mimicked by exposing cells to physiologically or chemically relevant stimuli. Since NETosis has been previously demonstrated to depend upon NOX activity and ROS generation (Palmer *et al.*, 2012a; Remijsen *et al.*, 2010), neutrophil activation state in response to stimulation and experimental conditions applied was evaluated through the measurement of two parameters, the release of NETs and the production of intracellular and extracellular ROS. Notably, variation in type and duration of stimulation often results in qualitative and quantitative differences in NET release (Brinkmann *et al.*, 2004). Therefore, for the analysis of neutrophil activation status, current techniques focus on monitoring ROS production and quantifying extracellular NET-DNA using fluorometric assays (described in section 2.6.2) in time-course studies. NET quantification assays have the potential to be performed using HCA, however, analytical conditions required optimisation for this purpose. The aim of this chapter was therefore to test and identify appropriate conditions for NET release which could be applied for neutrophil investigations using a HCA platform. Research areas covered in this chapter include: i) the effect of physiological and non-physiological (chemical) stimuli on neutrophil activation; ii) analysis of stimulation threshold; iii) effect of temperature and CO_2 conditions on NET

production; iv) effect of ion-supplemented media on neutrophil activation; and v) the comparison between human and murine bone marrow neutrophils and their responses.

5.2 Stimuli selection

Stimuli tested for neutrophil activation were divided into the two categories of "physiological" and "non-physiological" (chemical). Physiological stimuli were considered those that have been previously related to periodontitis pathogenesis and are known to activate neutrophils through surface receptor-binding, and include single species oral pathogens, oral biofilms and *E. coli* LPS (described in section 2.3.1). Chemical stimuli utilised for the following experiments were HOCl and PMA as they are well characterised stimuli of NET production (Palmer *et al.*, 2012a; Ermert *et al.*, 2009; Gupta *et al.*, 2005). Data on stimulation obtained for both ROS and NET production were compared with unstimulated basal levels.

5.2.1 PMA stimulation

PMA is a cell permeable compound that simulates DAG upstream of the activation of the PKC pathway, thereby bypassing the surface receptor binding process necessary for NET stimulation (Fuchs *et al.*, 2007). Previous publications on neutrophil stimulation have used concentrations of PMA between 10-50nM (Fuchs *et al.*, 2007;Brinkmann *et al.*, 2004). In order to characterise the PMA dose dependency response, a range of concentrations between 0 and 50nM were assayed for ROS and NET production.

Time-course analysis of total ROS was evaluated for up to 4 hours following exposure to PMA using a chemiluminescence assay (section 2.6.3) in which oxygen radicals are quantified as relative light units (RLU) emitted by oxidised luminol. Data demonstrated that the ROS signal increased with the time of exposure to PMA (Figure 3.1a), reached its maximum production

between 60 and 100 minutes after stimulation and, subsequently decreased. Higher PMA dosages reduced the time period required for stimulation of the maximum level of ROS production (Figure 3.1a). The minimal concentration of PMA necessary to induce a detectable ROS response was 6nM, while concentrations above this resulted in a dose-dependent increase in ROS signal as confirmed by the analysis of peak ROS release (Figure 3.1b). Dose-response data indicated detectable amounts of ROS were generated only following exposure to concentrations of 25nM PMA and above. NET analysis was performed by exposing neutrophils to the same range of PMA concentrations for up to 4 hours and was quantified fluorometrically (section 2.6.5). Data presented in Figure 3.1c indicated a dose-response release of NETs of a similar profile to that observed for ROS production (Figure 3.1b). Similar to ROS production, PMA-induced NET release required a minimum concentration of 6nM or above for detection, and significant levels of NET-DNA were detected only after stimulation with 50nM PMA compared with unstimulated neutrophils.

a) Time-course PMA dose-response ROS production

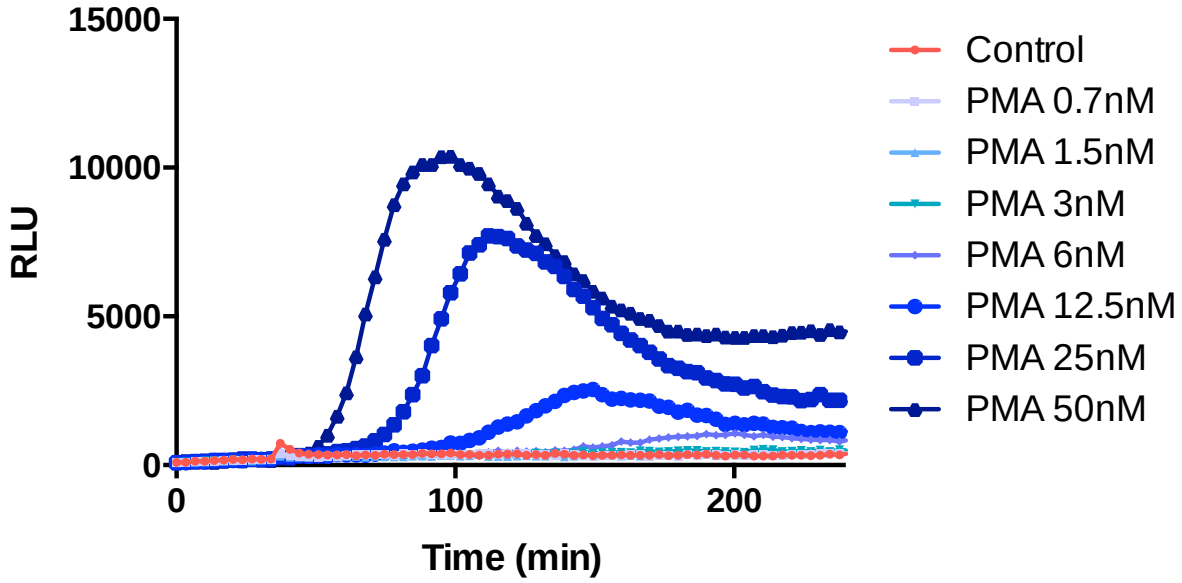

b) Peaks of ROS production: PMA dose-response

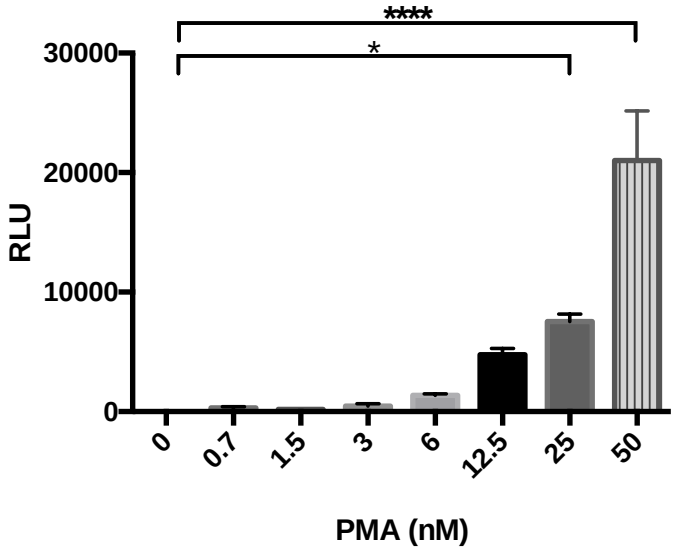

c) PMA dose-response NET release

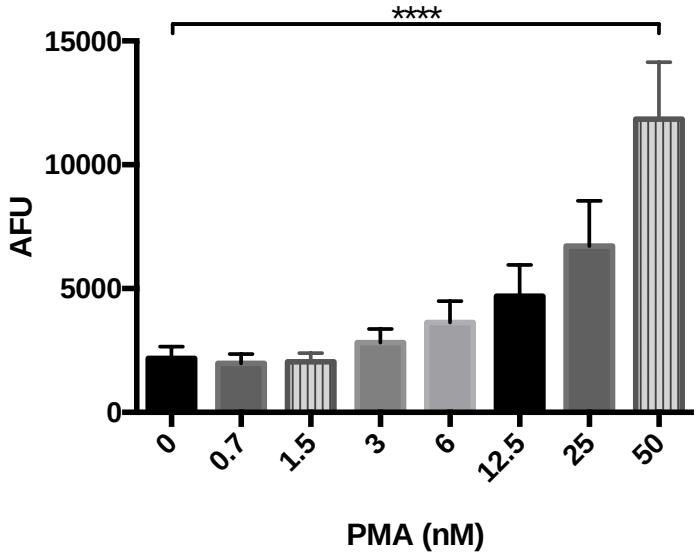

Figure 3.1:PMA dose-response for stimulation of ROS and NETs.
Stimulation of neutrophils with a range of PMA dosages (0 – 50nM) and its effect on a) time-course production of total ROS; b) peak ROS production, and c) NET production at 4 hours. Values are expressed as relative light units (RLU) or arbitrary fluorescence units (AFU) and as mean ± SEM. Statistical significance calculated with Dunnett's multiple comparison test (n= 5; *p<0.05, ****p<0.0001).

Ex vivo NET studies are routinely performed at 37°C in 5% CO_2 throughout the stimulation to provide physiologically relevant conditions. However, performing real-time HCA of NET formation would require incubation of neutrophils for extended time periods in the Arrayscan Cellomics equipment, which operates at room temperature and provides no CO_2 supplementation. Due to these logistic limitations, NET release was evaluated by fluorometric assay (section 2.6.5) in equivalent environmental conditions and compared with tissue culture incubation (37°C in 5% CO_2). For the following experiment, neutrophils were incubated with 50nM PMA for up to 3 hours at room temperature, 37°C, or 37°C in 5% CO_2 (section 2.6.4); and NETs quantified throughout the stimulation interval. Time-course analysis of NET formation (Figure 3.2a) indicated that incubation performed at 37°C in 5% CO_2 resulted in the highest amount of NET-DNA release in response to PMA, whereas in the absence of 5% CO_2 the levels of NETs decreased. Incubation at room temperature, however, considerably reduced the amount NET-DNA released and NETs remained at significantly lower levels throughout the entire stimulation period (Figure 3.2b).

a) Time-course of NET quantification

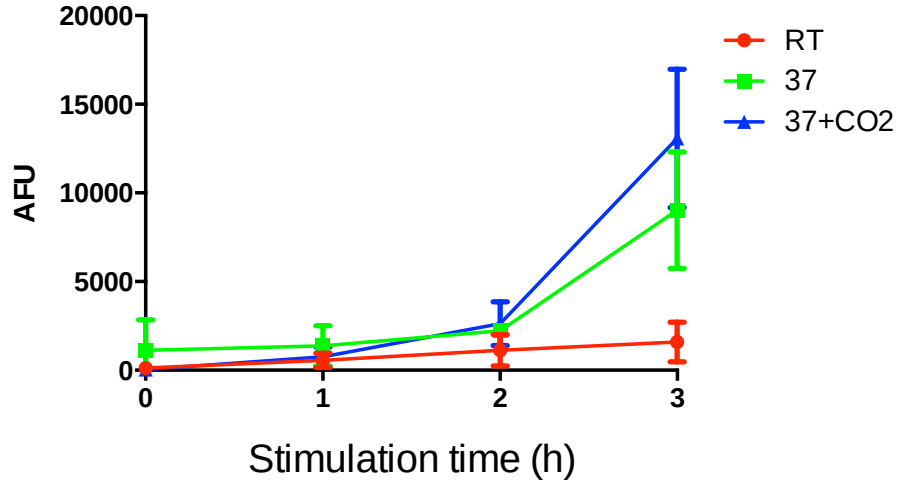

b) NET production: room temperature (RT), 37°C/atmospheric CO_2, and standard incubator 37°C/5% CO_2

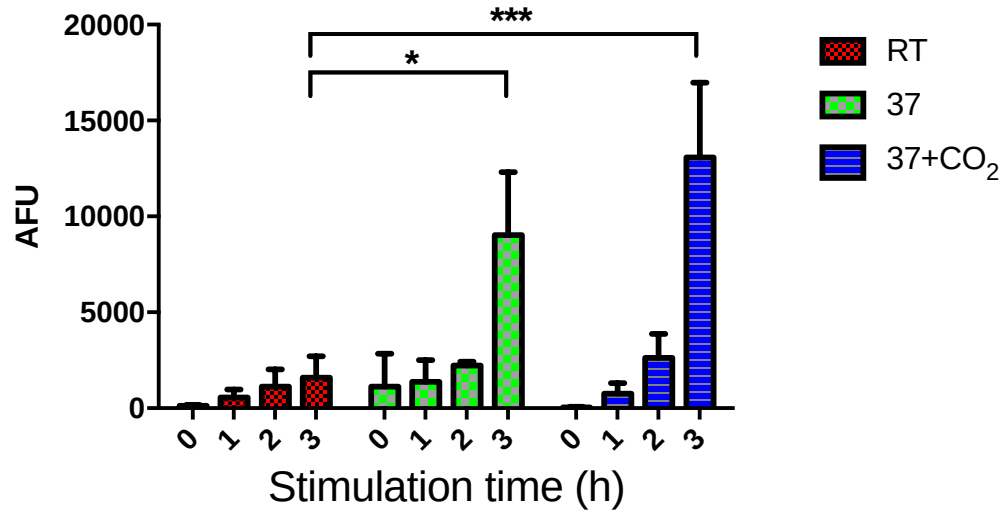

Figure 3.2: Time-course analysis of NET release following PMA stimulation under different environmental conditions.
PMA stimulated NET-DNA quantification over 3h incubation at room temperature (RT), at 37°C/atmospheric CO_2, and standard 37°C/5% CO_2. a) Time-course analysis of NET production and b) comparison between the different environmental conditions applied. Values are expressed as arbitrary fluorescence units (AFU) and as mean ± SEM. Statistical significance calculated with Tukey's multiple comparison test (n= 4; *p<0.05, ***p<0.001).

5.2.2 NET production following stimulation with periodontally relevant bacteria

To mimic the *in vivo* activity of neutrophils combatting a periodontal infection, two well characterised periodontal pathogens were assayed for neutrophil activation, namely *F. nucleatum* and *P. gingivalis*. Both periodontally-associated Gram negative bacteria trigger receptor-induced intracellular signalling cascades leading to ROS production and subsequent NET release (Prince *et al.*, 2011). Subsequently single-strain bacterial cultures were heat-killed and employed in time-course studies for total ROS production and NET release. Bacteria were used at a MOI of 100:1 according to previous studies which report the numbers of bacteria associated with periodontal pocket epithelium during active disease (Dierickx *et al.*, 2002).

Real-time total ROS production was recorded using the chemiluminescence assay (section 2.6.3) before and after stimulation for up to 10 hours. Neutrophil responses to *F. nucleatum* (MOI 100:1) were compared with PMA (50nM) exposure, which was used as a positive control and also with unstimulated cells as negative control. Figure 3.3a displays the differences in profiles generated between these two types of stimulation. The reaction to PMA began within 30 minutes of initial exposure to the stimulus and resulted in a sudden relatively high peak that slowly decreased up to 5 hours post-stimulation. Conversely, *F. nucleatum* stimulation resulted in a different curve profile and relatively slowly reached peak levels after approximately 4 hours exposure to bacteria, gradually decreasing to basal levels by 9 hours. Peak levels of ROS production are compared in Figure 3.3b. Consistent with the time-course data, peaks for both stimulations were significantly higher compared with basal levels of unstimulated cells, however, the difference between the two types of stimuli was not significant.

a) Time-course ROS production in response to PMA and *F. nucleatum*

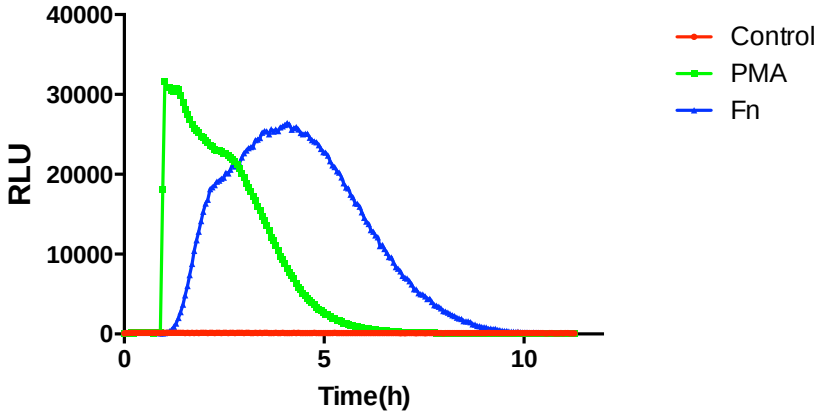

b) Peaks of ROS production in response to PMA and *F. nucleatum*

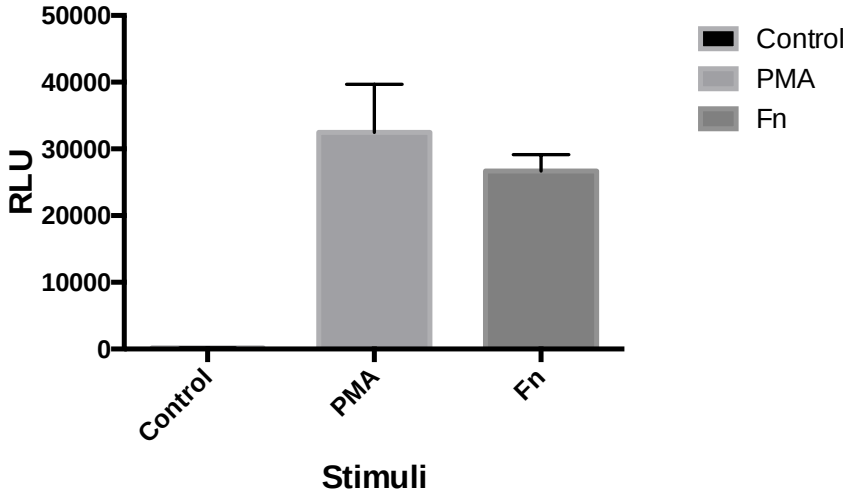

Figure 3.3: Analysis of ROS production by neutrophils in response to PMA and *F. nucleatum*.
Representative plots of total ROS production over 10h stimulation with PMA and *F. nucleatum* (Fn) are presented. a) Time-course quantification of ROS in response to PMA (green) and *F. nucleatum* (blue) compared with unstimulated neutrophils (red). b) Analysis of peak ROS production in response to PMA and *F. nucleatum* compared with unstimulated neutrophils (n=3). Values are expressed as relative light units (RLU) and as mean ± SEM.

To investigate differences between periodontally-pathogenic bacteria, neutrophils were exposed to *P. gingivalis* (MOI 100:1) for 4 hours. Neutrophil activation was quantified in terms of ROS production and NET release respectively using chemiluminescence and fluorometric assays. Peak levels of ROS were compared with *F. nucleatum* which was used as a positive control and unstimulated neutrophils were used as negative control. Data from *P. gingivalis* stimulation indicated a significant amount of ROS were produced compared with basal

unstimulated levels, however, significantly lower levels were detected compared with *F. nucleatum* stimulation (Figure 3.4a). Conversely, data on NET release indicated that stimulation with *P. gingivalis* induced a higher amount NET-DNA compared with *F. nucleatum* stimulation (Figure 3.4b).

a) Peaks of ROS production in response to *F. nucleatum* and *P. gingivalis*

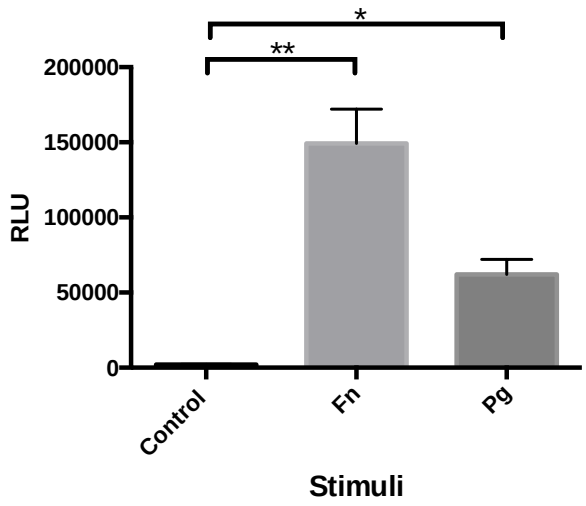

b) NET production in response to *F. nucleatum* and *P. gingivalis* exposure

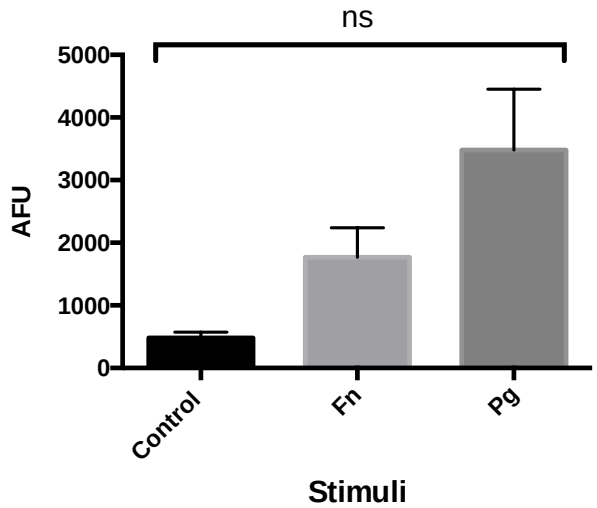

Figure 3.4: Total ROS and NET production in response to different bacterial stimuli. Neutrophil responses to *F. nucleatum* (Fn) and *P. gingivalis* (Pg) stimulation over 4h. Analysis of a) peaks of total ROS and b) NET production. Values are expressed as relative light units (RLU) or arbitrary fluorescence units (AFU) and as mean ± SEM. Statistical significance calculated with Dunnett's multiple comparison test (n= 3 individuals; ns=non significant, *p<0.05, **p<0.01).

Activation of neutrophils in response to bacterial stimuli is driven by receptor-binding processes which involve simultaneous activation of multiple receptors present on the cell surface as described by Futosi *et al.* (2013) and in section 2.3.1.1 of the Introduction. The concentration of bacteria required to trigger the activation of NOX complexes was determined using a range of *F. nucleatum* dosages. In order to test dose-response activation and mimic the immune response occurring in different stages of infection, neutrophils were stimulated with concentrations of *F. nucleatum* ranging between 0.1 and 100 bacteria per neutrophil. Data on time-course analysis indicated that the maximum level of ROS production occurred relatively early (at ~60 minutes) following stimulation with the highest *F. nucleatum* dosage (MOI 100:1) (Figure 3.5a). Concurrently, comparison of peak ROS production showed a dose-dependent increase in activation (Figure 3.5b).

a) Time-course study of ROS production

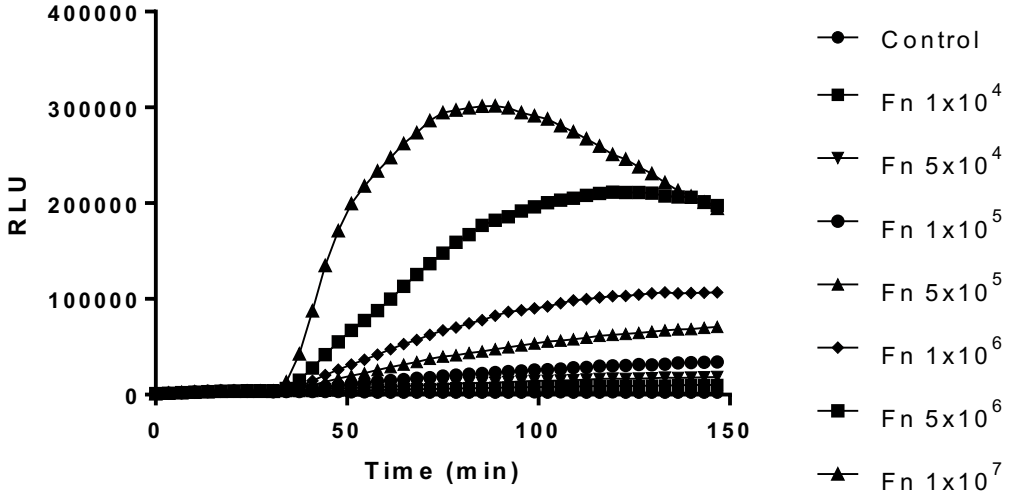

b) Peaks of ROS production

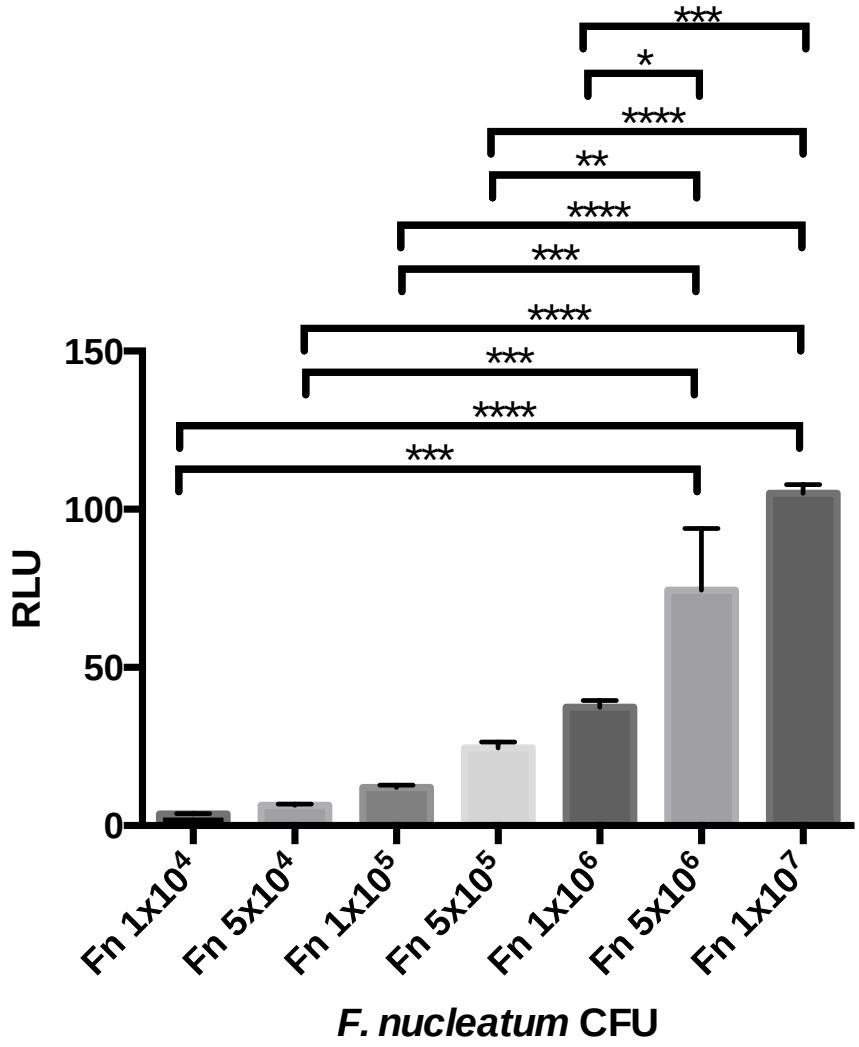

Figure 3.5: *F. nucleatum* dose-response stimulation of total ROS production.
Dose-response *F. nucleatum* induction of ROS production at 150 min stimulation (MOI 1:10, 5:10, 1:1, 5:1, 10:1, 50:1, 100:1). Data for a) time-course production and b) total ROS peak. Values are normalised to control and expressed as relative light units (RLU). Statistical significance calculated with two-way ANOVA and Tukey's multiple comparison test (n=3; *p<0.05, **p<0.01, ***p<0.001, ****p<0.0001).

Bacterial and chemical stimuli differentially activate neutrophils and responses vary in time and magnitude (Parker *et al.*, 2012a). In order to identify at what stage of the stimulation NET-DNA is first identified in neutrophils, samples were stimulated with *F. nucleatum*, PMA and HOCl for a 4 hour time-course and NETs were fluorometrically quantified at the time-points of 0, 30, 60, 120, 180 and 240 minutes post-exposure. Figure 3.6a represents an overview of all stimulations analysed along with differences in timing and relative amounts of NETs produced. Of the three stimuli tested, HOCl initiated NET release earlier than the other stimuli, data that is consistent with that previously described by Palmer *et al.* (2012a). The levels of HOCl-induced NET-DNA release were significantly higher compared with controls, and occurred as early as 30 minutes post-stimulation and increased up to four times by 240 minutes post-exposure. PMA resulted in delayed stimulation with significant levels of NET-DNA not being detected until 180 minutes post-exposure. Analysis of *F. nucleatum* stimulated NETs showed detectable NET-DNA induction at a later time-point compared with the other stimuli applied (Figure 3.6b).

a) NET production using three stimuli

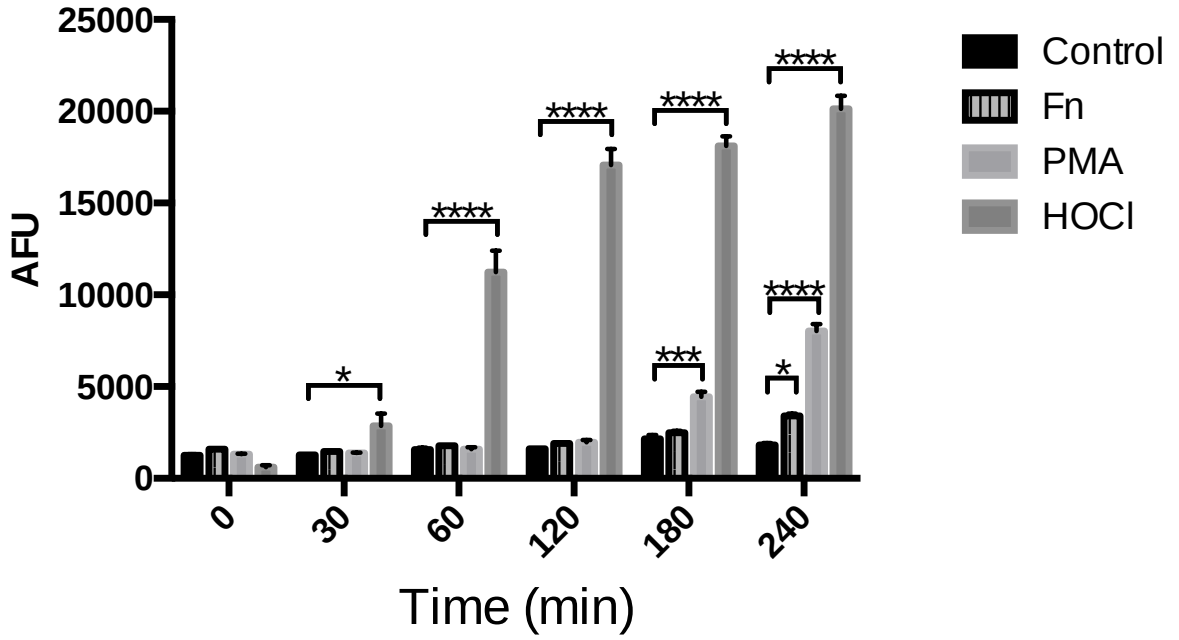

b) *F. nucleatum* stimulation (re-plotted from above graph)

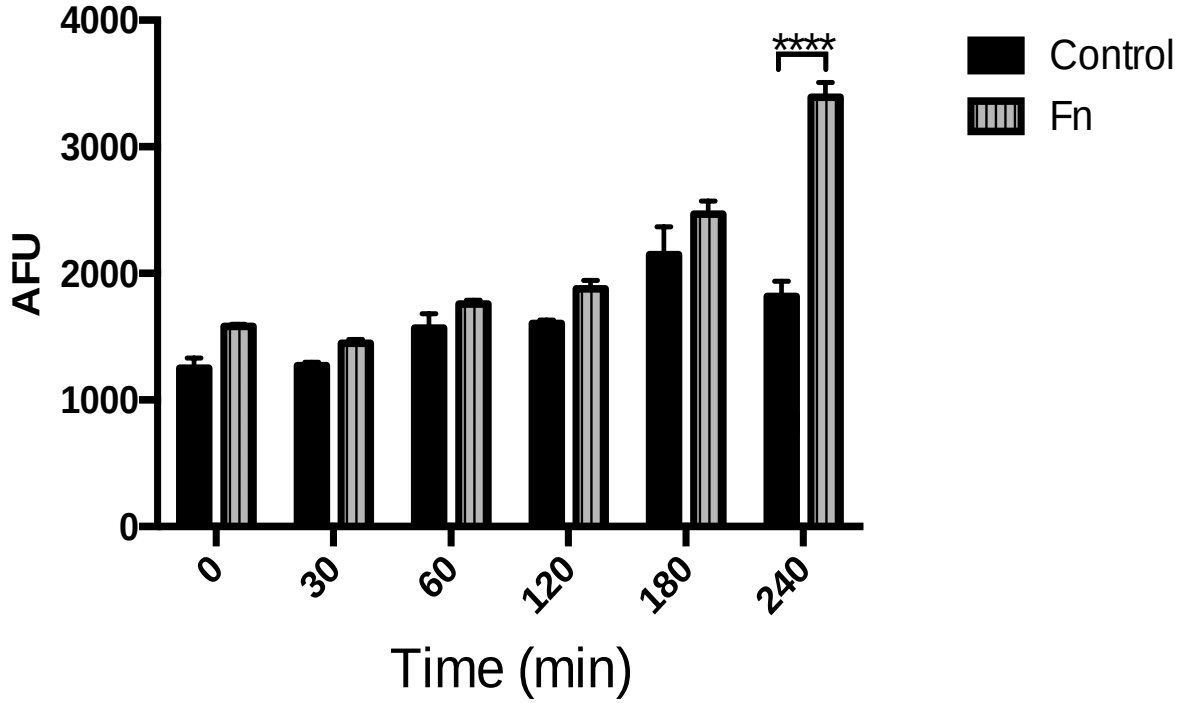

Figure 3.6: Time-course analysis of NET production in response to three different stimuli. NET quantification over 240 min stimulation with a) *F. nucleatum*, PMA and HOCl compared to unstimulated neutrophils; b) re-plotted data from graph presented in a) showing detailed *F. nucleatum* stimulation. Values are expressed as arbitrary fluorescence units (AFU) and as mean ± SEM. Statistical significance calculated with Tukey's multiple comparison test (n= 3; *p<0.05, ***p<0.001, ****p<0.0001).

Neutrophil exposure to *F. nucleatum* was also observed using a fluorescence microscope to determine the feasibility of using bacterial stimulation for further analysis by HCA. Subsequently, unstimulated and *F. nucleatum*-stimulated neutrophil preparations were stained with Sytox green® and analysed by epifluorescence microscopy. Images presented in Figure 3.7 demonstrate that bacterial cells were also stained by the DNA dye and created a notable background noise that may impact upon NET quantification using HCA image analysis techniques.

Control *F. nucleatum*

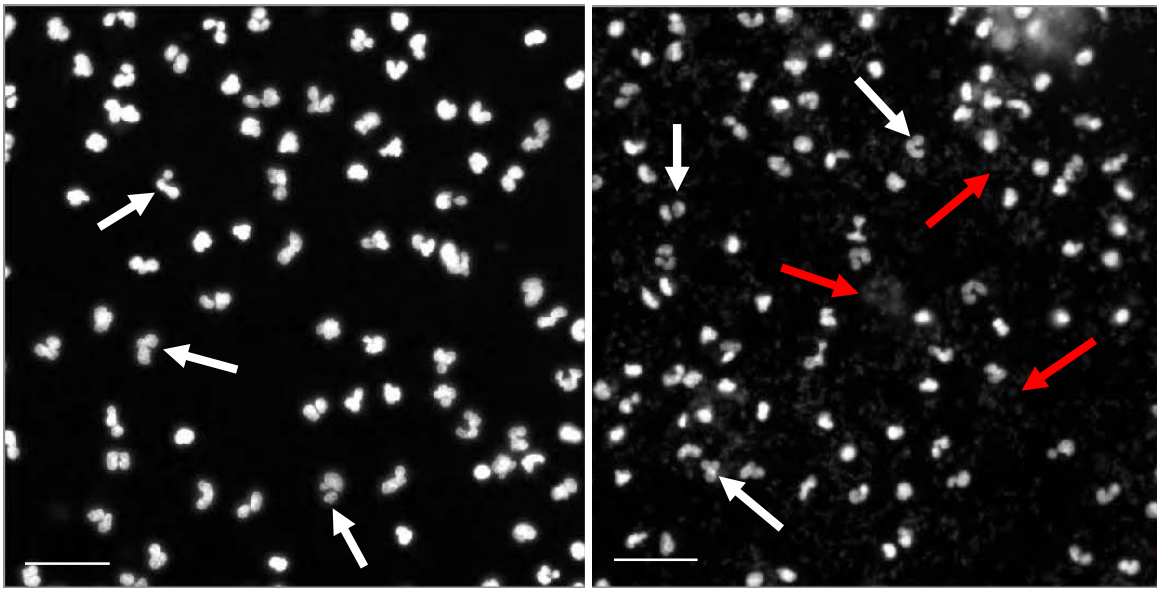

Figure 3.7: Fluorescence microscopy images of neutrophil co-localisation with F. nucleatum.
Neutrophils and *F. nucleatum* bacteria (heat-killed) were visible after staining with Sytox green and with fluorescence microscopy observation. Unstimulated cells on the left panel and bacteria stimulation on the right panel. Neutrophils are indicated by white arrows and *F. nucleatum* by red arrows. Scale bar represents 200µm. Images are representative of 3 independent experiments.

5.2.3 Lipopolysaccharide stimulation of NETs

Neutrophil stimulation is reportedly more rapid when triggered by multiple receptor being activated and bacterial components are also effective activators of several cell surface receptors,

as described in section 2.3.1.1. The advantages of using single bacterial components compared with using whole bacteria, is the absence of bacterial DNA and the possibility that the use of DNA dyes will subsequently not generate background noise which may interfere with future HCA. The following experiments aimed to identify optimal conditions for LPS stimulation of neutrophils.

LPS was diluted in standard PBS or PBS supplemented with 10% human plasma, 20% human plasma or 10% BSA; and used for neutrophil stimulation at 1μg/ml final concentration in order to verify whether these media would affect LPS stimulation. Production of ROS was evaluated using the chemiluminescence assay for up to 4 hours and ROS peak signals were compared. Figure 3.8a shows levels of ROS stimulation were similar with all four PBS buffer solutions used, however, LPS dilution in PBS supplemented with 10% BSA resulted in slightly lower, although non-significant, levels of ROS. Compared with unstimulated neutrophils, 1μg/ml LPS-stimulation resulted in increased ROS production although this was non-significant for all four tested buffer solutions used (Figure 3.8b).

a) LPS-stimulated total ROS production

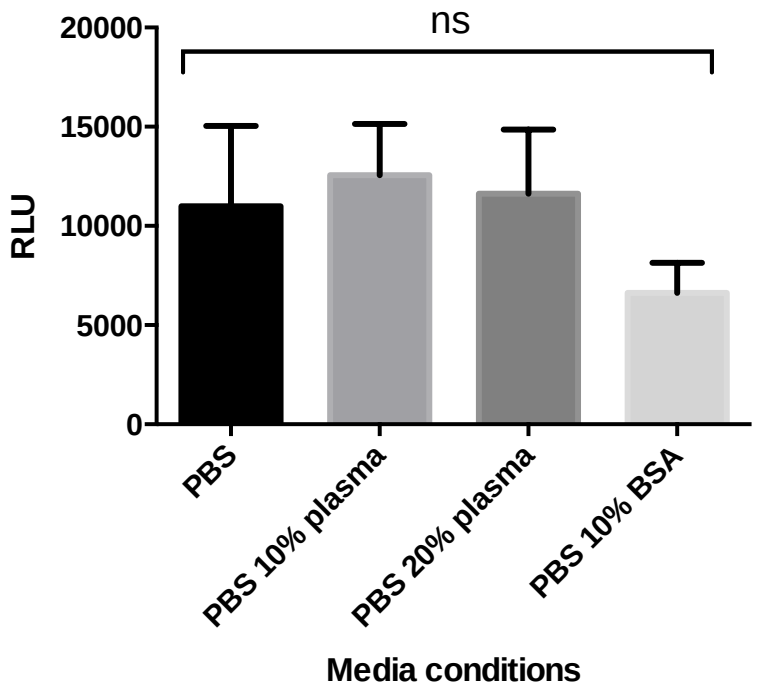

b) Peak total ROS production: LPS vs control

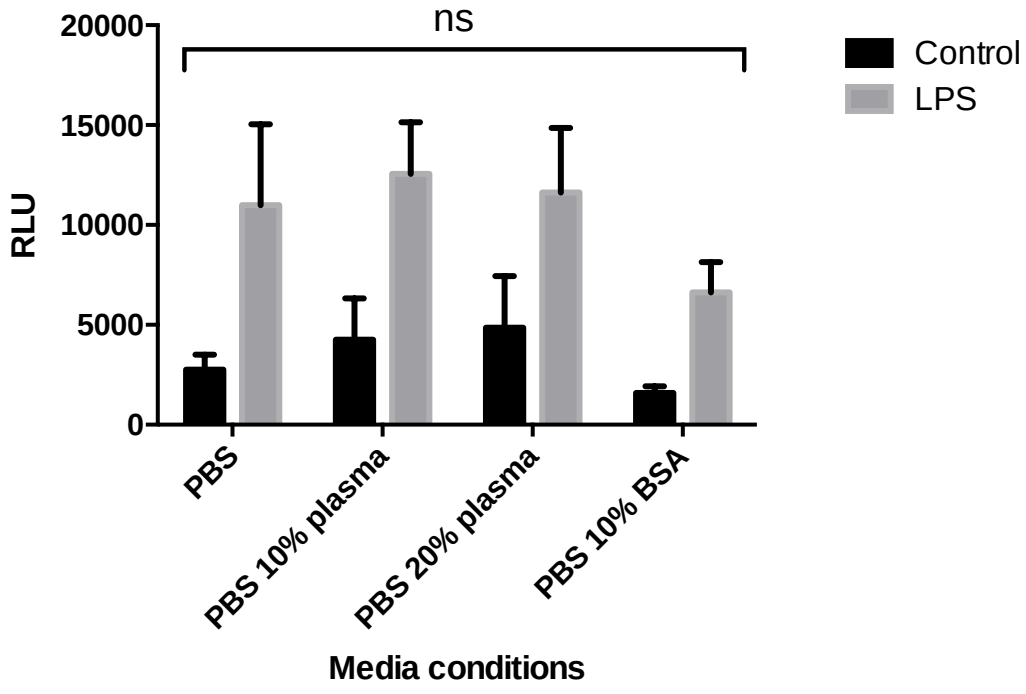

Figure 3.8: LPS-stimulated ROS production in different buffers.
LPS-induced total ROS formation, with peak analysis in a) standard PBS, 10% plasma supplemented PBS, 20% plasma supplemented PBS and 10% BSA supplemented PBS, and b) in comparison with unstimulated neutrophils. Values are expressed as relative light units (RLU) and as mean ± SEM. Statistical significance calculated with Tukey's multiple comparison test (n=3; ns= non significant).

The stimulation triggered by LPS in supplemented buffers was additionally tested for inducing NET formation at 4 hours post-exposure. Consistent with ROS data, addition of plasma or BSA to the standard PBS resulted in similar values of LPS-induced NETs as shown in Figure 3.9a. Similarly, compared with basal levels of unstimulated cells shown in Figure 3.9b, LPS was able to induce NET production although data were not statistically different from those in unstimulated cells. This result was consistent with the ROS data, nevertheless, for further experiments LPS was diluted in PBS buffer supplemented with 10% human plasma in order to facilitate receptor binding (Luchi & Munford, 1993).

a) LPS-stimulated NET production

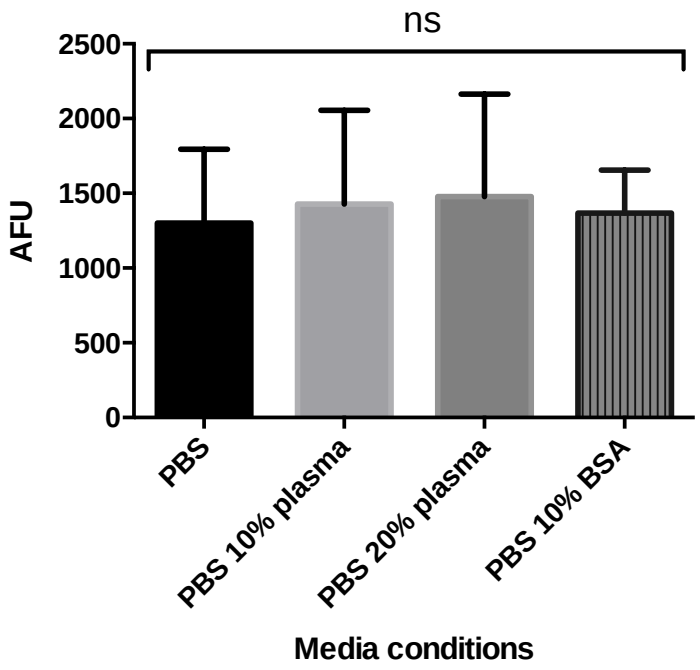

b) NET production: LPS vs control

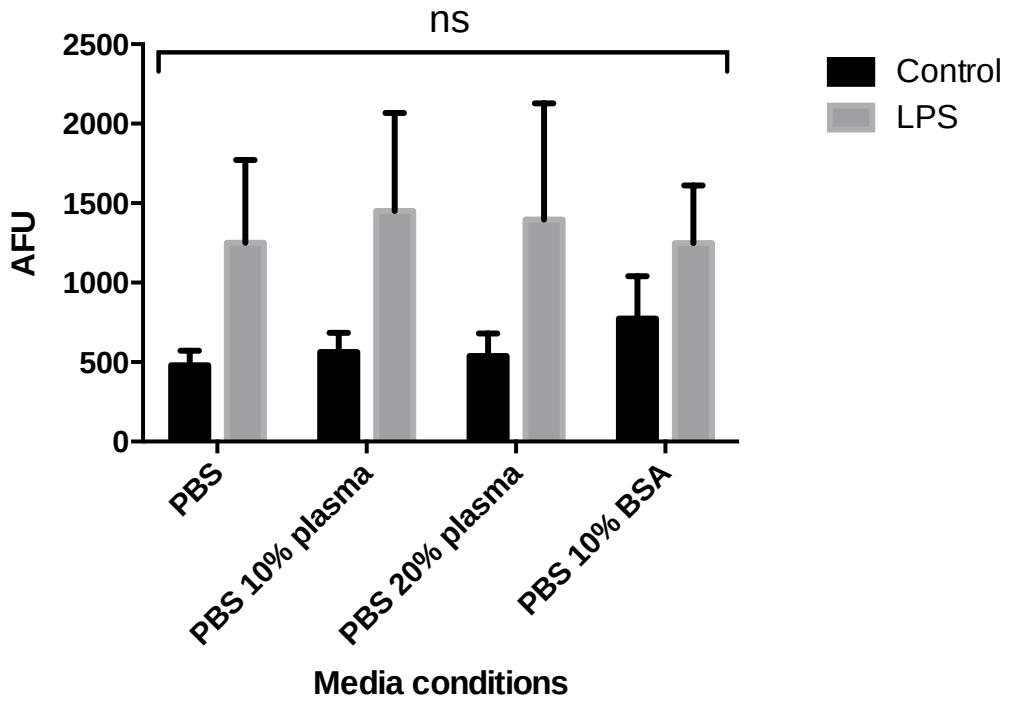

Figure 3.9: LPS-stimulated NET production in different buffers.
LPS-induced NET formation a) analysed in standard PBS, 10% plasma supplemented PBS, 20% plasma supplemented PBS and 10% BSA supplemented PBS, and b) in comparison with unstimulated neutrophils. Values are expressed as arbitrary fluorescence units (AFU) and as mean ± SEM. Statistical significance calculated with Tukey's multiple comparison test (n=3; ns= non significant).

As demonstrated above, 1μg/ml LPS did not induce significantly higher ROS or NET responses whether it was diluted in plasma or in standard PBS. Therefore, different dosages of LPS were tested as stimuli for both ROS and NET production. LPS was tested in a range of concentrations between 0.5 to 10μg/ml and neutrophil responses were analysed up to 4 hours exposure. Results presented in Figure 3.10a indicate all four concentrations induced a dose-dependent release of ROS compared with unstimulated neutrophils and the highest amount was registered upon stimulation with 10μg/ml LPS. Interestingly, NET quantification (shown in Figure 3.10b) indicated all four concentrations were ineffective in inducing significant NET release and, interestingly, stimulation with 10μg/ml LPS resulted in a significantly lower amount of NETs compared with unstimulated neutrophils. The high concentration of LPS may, actually, be associated with cell death do to the overwhelming signal or may activate an alternative killing mechanism such as phagocytosis.

a) LPS dose-response stimulation of total ROS

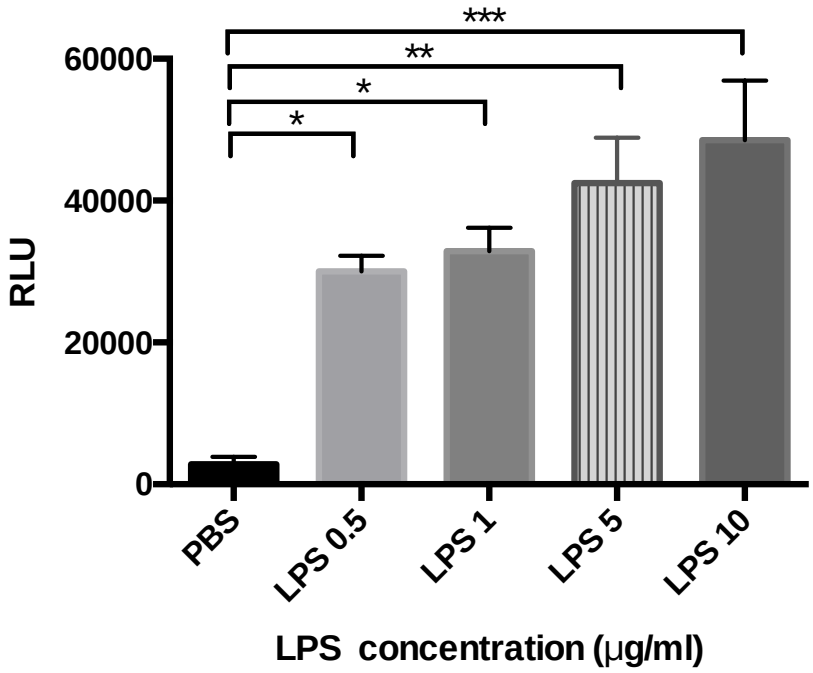

b) LPS dose-response of NET production

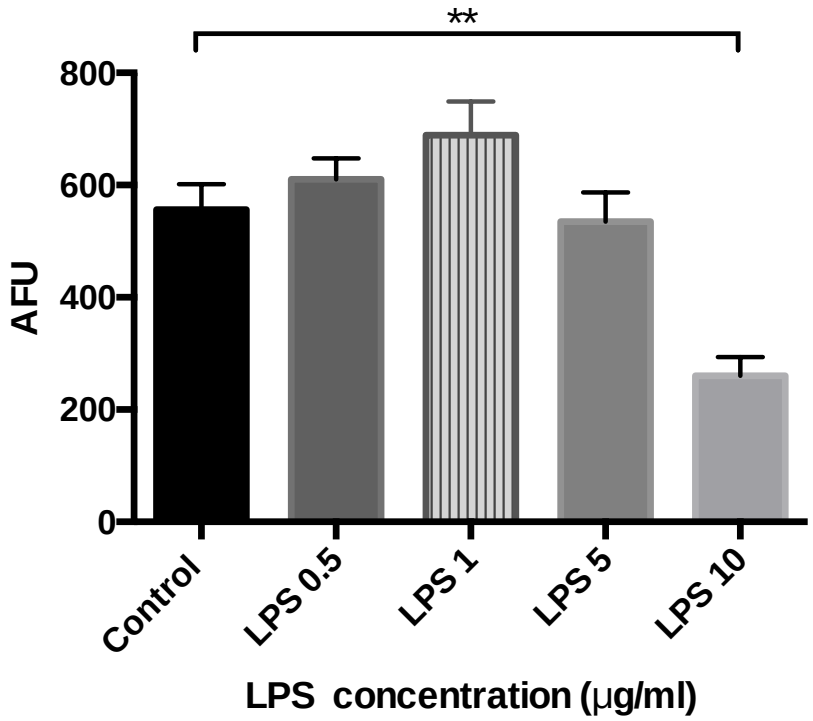

Figure 3.10: Dosage analysis for LPS stimulation of neutrophils.
LPS dose-response (0.5 - 10μg/ml) stimulation of a) peak total ROS production and b) NET production 4 hours post-stimulation. Values are expressed as relative light units (RLU) or arbitrary fluorescence units (AFU) and as mean ± SEM. Statistical significance calculated with Dunnett's multiple comparison test (n= 3; *p<0.05, **p<0.01, ***p<0.001).

5.2.4 Multi-species biofilms as stimulants for NET release

In periodontitis pathogenesis excess inflammation is driven by the dysregulation of the host immune response following microbial challenge (Darveau, 2010). More than 400 bacterial species have been identified within the oral biofilm to form the subgingival plaque (Xiao *et al.*, 2016) and subdivided into categories based on their association with the disease (Socransky *et al.*, 1998). To study the complex interaction between the host immune-inflammatory response and microbial plaque, Millhouse *et al.* (2014) developed a simplified model of oral multi-species biofilms and analysed the ability of these bacterial complexes to induce inflammatory responses in oral epithelial cells. This study identified that the co-culturing of oral epithelial cells with a disease-associated biofilm resulted in elevated expression of pro-inflammatory cytokines, such as IL-8 and TNF-α. Therefore, in the following experiments neutrophils were exposed to supernatants from 3-, 7- and 10-species biofilms which represents model for the healthy or disease-associated plaque as described in section 2.4.1.2 of the Materials and Methods. Additionally, supernatants from co-cultures of oral epithelial cells with biofilm models were used to stimulate neutrophils to mimic the local immune-response occurring during periodontal inflammation.

To analyse neutrophil responses to pathogenic and non-pathogenic biofilms directly, cells were incubated with supernatants from the culture of 3-, 7-, 10-species biofilms and compared with PMA induction as a positive control, the carrier diluent artificial saliva or unstimulated neutrophils were used as negative controls. Time-course ROS release was monitored by chemiluminescence assay, while NET production was fluorometrically evaluated following 4 hours of incubation. Data presented in Figure 3.11a indicate ROS production was elevated after exposure to all three types of biofilms, the highest response was obtained with the 3-species

biofilm stimulation, however, sterile artificial saliva was also able to induce significant ROS production. Conversely, data shown in Figure 3.11b indicated all three multispecies biofilm supernatants were insufficient to stimulate significant NET production after 4 hours.

a) Peak ROS production

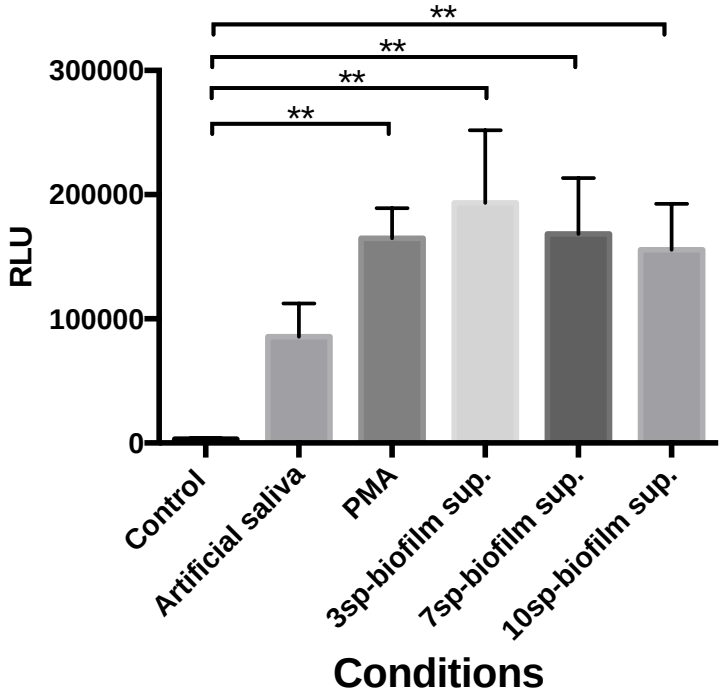

b) NET production

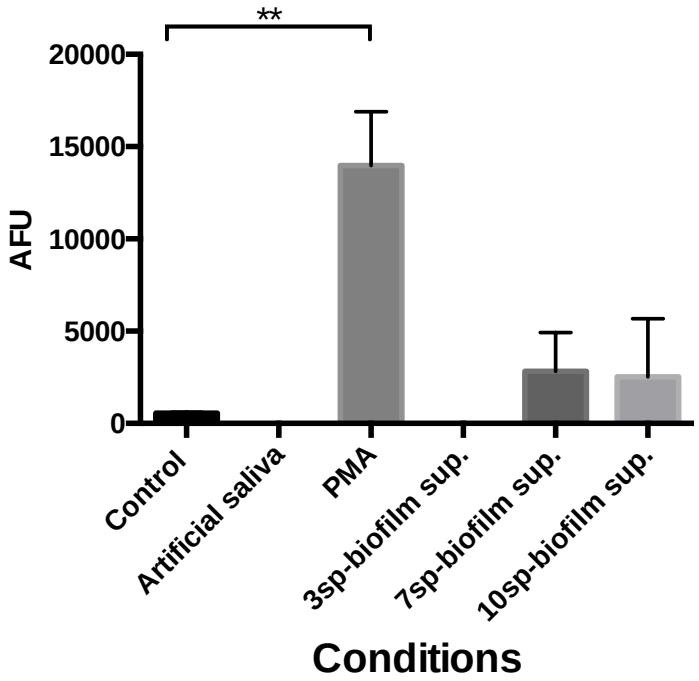

Figure 3.11: Neutrophil response to multi-species biofilms.
Stimulation with 3-, 7-, and 10-species biofilm supernatants compared with PMA, artificial saliva and unstimulated neutrophils. a) Effect on ROS production and b) quantification of NET-DNA release. Values are expressed as relative light units (RLU) or arbitrary fluorescence units (AFU) and as mean ± SEM. Statistical significance calculated using the Dunnett's multiple comparison test (n= 3; *p<0.05, **p<0.01).

In order to study neutrophil responses to pro-inflammatory stimuli released by oral epithelial cells when exposed to multispecies biofilms, supernatants from 24 hour co-cultures were used to stimulate ROS and NET-DNA release. Time-course ROS production was evaluated by real-time chemiluminescence quantification and compared with unstimulated oral epithelial cell supernatant, unstimulated neutrophils and PMA-stimulation. The analysis of peak ROS levels for each condition showed an increased and significant signal in response to the supernatants from oral epithelial cells co-cultured with 7- and 10-species biofilms (Figure 3.12a). However, fluorometric quantification of NET production after 4 hours stimulation showed minimal increase of NET-DNA (Figure 3.12b).

a) ROS production following exposure to epithelial cell supernatants

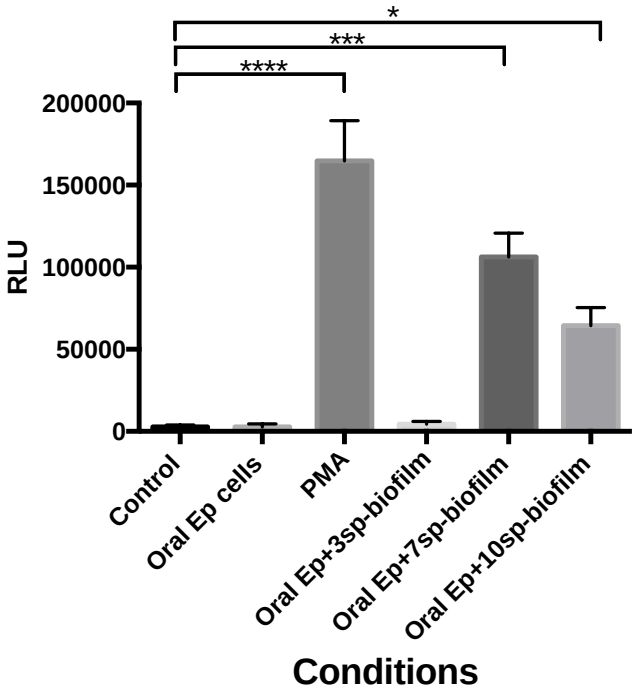

b) NET production following exposure to epithelial cell supernatants

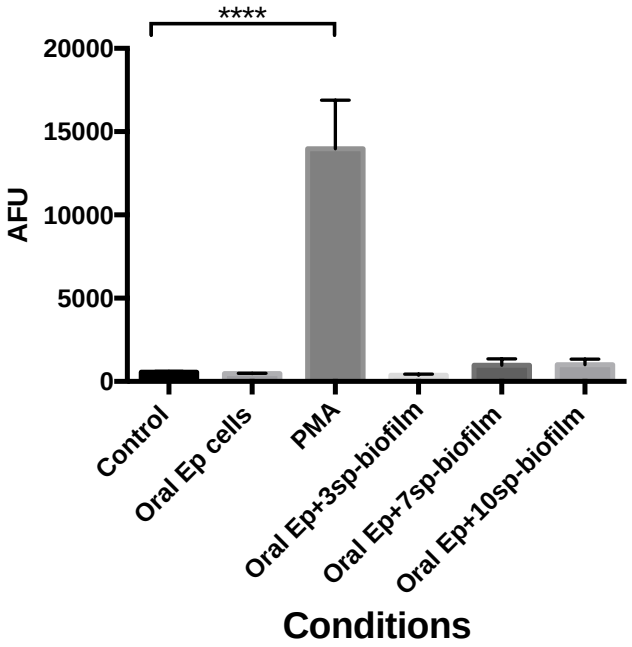

Figure 3.12: Neutrophil responses to supernatants obtained from co-cultures of oral epithelial cells with multi-species biofilms.
Stimulation with the supernatant from oral epithelial cell cultures (Oral Ep cells) or co-cultured with 3-, 7-, and 10-species biofilms (Oral Ep+3sp-, 7sp-, 10sp-biofilm) compared with PMA and unstimulated neutrophils. a) Effect on ROS production and b) quantification of NET-DNA release. Values are expressed as relative light units (RLU) or arbitrary fluorescence units (AFU) and as mean ± SEM. Statistical significance calculated using the Dunnett's multiple comparison test (n= 3; *$p<0.05$, ***$p<0.001$, ****$p<0.0001$).

5.3 Ion supplemented media as stimuli for NETs

Increased levels of salivary calcium have been related to oral diseases and extracellular calcium flux has a major role in neutrophil activation as described in section 2.2.1.3 of Introduction. Although salivary ionic levels differ from serum levels, alterations in saliva components mirror the fluctuations occurring in the human blood following disease progression (Greabu *et al.*, 2009). Therefore, the following experiments were performed to determine whether increased levels of serum extracellular calcium, as a salivary mimic for periodontitis, affect ROS generation and NET production in peripheral blood neutrophils.

5.3.1 Effects of calcium and magnesium ions on ROS production

$CaCl_2$ and $MgCl_2$ at a final concentration of 1mM were used to supplement PBS in order to represent ionic levels found in serum (Sullivan *et al.*, 1979) and neutrophil activity was compared with glucose-supplemented PBS (gPBS) and non-supplemented PBS. Neutrophils were seeded in supplemented PBS and stimulated with PMA to analyse ROS production in the presence of these cations. Figure 3.13a shows how supplementation of PBS with cations modified the profile of ROS release over time. Calcium supplementation resulted in a reduction in the peak signal detected at 60 minutes after exposure to non-supplemented media, however, at 100 minutes levels of ROS were equivalent. Conversely, the magnesium supplementation resulted in similar ROS levels over time to those of the non-supplemented conditions, however levels of ROS were marginally reduced. Supplementation with both calcium and magnesium compared with non-supplemented PBS resulted in an overall reduced level of ROS production. PMA stimulation, in both supplemented and non-supplemented media resulted in a significant increase in ROS compared with unstimulated neutrophils (Figure 3.13b).

a) Time-course of total ROS production in response to PMA

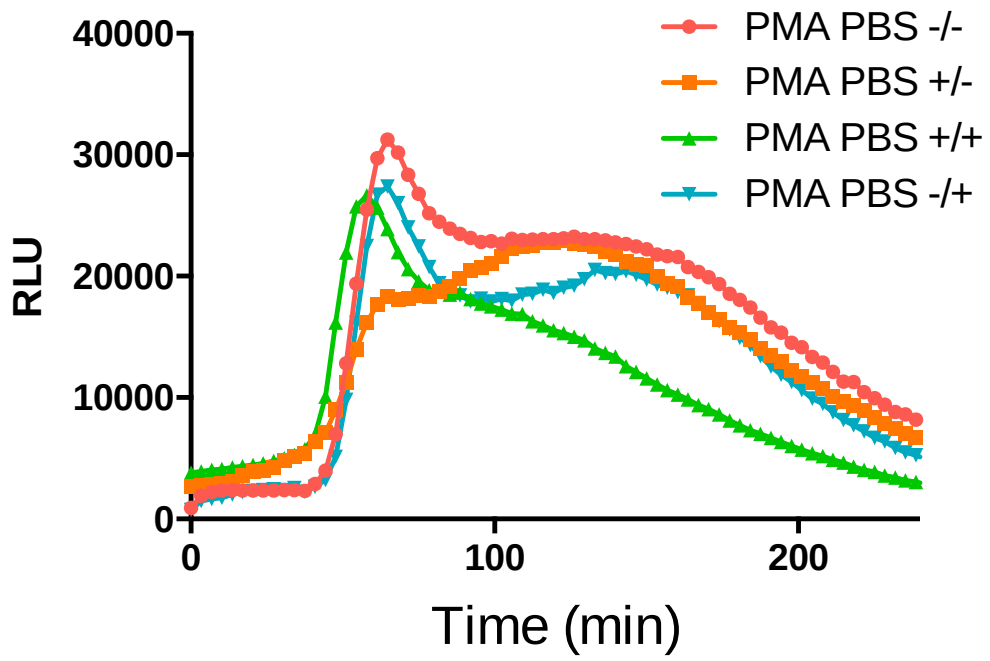

b) Peak ROS production: control vs PMA

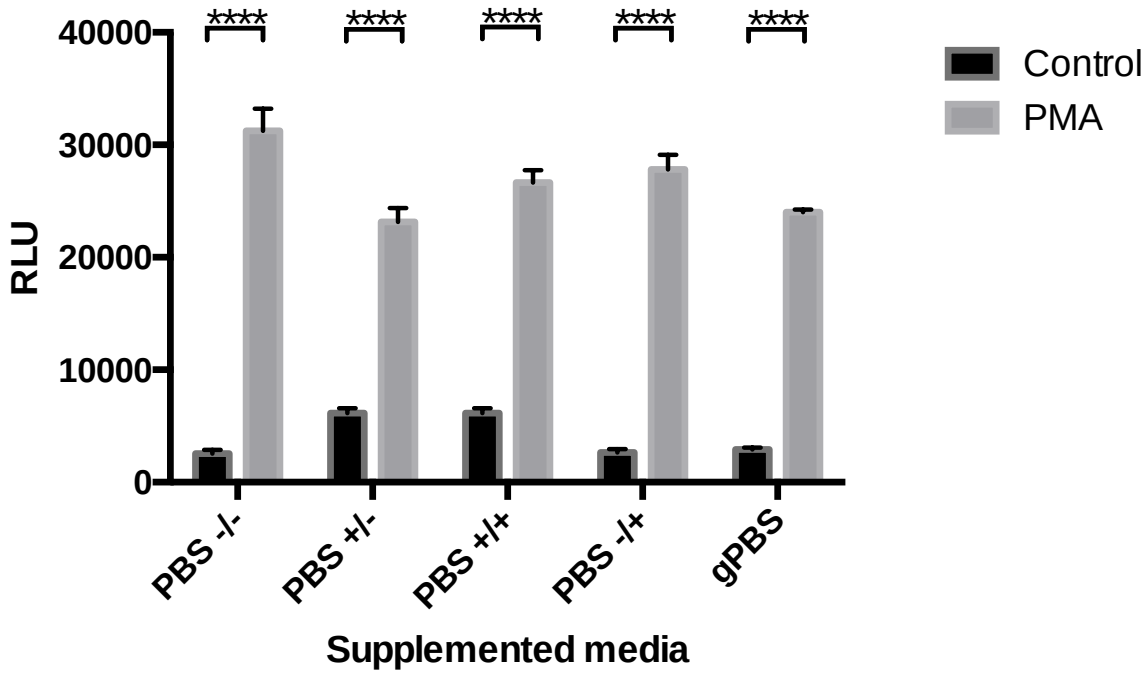

Figure 3.13: PMA induced ROS production in ion-supplemented PBS.
Neutrophils were stimulated with PMA in standard PBS (-/-), Ca^{+2} PBS (+/-), Mg^{+2} PBS (-/+), Ca^{+2}/Mg^{+2} PBS (+/+) and gPBS. a) Time-course analysis of total ROS production and b) analysis of peak ROS production in comparison with unstimulated neutrophils. Values are expressed as relative light units (RLU) and as mean ± SEM. Statistical significance was calculated with Tukey's multiple comparison test (n= 3; ****p<0.0001).

Following analysis of peak ROS production with supplemented and non-supplemented media in unstimulated neutrophils, the amount of ROS quantified was found to be significantly higher in the presence of calcium alone or when supplemented with both calcium and magnesium, while magnesium supplementation alone resulted in similar levels of peak ROS production compared with non-supplemented and glucose supplemented PBS (Figure 3.14a). However, in PMA-stimulated neutrophils, all supplementations resulted in lower levels of ROS release compared with non-supplemented PBS, while calcium supplemented PBS resulted in a significant reduction compared with non-supplemented PBS and gPBS (Figure 3.14b).

a) Unstimulated neutrophils

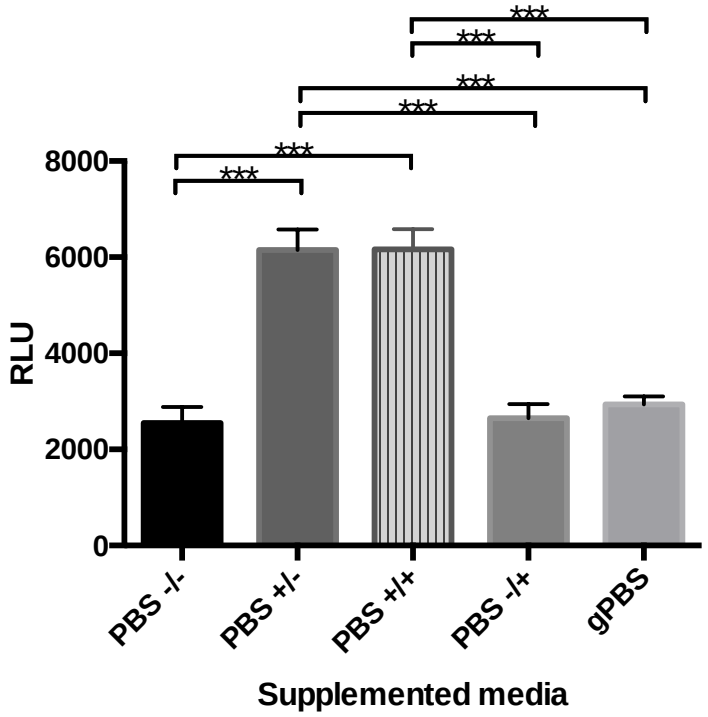

b) PMA stimulated neutrophils

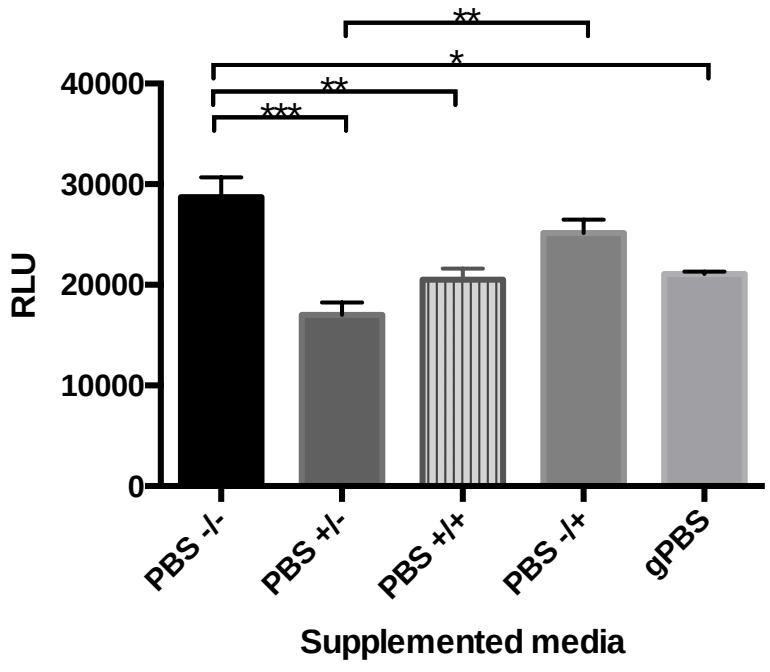

Figure 3.14: Effect of ion supplementation on ROS production.
Analysis of peak ROS production in a) unstimulated and b) PMA stimulated neutrophils in standard PBS (-/-), Ca^{+2} PBS (+/-), Mg^{+2} PBS (-/+), and Ca^{+2}/Mg^{+2} PBS (+/+) compared with gPBS. Values are expressed as relative light units (RLU) and as mean ± SEM. Statistical significance was calculated using Tukey's multiple comparison test (n= 3; *p<0.05, **p<0.01, ***p<0.001).

5.3.2 Effect of calcium and magnesium supplementation on NET production

Calcium and magnesium supplemented PBS was also assayed for NET production upon stimulation with PMA. Figure 3.15 shows levels of NETs produced in response to PMA. In enriched media with magnesium or both elements, PMA stimulation resulted in significantly higher levels of NETs compared with unstimulated cells, however, with calcium alone the difference was not significant.

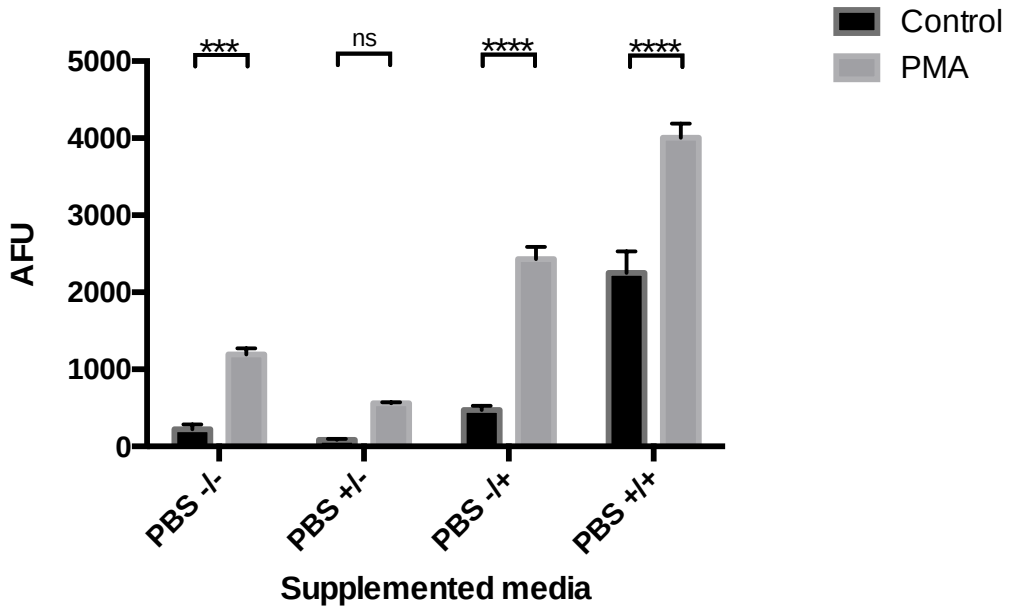

Figure 3.15: PMA stimulated NET production in ion-supplemented media.
PMA stimulation compared to unstimulated neutrophils in standard PBS (-/-), Ca^{+2} PBS (+/-), Mg^{+2} PBS (-/+), and Ca^{+2}/Mg^{+2} PBS (+/+). Values are expressed as arbitrary fluorescence units (AFU) and as mean $\pm$ SEM. Statistical significance was calculated with Tukey's multiple comparison test (n= 3; ns= non significant, ***p<0.001, ****p<0.0001).

Supplementation of PBS with both calcium and magnesium resulted in significantly higher levels of basal NET production in unstimulated neutrophils compared with the other conditions assayed (Figure 3.16a). Similarly, upon PMA stimulation, cells produced a significantly higher amount of NETs in the presence of magnesium alone or with both elements added, while significantly lower NETs were quantified in the presence of calcium supplementation (Figure 3.16b).

a) Unstimulated neutrophils

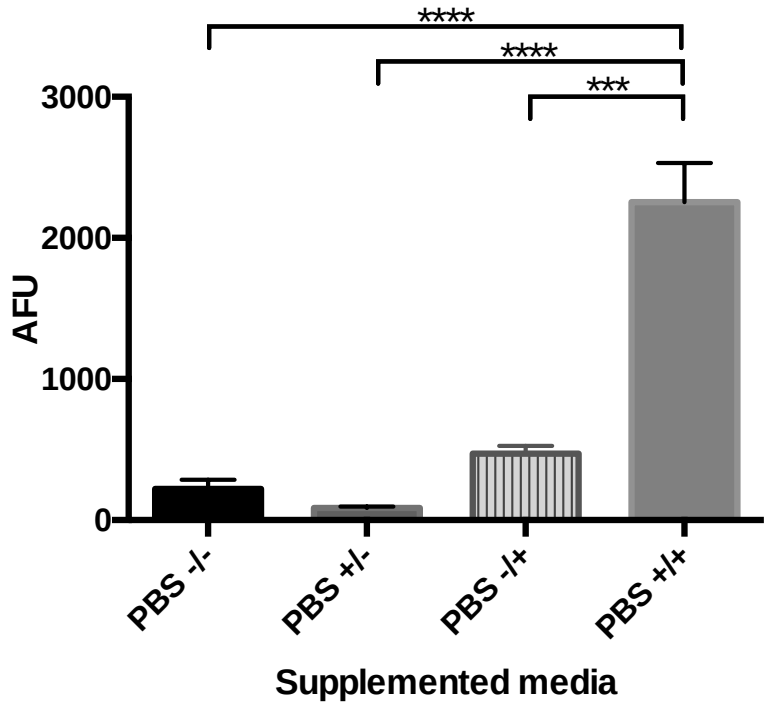

b) PMA stimulated neutrophils

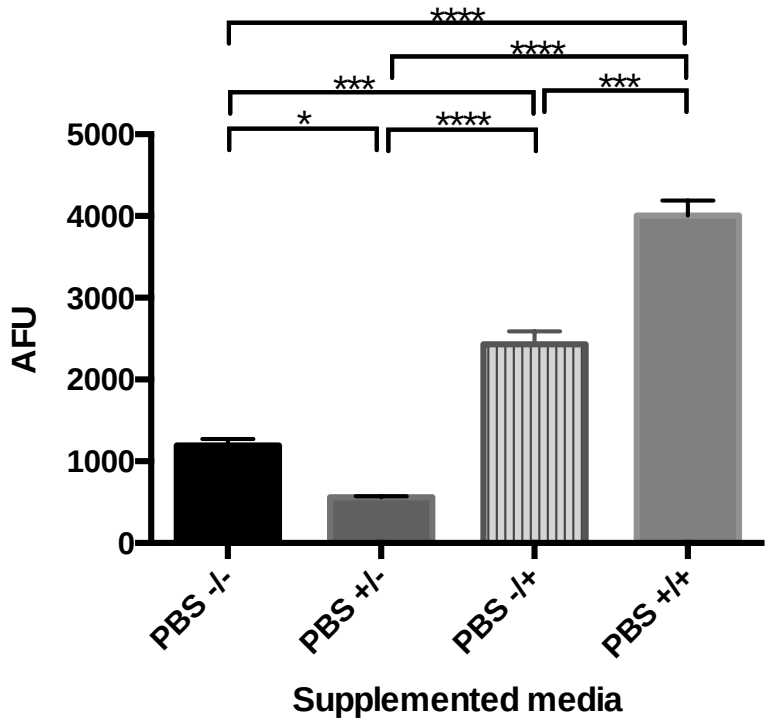

Figure 3.16: Effect of calcium and magnesium on NET production.
Analysis of NET production by a) unstimulated and b) PMA stimulated neutrophils in standard PBS (-/-), Ca^{+2} PBS (+/-), Mg^{+2} PBS (-/+), and Ca^{+2}/Mg^{+2} PBS (+/+). Values are expressed as relative light units (RLU) or arbitrary fluorescence units (AFU) and as mean $\pm$ SEM. Statistical significance calculated with Tukey's multiple comparison test (n= 3; *p<0.05, ***p<0.001, ****p<0.0001).

5.4 Behavioural analysis of murine bone marrow-derived neutrophils

Murine models have been extensively used for research on inflammatory processes as reviewed in section 2.4.1 of the Introduction. In the section below PAD4 knockout and wild-type bone marrow murine neutrophils were compared with healthy peripheral blood human neutrophils with the aim of validating murine models for NET studies and to evaluate the possibility of using murine derived neutrophils for HCA studies.

5.4.1 Validation of murine models for ROS production

To determine the ability of human and bone marrow murine neutrophils to produce ROS in response to non-physiological stimuli, cells were incubated for up to 18 hours with PMA, and ROS were measured using the chemiluminescence assay. Human neutrophils produced a considerably higher amount of ROS in response to PMA compared with murine neutrophils (Figure 3.17a). However, both types of murine neutrophils responded to PMA stimulation producing significantly higher amounts of ROS compared with unstimulated cells (Figure 3.17b).

a) ROS production: human vs murine neutrophils

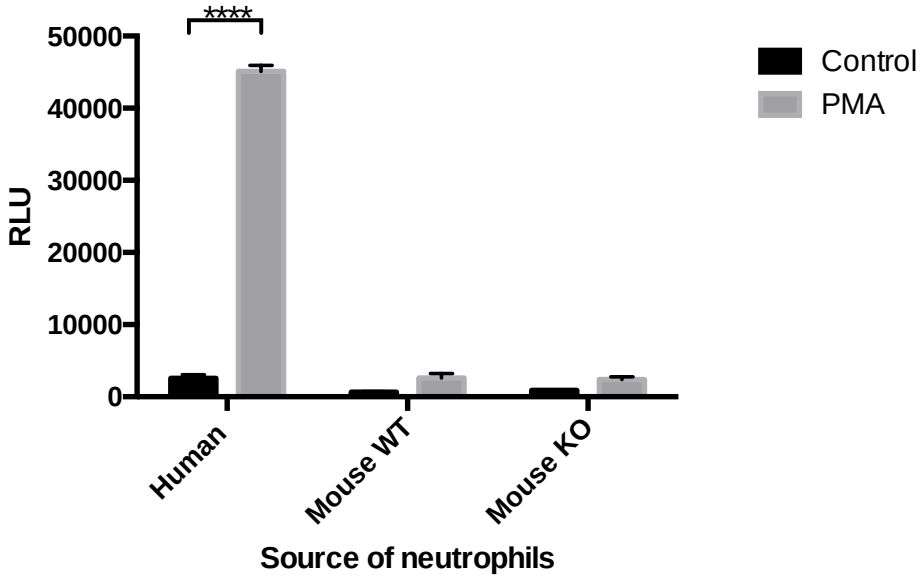

b) ROS production: wild type vs knockout

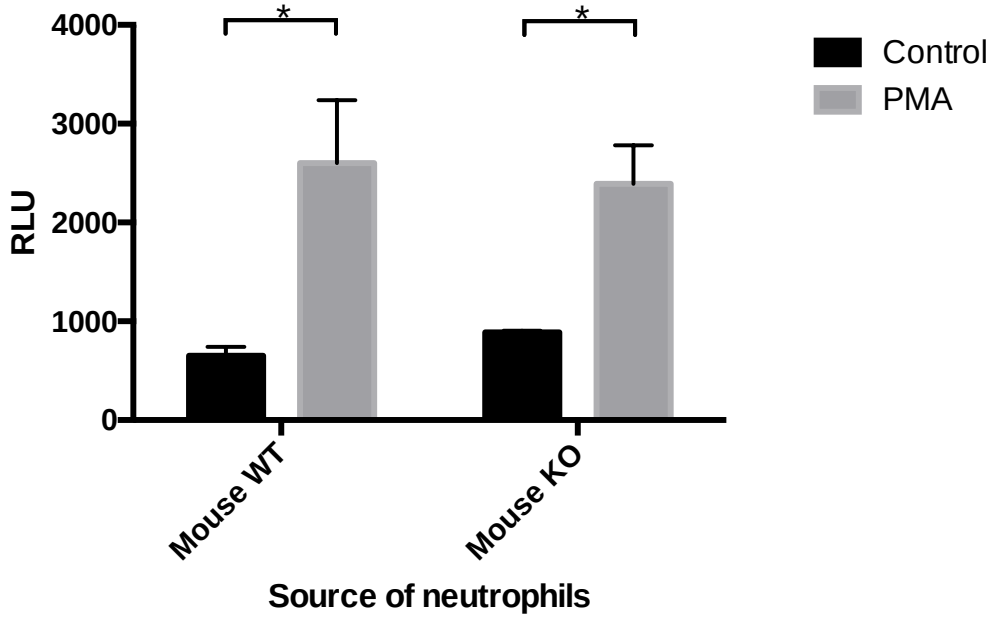

Figure 3.17: ROS production by bone-marrow derived murine neutrophils.
Analysis of peak ROS production by unstimulated and PMA-stimulated a) bone-marrow murine compared to human neutrophils and b) wild type (WT) compared with PAD4-knockout (KO) bone-marrow murine neutrophils. Values are expressed as relative light units (RLU) and as mean ± SEM. Statistical significance was calculated with Tukey's multiple comparison test (n= 3; *p<0.05, ****p<0.0001).

Although the difference with human and murine neutrophil responses was substantial, the bone marrow derived murine cells still exhibited a significant level of activation as a result of PMA stimulation. Such a differential response between the human and murine neutrophils may be due to the relatively immature nature of the murine bone marrow cells which are still in a naïve state compare with mature human peripheral blood neutrophils. In order to test this hypothesis, cells were exposed to the cytokine GM-CSF for 30 minutes before being stimulated with PMA in order to prime cells (section 2.3.3). Figure 3.18 shows there was no significant differences in term of ROS production between GM-CSF-treated and untreated cells for both human and mouse neutrophils.

a) ROS production: human vs murine neutrophils

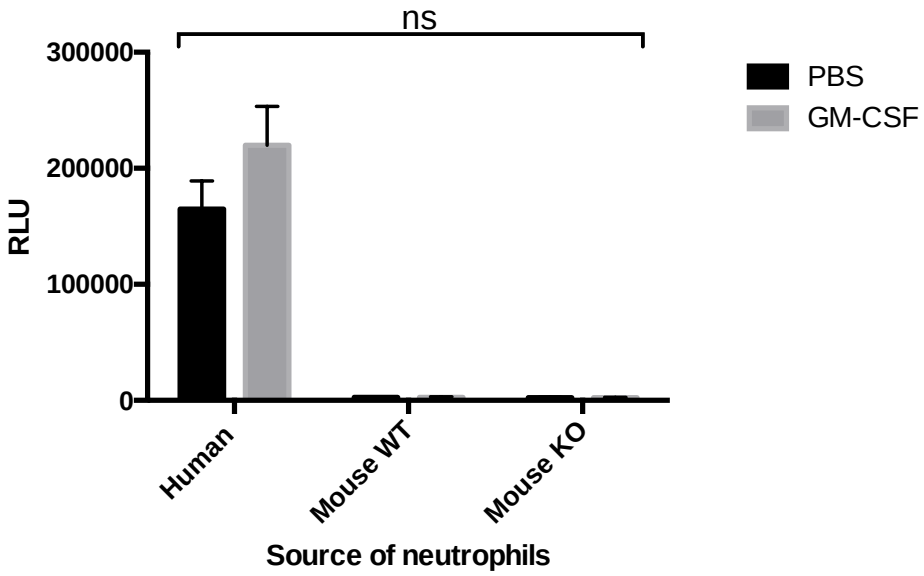

b) ROS production: wild type vs knockout

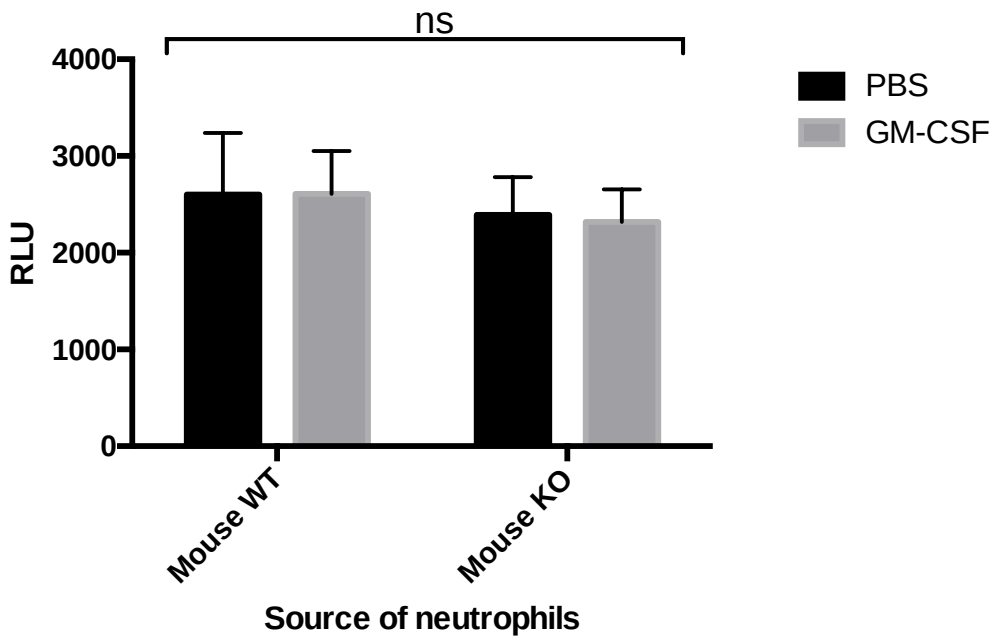

Figure 3.18: Primed ROS production in bone-marrow murine neutrophils.
Analysis of peak ROS production by PMA-stimulated and GM-CSF primed a) bone-marrow murine neutrophils compared with human and b) wild type (WT) compared with PAD4-knockout (KO) bone-marrow murine neutrophils. Values are expressed as relative light units (RLU) and as mean ± SEM. Statistical significance calculated with Tukey's multiple comparison test (n= 3; ns=non significant).

5.4.2 Identification of NET structures produced by bone marrow-derived murine neutrophils

Alongside ROS production, NET release by human and murine neutrophils was observed using fluorescence microscopy. Cells were exposed to PMA or were unstimulated for up to 5 hours and then stained with Sytox green prior to microscopic observation. Unstimulated neutrophils from both human and murine sources did not show the presence of NET structures at any time point (Figure 3.19 top row panel) and were therefore used as negative controls. PMA-stimulated human neutrophils presented few NET structures after 1 hour of exposure, while the amount of visible NETs notably increased at 3 and 5 hour time-points (Figure 3.19 left column). PAD4 knockout murine neutrophils presented a similar visual profile as compared with unstimulated cells up to 5 hours post-exposure to PMA (Figure 3.19 right column). In addition, relatively few NETs were visible in wild-type murine samples after 3 hours exposure to PMA and this number appeared to marginally increased at 5 hours post-stimulation (Figure 3.19 central column).

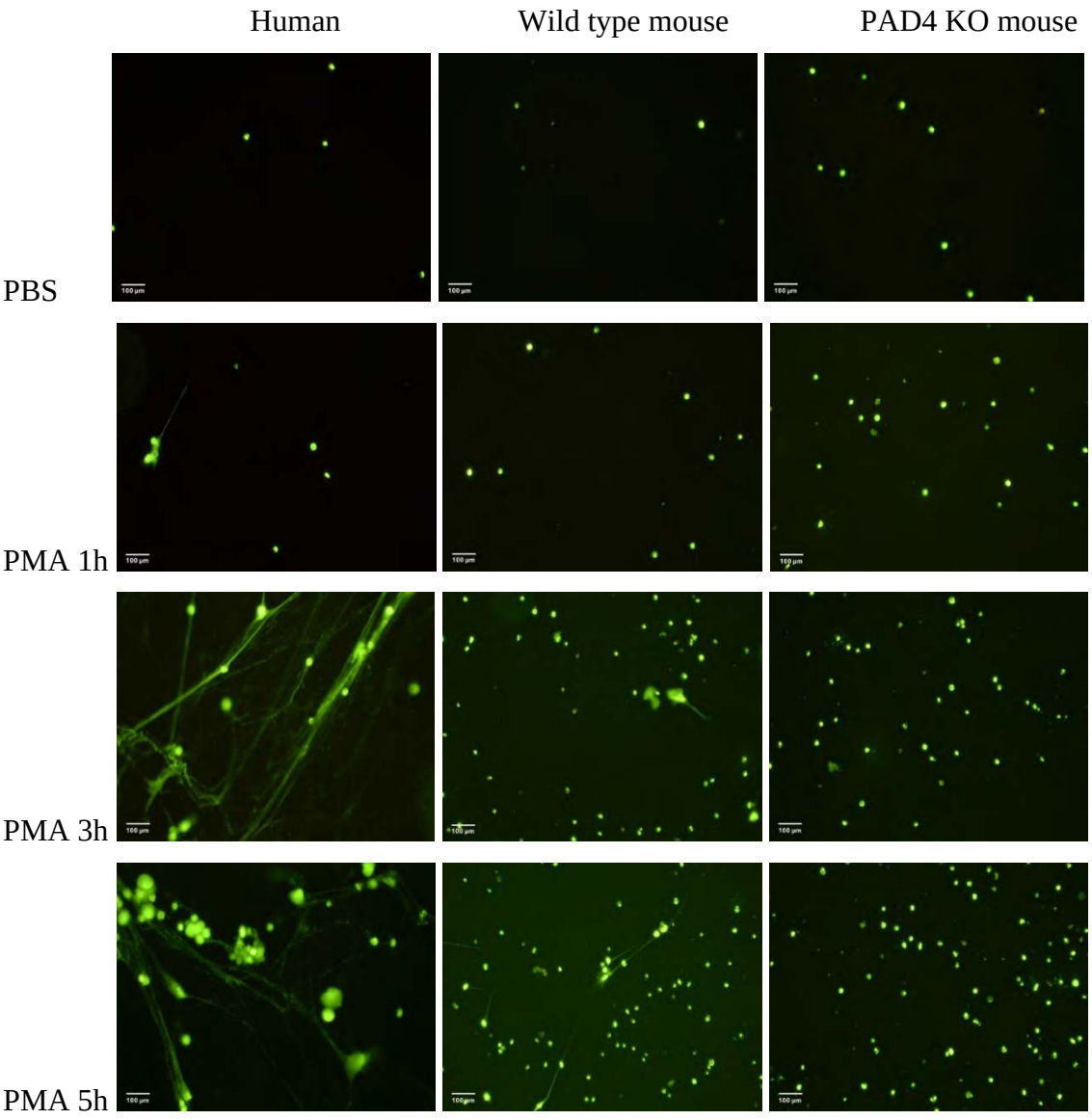

Figure 3.19: NET visualisation in human and murine neutrophils.
Images of neutrophils from human wild-type and PAD4 knockout (KO) mice were stimulated up to 5h with PMA or were unstimulated (PBS). NETs were stained with Sytox green® and visualised (X20 magnification) with an epifluorescence microscope. Images are representative of two independent experiments. Scale bar represents 100μm.

5.5 Discussion

HCA offers a powerful platform for observing NETs, their characteristic structures and all those features related to their formation, including nuclear decondensation and protein localisation; and provides a faster and more effective quantification technology for future studies of NET biology. Before applying HCA for neutrophil investigation, however, a reliable protocol needed to be developed. Several conditions and stimuli were therefore tested in the above experiments and results were considered for further protocol optimization.

PMA is the most commonly used stimulus in NET studies and the dose-response analysis reported here confirmed that concentrations above 6nM are required for activation of neutrophils. This suggests that concentrations below 6nM are not sufficient for triggering the PKC inflammatory pathway, which is in agreement with previous publications (Brinkmann *et al.*, 2004). However, exposure to 50nM PMA resulted in the most robust response for NET investigation and development of a HCA protocol. The highest PMA concentration was therefore used for subsequent analysis and for the evaluation of different environmental conditions on neutrophil responses.

NET production was negatively affected by decreased incubation temperature and decreased CO_2 levels, conditions which have been also identified in the subgingival environment in periodontitis patients. These data may indicate a possible failure of *in vivo* responses at epithelial or mucosal surfaces exposed to pathogen invasion and infection at the gingival margin. Lack of response by the immune system may allow microbial proliferation and the infection to disseminate more widely, representing a potential link to associated systemic diseases (Seymour *et al.*, 2007). Interestingly, the periodontal bacteria, *F. nucleatum* and *P. gingivalis,* induced a significant response in neutrophils in terms of ROS production. Both ROS

and NET production required longer exposure to bacteria compared with PMA and HOCl stimulation, however, this analysis is consistent with pathways usually triggered in neutrophils by bacteria (Prince *et al.*, 2011). This finding confirms that the accumulation and persistence of microbial plaque resulting from poor oral hygiene (Dahlén *et al.*, 1992) has the potential to trigger an inflammatory response. In this case ROS and NET production could contribute to periodontal tissue damage, as previously shown by our group (Matthews *et al.*, 2007b). Although *F. nucleatum* represents a good example of a physiological stimulus and is able to induce a notable response in term of ROS and NET production, bacterial DNA interferes with neutrophil staining and causes an elevated background in NET microscopic images potentially affecting future HCA results. Therefore, stimulation of neutrophils with bacterial components rather than whole bacteria may represent a solution for HCA. LPS extracted from *E. coli* was tested under different conditions and concentrations, notably the stimulation was effective for ROS production but, ineffective in inducing a significant amount of NET release despite numerous papers (Brinkmann *et al.*, 2004; Fuchs *et al.*, 2007; Yousefi *et al.*, 2009) publishing different findings. Concomitant dilutions of LPS in human plasma or bovine albumin failed to improve these neutrophil responses. The lack of NET production in neutrophils stimulated with *E. coli*-derived LPS may be attributed to the non-pathogenicity of the strain, however similar responses were identified upon stimulation with LPS from *P. gingivalis* (Figure 3.20).

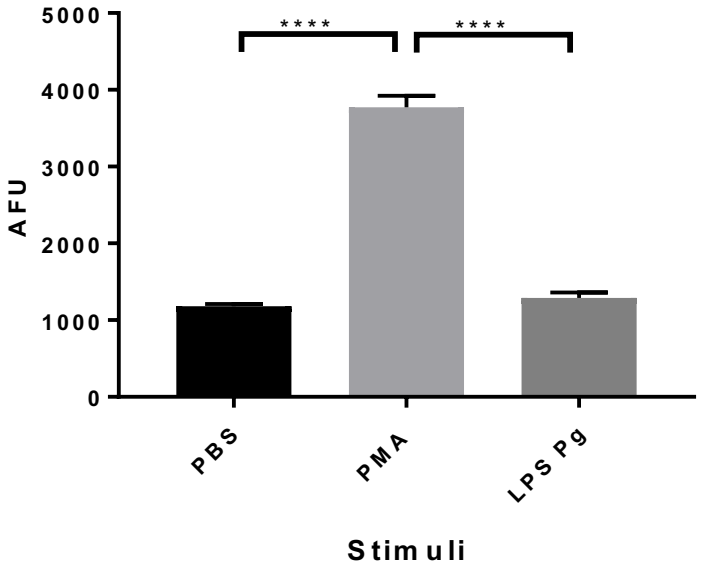

Figure 3.20: Neutrophil stimulation with *P. gingivalis*-derived LPS.
NET formation induced by P. gingivalis derived LPS (LPS Pg) and compared with unstimulated (PBS) and PMA-stimulated conditions. Values are expressed as arbitrary fluorescence units (AFU) and as mean ± SEM. Statistical significance calculated with Tukey's multiple comparison test (n= 3; ****p<0.0001).

Dental plaque is a complex bacterial biofilm which is able to trigger a substantial and sustained immune system response in humans (Peyyala & Ebersole, 2013). Therefore, to better mimic the *in vivo* situation, biofilm models developed by Millhouse *et al.*, (2014) were used here to invistigate the interaction between neutrophils and dental plaque. Both health and diseases relevant biofilm models were able to induce an inflammatory response in neutrophils in regard to ROS production, supporting previous study findings on the association between periodontal bacteria and neutrophil activation (White *et al.*, 2016a). The 7- and 10-species biofilms also demonstrated ability to induce NET release, although only at relatively low levels, indicating a possible NET degradation by bacterial DNase release, a well know virulence strategy used by bacteria in order to evade NET killing (Palmer *et al.*, 2012b).

Interaction between pathogenic biofilms and oral epithelial cells simulates local inflammation and cytokine release within the gingiva (Millhouse *et al.*, 2014; Peyyala *et al.*, 2012), the exposure of neutrophils to such an inflammatory environment was sufficient to trigger ROS production, although resulted in relatively low levels of NET formation. Results suggest NET activation may require a more complex pattern of stimulation or extended periods of stimulation. These data indicate *in vivo* NET production may act as a secondary antimicrobial strategy once other processes have failed.

Neutrophil exposure to elevated levels of calcium resulted in partial cell activation and increased basal levels of ROS production suggesting a possible role for ion levels present in periodontal pockets (Sewón *et al.*, 1995) in priming the immune system during periodontal inflammation. Surprisingly, magnesium supplementation had a priming effect on neutrophils which resulted in the release of an increased amount of NET-DNA in response to PMA. These results indicate a possible role for magnesium in neutrophil biology which requires further characterisation since altered magnesium levels have been associated with chronic diseases (Swaminathan, 2000).

Murine models are convenient and informative for studying disease pathogenesis and identifying new therapeutic approaches (Németh *et al.*, 2016), however, neutrophil biology differs between humans and mice. These differences were also identified in ROS production as described above. Priming bone marrow-derived murine neutrophils with growth factors/cytokines was also ineffective in inducing an adequate response to PMA as compared with human neutrophils. NET visualisation confirmed a considerably lower amount of DNA structures being released in response to PMA. This finding suggests the bone marrow neutrophils are unable to produce NETs as previously concluded by Martinelli *et al.* (2004) and their maturation requires a more complex combination of cytokines which has not been

determined yet. Notably, PAD4 knockout mouse were unable to produce NETs however prolonged the stimulation with PMA was. These data support previous findings which indicate that the activity of PAD4 is necessary for PMA-induced NET formation (Li *et al.*, 2010; Wang *et al.*, 2009). Murine models may help in better understanding intracellular pathways involved in neutrophil activation, however, currently they remain unsuitable for HCA application due to their different activation processes.

CHAPTER 4: PROTOCOL OPTIMISATION FOR HIGH-CONTENT ANALYSIS OF NETs

7.1 Background

Investigating biological samples using High Content Analysis (HCA) requires cell imaging for accurate and rapid examination. A key advantage of HCA is the ability to simultaneously observe thousands of cells, multiple samples and different conditions in a relatively short time span (Shariff *et al.*, 2010). However, imaging biological samples requires their fixation and appropriate staining to preserve their characteristic features (Corfe *et al.*, 2013). Neutrophils, and in particular NETs, have the potential to be studied using high-throughout analysis as previously discussed in section 2.6.4 of the Introduction, however, careful processing is required before imaging. Fixation protocols available for neutrophils currently involve several washing stages which may damage and alter the relatively fragile NET structures. This chapter aimed to establish the effects of different fixation protocols on NET samples and to identify optimal conditions to allow sample conservation while preserving NET-DNA structure integrity. The overall goal was to develop a suitable protocol for the application of HCA to NET samples.

7.2 Neutrophil cell densities for use in multi-well plate formats

Neutrophils are routinely imaged on glass slides by confocal microscopy. However, HCA technology requires the image acquisition from samples in microplate formats, therefore it was necessary to establish a suitable protocol to allow visualisation of cell and component using a 96-well plate format. Initially, neutrophil density studies were performed using multi-well plate formats. Neutrophils were seeded at 1,000, 10,000 and 100,000 cells/well in 24-, 48- and 96-well plate formats and stimulated as described in section 2.6.4. Neutrophil densities calculated according to manufacturer recommendation (Corning, 2010) are summarised in Table 4.1.

NETs were also qualitatively visualised using fluorescence microscopy following staining with Sytox green® (see section 2.6.6).

Multi-well plate format	Well surface area (cm^2)	Volume of medium/well (µl)	Cell seeding (cells/well)	Cell densities (cells/cm^2)
24-well	1.9	600	1,000	526
			10,000	5,263
			100,000	52,632
48-well	0.95	400	1,000	1,053
			10,000	10,526
			100,000	105,263
96-well	0.32	200	1,000	3,125
			10,000	31,250
			100,000	312,500

Table 4.1: Multi-well plate formats used and neutrophil seeding cell densities.

Images displayed in Figure 4.1a are representative of unstimulated and PMA stimulated neutrophils as seeded at different densities in a 24-well plate. Seeding 526 neutrophils/cm^2 resulted in relatively few cells being identifiable in each field of view for both PMA-stimulated and unstimulated conditions. Following 3 hours of PMA-stimulation, no NETs were observed. Seeding at 5,263 neutrophils/cm^2 resulted in more cells being visible and an average of 6 neutrophils could be seen in each field of view. Few short NET structures were also identified at 3 hours post PMA-stimulation. However, more numerous complex structures were visible with the higher seeding density (52,632 cells/cm^2). Representative images obtained by seeding 1,000, 10,000 and 100,000 cells/well in a 48-well plate are shown in Figure 4.1b. Detection and complexity of NET structures increased with increased cell density. The lowest density showed one NETosing cell in the field of view, while numerous NETosis events were observed in wells with higher densities (105,263 cells/cm^2). Similar results were observed in the 96-well plate

format with 1,000, 10,000 and 100,000 cells/well as shown in Figure 4.1c. The lower seeding density of 3,125 cells/cm^2 captured relatively few cells in NETosis, while, increasing the cell density resulted in increased number of NET structures visible within the field of view. In the PMA-stimulated 312,500 cells/cm^2 density wells NETs appeared as complex aggregate structures. Higher densities of 31,250 and 312,500 cells/cm^2, showed the presence of a relatively small amount of NET filaments also evident in unstimulated control cells. Low density seeding resulted in an uneven distribution of cells within the well surfaces, which presented many fields of view deprived of cells (black) when observed by fluorescence microscopy. The autofocus setting, operating during the HCA image acquisition phase, becomes inoperative on black fields of view producing faulty and unreliable data. Therefore, based on these results, neutrophils required seeding at a minimum of 100,000 cells/well in 24- and 48-well for NET detection, while 10,000 cells/well was the lowest threshold suitable for use in the 96-well plate format.

a) 24-well plate

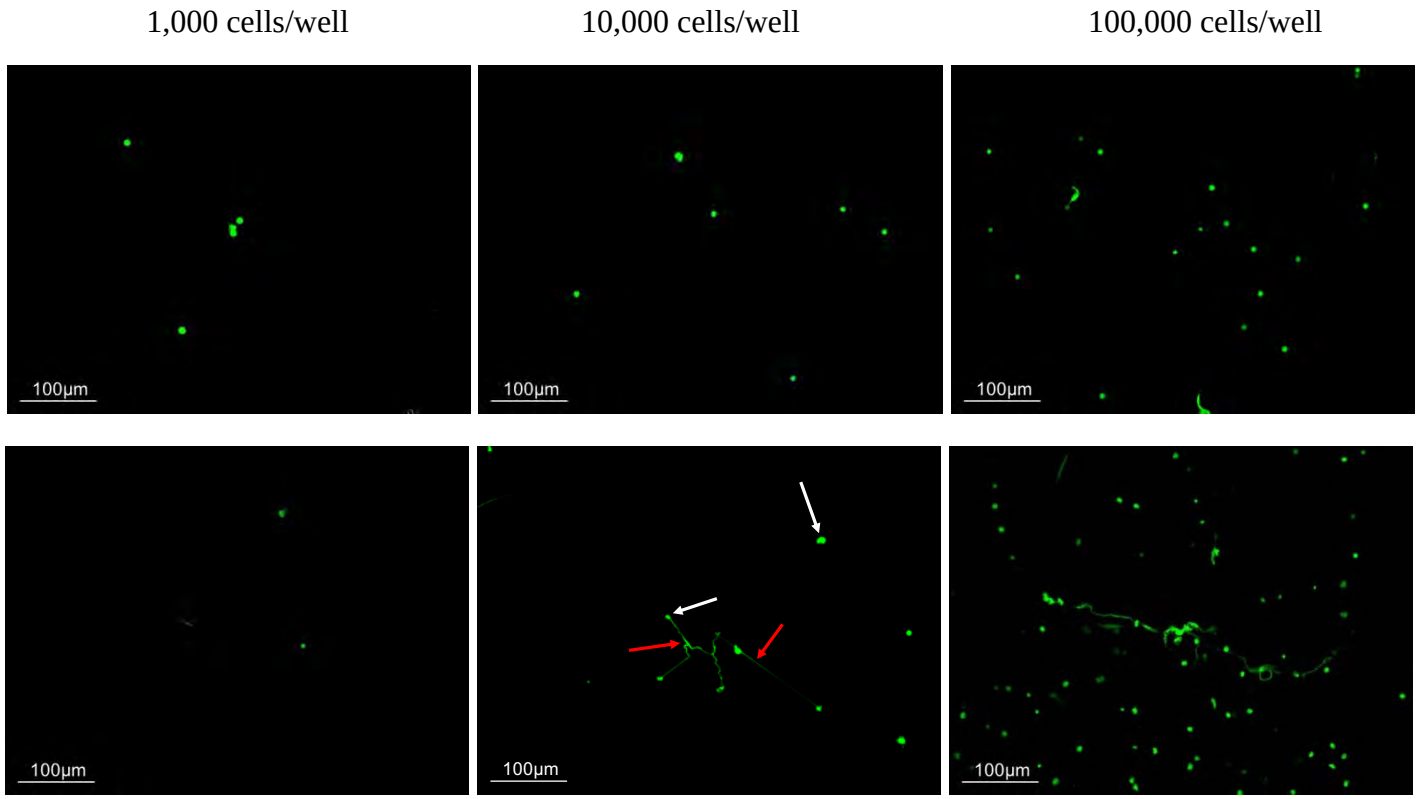

b) 48-well plate

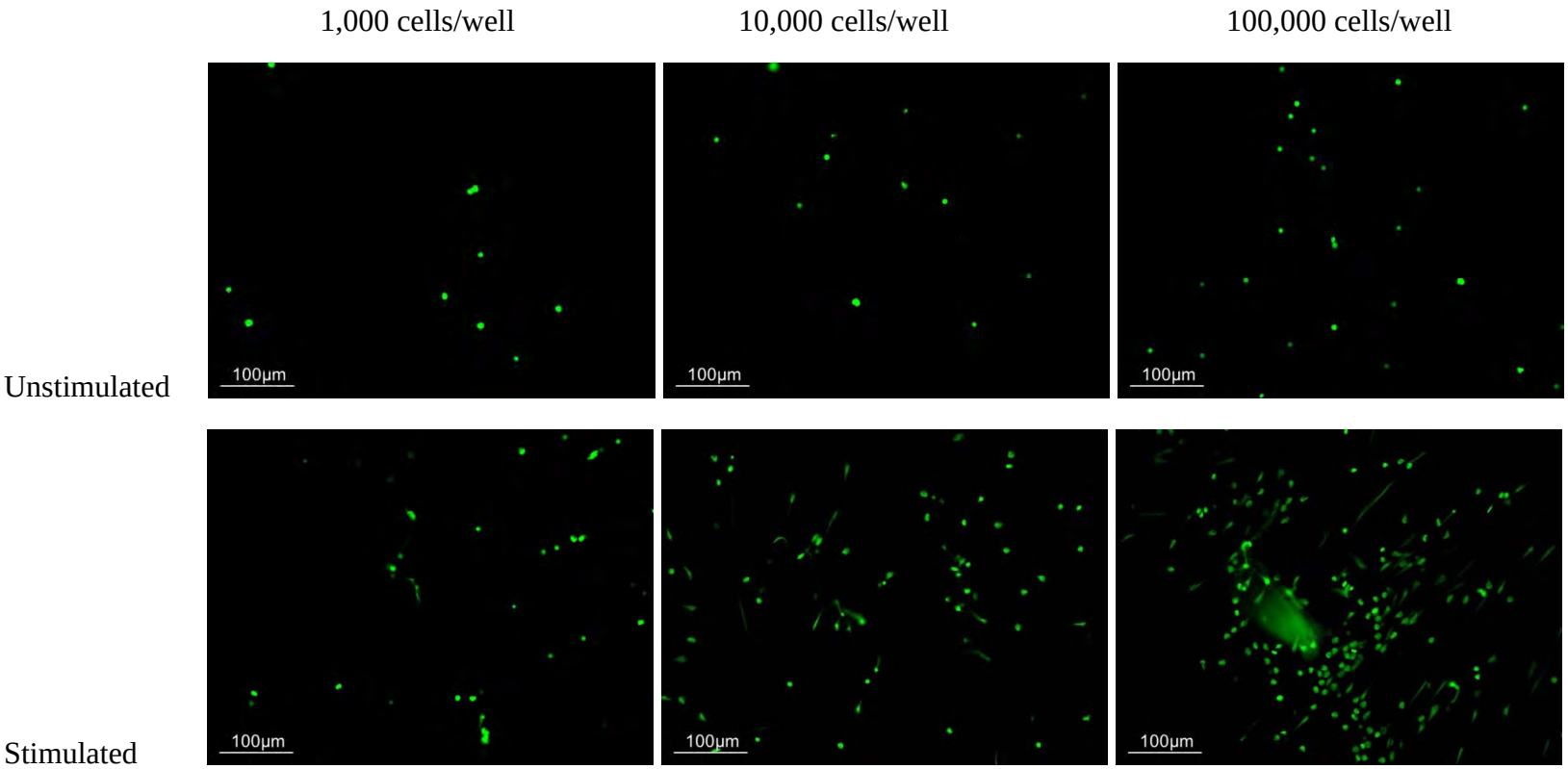

c) 96-well plate

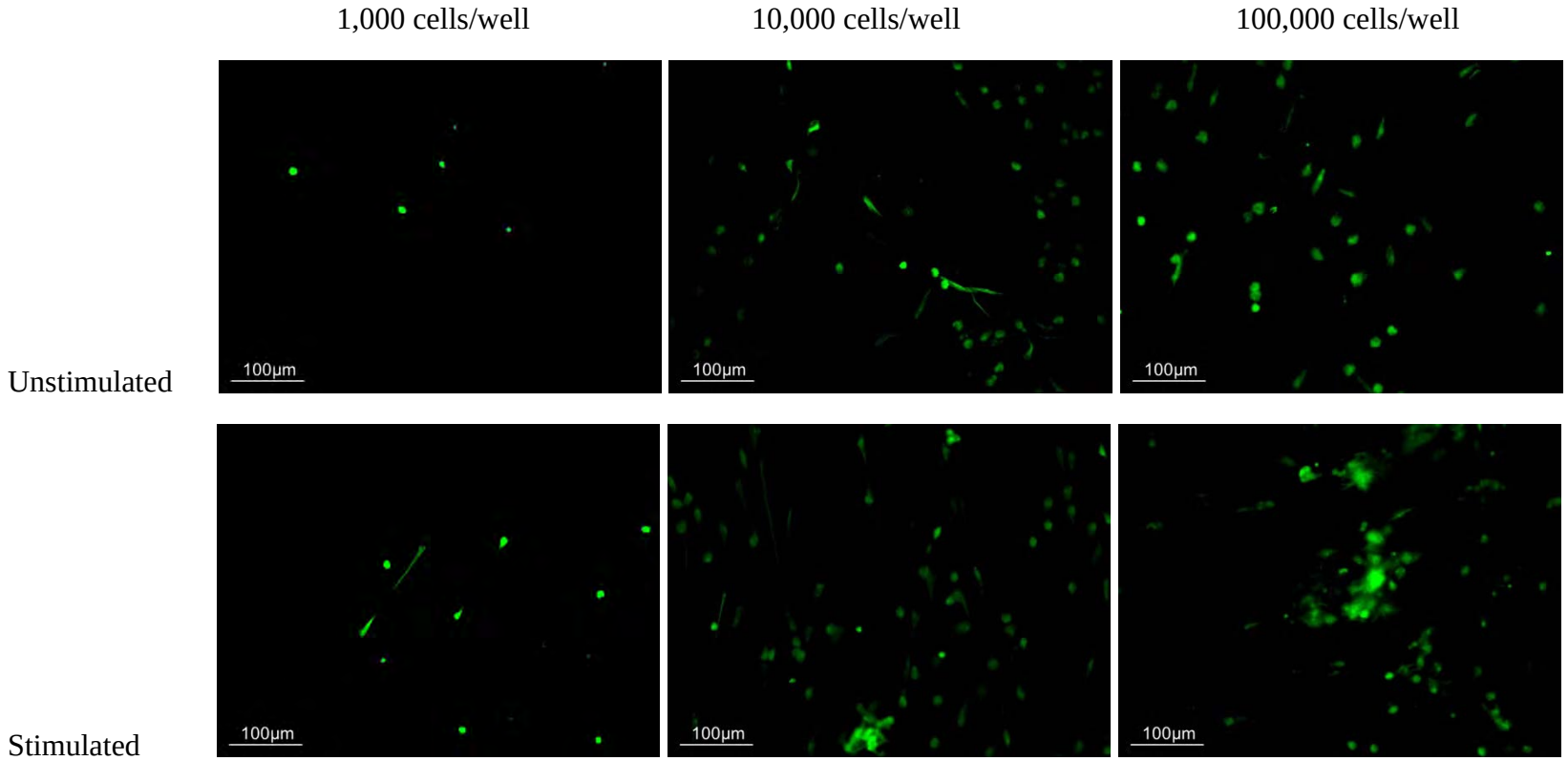

Figure 4.1: Studies for determination of neutrophil seeding densities for use in HCA in different multiwell plate formats.
Fluorescence microscopic visualisation of Sytox green® stained neutrophils seeded at 1,000, 10,000 and 100,000 cells/well unstimulated or stimulated with PMA for 3 hours in a) 24 well plate, b) 48-well plate and c) 96-well plate. Images are representative of 2 independent experiments. Representative neutrophils are indicated with white arrows and NETs with red arrows. Scale bars are shown.

7.3 Identification of a suitable NET fixation protocol for use in HCA

Commonly reported fixation protocols suitable for use with neutrophils involve numerous wash steps prior to image acquisition and analysis (Elliott *et al.*, 1995). The mechanical action applied during these wash steps can result in the loss of sample material, resulting in disruption of NET structures. The effects of these fixation procedures on NET images were analysed, and techniques optimised to minimise NET disruption.

7.3.1 Mechanical removal of NETs during fixation procedures

The mechanical forces of pipetting and washing samples during the fixation protocol may also affect NET structures. Images of NETs before and after the washing process were subsequently observed to identify the effect of washing on sample integrity. Following stimulation with PMA, NETs were fixed by the addition of 4% PFA solution directly into the well, and after 10 minutes incubation Sytox green® was added and 20 images per well, representing almost entirely the well surface, were captured with the ArrayScan (section 2.8.6). Afterwards, the media was removed, samples were washed twice with PBS and images were captured again. Figure 4.2 shows resulting images of neutrophils and NET structures following application of this technique. A considerable amount of NET production is apparent in images in Figure 4.2a as would be expected following PMA stimulation. A qualitative observation of the images indicated that NETs were evenly distributed and DNA filaments appeared of variable staining intensity, suggesting NETs are characterised by variable states of DNA condensation, as Pires *et al.* (2016) has already identified by atomic force microscopy. In Figure 4.2b images following the washing procedures are shown. This visibly contained fewer NETs suggesting most of NET structures were removed during the wash steps.

a)

Pre-wash 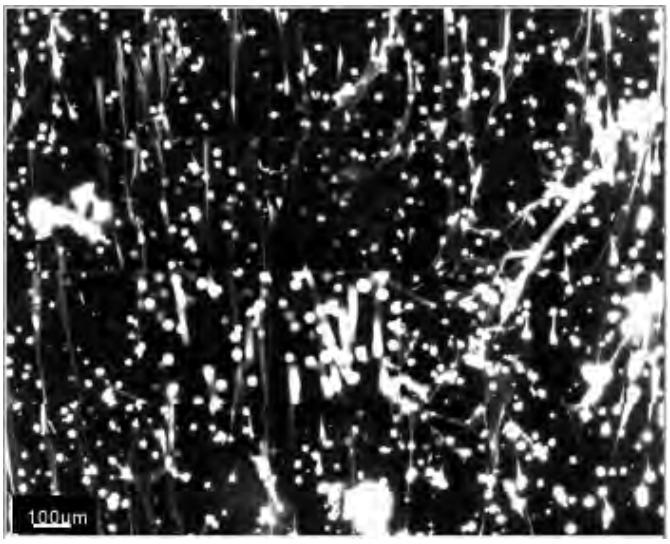

b)

Post-wash 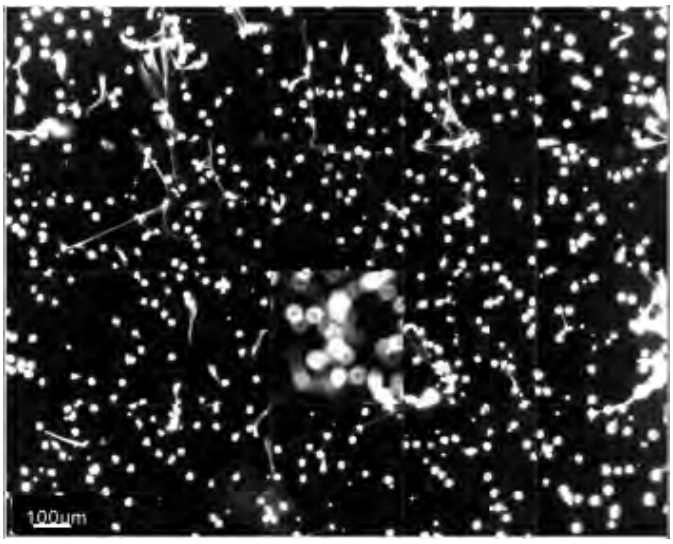

Figure 4.2: NET structures are removed during washing procedures.
Microscopic visualisation of Sytox green® stained neutrophils stimulated with PMA for 3 hours. Images are representative of 20 fields of view per well in a 96-well plate and were acquired before and after PBS washing. Results are representative of 2 independent experiments. Scale bars are shown in the lower left of image box.

7.3.2 Variations of fixation protocols

Accurate imaging of biological samples generally requires prior fixation. However, acquired images should provide an accurate representation for an effective application of HCA for NET studies. Hence, the mechanical alteration arising due to the fixation procedure needed to be minimised. For this reason, modifications of the fixation protocol for NETs were tested to identify the approach most likely to minimise loss of material. Neutrophils were stimulated with PMA or were unstimulated (controls) for 3 hours, prior to addition of Sytox green® and image captured by epifluorescence microscopy before and after the fixation procedures (see section 2.6.6.3). Three main steps of the protocol were evaluated and tested in different sequences, these were: i) centrifugation of samples for 10 minutes at 1800rcf; ii) addition of 4% PFA solution (see section 2.6.6.1); iii) media removal and subsequent PBS washing. Images of unstimulated and PMA-stimulated neutrophils before and after 5 different fixation approaches were compared with unfixed samples. Representative images for each combination of steps are provided in Figure 4.3. In Figure 4.3a post-incubation samples were firstly centrifuged, followed by PFA addition and PBS washing after 10 minutes incubation. The mechanical force of the centrifugation appeared to alter NET morphology and reduce the number of NETs when comparing images produced before and after processing. Images shown in Figure 4.3b were obtained by fixing samples with PFA initially, and then incubating for 10 minutes followed by centrifugation and washing with PBS. Unstimulated neutrophils prior to the fixation procedure demonstrated the presence of NET structures, which were absent in images post-fixation. However, compared with PMA-stimulation, the presence of NETs in unstimulated neutrophils was considered a basal level of cell activation and NET production, as expected in experiments using peripheral blood neutrophils which circulate the body at different stages of activation. Images of PMA-stimulated neutrophils showed a similar amount of NET staining before and

after fixation. In Figure 4.3c images are representative of the centrifuged sample, then subjected to medium removal, and finally fixed with PFA solution. PMA-induced NET organisation and direction appeared altered indicating that NET material may have been mechanically removed by the washing procedure. Images in Figures 4.3d) & e) provide representative results obtained without the inclusion of the centrifugation steps. In panel d) images represent samples treated with PFA for 10 minutes directly after the 3-hour stimulation, followed by media removal and PBS washing. Images pre- and post- fixation indicated NET structures were well preserved and the level of DNA staining appeared to be consistent in both images. In panel e) the medium was initially removed, followed by treatment with PFA for 10 minutes and PBS washing. PMA-stimulated neutrophils showed relatively high levels of NETs before the fixation procedure, however, after the procedure only few structures remained. Images showed in panel f) represent unfixed samples before and after centrifugation. Unstimulated neutrophils were not affected by the centrifugation step, however, PMA-stimulated samples showed an accumulation of DNA staining following this procedure. A qualitative evaluation of above fixation procedures suggested NETs were well preserved following the methods applied for images presented in Figures 4.3a) & d).

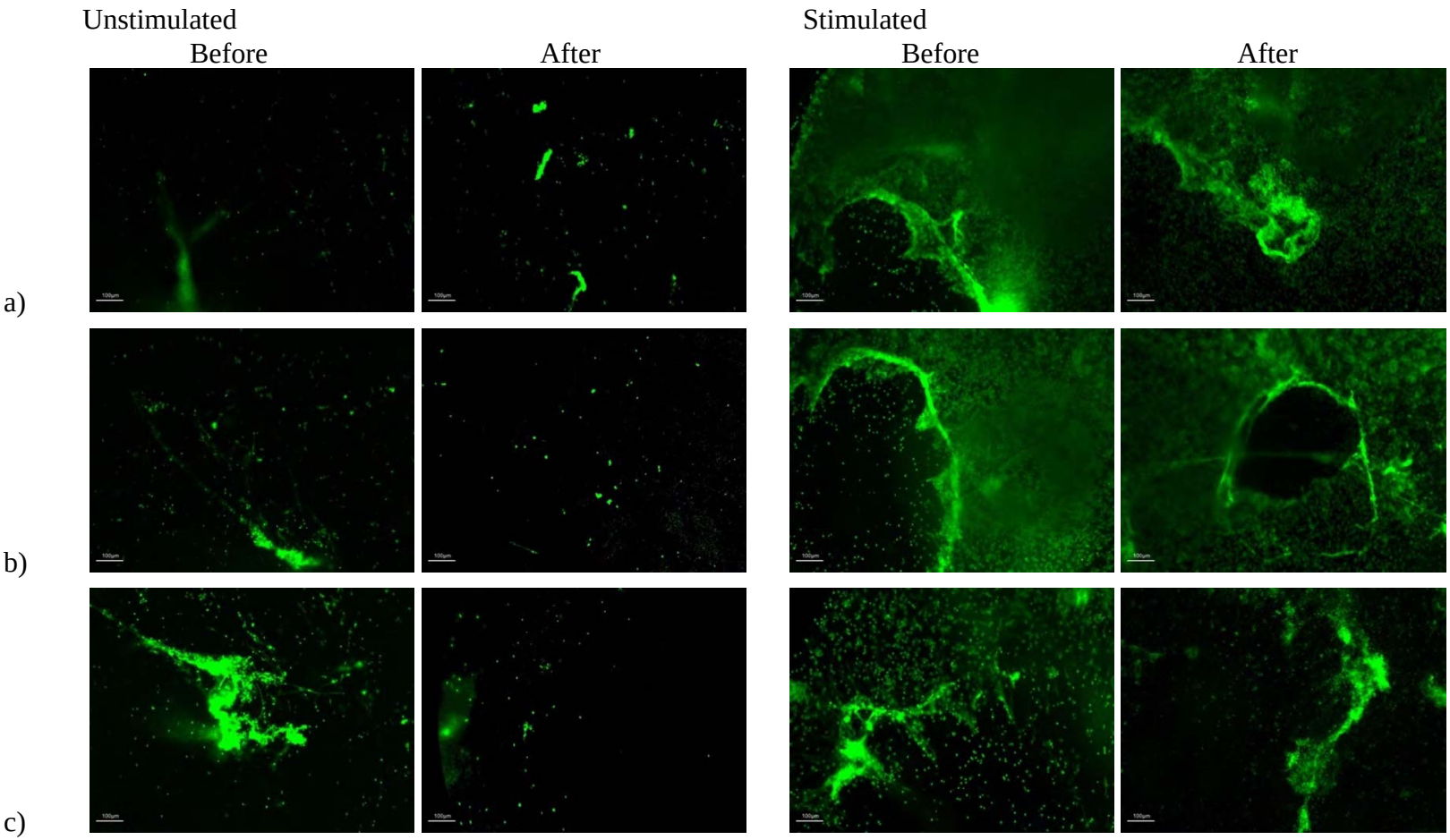
Unstimulated
Before
After
Stimulated
Before
After
a)
b)
c)

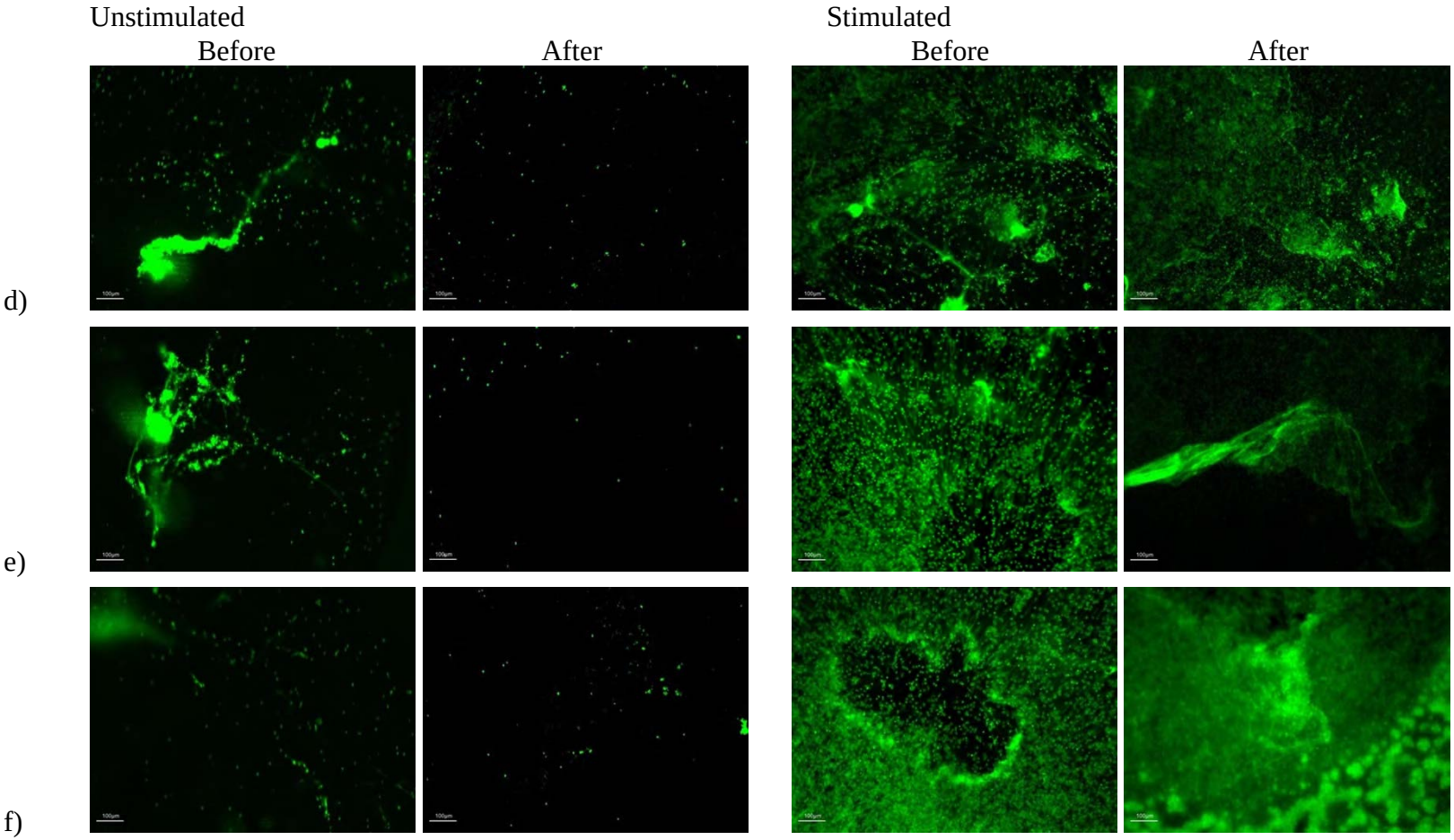

Figure 4.3: Assessment of fixation protocols for NET analysis.
Visualisation of Sytox green® stained neutrophils stimulated with PMA for 3 hours or unstimulated. Images were acquired before and after the fixation procedures as for: a) centrifugation, adding PFA and washing; b) adding PFA, centrifugation and washing; c) centrifugation, removing media, adding PFA and washing; d) adding PFA, removing media and washing; e) removing media, adding PFA and washing; f) centrifugation only. Results are representative of 2 independent experiments. Scale bars are shown.

7.3.3 Efficacy of the fixation protocol

In order to study neutrophil biology and specifically NETs using HCA, samples need to be transported for analysis to a distant site in Manchester (UK). Therefore, the fixation protocol was tested to evaluate its efficacy in preserving NET samples for up to 24 hours. Neutrophils were stimulated with PMA or remained unstimulated (controls) for 3 hours. Subsequently, samples were fixed (as described in section 2.6.6.2), Sytox green® was added to samples and images were captured under epifluorescence microscopy at 0 and 24 hours after fixation. Figure 4.4 shows representative images for each condition tested. Representative images of unstimulated neutrophils showed no visible difference between the two time-points analysed for both fixed and unfixed samples. However, while unfixed PMA-stimulated samples exhibited a higher NET presence, fixed PMA-induced NETs were unaffected in images after 24 hours, indicating the fixation protocol successfully preserved the samples for transport.

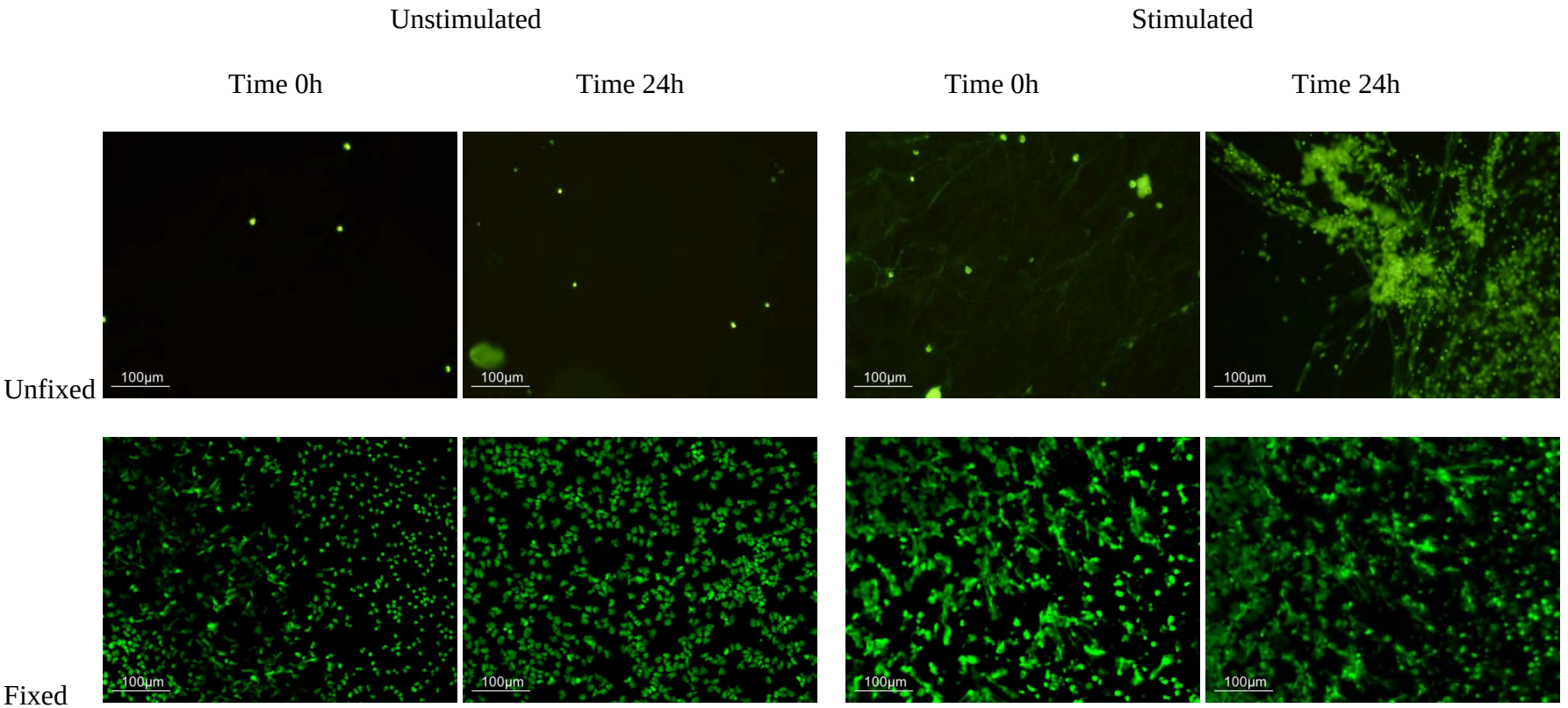

Figure 4.4: Efficacy of fixation protocol for preserving NET structures.
Visualisation of Sytox green® stained neutrophils stimulated with PMA for 3 hours or unstimulated (negative control). Images were obtained at time 0 and 24 hours after application of the fixation procedures or were left unfixed. Results are representative of 2 independent experiments. Scale bars are shown.

7.4 Poly-L-lysine effects on NET formation

Once released into the extracellular space, NET structures become suspended in the culture medium and may be subjected to damage during sample processing or handling, as demonstrated in the above experiments (section 7.3.1). To maintain the integrity of NET structures and have suitable material for HCA, neutrophil NET responses were assayed following poly-L-lysine coating of cultureware. Poly-L-lysine is a synthetic cationic polymer commonly employed in tissue culture to promote cell adhesion by electrostatically bonding with negatively charged cells and molecules (Khademhosseini *et al.*, 2004). Although poly-L-lysine has applications for the non-adherent neutrophil visualisation on glass slides (Fuchs *et al.*, 2007; Wang *et al.*, 2009; Yousefi *et al.*, 2008), there is currently a lack of knowledge on its effect on NET formation and NET structures. The following experiments aimed to analyse how the pre-treatment of cultureware with poly-L-lysine influenced neutrophil behaviour and in particular NET release.

A layer of poly-L-lysine was deposited on the surface of each well prior to neutrophil seeding and stimulation (section 2.6.2). NETs were then produced and visualised as described in sections 2.6.4 & 2.6.6.3 respectively. Figure 4.5 provides images of unstimulated and stimulated neutrophils obtained with or without pre-treatment of wells with poly-L-lysine. A PMA dose-response stimulation was also applied to identify a potential threshold for neutrophil activation in conjunction with the polymer. Images revealed a visible increase in NETs numbers which correlated with PMA dosage for both untreated and poly-L-lysine treated well conditions. However, in poly-L-lysine pre-treated plates, NETs appeared to accumulate as flat structures on the bottom of the well, while without the adhesive agent NETs appeared as three-dimensional structures distributed across several focal planes of the well.

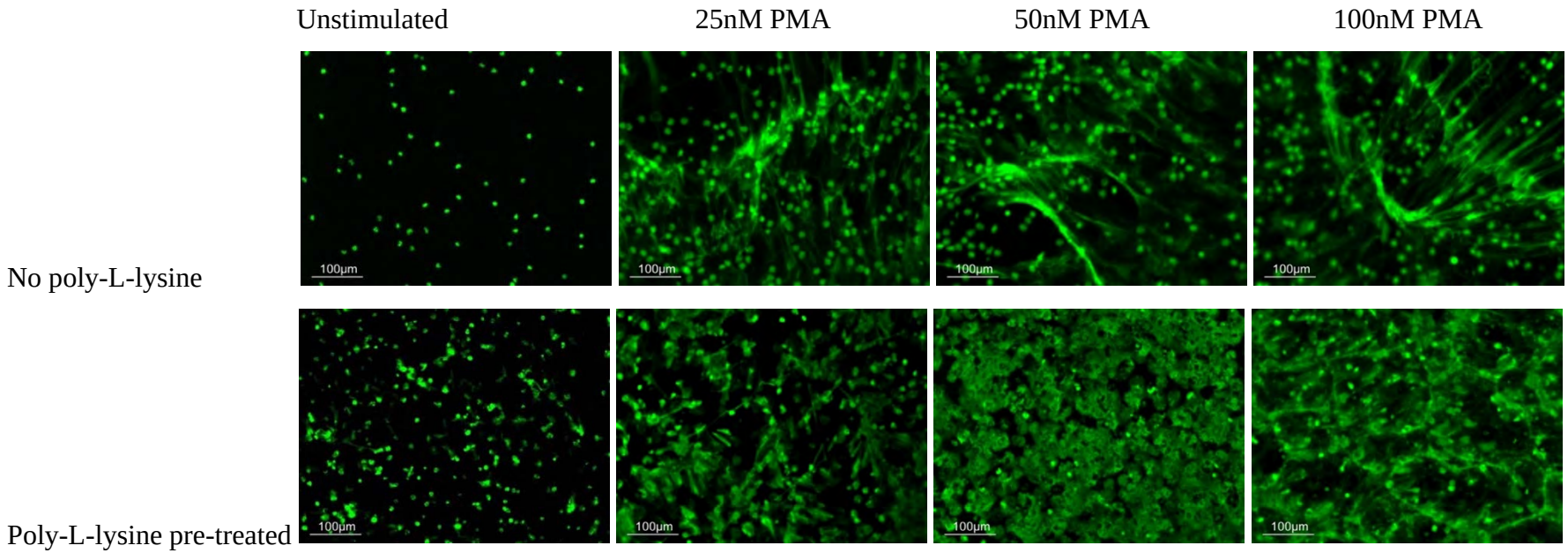

Figure 4.5: Effect of poly-L-Lysine pre-treatment of cultureware for NET visualization.
Visualisation of Sytox green® stained neutrophils stimulated with 25, 50, 100nM PMA for 3 hours or unstimulated (negative control). Comparison of untreated 96-well plate with poly-L-lysine pre-treated cultureware. Results are representative of 3 independent experiments. Scale bars are shown.

Inhibition of NET formation in poly-L-lysine pre-treated cultureware was further investigated through fluorometric quantification (section 2.6.5). As previously described, neutrophils were stimulated with three concentrations of PMA for 3 hours. Results obtained from both poly-L-lysine pre-treated and untreated cultureware showed a similar trend towards dose-dependent NET production as determined by fluorometric analysis (Figure 4.6). However, the NET-DNA quantified in poly-L-lysine pre-treated wells appeared reduced by approximately 5-fold for 25 and 50nM PMA and 3.5-fold for 100nM PMA treatment compared with NET-DNA generated in poly-L-lysine untreated wells. This was in contrast to the NET visualisation data, which indicated a similar amount of NETs were produced in poly-L-lysine pre-treated cultureware compared with poly-L-lysine untreated wells, and can be attributed to the differences in the methodologies utilised for NET analysis.

a) No poly-L-lysine

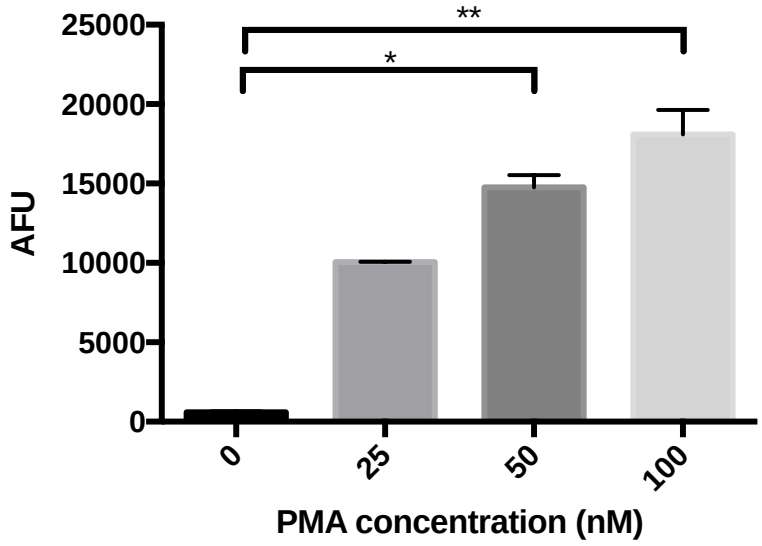

b) Poly-L-lysine pre-treatment

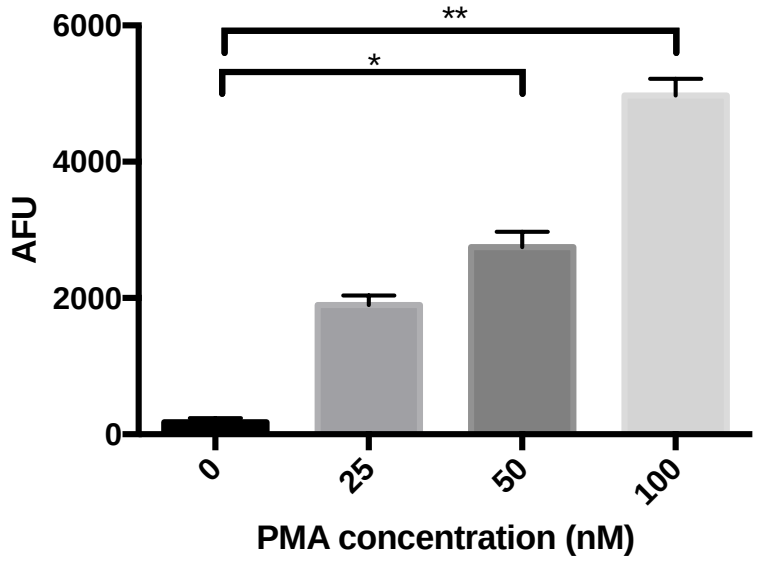

Figure 4.6: Effects of poly-L-lysine pre-treatment on NET quantification.
Dose-response with fluorometric quantification of PMA stimulated NET production in neutrophils upon incubation in poly-L-lysine pre-treated and untreated 96-well plates. Values are expressed as arbitrary fluorescence units (AFU) and as mean ± SEM. Statistical significance calculated with Uncorrected Dunn's test (n= 3; *p<0.05, **p<0.01).

7.5 Comparison of different DNA staining approaches for image analysis of NETs

Sytox green® is a DNA-binding fluorescent dye non-permeant to the outer cell wall. Once bound to DNA, its fluorescent signal is enhanced up to 500-fold and is visualised as a bright green stain (Suzuki *et al.*, 1998). Sytox green® only stains neutrophil nuclei following cell wall damage, such as during cell death. Hoechst, conversely, is a fluorescent DNA dye which can penetrate the cell wall and stain nuclei of viable neutrophils, and is visualised as a blue fluorescence signal (Lakowicz *et al.*, 1997). However, the Hoechst signal has lower intensity compared with Sytox green® stain, therefore it may be unsuited for staining of NETs, given their decondensed structures. In order to determine the difference between the two types of fluorescent staining for assaying NET production, unstimulated and PMA-stimulated neutrophils were observed using the ArrayScan (section 2.8.6). Samples were excited at wavelengths of 360nm and 472nm and visualised using a 490nm and 520nm filter, for Hoechst and Sytox green® stained DNA, respectively. Imaging with the brightfield filter was concomitantly employed to ensure the presence of cells within the analysed fields. Unstimulated neutrophils are shown in Figure 4.7a. Both Hoechst and Sytox green® appeared to stain nuclear DNA, however, approximately 20% of unstimulated nuclei were visible with a Sytox green® signal, while 100% were visible using the Hoechst stain. Conversely, in images of PMA-stimulated cells (Figure 4.7b) many NET filaments were visible with Sytox green® staining while relatively few NETs were visible using the Hoechst stain. Although the dyes have different properties, it appears that both have potential application for HCA of neutrophils. In particular, Hoechst appears appropriate for studying nuclear activation states and morphology in viable or NETosing cells, while Sytox green® is appropriate for NET structure

analysis. However, potentially, for the HCA platform, both dyes could be applied concomitantly for an accurate and more complete sample characterisation.

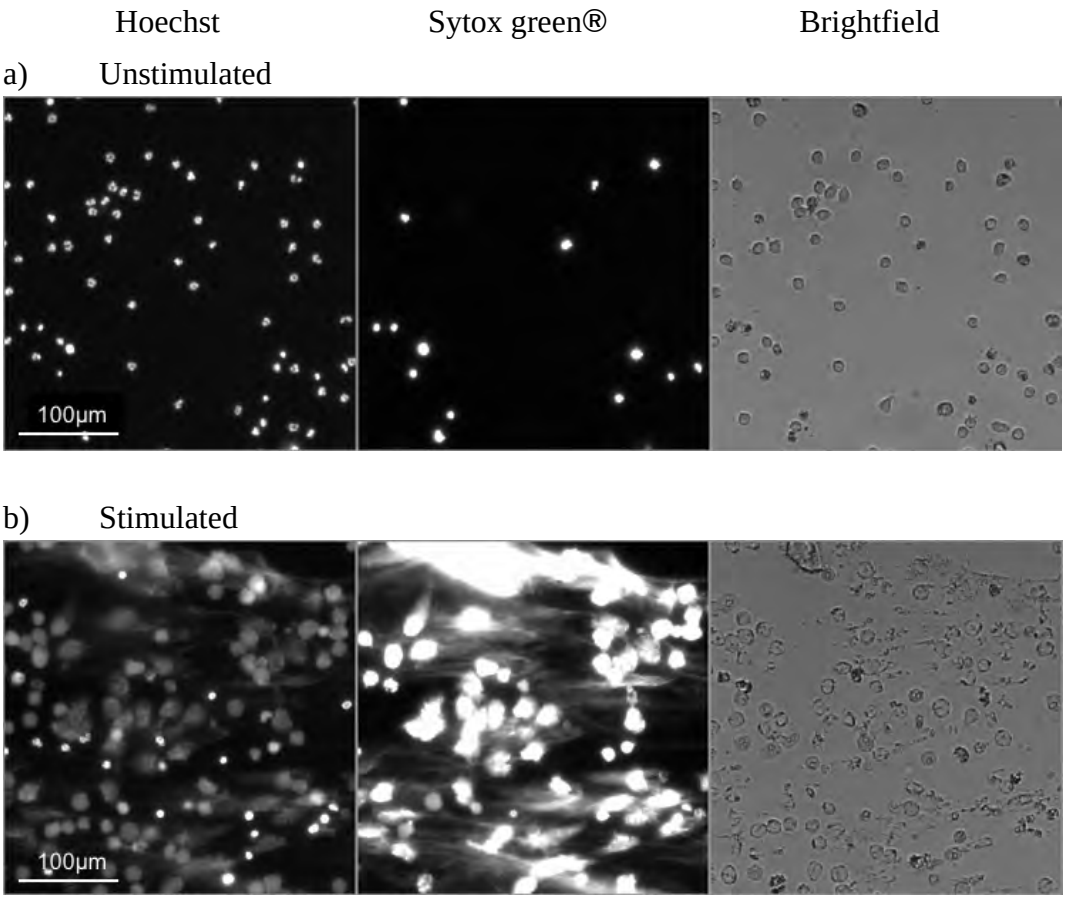

Figure 4.7: Hoechst and Sytox green® neutrophil staining.
Visualisation of Hoechst and Sytox green® stained neutrophils a) stimulated with 50nM PMA for 3 hours or b) unstimulated (negative control). Unprocessed images represent Hoechst staining on left panel, Sytox staining in the middle panel and brightfield channel on the right panel. Images are representative of 3 independent experiments. The scale bar shown is representative for all images.

7.6 Discussion

In order to develop a suitable protocol for studying NETs using HCA, neutrophils needed to be appropriately prepared and fixed for preservation and transportation. An appropriate fixation protocol, therefore, needed to be identified in which biological material especially the fragile NET structures was not lost.

Initially, neutrophil cell density was investigated in different multi-well plate formats to identify the minimal seeding density for each format required for even cell distribution and substantial NET detection. The results suggested that neutrophil densities in 24-well plate had to be equal to or above 50,000 cells/cm^2 to obtain a suitable amount of NET forming cells within the well. Similar to the 24-well plate format, 48- and 96-well plates required a relatively high density of cells, respectively 100,000 cells/cm^2 and 310,000 cells/cm^2 to avoid black fields of view with no cells and also ensure abundant NET production. These data also indicate that NET formation may be connected to neutrophil cell density which suggests a potential mechanism of cross-talking among neutrophils in order to regulate NET production, which may, in turn, regulate the antimicrobial potential, as has already been proved for other immunity events (Bennouna *et al.*, 2003). Once the adequate cell density for NET formation was established for the 96-well plate format, this was employed for all subsequent experiments.

The washing stages required in the fixation procedures may affect sample integrity due to their mechanical actions and disruption of NET structures, as has also been identified for NETs using atomic force microscopy (Pires *et al.*, 2016). Results from images captured after washing procedures indicated that the majority of NETs were indeed removed by the washing step. Clearly, NETs require careful handling and less aggressive fixation protocols in order to preserve their structural integrity for downstream analysis. Variations in the fixation protocol

were tested to identify which step most significantly affected the integrity of NET structures. All assayed protocol variations were analysed included the addition of PFA, a washing step and a centrifugation step, but they were applied in different orders. The majority of the protocols applied resulted in the loss of sample material or apparent alterations in NET filament structure. Following assessment of the results of these experiments, it was concluded that the most appropriate protocol consisted of careful addition of PFA directly onto stimulated NETs, thus the fixation agent directly interacts with NETs, potentially protecting them from further mechanical disruption. While such a fixation method may be sufficient for general NET visualization, an additional centrifugation stage for immune-staining applications is appropriate to ensure all NET material sediments.

The modified fixation protocol was further tested before application to NET samples. Images of NETs were captured immediately following fixation and once again 24h later to identify whether the fixation was able to preserve NET structures over this time period. The protocol resulted in effective preservation of NETs compared with unfixed samples which were exposed to the stimulating agent for prolonged time and, hence, lead to cell damage. Indeed, images of unfixed unstimulated neutrophils after 24h demonstrate minimal levels of spontaneous NET production.

The major issue encountered during the fixation procedure consisted of the loss of sample material, therefore, an adhesive agent was tested to overcome this. Poly-L-lysine acts as an adhesive layer which aids cells to settle and bind to cultureware. NET experiments performed using poly-L-lysine treated cultureware indicated that the polymer had a negative effect on NET formation. While images of PMA-stimulated neutrophils showed NET formation in the presence of poly-L-lysine treatment, NET quantification data demonstrated a considerable lower amounts of NET-DNA compared with experiments performed in untreated cultureware.

Imaged NETs demonstrated relatively flat structures formed on the bottom of the well in poly-L-lysine pre-treated plates, supporting the assumption that they adhere to the cultureware. Data suggest that poly-L-lysine is unsuitable for use in fluorometric quantification of NETs, possibly due to the interaction between the positive charge on the polymer structure and the negative charges associated with NET-DNA (Liu *et al.*, 2001), causing NETs to adhere to the layer of lysine and consequential inaccurate quantification. As fluorometric NET quantification has been used in future experiments as a positive control for NET formation, poly-L-lysine was deemed unsuitable for further application.

NET filaments are relatively long and thin structures comprised of decondensed DNA which renders them difficult to identify with most commercially available staining approaches. The most common fluorescent dye used for NET assays is Sytox green® (de Buhr & von Köckritz-Blickwede, 2016; Fuchs *et al.*, 2007; Palmer *et al.*, 2012a) as its signal increases up to 500 fold once bound to DNA. Thus, NETs appear as bright green structures in contrast to a black background 'speckled' with green cells. However, Sytox green® is unable to stain live or undamaged cells since the dye does not permeate the neutrophils outer cell wall. Another fluorescent DNA dye was tested alongside Sytox green® to investigate both cells and NETs in unfixed neutrophil samples. Notably, neutrophil nuclei and their features were more clearly visible using Hoechst staining. Unstimulated neutrophils exhibited their characteristic multi-lobulated nuclear shape which was subsequently lost as a consequence of NET production. Furthermore, PMA-stimulated nuclei appeared of lager size and spherical with decreased intensity compared with unstimulated nuclei, a characteristic which has already been attributed to the early stages of NET formation and successfully employed for the quantification of NETosing cells (Brinkmann *et al.*, 2012; Zhao *et al.*, 2015). Conversely, Sytox green® only stained a small percentage of nuclei and in particular those with damaged outer cell walls.

However, PMA-stimulated NETs were clearly visible as bright filamentous structures upon Sytox green® staining, while Hoechst staining only highlighted faded structures. The two staining approaches require different excitation/emission filters, which allows their simultaneous application, without the risk of interference, broadening the amount of detectable features in a single HCA readout. While Hoechst has application for studying nuclear activation and nuclear morphologic changes in different conditions, simultaneous Sytox green® staining will serve better for studying NET structures and their release.

CHAPTER 5: OPTIMISATION AND VALIDATION OF HCA PARAMETERS FOR NET ANALYSIS

5.1 Background

Many publications on NET analysis and their characterisation as an anti-microbial strategy utilise qualitative microscopic image analysis (Brinkmann *et al.*, 2004; Fuchs *et al.*, 2007). Furthermore, studies that aim to elucidate the intracellular processes leading to NET release and the nature of its DNA backbone utilise similar approaches (Aleyd *et al.*, 2014; Yousefi *et al.*, 2009). Three main theories, described in more details in section 2.2.3 of Introduction, regarding the signalling regulation of NET generation, have been proposed. The first two, introduced respectively by Fuchs *et al.* (2007) and Yousefi *et al.* (2009), describe NETs as nuclear DNA-made structures released following an ultimate fate of programmed cell death or as mitochondrial-derived ETs which leave the cells in a vital state. A third mechanism as been proposed for vital NETosis which suggested a-nuclear although functional neutrophils are left upon release of nuclear NETs in vesicles in response to *Staphylococcus aureus* (Pilsczek *et al.*, 2010).

As previously described (section 2.6), frequently used NET assays are based on the identification of their components, including DNA or NET-related proteins, with levels determined by immunostaining, immunoblotting or ELISA (Palmer *et al.*, 2012a; Urban *et al.*, 2009; Wang *et al.*, 2009). These methods are relatively low-throughput, time consuming, expensive and currently there is lack of consistency in findings in the field. Subsequently, in recent years several alternative approaches have been developed for the high-throughput analysis of NETs (Brinkmann *et al.*, 2012; Gavillet *et al.*, 2015; Moussavi-Harami *et al.*, 2016; Zhao *et al.*, 2015) (as described in section 2.6.4).

In this chapter, HCA parameters were explored and optimised in order to develop an innovative high-throughput approach for NET analysis. The aim was to develop an automated technique

that utilises quantitative imaging for the monitoring of neutrophils, their nuclei and NET-related responses. Furthermore, one of the key advantages of HCA compared with traditional assays is the potential for combining readouts acquired for protein staining intensity, subcellular protein localisations and independent cell information (Drake *et al.*, 2009). Image analysis is subsequently performed using a bioinformatic software with built-in algorithms for a diverse range of biological applications (Ghosh *et al.*; Mandavilli; Miller *et al.*). Notably this technique has not previously been applied for neutrophils or for NET analysis.

Research areas covered in this chapter include: i) the optimisation of pre-existing HCA algorithms and their application in NET analysis; ii) the development of specific algorithms for NET analysis; iii) the use of HCA for analysis of intracellular proteins in H400 cells and neutrophils; and iv) the validation of HCA for NET quantification against previously established NET analysis assays.

5.2 Adapting pre-determined algorithms for NET analysis

For appropriate image interpretation and, therefore, accurate HCA of NET structures, the settings of two algorithms, suitable for the analysis of extruded DNA material, already built-into the HCS Reader software (Cellomics, ThermoFisher) were optimised and tested. NETs were generated as described in section 2.6.4 and fixed as per section 2.6.6.2. Neutrophil nuclei and NET structures were stained with Hoechst and Sytox green® as previously described in section 2.8.1. Images were acquired using the ArrayScan equipment (Cellomics, ThermoFisher) and analysed by the HCS Reader software (sections 2.8.7) applying the Compartmental Analysis and the Tube Formation algorithms.

Images of neutrophils and NET recognition by each algorithm are illustrated in Figure 5.1. The Compartmental Analysis algorithm was designed to monitor the presence and the movements

of macromolecules in and between subcellular locations (as described in the Thermo Scientific Cellomics® Compartmental Analysis guide). The Compartmental Analysis algorithm operates by identifying neutrophil nuclei as circular objects which correspond to pre-determined parameters for both size and intensity. Subsequently the object identification settings were adapted to size and staining intensity based on neutrophil nuclear features, to enable the algorithm to recognise nuclei as small lobulated objects (coloured in pink in Figure 5.1a). Rejection criteria were established for the exclusion of cell debris or aggregates or objects located at image edges. Algorithm settings were adjusted to create a relatively wide ring around nuclei (shown as green circles in Figure 5.1a) and to quantify the extracellular DNA within that space (shown coloured in blue in Figure 5.1a).

The Tube Formation algorithm was designed to analyse cellular structures which exhibited tube-like shapes (from the Thermo Scientific Cellomics® Tube Formation guide). The algorithm identifies neutrophil nuclei as circular objects in the image and selects as valid those presenting extruded DNA (circled in blue in Figure 5.1b). Selection and rejection criteria were optimised as previously described above for the Compartmental Analysis algorithm, with the exception of rejecting every nucleus lacking DNA extrusions. Subsequently the Tube Formation algorithm identifies, encloses and analyses extrusions of DNA in the surrounding extracellular space (shown in orange, green, purple and yellow in Figure 5.1b).

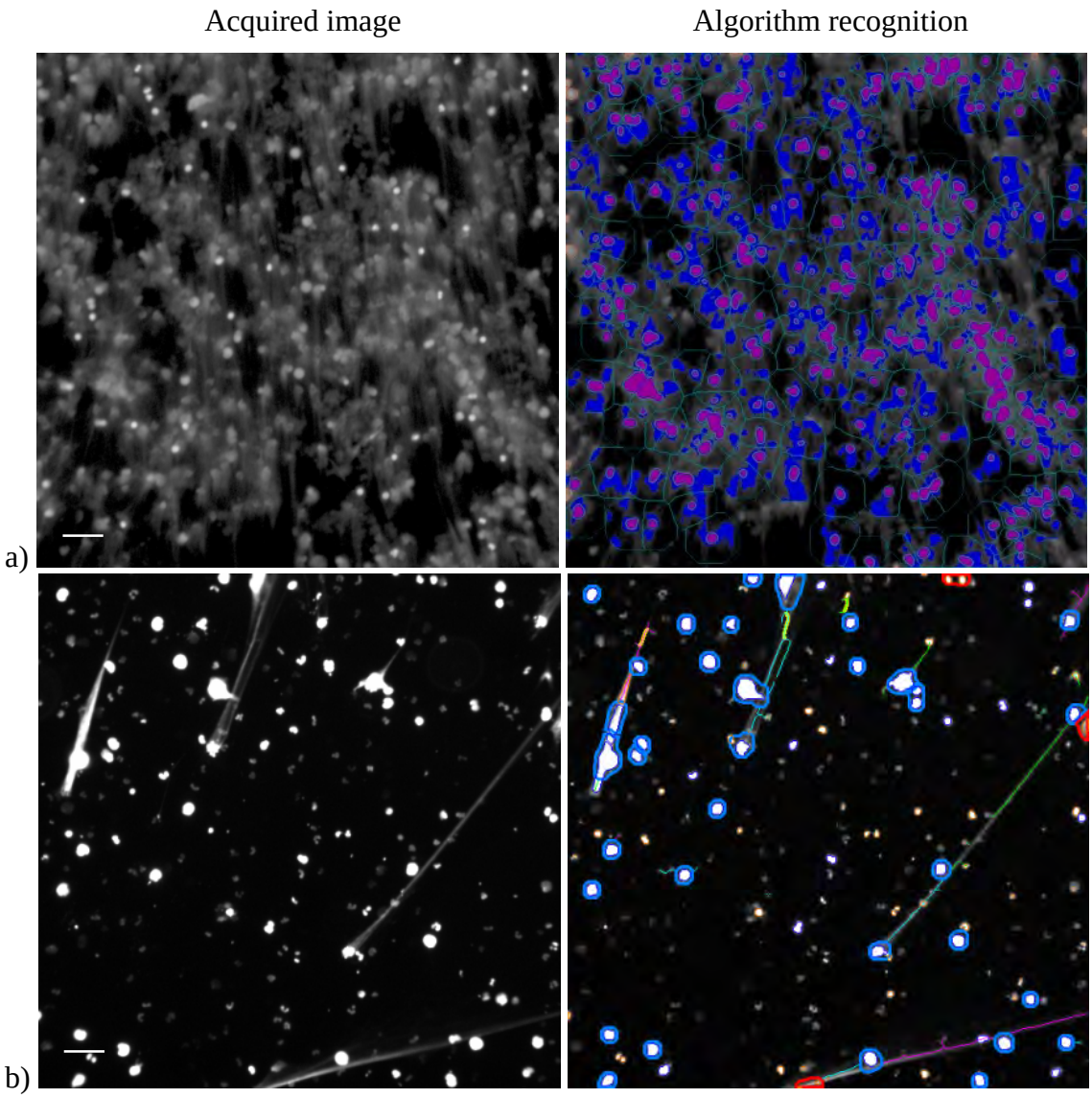

Figure 5.1: HCA algorithm recognition of neutrophils and NETs.
Images of PMA-stimulated neutrophils stained with Hoechst and Sytox green® acquired using the ArrayScan. a) Application of the Compartmental Analysis algorithm for the identification of neutrophil nuclei (purple) and NETs (blue). b) Application of the Tube Formation algorithm for the identification of neutrophil nuclei (blue circles) and NETs (green, orange, yellow and purple). Scale bar represents 200μm and applies for all images.

5.2.1 Application of the Compartmental Analysis algorithm for NET analysis

The Compartmental Analysis algorithm allows extracellular DNA to be identified in the area surrounding the nuclei of activated neutrophils. The algorithm, optimised as described above, was applied to the analysis of NETs. Neutrophils were seeded at 10,000, 100,000 and 500,000

cells/well in a 96-well plate and stimulated with PMA and HOCl or were unstimulated (negative control) for 3 hours (as described in section 2.6.4). HCA was performed as described in section 2.8.3 and the Compartmental Analysis algorithm was applied to determine the average DNA staining registered within the annular detection area around neutrophil nuclei, also termed 'ring' in the Thermo Scientific Cellomics® Compartmental Analysis guide. Results presented in Figure 5.2 indicate that the Compartmental Analysis algorithm identified a significant increase in NET areas in HOCl-stimulated neutrophils compared with unstimulated controls. However, the increase in the NET area was only detected with 100,000 and 500,000 cell/well densities, and not in the 10,000 cells/well of neutrophil densities. Interestingly, among the HOCl-stimulated neutrophil densities the Compartmental Analysis algorithm identified significant differences in detected NET areas. Seeding neutrophils at 10,000 cells/well resulted in significantly smaller area of NETs detected than in the 100,000 and 500,000 cells/well seeding. These data suggest the application of the Compartmental Analysis algorithm was limited to HOCl-stimulated neutrophils. However, this approach was ineffective in quantifying PMA-induced NETs (Figure 5.2). Other limitations of this software algorithm for NET detection were related to the lack of detection of the early time-point of NETosis and those NETs which extended outside the detection area or ring (annular extracellular region around nuclei).

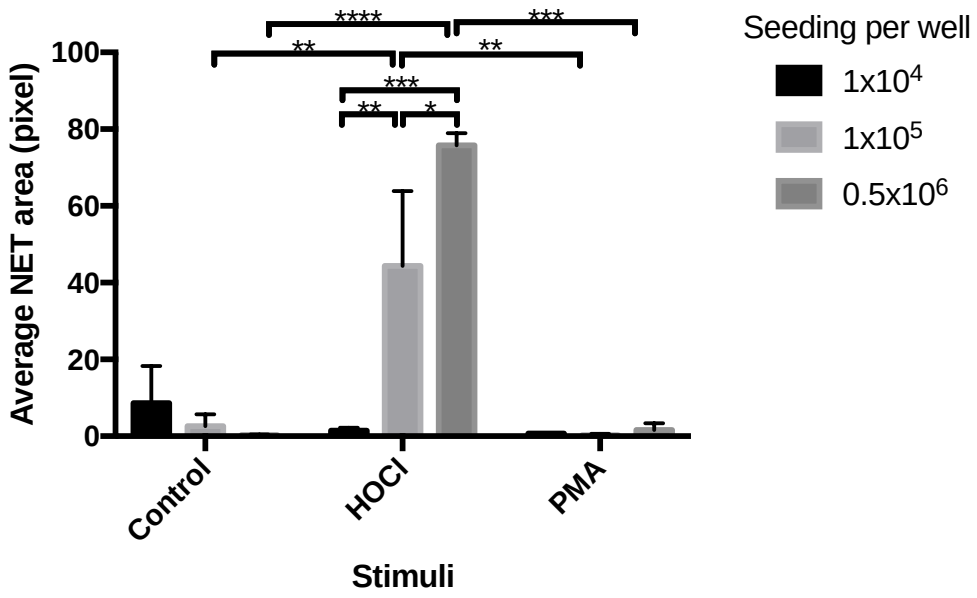

Figure 5.2: NET area variation in stimulated neutrophils calculated using the Compartmental Analysis algorithm.
Average of NET area detected by the Compartmental Analysis algorithm for the HCA of neutrophils seeded at 10,000, 100,000 and 500,000 cells/well and stimulated for 3 hours with PMA, HOCl or unstimulated controls. Values are calculated as pixels of staining, are expressed as mean ± SEM and statistical significance was calculated with Sidak's multiple comparison test (n=6; *p<0.05, **p<0.01, ***p<0.001, ****p<0.0001).

5.2.2 Application of the Tube Formation algorithm for NET analysis

The Tube Formation algorithm, optimised as described above (section 5.2), was applied for the quantification and the characterisation of NETs. Neutrophils were seeded at a range of densities of between 1,000 and 100,000 cells/well in a 96-well plate and stimulated with PMA or were unstimulated for up to 3 hours as described in section 2.6.4. HCA was performed as described in section 2.8.3 and the Tube Formation algorithm was applied for analysing the number of extruded NETs and their average size, including total NET covered area and filament length, under each experimental condition. Interestingly, the Tube Formation algorithm identified a relatively high amount of NETs which were relatively large in size in unstimulated neutrophils, identifying no differences compared with PMA-stimulated neutrophils at all 5 densities studied

(Figure 5.3a, b and c). The NET count was higher and structures were longer and wider in the 10,000 cells/well seeding conditions compared with the other 4 seeding densities. This result suggested that neutrophils and NETs at this density assume a conformation and orientation which resulted in high values of NET units and size as registered by the Tube Formation algorithm. Furthermore, PMA-induced NETs are not always associated with intact nuclei, since nuclear decondensation and loss of the nuclear membrane occur during NETosis, and in this may, therefore, may escape algorithm recognition. These limitations suggest the Tube Formation algorithm was not suitable for NET quantification.

a)

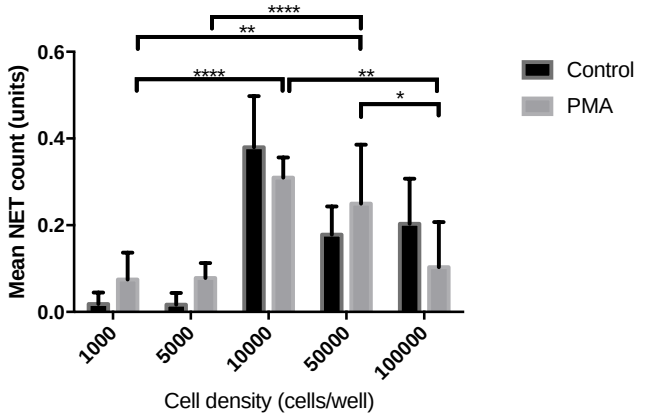

b)

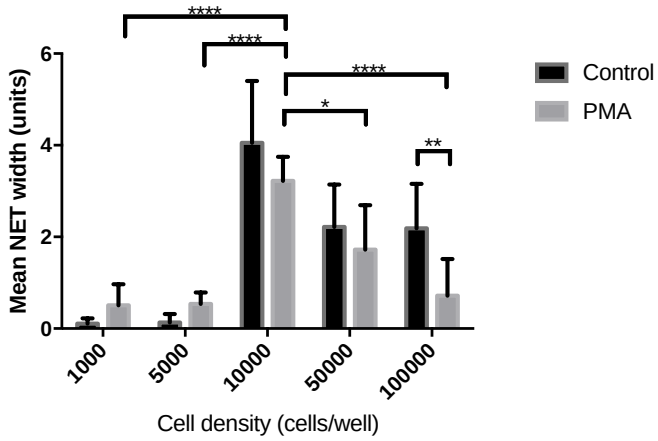

c)

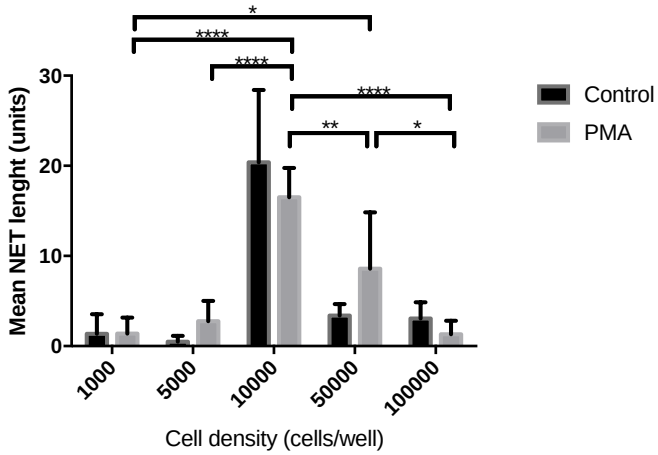

Figure 5.3: NET analysis as determined by the Tube Formation algorithm.
HCA of neutrophils seeded up to 100,000 cells/well stimulated with PMA or unstimulated (control) for 3 hours. Analysis of a) NET numbers, b) average NET width and c) average NET length calculated by the Tube Formation algorithm. Values are expressed as units of staining and as mean ± SEM and the statistical significance was calculated with Sidak's multiple comparison test (n=2; *p<0.05, **p<0.01, ***p<0.001, ****p<0.0001).

5.3 Development of bespoke algorithms for NET analysis

Alongside adapting the pre-existing algorithms of the HCS Reader software, two more algorithms were developed specifically for NET analysis. These algorithms, were termed “NET Detection” and “Nuclear Decondensation”, and were developed for the simultaneous monitoring of two fundamental characteristics of NETosis, respectively the release of DNA in the extracellular space and the preceding nuclear decondensation. In Figure 5.4 images of unstimulated and PMA-stimulated neutrophils are shown. Samples were isolated and stimulated as described in sections 2.1 & 2.6.4, and were unfixed in order to monitor cell integrity during NET formation. Hoechst and Sytox green® were used to stain the nuclear and extracellular DNA respectively (section 2.8.1). Images for Hoechst and Sytox green® staining were acquired independently by the ArrayScan (Figure 5.4a & b) and merged using different colorations (Figure 5.4c) by the HCS Reader software (sections 2.8.7). Unstimulated neutrophil nuclei, visible by Hoechst staining, exhibited a characteristic multilobulated shape and bright staining intensity indicating nuclei were in a compact state, while no NETs were visible by Sytox green® staining and only a few cells appeared to have a compromised plasma membrane. Conversely, in neutrophils stimulated for 3 hours with PMA considerable numbers of nuclei had lost their original morphology and exhibited an enlarged rounded conformation while the staining intensity visibly decreased compared with cells which had compact nuclei. Staining using Sytox green® indicated numerous NET filaments were visible in association with decondensed nuclei.

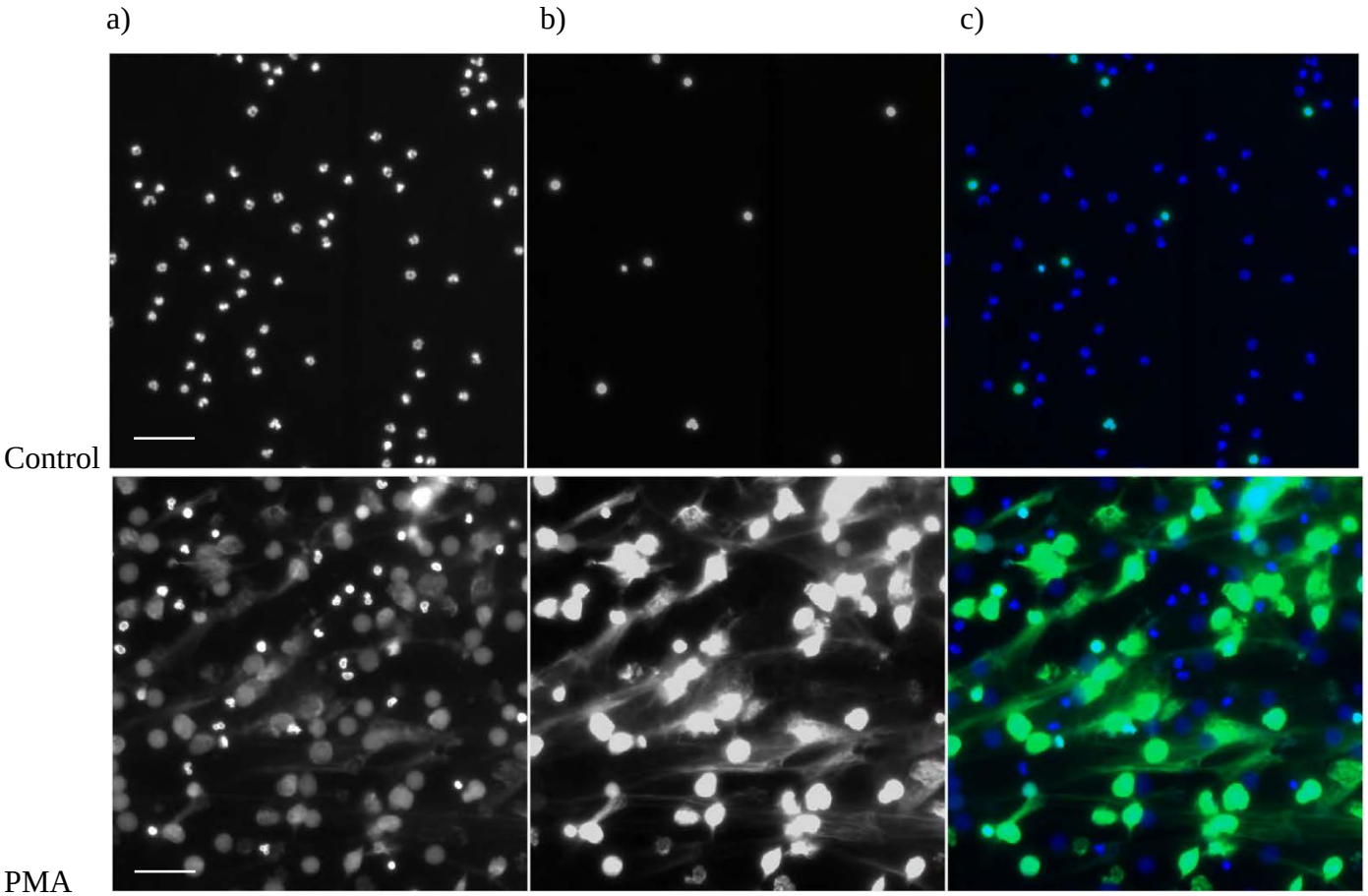

Figure 5.4: Images of nuclear decondensation related to NET formation.
Images acquired for HCA of neutrophils unstimulated or stimulated with PMA for 3 hours. Nuclei in compact and decondensed states are visible in a) following Hoechst staining, while compromised cells and NETs are visible in b) following Sytox green® staining. Images of Hoechst and Sytox green® are merged in c) respectively in blue and green. Images are representative of 3 independent experiments. Scale bars represent 200µm and apply for all images.

5.3.1 Application of the NET Detection algorithm

The NET Detection algorithm was also developed to provide information on NET length and area of extension. Neutrophils were stimulated with PMA or were unstimulated (controls) for up to 3 hours as described in section 2.6.4. Fixed samples were stained with Sytox green® and analysed by HCA (section 2.8.3). The NET Detection algorithm was designed to identify DNA staining areas in neutrophil images which corresponded to pre-determined parameters of size and intensity (Appendix I). Object identification settings were adapted to size and staining intensity based on NET-DNA features, therefore, the algorithm recognised all small lobulated objects as nuclei which were then rejected in order to exclude the nuclear DNA of intact cells from the analysis (circled in orange in Figure 5.5a). Algorithm settings were adjusted to identify filaments of extracellular DNA (green areas in Figure 5.5) and to provide information on area, size and intensity of those sections. Data shown in Figure 5.5.5b indicated that the NET Detection algorithm identified time-course increases in NETs in PMA-stimulated neutrophils at 3 and 4 hours, while the controls maintained values close to zero throughout the 4 hour period. Additional data on PMA-stimulated neutrophils indicated a time-dependent increase in NET area detected (Figure 5.5c), suggesting these structures increase in length and complexity as the stimulation is prolonged.

a)

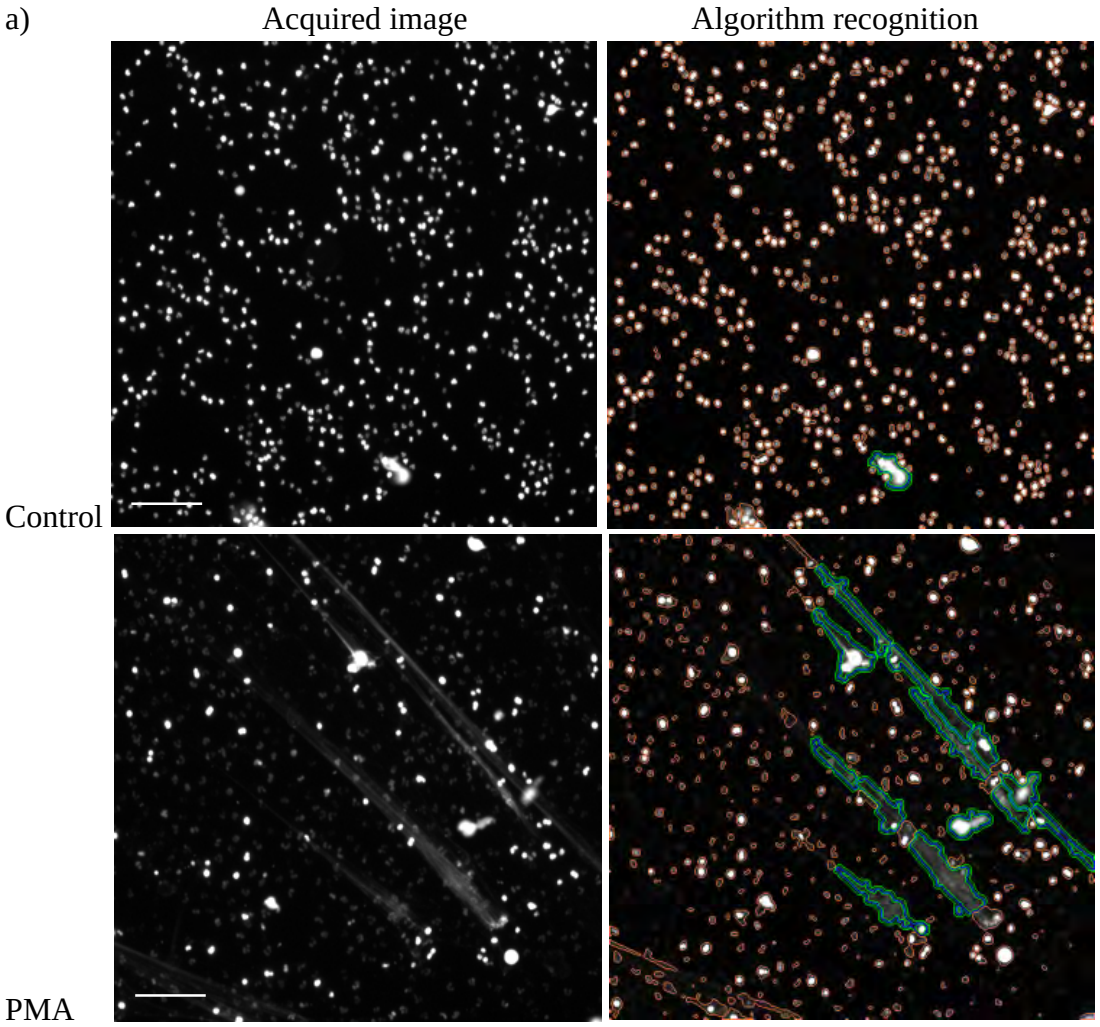
Acquired image
Algorithm recognition
Control
PMA

b)

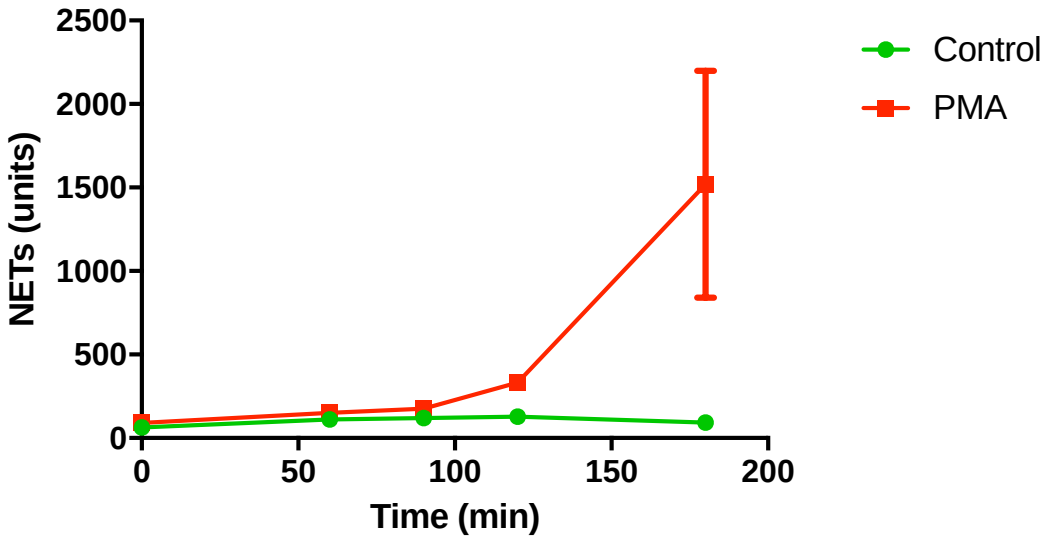
2500
2000
1500
1000
500
0
NETs (units)
0
50
100
150
200
Time (min)
Control
PMA

c)

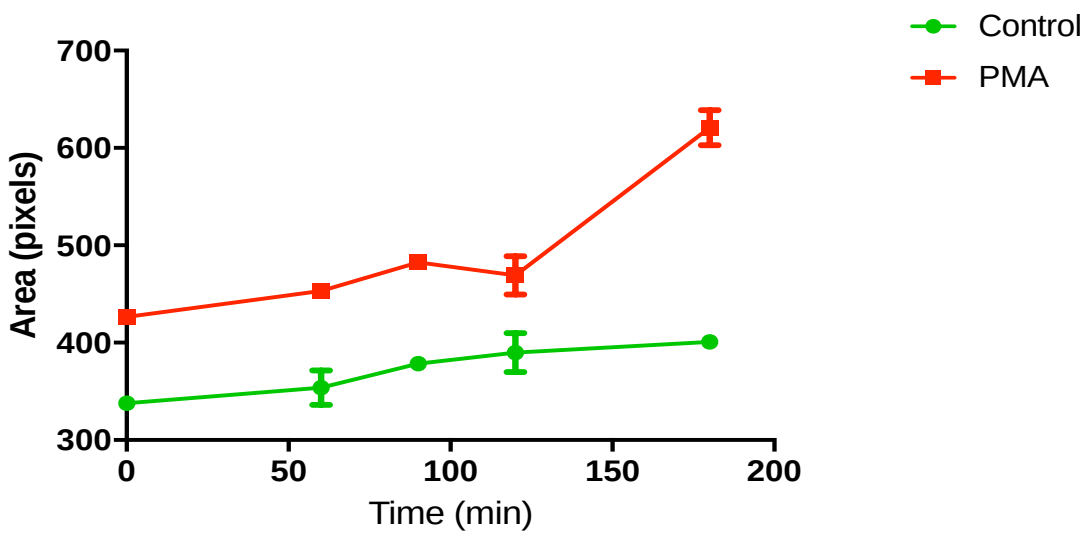

Figure 5.5: NET recognition and quantification by the NET Detection algorithm. Application of the NET Detection algorithm for the HCA of neutrophils stimulated with PMA or unstimulated (controls) for 3 hours. Representative images of unstimulated and PMA-stimulated neutrophils, relative algorithm recognition (a) and time-course NET quantification (b). c) Time-course analysis of NET areas detected in unstimulated and PMA-stimulated neutrophils at up to 3 hours. Values are expressed as units of NETs and pixels of staining and as mean ± SEM. Scale bar represents 400μm and applies to all images shown.

5.3.2 Application of the Nuclear Decondensation algorithm

Alongside the algorithm for NET structure analysis, another algorithm was developed to acquire information on the early stages of NETosis based on monitoring changes in nuclear morphology and chromatin decondensation. Monitoring nuclear area and staining intensity provides information on the state of chromatin decondensation and, therefore, can reportedly be quantified as indicator of the early stages of NETosis (Zhao *et al.*, 2015).

The algorithm, termed “Nuclear Decondensation”, was designed to identify neutrophil nuclei as circular objects which correspond to pre-determined parameters for size and intensity (Appendix II). Object identification settings were adapted to size and staining intensity based on neutrophil nuclear features, therefore, the algorithm recognised small lobulated objects as nuclei (circled in red in Figure 5.6). Rejection criteria were established for the exclusion of cell

debris or aggregates or objects located at the image edges (Appendix II & circled in green in Figure 5.6). The Nuclear Decondensation algorithm provided a wide range of information on Hoechst-stained neutrophil nuclei and identified as NETosing those cells with relatively large areas and low signal intensity (shown in Figure 5.6) compared with controls.

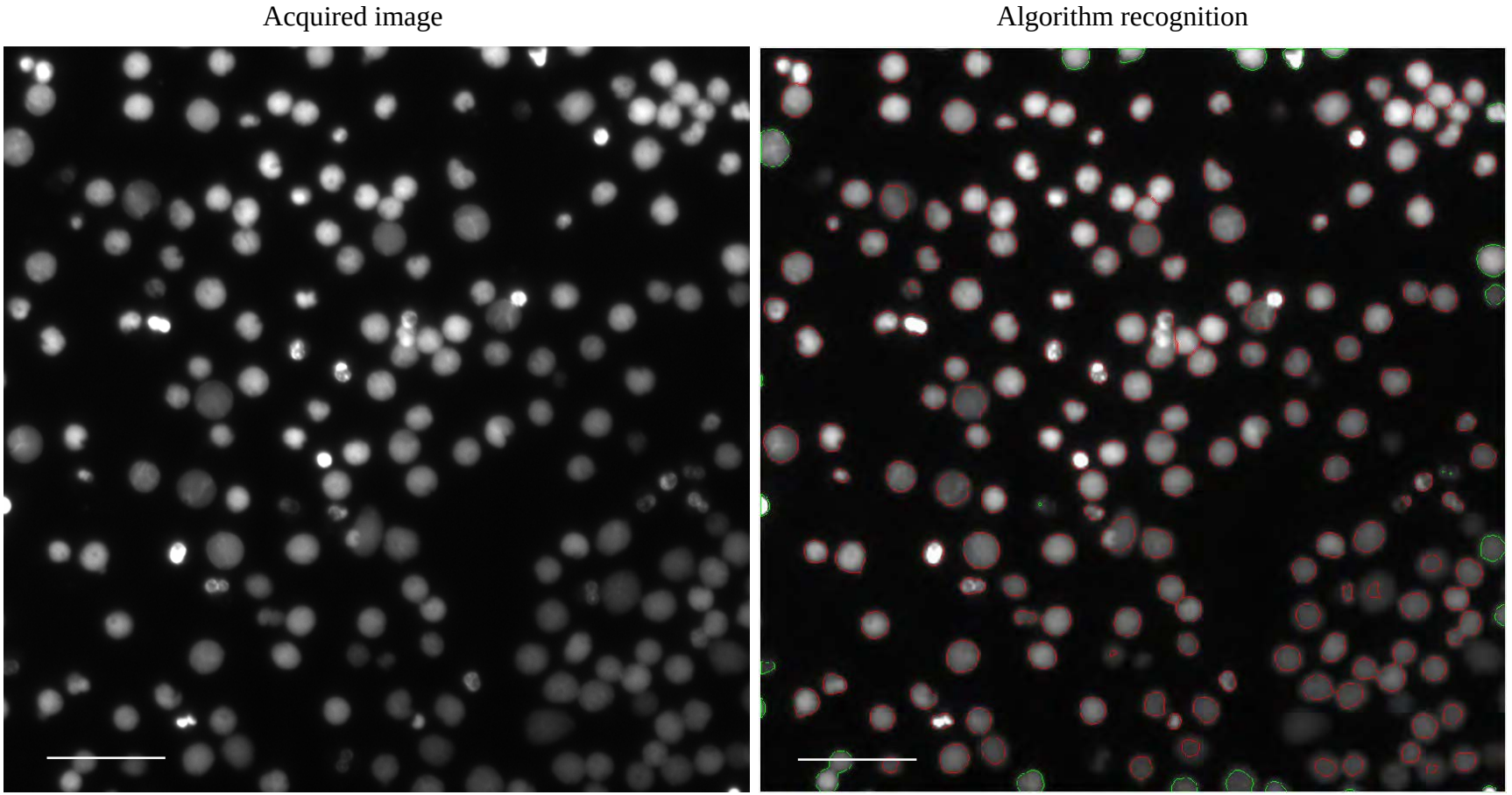

Figure 5.6: Images of neutrophil nuclei identification by Nuclear Decondensation algorithm.
Representative images of PMA-stimulated neutrophil nuclei acquired with the ArrayScan and relative algorithm recognition. Nuclei are automatically identified and selected (red circles in the right hand image) based on morphology and intensity by the Nuclear Decondensation algorithm. Objects adjacent to the image edges are rejected (green circles in the right hand image). Scale bar represents 100 μm.

Neutrophils were stimulated with PMA or were unstimulated (controls) for 3 hours. Upon fixation, samples were stained with Hoechst and HCA was performed. The Nuclear Decondensation algorithm was applied as described above. Thresholds for nuclear areas and staining intensity were manually adjusted based on images of control nuclei (Appendix II). The algorithm determined the portion of cells with areas above, and with staining intensity below, the specified thresholds. Results shown in Figure 5.7a indicated the Nuclear Detection algorithm in unstimulated neutrophil nuclei calculated an average nuclear area of between 500 and 700 pixels throughout the 4 hour incubation period. A similar nuclear area was calculated in PMA-stimulated neutrophils for up to 3 hours and increased above 1,000 pixels after 4 hours. Opposite trends were seen for the analysis of nuclear staining intensity. PMA-stimulated neutrophil nuclear intensity was constantly 200 units below the measured intensity in unstimulated neutrophils during the initial 3 hours of exposure to PMA and decreased to 500 units at 4 hours (Figure 5.7b). Nuclei which presented simultaneously enlarged areas and a diminished nuclear intensity were considered by the algorithm as NETotic events. The graph presented in Figure 5.7c represents the percentage of NETotic events calculated in unstimulated and stimulated neutrophils related to the previously described area and intensity data. The percentage of NETotic events remained approximately 0% in unstimulated neutrophils, while in PMA-stimulated neutrophils approximately 60% of cells were determined to be in a NETosing state at 4 hours exposure to PMA. Interestingly, the trend for NETosing cells calculated with the Nuclear Detection algorithm was similar to the trend of NET release calculated using the NET Detection algorithm (Figure 5.5b). Taken together these data confirm that monitoring nuclear decondensation appears to be a valid indicator of NET forming activity and directly relates to NET formation.

a)

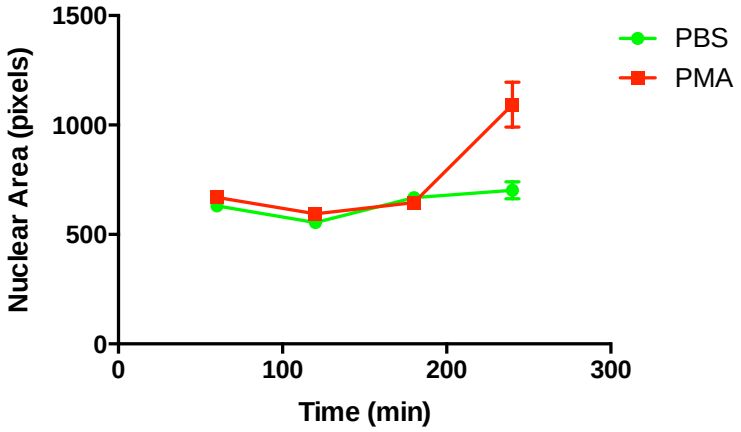

b)

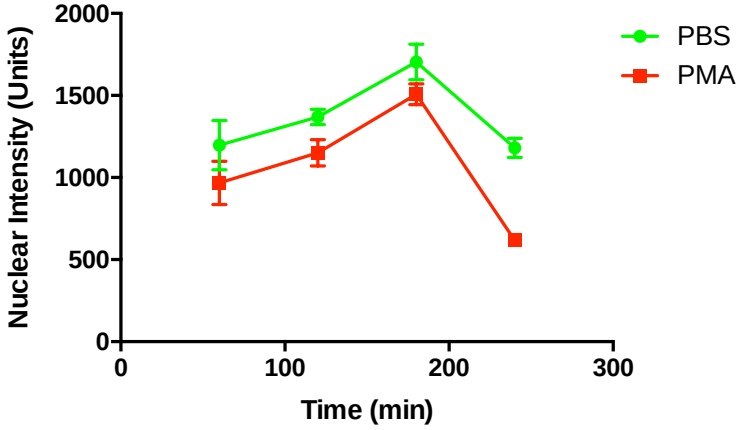

c)

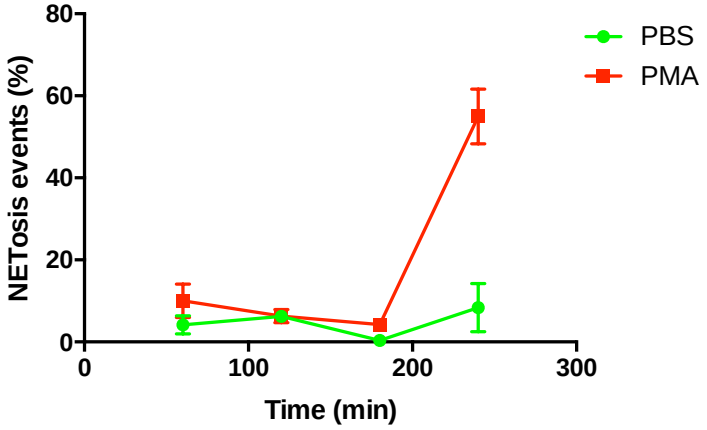

Figure 5.7: Time-course of NETosis as determined using HCA.
Data from HCA of unstimulated (PBS/green) and PMA-stimulated (red) neutrophils at up to 4 hours. Time-course average nuclear area (a) and average nuclear intensity data (b) are combined to calculate the percentage of NETosing neutrophils at each time-point (c). Values are expressed as pixels or units of fluorescent signal and as mean ± SEM. Data represent the mean of two independent experiments.

5.4 Sub-cellular localisation of proteins

Nuclear decondensation in neutrophils has been related to the activity of specific proteins, including PAD4 and NE (Li *et al.*, 2010; Papayannopoulos *et al.*, 2010). Tracking specific proteins during the NET stimulation phase provides valuable information on neutrophil activation and the NET release processes which still require further elucidation and may enable the identification of novel therapeutic approaches for NET-related diseases.

The Compartmental Analysis algorithm, as previously described, has application for monitoring protein translocations in biological systems (Drake *et al.*, 2009). However, HCA has not previously been applied in the localisation of neutrophil proteins. The Compartmental Analysis algorithm, as optimised above for neutrophil recognition, was subsequently employed with the aim of tracking PAD4 during the neutrophil stimulation phase. Initially however, HCA was applied in this thesis to study the nuclear translocation of the NF-κB transcription factor in oral keratinocytes, which represents a well characterised process (Milward *et al.*, 2007). As HCA has already been successfully applied to the analysis of NF-κB localisation in oral keratinocytes (Milward *et al.*, 2013) it was therefore utilised to validate and optimise the approach for the analysis of protein intracellular localisation and tracking.

5.4.1 NF-κB nuclear translocation in H400 cells

Bacterial products trigger a wide range of intracellular pro-inflammatory processes in H400 cells, including the activation of NF-κB which plays a key role in regulating cytokine transcription and production (Perkins, 2007). In the resting state, NF-κB is located in the cytoplasm bound to its inhibitor IκB which is disassembled upon ubiquitination as a result of

cellular activation. Once released, NF-κB translocates to the nucleus and binds to DNA promoting the transcription of several inflammation-related genes (Barnes, 1997).

Activation of the inflammatory response in H400 cells was induced by LPS stimulation as described in section 2.5 of the Materials and Methods. NF-κB translocation in H400 cells was assessed in parallel by semi-quantitative conventional immunohistochemistry and HCA (sections 2.7 & 2.8.4) and data obtained using the two techniques were compared. For immunohistochemistry purposes H400 cells were cultured and stimulated on multi-well glass slide as described in sections 2.3.3. For HCA application, H400 cells were cultured and stimulated in black, clear bottom 96-well plates as described in sections 2.3.3 & 2.5. Representative images in Figure 5.8 show NF-κB staining in H400 cells unstimulated or stimulated with LPS for 1 hour with or without pre-treatment with celastrol. Notably, celastrol inhibits the intracellular pathway upstream of IκB degradation and, therefore, abrogates NF-κB translocation to the nucleus (Wu *et al.*, 2009). Using both immunohistochemistry and immunofluorescence techniques NF-κB was shown to locate in the nuclei of LPS-stimulated H400 cells, while in unstimulated cells the staining was predominantly cytoplasmic. Similar to control samples, NF-κB staining was identified in the cytoplasm of celastrol pre-treated LPS-stimulated H400 cells in agreement with data demonstrating the compounds inhibitory activity of this process (He *et al.*, 2009).

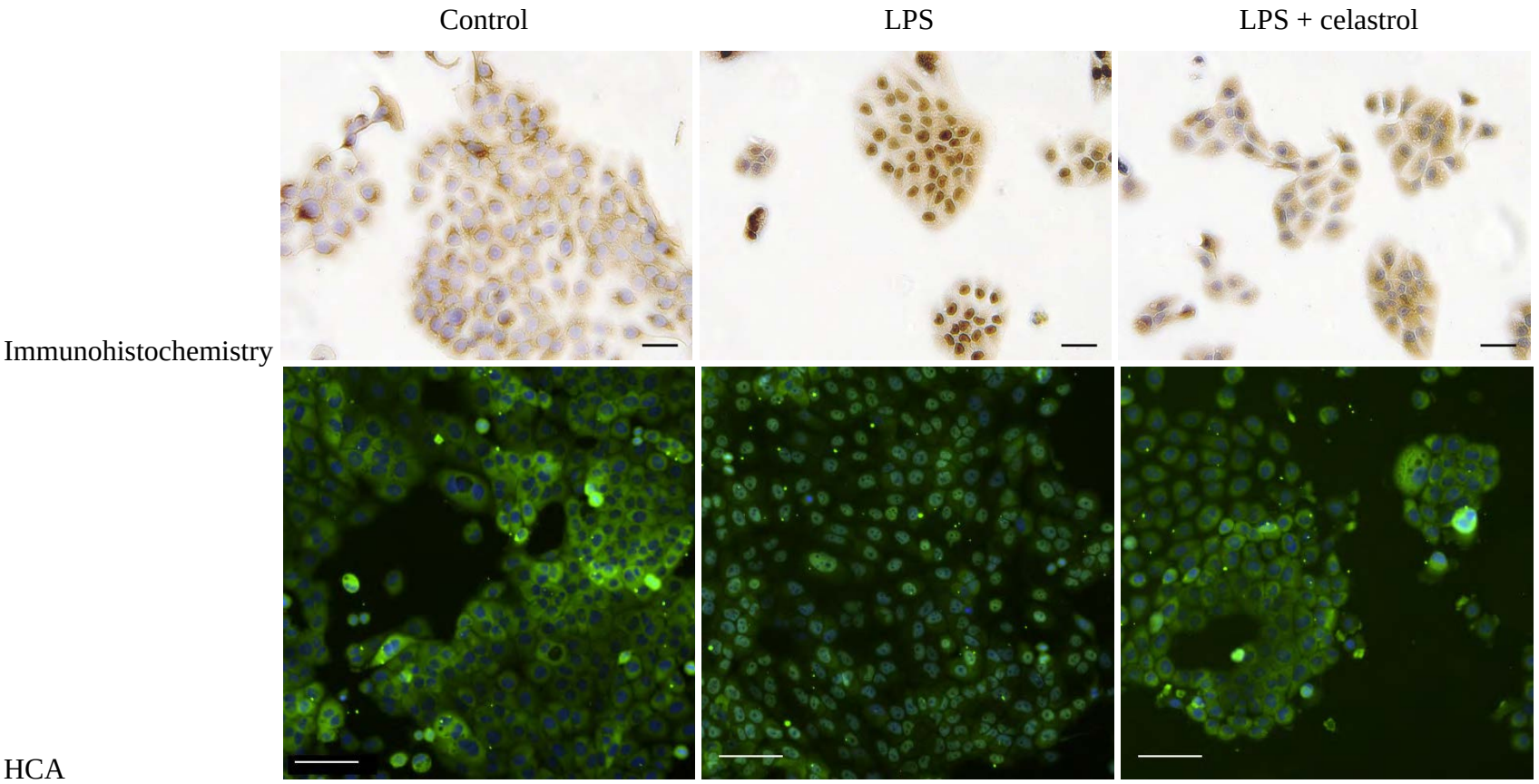

Figure 5.8: Images of LPS-induced NF-κB nuclear translocation in the H400 cell line: Immunohistochemistry analysis vs HCA. Representative images of NF-κB nuclear translocation in H400 cells unstimulated or stimulated with LPS for 1 hour, untreated or pre-treated with celastrol. Immunohistochemistry images show H400 nuclei in blue and NF-κB proteins in brown, while HCA images show nuclei in blue and NF-κB proteins in green. Images are representative of two independent experiments. Scale bars represent 50 μm.

Images obtained by conventional immunohistochemistry were analysed to determine the proportion of H400 cells positive for NF-κB nuclear localisation. The cell count was performed as described in section 2.7.2 and results are presented in Figure 5.9. LPS-stimulation induced NF-κB nuclear translocation in the majority of analysed cells, while in unstimulated conditions NF-κB maintained a cytoplasmic localisation. Celastrol pre-treatment of LPS-stimulated H400 cells significantly reduced the percentage of cells positive for NF-κB nuclear localisation, restoring levels to those found in unstimulated H400 cells.

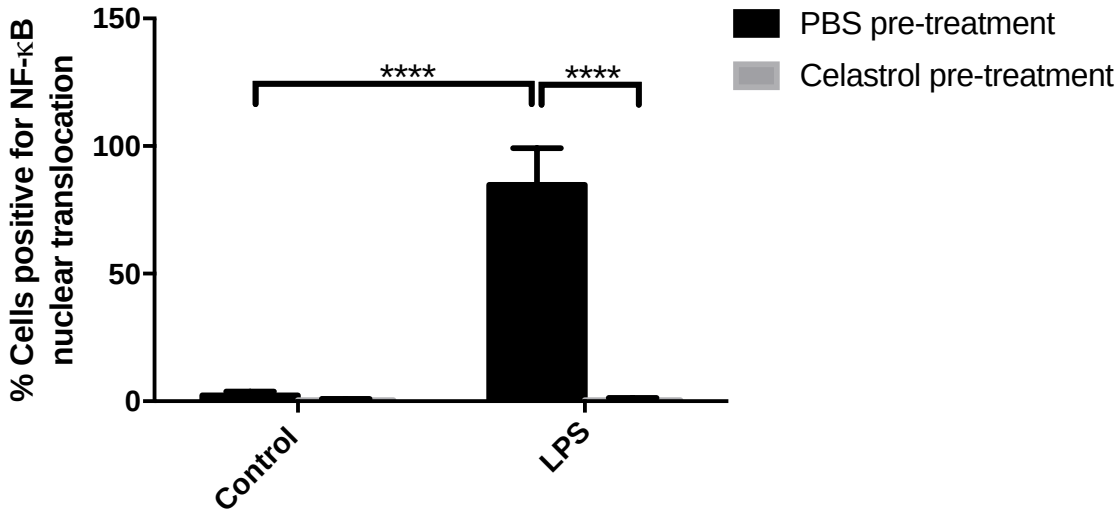

Figure 5.9: Semi-quantitative analysis of NF-κB nuclear localisation in H400 cells as determined from immunohistochemistry images.
Analysis of immunohistochemistry staining for NF-κB nuclear localisation in H400 cells unstimulated or stimulated with LPS for 1 hour, untreated (black bars) or pre-treated with celastrol (grey bars). Values are expressed as percentage of positive cells and as mean ± SEM. Statistical significance calculated with Tukey's multiple comparison test (n=4; ****p<0.0001).

NF-κB nuclear translocation in LPS-stimulated H400 cells was quantified by HCA with or without pre-treatment with celastrol and the Compartmental Analysis algorithm was applied as described above in section 5.2.1. Thresholds for nuclear area and staining intensity were manually adjusted based on images of H400 cell nuclei (Appendix III). Object identification and rejection settings were adapted to size and staining intensity based on H400 nuclear features

(Appendix III). Algorithm settings were adjusted for the subdivision of the cell into two main compartments which corresponded to the nucleus and cytoplasm surrounding it. The software subsequently identified and quantified the NF-κB staining signal within the two compartments. Results presented in Figure 5.10 indicated that the Compartmental Analysis algorithm identified a comparable number of cells for all conditions studied (Figure 5.10a). Celastrol treated cells presented a significantly decreased nuclear area compared with untreated cells, while the LPS-stimulated nuclei presented as a similar size to unstimulated nuclei (Figure 5.10b). The decreased size of celastrol-treated nuclei may be attributed to the inhibition of NF-κB and the consequentially reduced gene transcription since this activity has been previously related to nuclear morphology (Queisser *et al.*, 2011).

a)

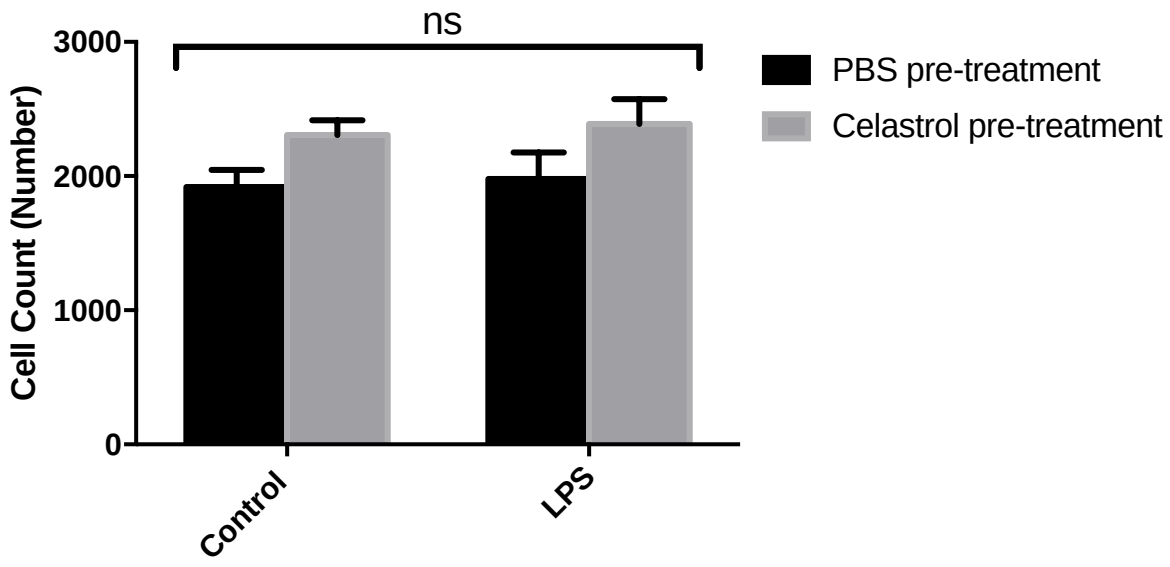

b)

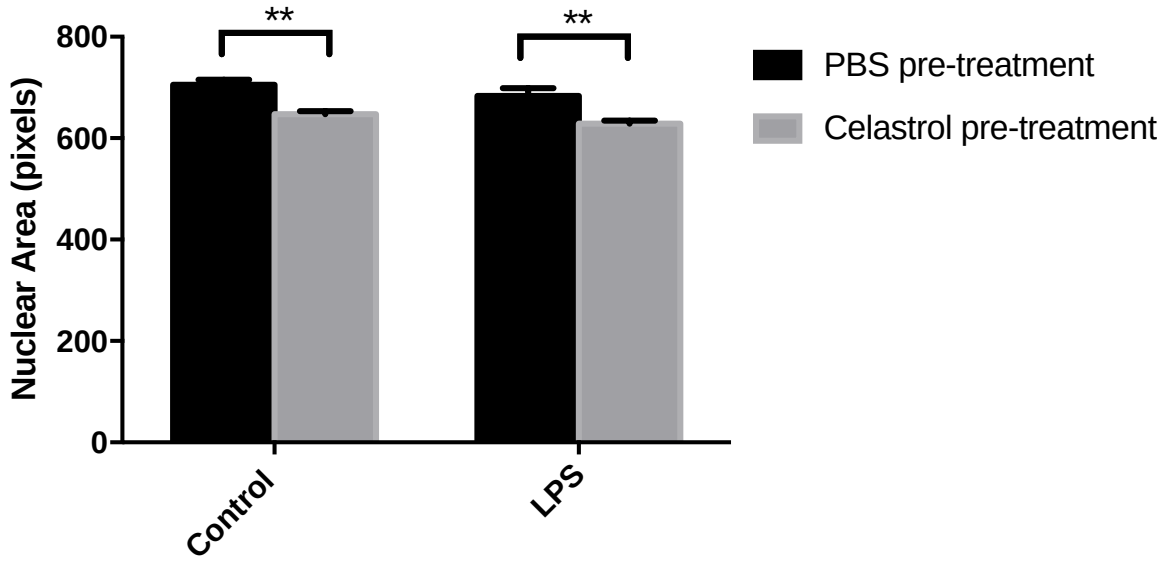

Figure 5.10: Effect of celastrol treatment and LPS stimulation on H400 cells.
Analysis of cell count (a) and average nuclear area (b) of H400 cells unstimulated or stimulated with LPS for 1 hour, untreated (black bars) or pre-treated with celastrol (grey bars). Values are expressed as number of cells or pixels of staining and as mean ± SEM. Statistical significance was calculated with Tukey's multiple comparison test (n=2; ns=non-significant, **p<0.01).

In Figure 5.11 data on NF-κB nuclear translocation is presented. The Compartmental Analysis algorithm identified similar levels of NF-κB cytoplasmic staining between untreated and celastrol-treated control cells, while LPS-stimulated cells exhibited a significantly lower amount of cytoplasmic staining, and this was restored to control levels in celastrol pre-treated cells (Figure 5.11a). An opposite trend was detected for the analysis of nuclear staining (Figure 5.11b). The NF-κB signal increased in LPS-stimulated cells compared with unstimulated cells which presented a similar amount of nuclear intensity as that determined with celastrol pre-treatment of LPS-stimulated cells. Interestingly, celastrol-treated control cells presented higher levels or greater intensity of NF-κB nuclear staining compared with the untreated control condition. This suggests a partial activation of NF-κB potentially due to its anti-apoptotic activity, as proposed by Wright *et al.* (2011), in response to celastrol and relatively minor cytotoxicity has been identified in previous publications (Figure 4b in He *et al.*, 2009; Figure 1b in Sethi *et al.*, 2007). In Figure 5.11c values of nuclear intensity are presented in relation to those of cytoplasmic staining for each condition. Data indicate that LPS-stimulation resulted in a significantly higher ratio of nuclear staining versus cytoplasmic staining compared with unstimulated cells. LPS-induced activation, however, was efficiently inhibited by the pre-treatment with celastrol which exhibited levels comparable to controls for NF-κB nuclear staining.

a)

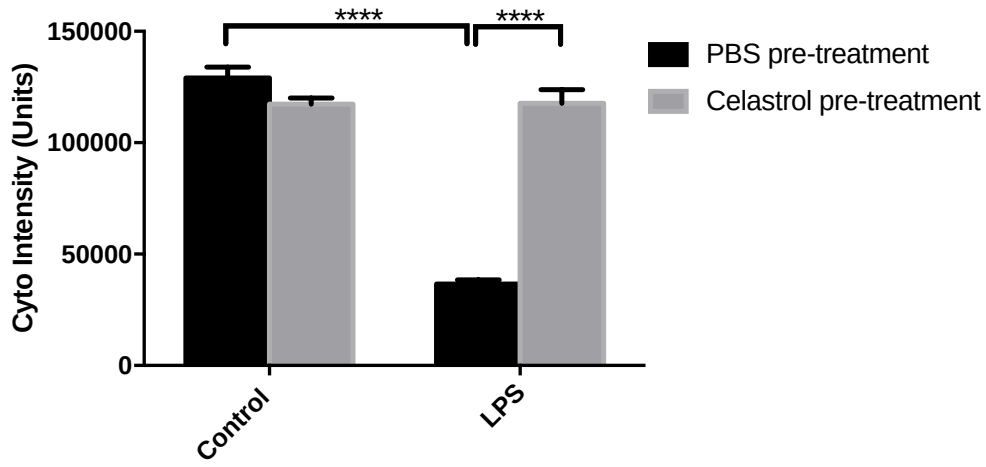

b)

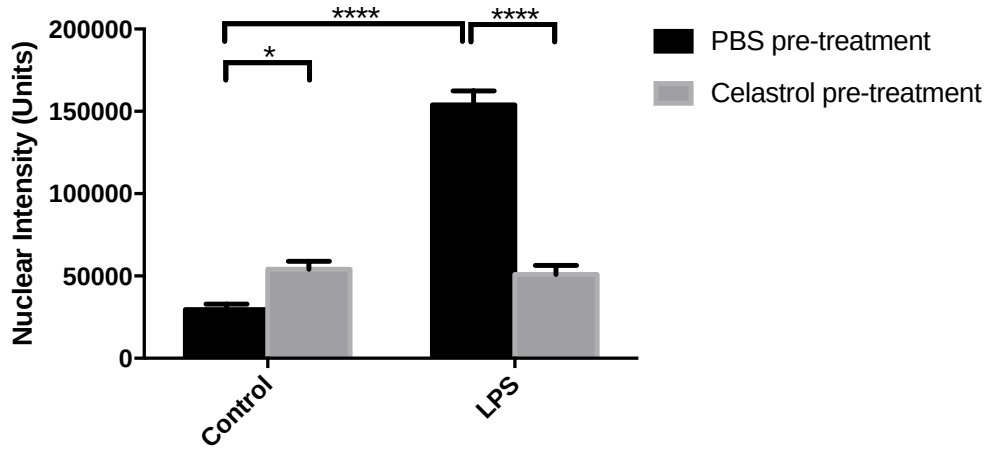

c)

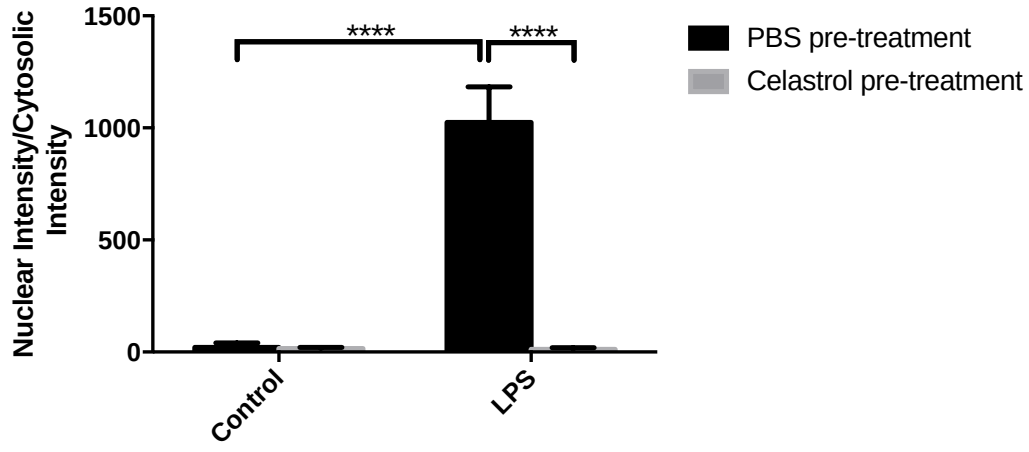

Figure 5.11: HCA of NF-κB localisation.
HCA of cytosolic (cyto) (a) and nuclear (b) fluorescent immunostaining signal for NF-κB and nuclear/cytosolic ratio (c) related to NF-κB translocation in H400 cells unstimulated or stimulated with LPS for 1 hour, untreated (black bars) or pre-treated with celastrol (grey bars). Values are expressed as units of fluorescent signal and as mean ± SEM. Statistical significance calculated with Tukey's multiple comparison test (n=2; *p<0.05, ****p<0.0001).

5.4.2 PAD4 cellular localisation in neutrophils

Previously experiments in murine bone marrow neutrophils (section 5.4.2) has demonstrated that PAD4 knockout mice were unable to produce NETs. PAD4 localises to the nuclei of neutrophils and has been extensively described in the literature as a key protein for regulating chromatin decondensation and NETosis processes (reviewed in section 2.2.1.2). In this section, PAD4 activation and its regulated process, histone citrullination, were investigated using HCA in order to characterise their association with NETosis.

Neutrophils were exposed to PMA for up to 4 hours to induce NETosis and subsequently fixed with PFA as described in section 2.6.6.2. Neutrophil nuclei and NETs were stained with Hoechst while immunostaining was performed for PAD4 as detailed in section 2.8.2. Images of DNA and PAD4 staining in neutrophils were acquired on distinct channels using the ArrayScan (section 2.8.6) and visualised with the HCS Reader software. In Figure 5.12 the PAD4 staining is presented both independently and merged with the DNA signal in images of neutrophils stimulated for 90 minutes with PMA. The majority of neutrophil nuclei appeared in a condensed state as characterised by their multilobulated morphology consistently with the time they had been exposed to the stimulus. However, some nuclei were identified in a NETosing state, having lost their multilobulation and exhibited a decreased intensity. Interestingly, PAD4 staining was particularly intense in those areas corresponding to NETosing nuclei. Furthermore, PAD4 staining appeared to localise with extruded extracellular filaments which exhibited a morphology consistent with NET structures.

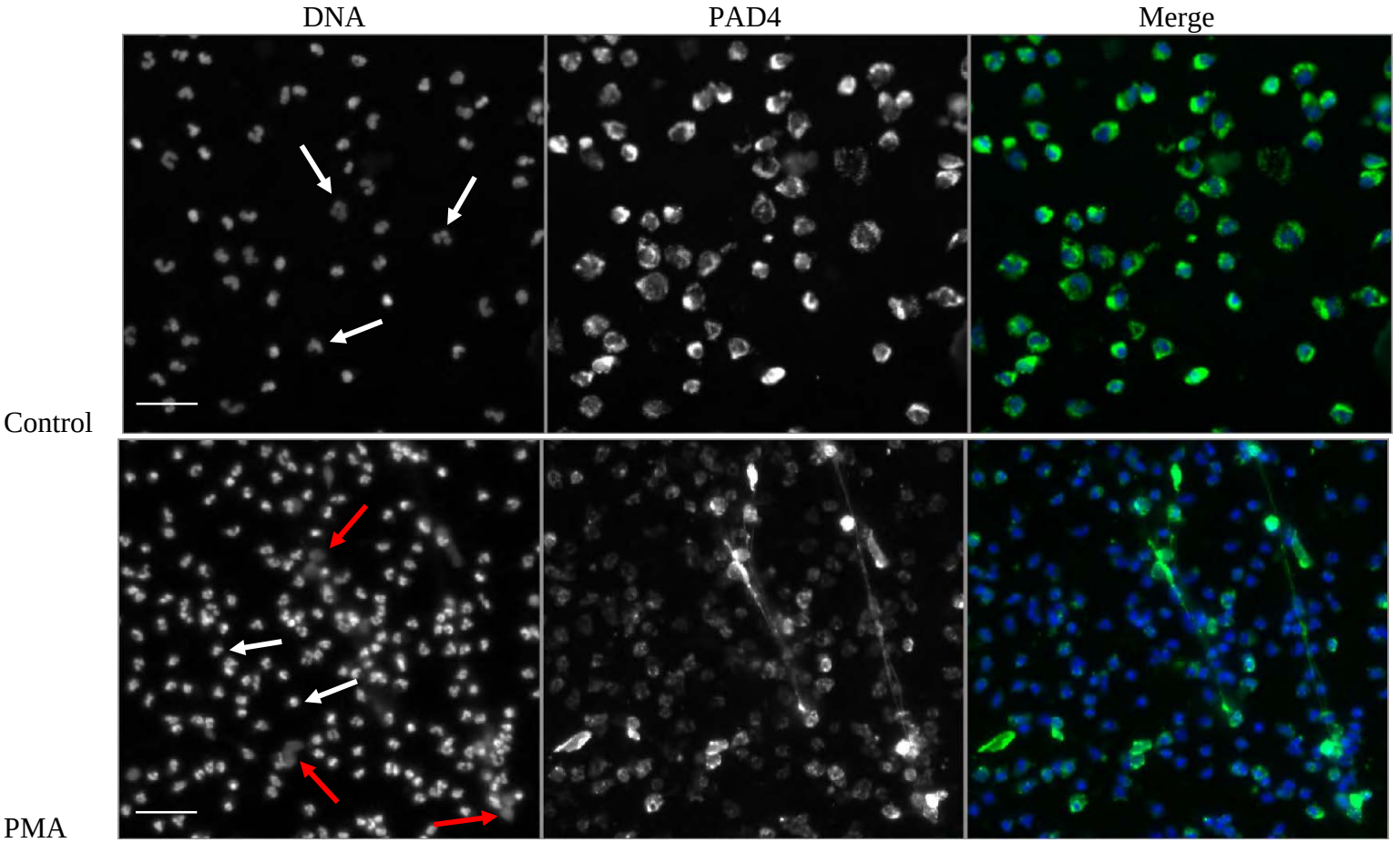

Figure 5.12: PAD4 staining co-localised with NETs.
Representative images of neutrophils unstimulated or stimulated for 90 minutes with PMA. In the far left images, nuclei are in condensed (white arrows) and decondensed (red arrows) states. The PAD4 immunostaining signal is shown independently in the central image and merged with the DNA staining in the right image (PAD4 is shown in green and DNA in blue). Images are representative of 3 independent experiments. Scale bars represent 200μm and apply for all images.

Time-course localisation of PAD4 staining in neutrophil nuclei was analysed following stimulation for up to 4 hours with PMA or HOCl and compared with unstimulated neutrophils using the Compartmental Analysis algorithm. The algorithm identification and rejection criteria were optimised for neutrophil nuclear morphology as described in section 5.2.1. For this application, the algorithm settings were adjusted to identify and encircle the area surrounding neutrophil nuclei that corresponded with the cytoplasm (Appendix IV). The Compartmental Analysis, then, localised and quantified the fluorescently stained signal within the nuclear and the cytoplasmic areas. Images shown in Figure 5.13a demonstrate how the PAD4 staining signal was recognised and localised by the algorithm in HOCl-stimulated and in unstimulated neutrophils. Interestingly, the PAD4 signal appeared strongly associated with the nuclear DNA in HOCl-stimulated neutrophils, while unstimulated neutrophils presented both a nuclear and a cytoplasmic signal. However, the cytosolic signal in control images appeared to be located in close proximity of the nuclear area. Time-course data on the quantification of PAD4 nuclear staining in stimulated and unstimulated neutrophils are presented in Figure 5.13b. PAD4 nuclear staining in unstimulated neutrophils remained at constant levels during all 4 hours. Conversely, HOCl stimulation resulted in maximum PAD4 nuclear signal after 30 minutes, subsequently, between 30 minutes and 2 hours, the signal decreased to relatively low levels and remained constant for the following 2 hours. Following PMA stimulation, the PAD4 nuclear signal increased in association with the time of exposure to the stimulus. Interestingly, the maximal levels of nuclear staining intensity were detected after 30 minutes and 4 hours stimulation respectively with HOCl and PMA which are both consistent with the previously determined exposure times required for NET production (see Figure 3.6).

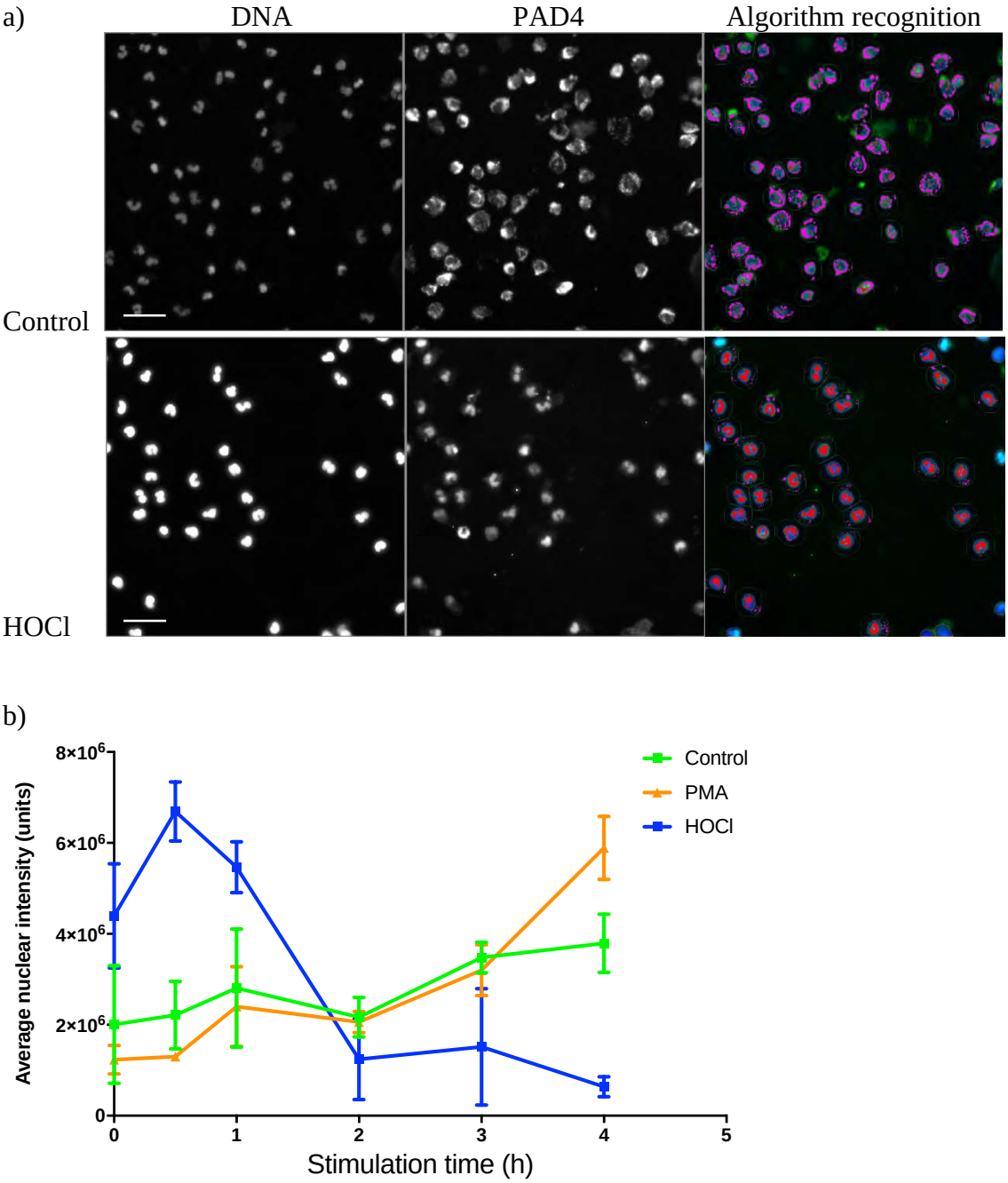

Figure 5.13: PAD4 nuclear localisation in stimulated neutrophils.
HCA of PAD4 nuclear localisation in neutrophils stimulated with PMA, HOCl or unstimulated for up to 4 hours. a) Representative images of neutrophils stimulated with HOCl for 30 minutes or unstimulated (controls). DNA and PAD4 signals are shown independently respectively in the left and central images. In the right hand images the algorithm identifies neutrophil nuclei in blue and PAD4 localisation as purple spots in the cytoplasm and red spots in the nuclei. b) Time-course analysis of PAD4 nuclear staining intensity in stimulated and unstimulated neutrophils. Images and data are representative of 3 independent experiments (n=3). Values are expressed as mean ± SEM. Scale bars represent 200μm and apply for all images.

Concurrent with PAD4 staining, citrullinated-histone 3 localisation was also investigated in relation to NET formation. Neutrophils were stimulated for up to 4 hours with PMA and HOCl and, upon fixation, immunostaining was performed simultaneously for PAD4 and citrullinated-histone 3. The Compartmental Analysis algorithm was applied as described above. Data presented in Figure 5.14 show the percentage of cells that were positive for PAD4 or citrullinated-histone 3 nuclear staining during the course of stimulation. Time-course analysis of PMA-stimulated neutrophils indicated between 30% and 40% of cells were positive for PAD4 nuclear staining after 3 and 4 hours exposure, which was consistent with previous data on PAD4 localisation shown in Figure 5.13. Data for citrullinated-histone 3 nuclear staining showed a similar increase at 3 and 4 hours, however, only 10% of cells were shown as positive. A different trend was detected in HOCl-stimulated neutrophils. The percentage of cells positive for PAD4 nuclear staining increased to 10% after 30 minutes of stimulation, remained at constant levels for the following 2 hours, and then increased further to 30% after 4 hours. Notably, the percentage of cells positive for citrullinated-histone 3 nuclear signal increased to 10% after 1 hour of stimulation, decreased for the following 2 hours to nearly 0%, and increased to 5% after 4 hours. The high percentage of cells detected as positive for PAD4 nuclear staining in both PMA- and HOCl-stimulated neutrophils may be a consequence of damage to nuclear and plasma membranes which induced loss of cellular compartments before DNA release. Since PAD4 has been shown to localise with NETs in the extracellular space (Figure 5.11 & Spengler *et al.*, 2015), the high percentage registered at 4 hours may be related to the association of PAD4 with NET-DNA rather than nuclear DNA.

PMA

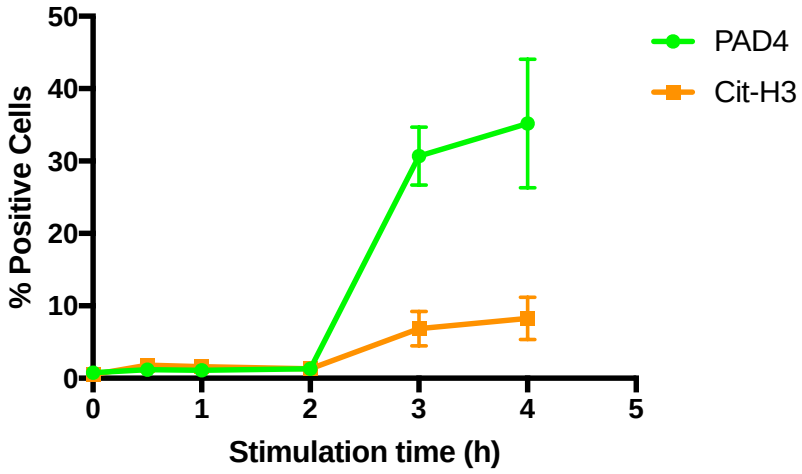

HOCl

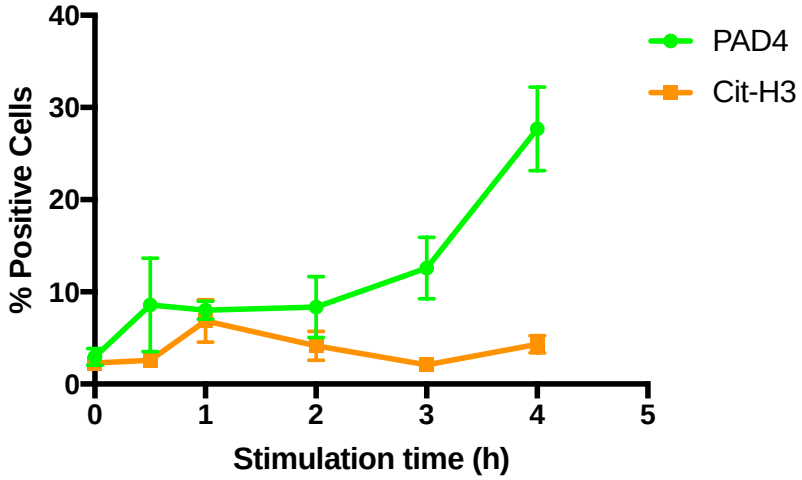

Figure 5.14: PAD4 and citrullinated-H3 associated with DNA.
HCA of PAD4 and citrullinated-H3 (Cit-H3) associated with DNA in neutrophils stimulated with PMA and HOCl for up to 4 hours. Analysis of the percentage of stimulated neutrophils positive for PAD4 and citrullinated-H3 association with DNA (n=3). Data are representative of 3 independent experiments. Values are expressed as mean ± SEM.

5.5 Validation of HCA for NET analysis

Once the HCA approach had been optimised for its application for neutrophil and NET analysis, further validation was required in order to confirm the accuracy of the technique. Therefore, NET analysis was performed by HCA and compared with the fluorometric quantification

approach which determines levels of extracellular NET-DNA post-MNase digestion. The HCA accuracy for the quantification of NETs was evaluated in time-course and cell density-related experiments. For HCA purposes, samples were prepared in a black, clear bottomed 96-well plates and fixed with PFA. Sytox green® was applied for staining NET structures and HCA was performed (as described in section 2.8.3) employing the NET Detection algorithm. For the fluorometric assay neutrophils were seeded in a clear 96-well plate and NET quantification was performed (as described in section 2.6.5).

5.5.1 Time-course analysis of NET formation

Neutrophils were isolated and stimulated with PMA for up to 3 hours as described in sections 2.6.4. Data on time-course NET quantification performed with HCA are presented in Figure 5.15a. Results indicated the technique detected increased NET units as early as 60 minutes after exposure to PMA. Subsequently, the amount of NETs further increased and reached its peak after 3 hours stimulation. Conversely, the algorithm identified relatively low amounts of NETs in unstimulated neutrophils, although this marginally increased by 90 minutes. Data obtained with the fluorometric quantification presented a similar trend of NET production for PMA-stimulated neutrophils (Figure 5.15b), validating the time-course quantification determined by HCA. However, the fluorometric assay registered 4 times higher levels of NETs after 3 hours stimulation compared with the previous time-point, while fewer differences were identified by HCA.

a)

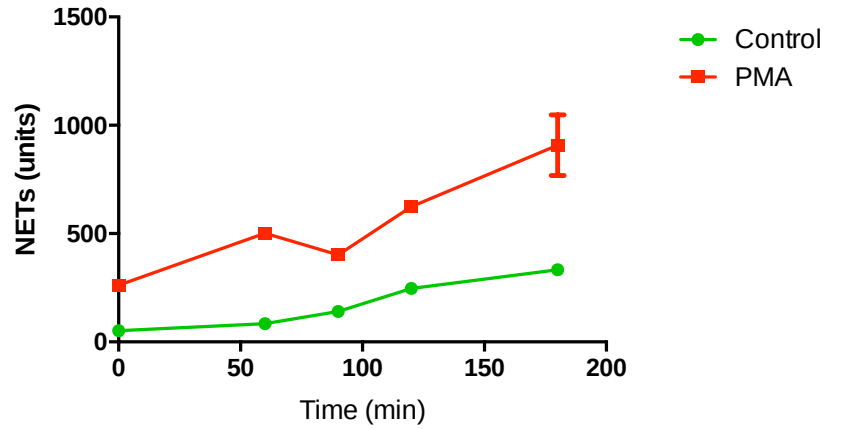

b)

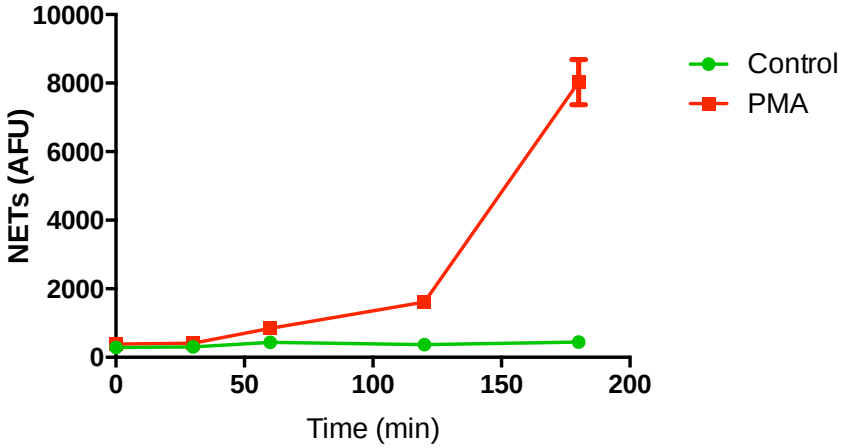

Figure 5.15: Time-course of NET quantification: HCA vs fluorometric assay.
Time-course NET quantification in unstimulated (green) and PMA-stimulated (red) neutrophils up to 3 hours of stimulation. Comparison between HCA (a) and fluorometric (b) quantification. Values are expressed as units of fluorescent signal or arbitrary fluorescence units (AFU). Data represent the mean of two independent experiments ± SEM.

5.5.2 Cell density-related NET formation

The sensitivity of the NET Detection algorithm was evaluated using a range of neutrophil densities between 1,000 and 100,000 cells/well, unstimulated or stimulated with PMA for 3 hours. The NET Detection algorithm outputs were compared with data obtained by fluorometric assay. The NET Detection algorithm registered significantly increased levels of NETs in PMA-

stimulated compared with unstimulated neutrophils seeded at 50,000 cells/well and greater (Figure 5.16a). A similar trend of NET production was confirmed by fluorometric quantification, which also showed significant increases in PMA-induced NETs compared with controls in neutrophils seeded at 50,000 cells/well and above. However, this increase was also detected in as little as 5,000 neutrophils/well (Figure 5.16b). This result indicates that the HCA algorithm allows a sensitive and accurate NET quantification in samples with seeding densities above 50,000 neutrophils/well in a microplate format.

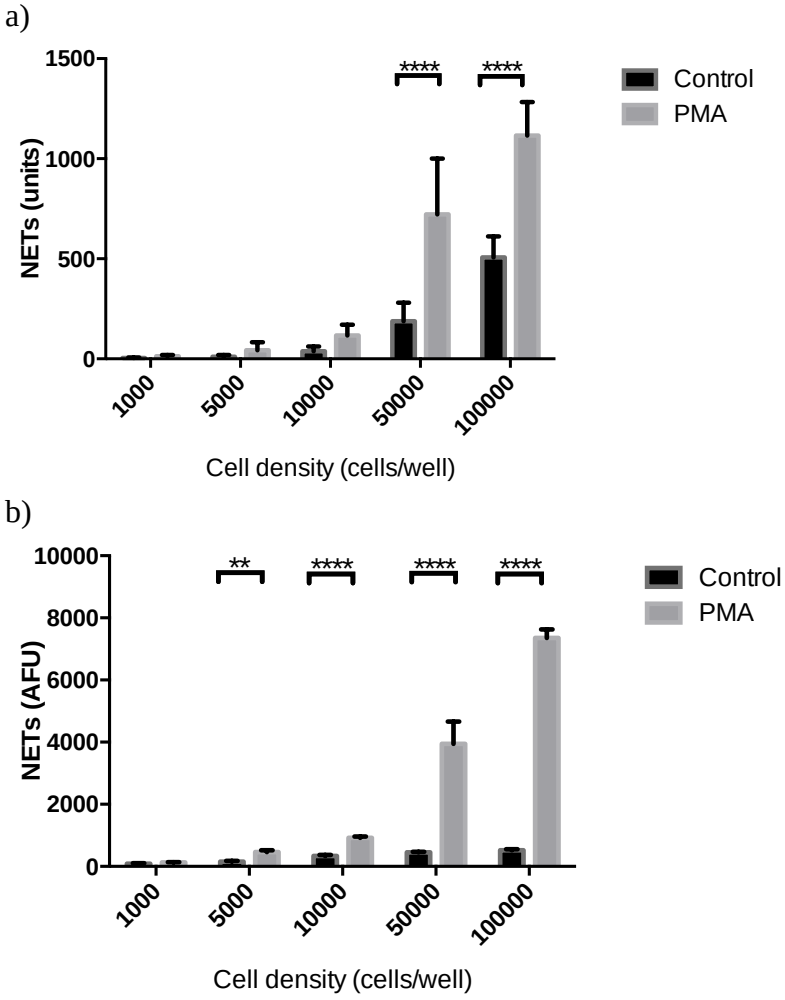

Figure 5.16: Cell-density related NET quantification: HCA vs fluorometric assay. Neutrophils seeded at 5 concentrations in a 96-well plate and stimulated for 3 hours with PMA (grey bars) or unstimulated (black bars). NET quantification by HCA (a) and fluorometric assay (b). Values are expressed as units of fluorescent signal or arbitrary fluorescence units (AFU) and as mean ± SEM. Statistical significance calculated with Sidak's multiple comparison test (n=3; **p<0.01, ****p<0.0001).

5.6 Discussion

In this chapter various algorithms available for HCA were tested for neutrophil and NET identification and quantification. Firstly, two pre-existing algorithms were manually adjusted and tested for this purpose: namely “Compartmental Analysis” and “Tube Formation”. NET recognition occurs in two diverse manners, on one hand the Compartmental Analysis algorithm quantifies the DNA in a circular space surrounding the nucleus, on the other hand the Tube Formation algorithm quantifies DNA filaments extruded into the extracellular space. Both algorithms were evaluated in cell-density experiments in order to determine their accuracy.

Analysis of NET areas registered by the Compartmental Analysis algorithm in PMA-stimulated neutrophils were similar to the values in control neutrophils. Conversely, HOCl-stimulation induced a significant increase in NET area compared with control registered in both 100,000 and 500,000 cells/well densities. Data suggest a different type of NET release may be induced by the two stimuli. For instance, PMA may induce the formation of long filaments, while HOCl could induce a cloud-like diffusion of NETs as previously shown in the supplementary material (video: link3) of Brinkmann & Zychlinsky (2012). Therefore, the Compartmental Analysis algorithm may effectively identify cloud-like NETs and neglect extruded NET filaments. Moreover, seeding at low density resulted in no significant difference between the NET area detected for unstimulated and stimulated neutrophils, suggesting that the cell density may also affect the type and amount of NETs released as previously reported in section 7.2.

The analysis performed with the Tube Formation algorithm resulted in a higher amount of NETs counted in unstimulated compared with PMA-stimulated neutrophils seeded at 10,000 cells/well and above. This results may be related to the excessive formation of cell aggregates or to the cell assuming an elongated phenotype, as shown in Figure 3a and b of Zhao *et al.*

(2015). This type of cell morphology may be mistaken for NETosing activity by the Tube Formation algorithm. Furthermore, PMA-induced NETs may be extruded from multiple sites within the cells simultaneously or may not be associated with intact nuclei and, therefore, escape algorithm recognition.

Both the Compartmental Analysis and the Tube Formation application presented limitations for NET analysis, therefore, two new algorithms were specifically developed for this purpose: namely “NET Detection” and “Nuclear Decondensation”. These algorithms targeted for two main features of NETosis, the extrusion of DNA filaments and the loss of nuclear multilobulated morphology respectively, which allows their simultaneous application to obtain multiparametric data on NETosis. Using dual staining with Hoechst/Sytox green®, the NET Detection and Nuclear Decondensation algorithm demonstrated a similar trend for NET release and nuclear decondensation, which indicates that the two parameters are directly related. The origin of NETs is somewhat controversial as some publications report mitochondrial DNA as the main component of these structures and that neutrophils remain viable following their release rather than undergoing cell death (Yousefi & Simon, 2016). However, results gathered with the Hoechst/Sytox green® approach and the strong stimuli employed in the present stimuli indicate that the association of NET production with nuclear decondensation support studies suggesting that these two mechanisms exist and occur as a result of different stimuli (Zhao *et al.*, 2015).

Time-course production of NETs in PMA-stimulated neutrophils was accurately measured by the NET Detection algorithm, as validated by the fluorometric quantification of NET-DNA. As expected, NET release increased with the time of exposure to the stimulus and this trend was confirmed by both types of quantification approach. However, differences were identified

between the two approaches which may be explained by the different types of quantification applied. On one hand, the fluorometric assay is based on fluorescent measurement of DNA in the supernatant and, on the other hand, HCA is applied to images of stimuli-induced NETs.

When performing the time-course analysis of neutrophils, an interesting morphological change induced by PMA stimulation was observed. Images of Hoechst-stained neutrophil nuclei were visualised and merged with brightfield images in order to monitor cellular changes associated with PMA-induced nuclear changes. Unstimulated neutrophils retained a rounded and compact shape visible in the images as a darker ring around the orange nuclei. Conversely, as early as 60 minutes into PMA-stimulation, the spherical shape disappeared and the cytoplasm appeared as an undefined area around nuclei (Figure 5.17). The altered morphology may be due to the activation of intracellular pathways upstream of the process of NET release. Consistently, similar morphology has been identified in numerous published images of stimulated neutrophils including Figure 1d in Brinkmann *et al.* (2004), Figure 2b in Fuchs *et al.* (2007) and Figure 1a in Zhao *et al.* (2015). This particular morphological change in neutrophils, described as "spreading on a surface", has already been related to cytoskeletal activities (Girard *et al.*, 1997). Furthermore, Neeli *et al.* (2009) demonstrated that cytoskeletal rearrangement is required for histone deimination and NET formation in LPS stimulated neutrophils. Therefore, the morphological changes observed in PMA-stimulated neutrophils and preceding NET release (as quantified in section 5.5.1) support the hypothesis that cytoskeletal rearrangement is an early stimulus-induced mechanism required for NET formation.

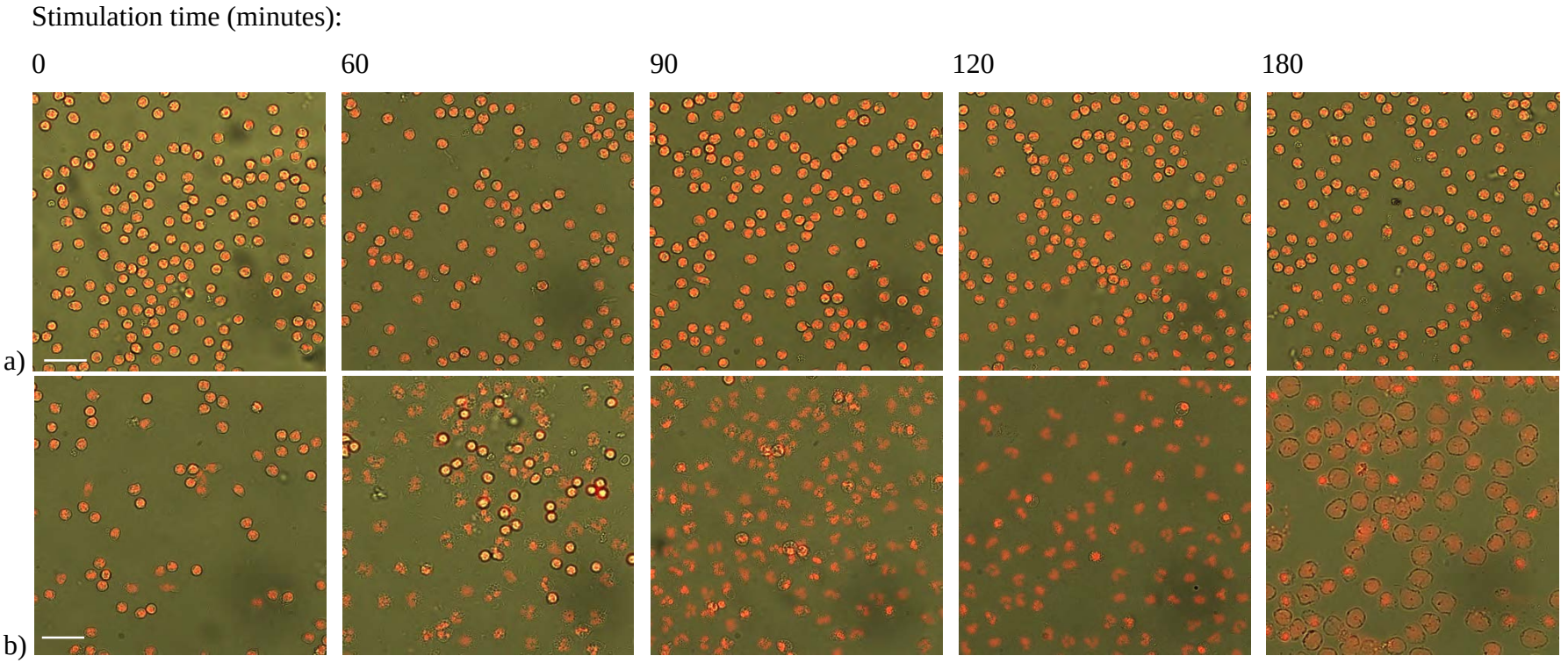

Figure 5.17: Time-point images of neutrophil stimulation showing altered cytoplasm appearance following PMA treatment. Representative HCA images of neutrophils unstimulated (a) or stimulated with PMA (b) for up to 3 hours. Hoechst-stained nuclei are shown in orange colouration and merged with brightfield images. Nuclei appeared in decondensed state at 180 minutes when are stimulated, while cytoplasm had lost the compact spherical shape in the majority of cells as early as 60 minutes after stimulation with PMA. Images are representative of two independent experiments. Scale bars represent 200μm and apply for all images.

The Nuclear Decondensation algorithm provided an accurate calculation of cells in a NETosing state based solely on chromatin observation, which has been related to NET release in previous publications (Brinkmann *et al.*, 2012; Zhao *et al.*, 2015). This type of recognition allows the identification of NETosing nuclei and excludes other cell death phenotypes including necrotic nuclei which lose their multilobulation, however, which remain in a condensed state (Fuchs *et al.*, 2007). The main advantages of monitoring nuclear decondensation are the possibility to study early phases of NET formation and the benefit of obtaining information on a cell-to-cell basis. Analysis of PMA-stimulated neutrophils demonstrated that the Nuclear Decondensation algorithm was effective in identifying and quantifying the portion of cells in a NETosing state. Results presented in Figure 5.7 are in agreement with those presented in Zhao *et al.* (2015) which proposed a modified flow cytometry method for NETosis quantification based on area and bright detail intensity.

The Compartmental Analysis algorithm was successfully applied for the localisation of proteins in both H400 cells and neutrophils. The method was validated for nuclear translocation of NF-κB in stimulated H400 cells by immunohistochemistry. The analysis performed on immunohistochemistry images and the HCA resulted in similar distributions of localisation for NF-κB in unstimulated and stimulated cells suggesting both techniques provide accurate and reliable data. NF-κB identification by immunohistochemistry and by HCA was also performed in neutrophils unstimulated and stimulated with PMA (data not shown). However, neither the immunohistochemistry staining nor the HCA identified translocation of NF-κB in the nuclei of neutrophils upon stimulation within the time-point observed. A previous report has identified nuclear translocation of NF-κB in neutrophils following 10 minutes stimulation with LPS, which was sustained up to 2.5 hours (McDonald *et al.*, 1997). In the same study, PMA stimulation also induced NF-κB activation and nuclear translocation after 45 minutes of

exposure. Therefore, it is plausible that in the time-points observed, of 30 and 60 minutes post-stimulation, NF-κB was present in the cytoplasm respectively before and after nuclear translocation.

PAD4 specific activation and function in neutrophils has not been fully described, which further strengthens the argument raised in Yousefi & Simon (2016) which suggested that the citrullination process is operated by PAD2 rather than PAD4, and occurs extracellularly, rather than in the nucleus. HCA in stimulated neutrophils demonstrated PAD4 co-localised with nuclear DNA and NET filaments which suggests that PAD4 is released into the extracellular space bound to NETs, from where it may operate its citrullination activity as already recently proposed by Spengler *et al.* (2015) and confirmed in section 5.4.2. However, data shown in Figure 5.14 are a representation of PAD4 staining intensity and the strong signal registered in stimulated neutrophils may be related the protein activation state. Notably, previous studies have shown that dimerisation is required for PAD4 enzymatic activity while the monomeric form exhibits less activity (Liu *et al.*, 2011). Therefore, the increased signal intensity registered upon stimulation suggests the enzyme was in its dimer form and its active state. Citrullinated-histone 3 was identified in the nuclear DNA of stimulated-neutrophils in association with PAD4. The registered signal, however, was relatively low compared with the PAD4 signal, suggesting that the citrullination activity is not proportionally related to the enzyme concentration in the cell.

CHAPTER 6: HIGH-THROUGHPUT SCREENING OF NETOSIS MODULATORS

6.1 Background

Despite their important antimicrobial role at sites of infection, NETs have also been associated with the pathogenesis of several auto-inflammatory and auto-immune disorders. In particular, NET under and over-production or aberrant clearance has been proposed to play a role in the pathogenesis of several diseases (summarised in section 2.4). Hence, due to their potentially conflicting functions in human health, NETs have been described as a "double-edged sword" and it is apparent that a fine homeostatic balance may determine the difference between health and disease (Cooper *et al.*, 2013). Consequently, the pharmacological modulation of NETosis offers the potential for developing novel treatments for a range of diseases (Cheng & Palaniyar, 2013; Hahn *et al.*, 2013). Indeed, researchers have already identified compounds that regulate NETosis and may therefore serve as possible treatments in auto-inflammatory/-immune diseases (Lapponi *et al.*, 2013; Mcinturff *et al.*, 2013; Yu *et al.*, 2015). Notably, however, research to date has been limited as the current methods used for screening for modulators of NETosis lack consistency and reproducibility. An example of this is the compound Rapamycin, an inhibitor of the mTOR pathway, which has been found to reduce NET formation in a study employing LPS stimulated neutrophils (Mcinturff *et al.*, 2013), however, in another study it was shown to have no effect on ionomycin and PMA induced NETosis (Gupta *et al.*, 2014) raising concerns over its use.

Chapter 8 in this thesis described the development and optimisation of a novel approach for HCA of neutrophils ET release. This technology has application for the screening of small molecule libraries and is employed in the pharmaceutical industry for drug discovery processes and intracellular molecular tracking (Posner, 2005; Korn & Krausz, 2007). In the current chapter the HCA method previously developed (see Chapter 5) was applied for High-Content Screening (HCS) of a pharmaceutically-derived compound library to identify modulators of

NETosis. The utilised library comprised 56 compounds that have previously been applied to cancer treatment and includes a number of immunosuppressive molecules which have been shown to regulate neutrophil and other immune cell functions (Dr Gareth Griffiths, Imagen Therapeutics - personal communication). Subsequently, the individual compounds identified by HCS to modulate NETosis were then characterised using low-throughput approaches to validate findings and further investigate their modulation of neutrophil activity.

6.2 High-throughput screening for compounds that modulate NET production

In order to perform HCS of the 56 member compound library, neutrophils were isolated and seeded in black, clear bottomed 384-well plates (as described in section 2.8.5.3). Neutrophil seeding and handling was performed using the robotic benchtop workstation (section 2.8.5.1). Individual compounds from the library were applied to the neutrophil preparations for 30 minutes using a range of 5 concentrations pre-determined for each compound (Dr Gareth Griffiths, Imagen Therapeutics - personal communication and as detailed in section 2.8.5.2). Celastrol-treated cells were used as inhibitory controls while Benzethonium Chloride was used to induce cytotoxicity and to discern NETosis from other types of cell death. After 30 minutes, neutrophils were stimulated with PMA or were left unstimulated for 3 hours. Following fixation, Hoechst was applied for nuclear staining and images were acquired using the ArrayScan (section 2.8.6). HCA was performed using the Nuclear Detection algorithm as described in section 5.3.2. Image analysis was performed using two distinct methods for unstimulated and PMA-stimulated images. To identify whether compounds were able to induce NETosis in unstimulated conditions, rejection and threshold criteria for nuclear size and nuclear staining intensity were defined based on images of unstimulated and untreated neutrophils as previously described in section 5.3.2 of Chapter 5 and as listed in Appendix V. The algorithm subsequently identified those cells with increased nuclear size and with decreased nuclear

intensity. Concomitant increased size and decreased staining intensity was calculated by the algorithm and used as an indication of NETosing activity, which is reported in the unstimulated panel of Figure 6.1 using shades of grey, while control levels are shown in black. Conversely, in order to identify whether compounds inhibited PMA-induced stimulation, rejection and threshold criteria were established based on images of PMA stimulated neutrophils and untreated neutrophils were used as controls. In this case, the algorithm determined the proportion of cells with increased or decreased levels of both nuclear size and staining intensity compared with control cells. The NETosing activity registered in PMA-stimulated and untreated neutrophils are reported in shades of grey in the PMA panel of Figure 6.1; increased NETosis is reported in colours towards white and inhibitory activity in colours towards black. Celastrol treatment, used as control for inhibitory activity, resulted in a complete inhibition of PMA-induced NETosis and is represented in black in both panels of Figure 6.1. The HCS identified 17 compounds potentially inducing NETosis in unstimulated neutrophils, while 13 compounds potentially were identified as inhibiting NETosis and 13 compounds potentially enhanced PMA-induced NETosis. Rapamycin and Lapatinib treatments resulted in inhibition at low dosages and increased NETosis at high dosages, while Bosutinib treatment resulted in an opposite effect. Compounds showing modulatory activity in unstimulated and PMA-stimulated neutrophils were selected for further screening.

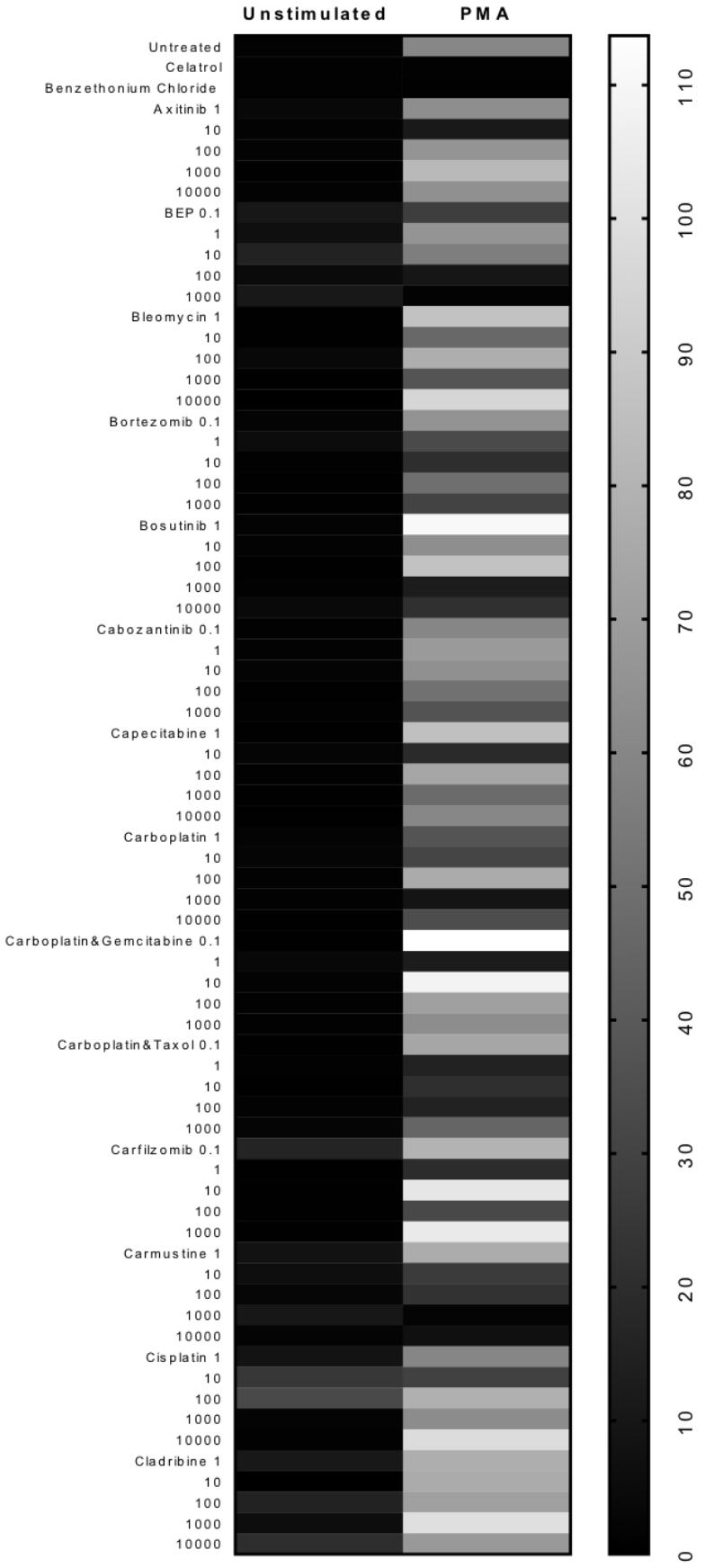
Unstimulated
PMA
Untreated
Celatrol
Benzethonium Chloride
Axitinib 1
10
100
1000
10000
BEP 0.1
1
10
100
1000
Bleomycin 1
10
100
1000
10000
Bortezomib 0.1
1
10
100
1000
Bosutinib 1
10
100
1000
10000
Cabozantinib 0.1
1
10
100
1000
Capecitabine 1
10
100
1000
10000
Carboplatin 1
10
100
1000
10000
Carboplatin&Gemcitabine 0.1
1
10
100
1000
Carboplatin&Taxol 0.1
1
10
100
1000
Carfilzomib 0.1
1
10
100
1000
Carmustine 1
10
100
1000
10000
Cisplatin 1
10
100
1000
10000
Cladribine 1
10
100
1000
10000
0
10
20
30
40
50
60
70
80
90
100
110

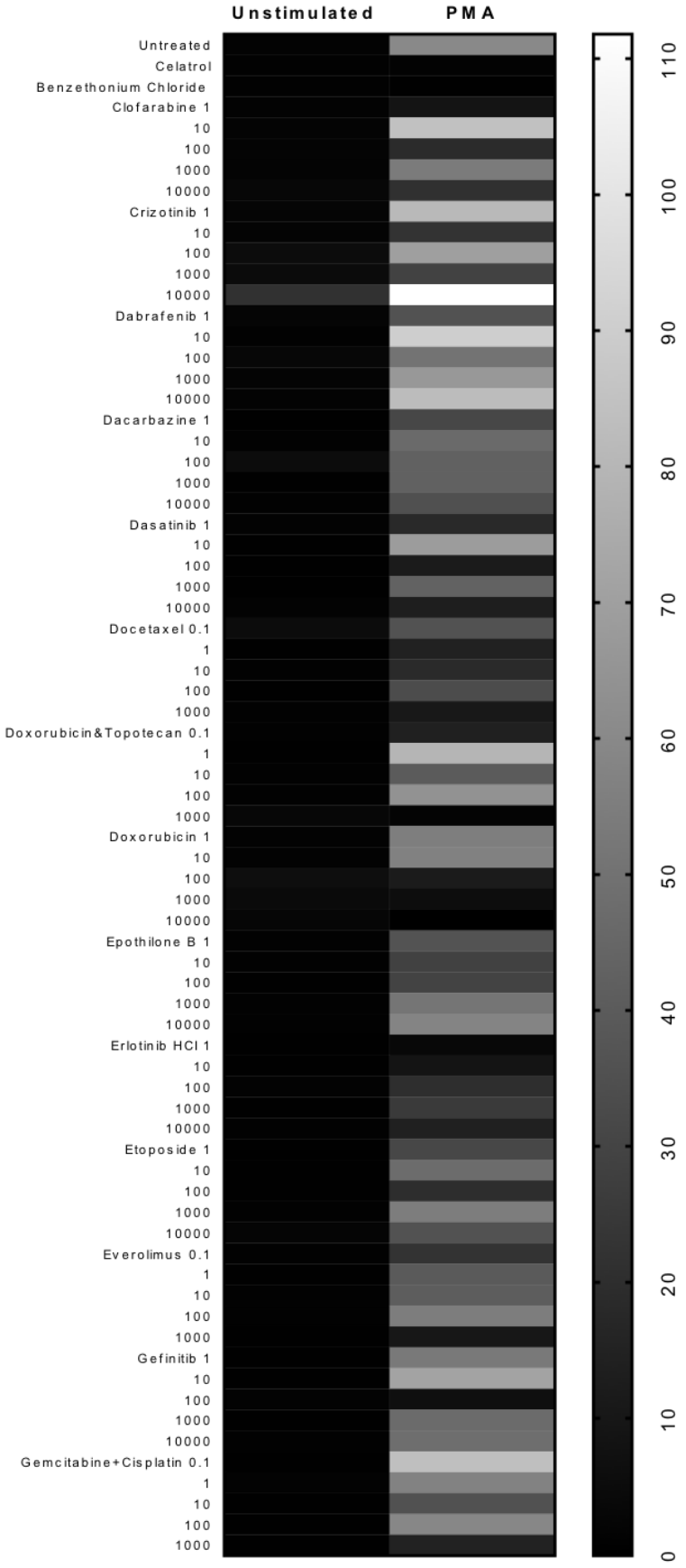
Unstimulated
PMA
Untreated
Celatrol
Benzethonium Chloride
Clofarabine 1
10
100
1000
10000
Crizotinib 1
10
100
1000
10000
Dabrafenib 1
10
100
1000
10000
Dacarbazine 1
10
100
1000
10000
Dasatinib 1
10
100
1000
10000
Docetaxel 0.1
1
10
100
1000
Doxorubicin&Topotecan 0.1
1
10
100
1000
Doxorubicin 1
10
100
1000
10000
Epothilone B 1
10
100
1000
10000
Erlotinib HCl 1
10
100
1000
10000
Etoposide 1
10
100
1000
10000
Everolimus 0.1
1
10
100
1000
Gefinitib 1
10
100
1000
10000
Gemcitabine+Cisplatin 0.1
1
10
100
1000
0
10
20
30
40
50
60
70
80
90
100
110

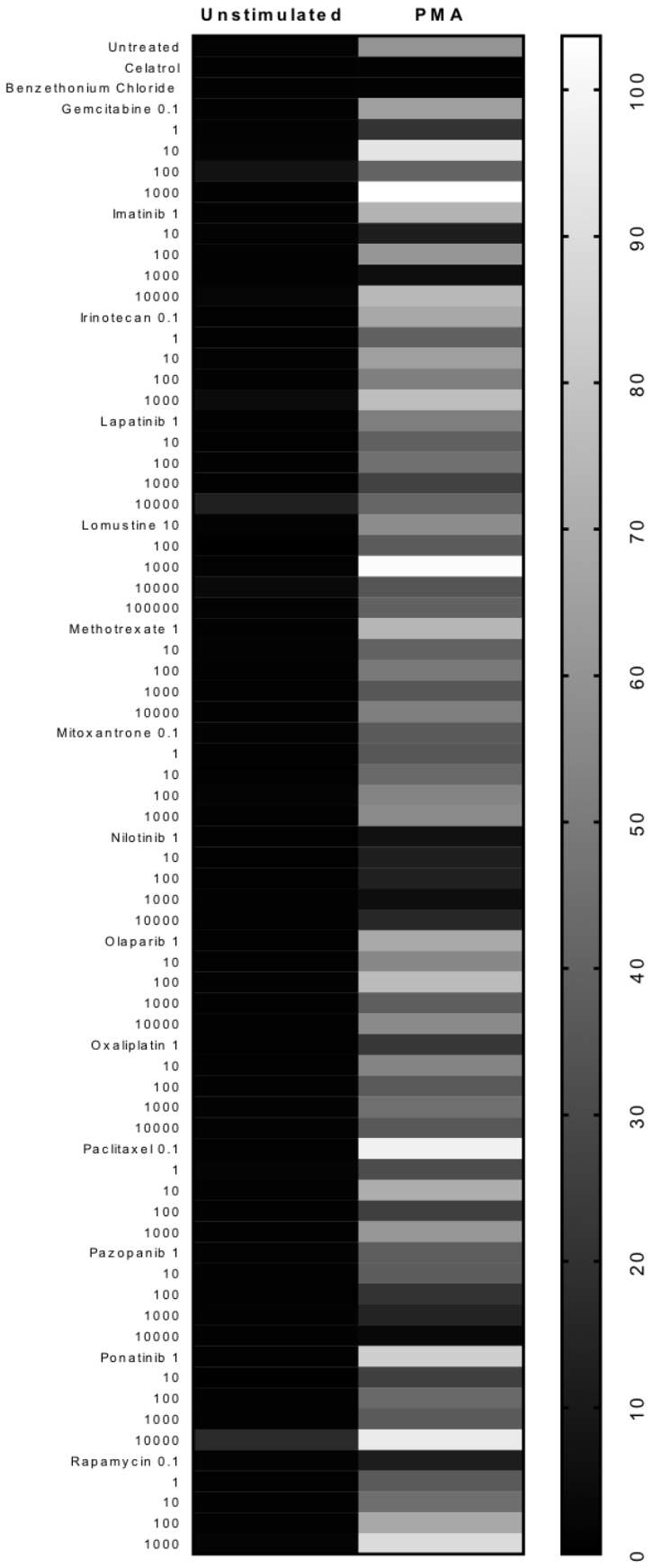
Unstimulated
PMA
Untreated
Celatrol
Benzethonium Chloride
Gemcitabine 0.1
1
10
100
1000
Imatinib 1
10
100
1000
10000
Irinotecan 0.1
1
10
100
1000
Lapatinib 1
10
100
1000
10000
Lomustine 10
100
1000
10000
100000
Methotrexate 1
10
100
1000
10000
Mitoxantrone 0.1
1
10
100
1000
Nilotinib 1
10
100
1000
10000
Olaparib 1
10
100
1000
10000
Oxaliplatin 1
10
100
1000
10000
Paclitaxel 0.1
1
10
100
1000
Pazopanib 1
10
100
1000
10000
Ponatinib 1
10
100
1000
10000
Rapamycin 0.1
1
10
100
1000
0
10
20
30
40
50
60
70
80
90
100

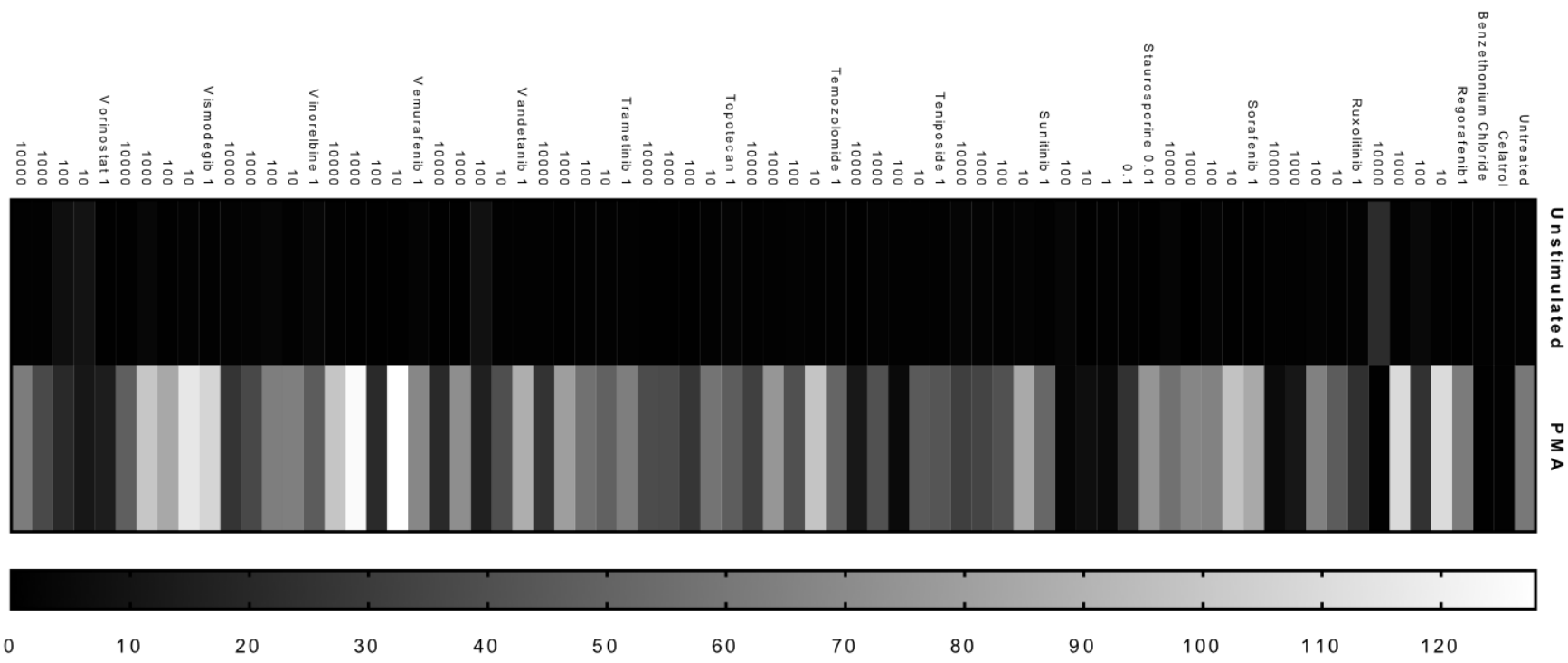

Figure 6.1: Heatmap representation of the range of activities induced by the compounds on NETosis.
Heatmap representing the NETotitc events calculated by HCS in unstimulated and PMA-stimulated neutrophils untreated or pre-treated with members of the 56-compound library. Values are calculated as the mean of two independent experiments and are expressed in a grey scale where black represents no NET detection and white represent the maximal NETotitc activity registered in the experiment. The untreated condition is represented as black due to the absence of stimulation and grey represents PMA-stimulated neutrophils.

6.3 Selection of compounds which modulate NETosis

Images associated with the compounds identified by the initial HCS were further analysed using the HCS Reader software. The nuclei in each image were analysed for false negative or false positive events. For instance, images captured out of focus presented nuclei with size and nuclear intensity inaccurately identified by the Nuclear Decondensation algorithm and were manually excluded from the selection process. Furthermore, nuclei were screened for apoptosis-related phenotypes as shown in Figure 6.2 and previously identified in neutrophils by Fuchs *et al.* (2007). Although apoptotic bodies were visible as black spots, the nuclei still presented similar features to NETosing activity which was misinterpreted by the algorithm and these were also manually excluded from the selection process.

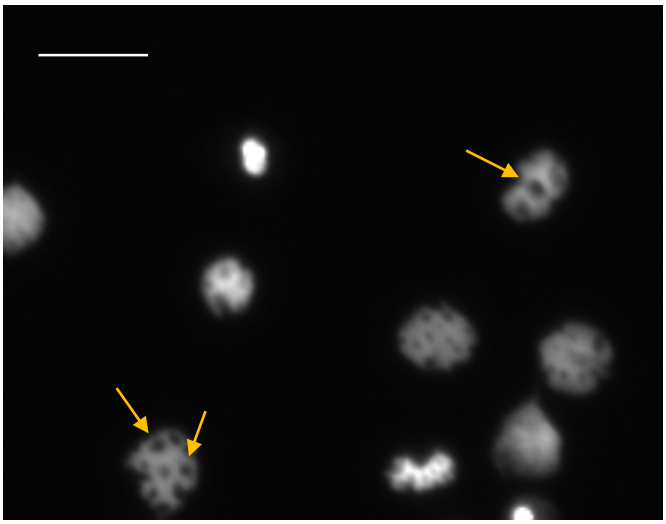

Figure 6.2: Apoptotic body detection in neutrophil nuclei.
Representative image of apoptotic body formation (yellow arrows) in Hoechst-stained neutrophil nuclei following treatment with Cladrabine. Scale bar represents 100μm.

Following an extensive literature search, those compounds that were associated with neutropenia or other forms of neutrophil cell death were also excluded from further study. Subsequently, of the 56 compounds initially screened for modulation of NETosis, 8 were selected for further downstream characterisation. In Figure 6.3 images of PMA stimulated and

compound-treated neutrophils are shown. PMA stimulated nuclei, utilised for the determination of nuclear size and intensity thresholds, presented characteristic NETosing morphology. Adjacent to this, celastrol treated neutrophils are shown, and as would be expected, these cells exhibited nuclei with unstimulated features which were used as controls for inhibitory activity.

6.3.1 NETosis inducers

Crizotinib and Ponatinib were selected as inducers of neutrophil activation since their application to PMA-stimulated neutrophils enhanced NETotic events to a greater level compared with PMA-alone treated neutrophils. Indeed, the majority of nuclei presented a decondensed morphology and numerous NET structures were visible in association with them.

6.3.2 NETosis inhibitors

Conversely, neutrophils treated with Carmustine, Erlotinib and Nilotinib, prior to PMA exposure, exhibited nuclear features consistent with celastrol treated cells and were, therefore, selected as inhibitors of NETosis.

6.3.3 Compounds causing biphasic effects on NETosis

Lapatinib, Bosutinib and Rapamycin displayed both inhibiting and enhancing activities when applied at different doses which correlated with the HCS findings. Bosutinib and Lapatinib were selected for further analysis, after HCS and manual screening, for their predominantly inhibitory activity, while Rapamycin was selected for its ability to increase PMA-induced stimulation.

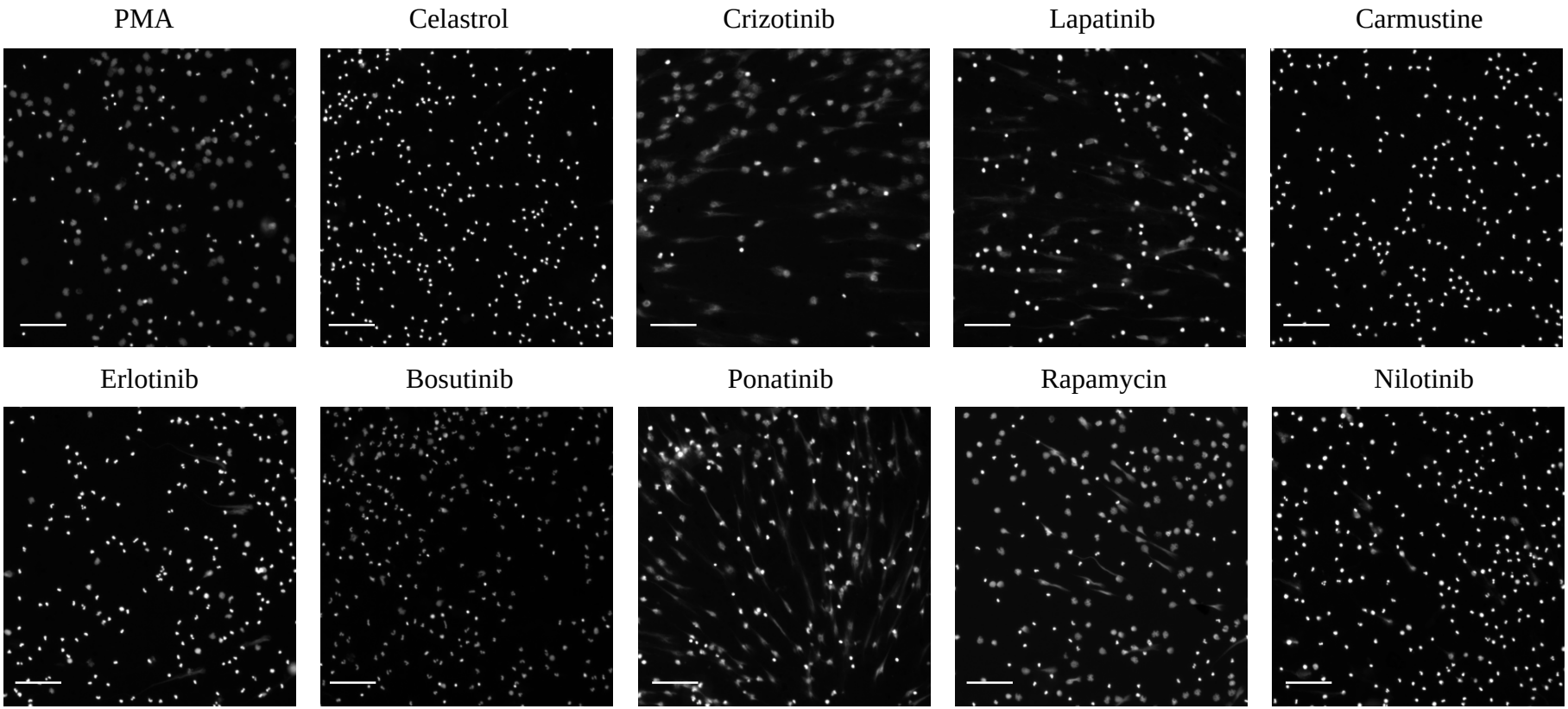

Figure 6.3: Images of compound-treated neutrophil nuclei.
Representative images of 3 hour PMA-stimulated neutrophil nuclei untreated or pre-treated with celastrol and the 8 compounds selected using HCS and manual screening applied at their highest concentration (10,000nM). Nuclei and NETs are visible following Hoechst staining. Images are representative of three independent experiments and are shown for comparison purposes. Scale bars represent 400μm.

6.4 Neutrophil dose-responses

The 8 selected compounds were characterised further for their neutrophil modulatory activity using more targeted approaches. The 8 compounds were simultaneously tested in neutrophils from 3 donors. Isolated neutrophils were seeded in clear 96-well plates and the 8 compounds were applied at a range of concentrations from 1nM and 10,000nM and samples incubated for up to 3 hours. PMA treatment was used as a positive control for stimulation, while celastrol and media alone were used as a negative control and to provide baseline readouts, respectively. To determine whether compounds induced a neutrophil response through the activation of NOX complexes, intracellular and extracellular ROS production were monitored by chemiluminescence assay (section 2.6.3). Simultaneously, their ability to induce NETosis was evaluated by fluorometric quantification after 3 hours incubation (section 2.6.5).

6.4.1 ROS production

Neutrophil ROS production was evaluated for 3 hours following compound treatment. The maximum values registered within the incubation time for each treatment are presented in Figure 6.4. PMA stimulation effectively induced ROS production, while data indicated none of the 8 compound treatments induced the activation of the ROS cascade (Figure 6.4a & b). Celastrol treatment resulted in statistically significant lower levels of ROS compared with media control, suggesting the compound-driven inhibition may also suppress the normal metabolic activity of unstimulated cells. Similar statistically significant differences were detected with Bosutinib and Ponatib treatments at relatively high doses (respectively at 10,000nM and at 1,000nM and 10,000nM), indicating the two compounds have inhibitory effects similar to celastrol (Figure 6.4b).

a)

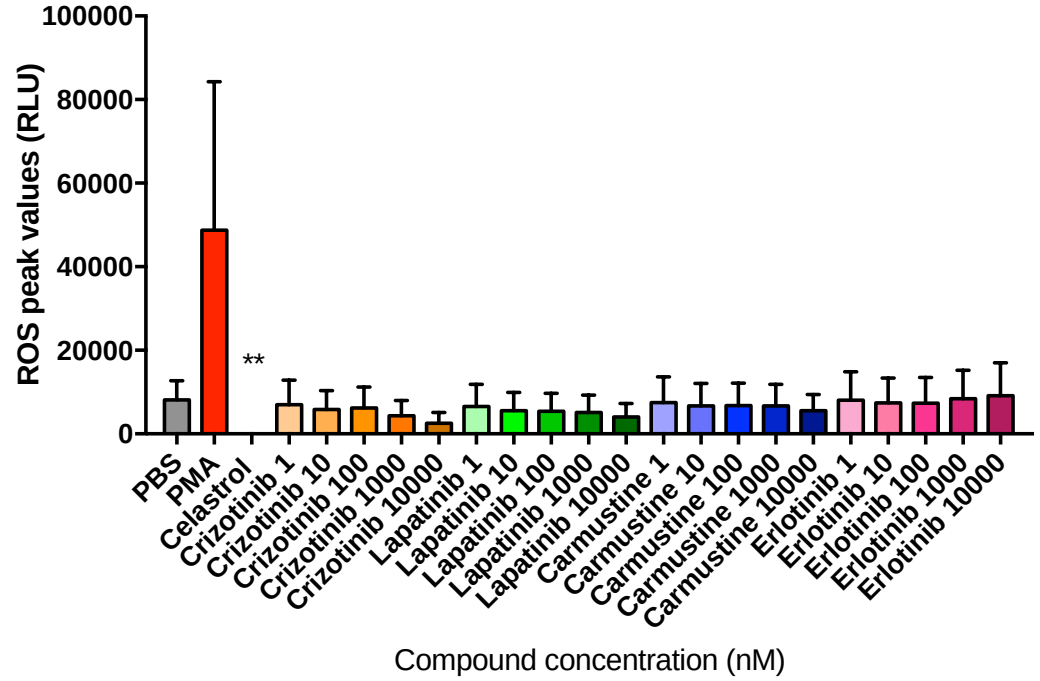

b)

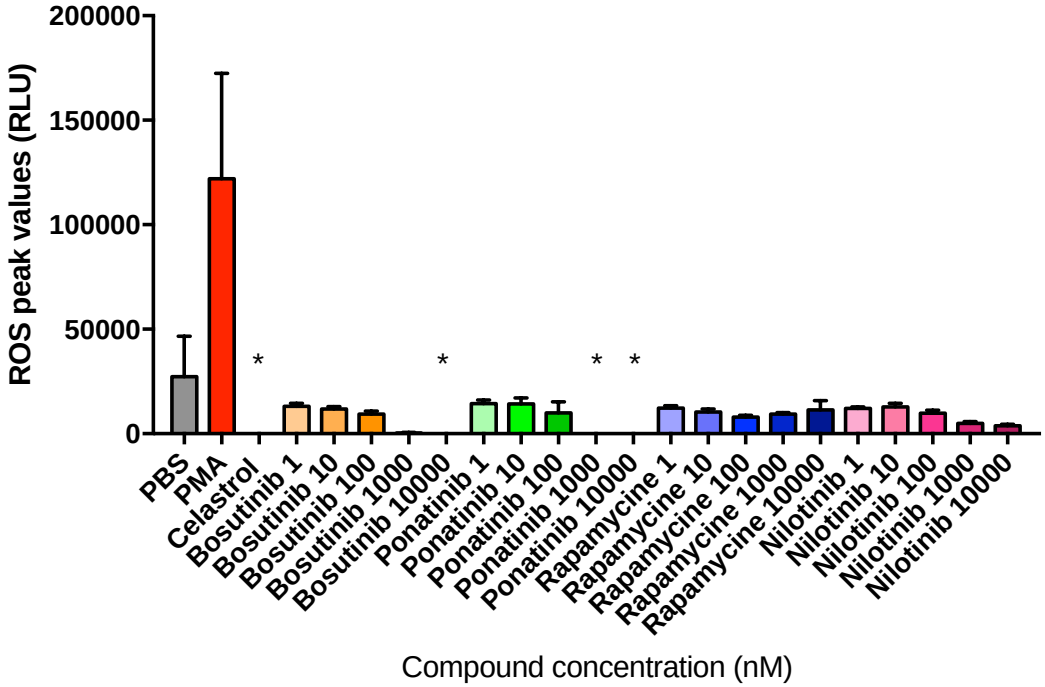

Figure 6.4: ROS production quantified in compound-treated neutrophils.
ROS production in unstimulated neutrophils which were untreated or pre-treated with 10µM celastrol or the 8 selected compounds at concentrations ranging from 1nM to 10,000nM, or stimulated with 50nM PMA for 3 hours. Values are expressed as relative light units (RLU) and mean ± SEM. Statistical significance was calculated using the Kruskal-Wallis's multiple comparison test (n= 3; *p<0.05, **p<0.01 compared with PBS control values).

6.4.2 NET production

Dose-response induction of NETosis in unstimulated neutrophils was evaluated by fluorometric measurement of extracellular NET-DNA release following 3 hours treatment with the selected compounds. Among the 8 tested compounds, only Crizotinib treatment at 10,000nM induced a significantly higher amount of NET-DNA release compared with the unstimulated/untreated control (Figure 6.5a). Furthermore, Bosutinib and Ponatinib treatments at 10,000nM resulted in increased NET-DNA release, although the difference compared with the media control was not statistically significant (Figure 6.5b). The other 5 compounds exhibited similar NET-DNA levels to that of the untreated control indicating their application to neutrophils did not trigger NETosis. Notably, the data for Crizotinib and Ponatinib treatments were consistent with the NET-inducing activity as determined by the HCS.

a)

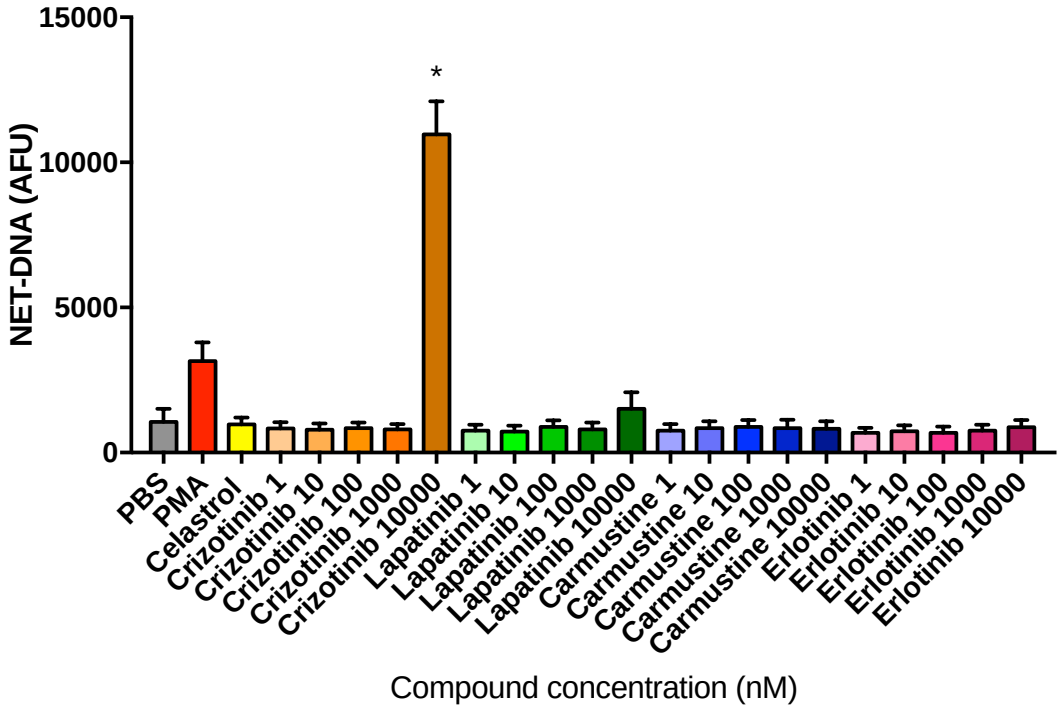

b)

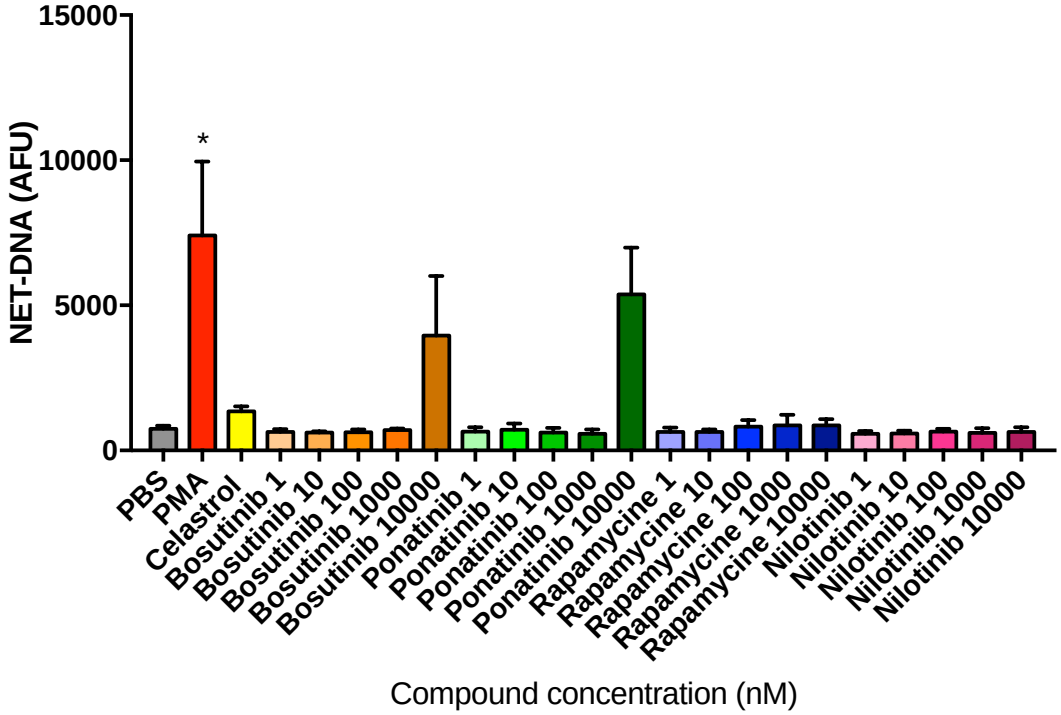

Figure 6.5: NET production quantified in compound-treated neutrophils.
Fluorometric NET quantification at 3 hours in unstimulated neutrophils untreated or pre-treated with 10μM celastrol or the 8 selected compounds using concentrations ranging from 1nM to 10,000nM, or stimulated with 50nM PMA. Values are expressed as arbitrary fluorescence units (AFU) and mean ± SEM. Statistical significance was calculated with Kruskal-Wallis's multiple comparison test (n= 3; *p<0.05 compared with PBS control values).

6.5 Dose-response inhibition of PMA-induced neutrophil activation

The 8 selected compounds were characterised for their ability to modulate responses in PMA activated neutrophils from 3 donors. Neutrophils were seeded in clear 96-well plates (as described in section 2.1) and were treated with the selected compounds at a range of concentrations from 1nM to 10,000nM and incubated for 30 minutes. Neutrophil stimulation was subsequently induced by PMA exposure (as described in section 2.4) for up to 3 hours. Treatment with PMA only was utilised as the positive control, while celastrol treatment was used as a control for inhibitory activity. In order to identify whether compounds were able to inhibit or enhance the PMA-induced NOX activation, intracellular and extracellular ROS production was monitored by chemiluminescence assay (section 2.6.3). Simultaneously, their ability to inhibit or increase PMA-induced NET release was evaluated by fluorometric quantification after 3 hours incubation (section 2.6.5).

6.5.1 Compound inhibition of PMA-induced ROS production

The dose-response modulation of PMA-induced ROS release was monitored for 3 hours and the maximum levels of ROS production following treatment were compared with the maximum levels registered in untreated cells throughout the stimulation period. Data presented in Figure 6.6 were normalised using the media-only control values in order to minimise the physiological differences between donors. Consistently, celastrol treatment significantly reduced PMA-induced ROS activity. Results presented in Figure 6.6a & b show an overall dose-response inhibition of NOX activity following compound treatment compared with PMA-stimulated neutrophils, although, in general, these results were not statistically significant. Interestingly, Crizotinib treatment at the highest dose (10,000nM) was able to significantly reduce the amount of ROS produced in response to PMA stimulation (Figure 6.6a). Notably, Carmustine,

Bosutinib and Ponatinib treatments, all at the highest dose (10,000nM), also reduced the levels of PMA-induced ROS (Carmustine in Figure 6.6a, Bosutinib and Ponatinib in Figure 6.6b). These differences were, however, not statistically significant.

a)

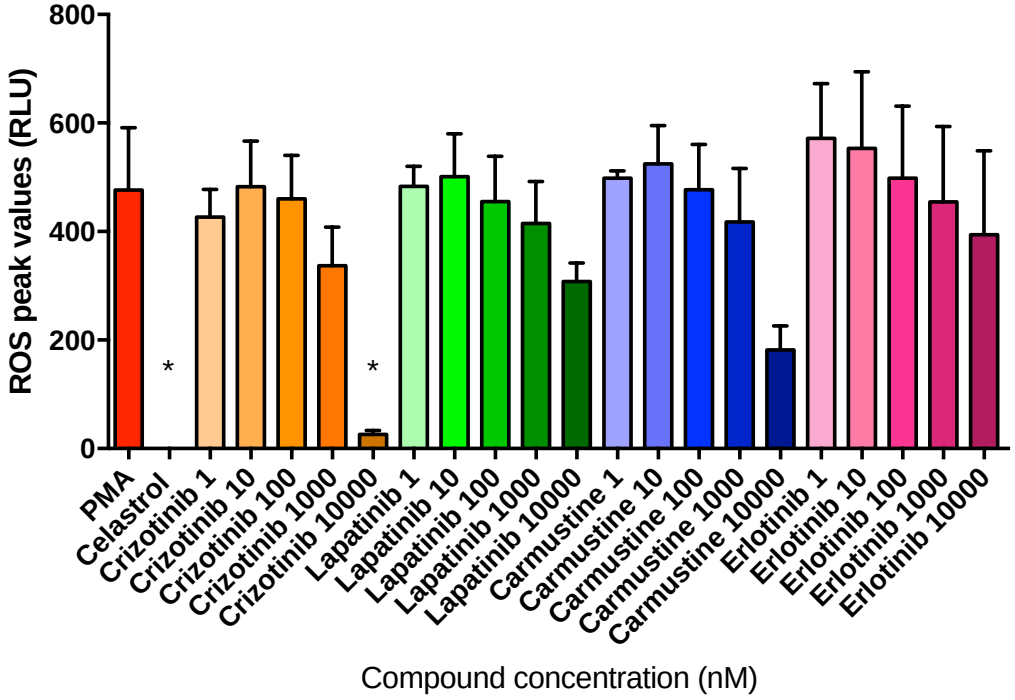

b)

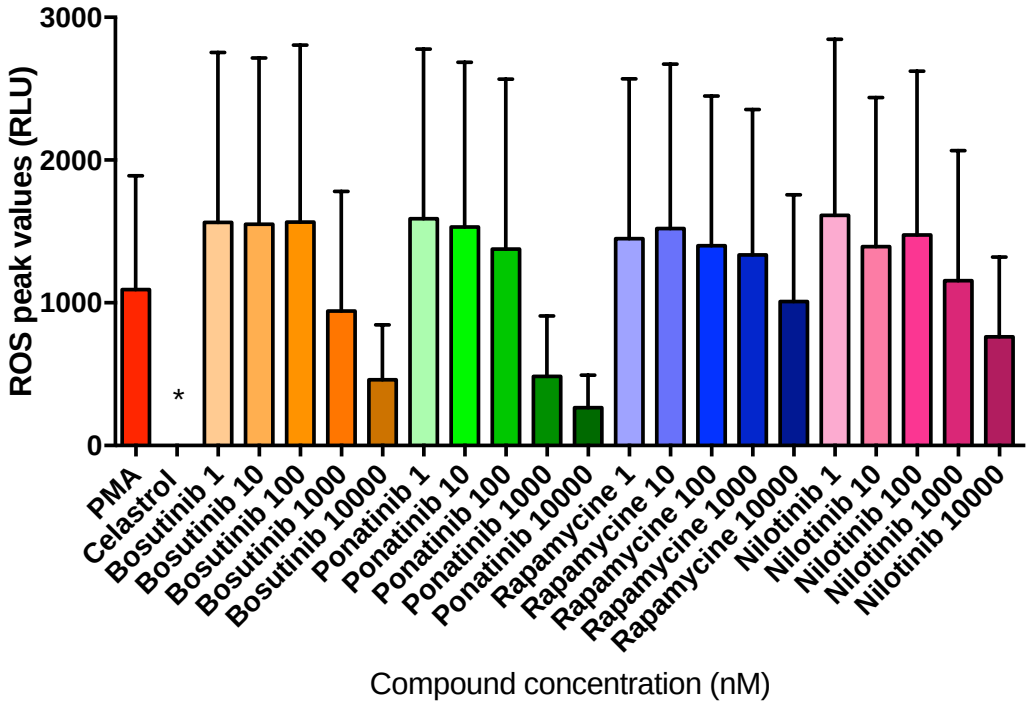

Figure 6.6: Compound inhibition of PMA-induced ROS.
ROS quantification in neutrophils stimulated for 3 hours with 50nM PMA and untreated or pre-treated with 10μM celastrol and the 8 selected compounds at concentrations of between 1nM and 10,000nM. Values are normalised to the media control and expressed as relative light units (RLU) and mean ± SEM. Statistical significance was calculated using the Kruskal-Wallis's multiple comparison test (n= 3; *p<0.05 compared with PMA control values).

6.5.2 Compound inhibition of PMA-induced NET production

Neutrophils were treated for 30 minutes with the selected compounds prior to stimulation with PMA. Compound dose-response modulation of PMA-induced NETosis was evaluated by fluorometric measurement of extracellular NET-DNA release following 3 hours incubation. Data presented in Figure 6.7 were normalised by media control values in order to minimise physiological differences between donors. Inhibition of NET release was identified following treatment with Lapatinib at 10nM and 1,000nM, Carmustine at 1nM, 10nM and 10,000nM and Erlotinib at 10nM and 1,000nM. Interestingly, Crizotininb treatment at the highest dosage (10,000nM) resulted in more than 3-fold higher DNA release, although this was not statistically significant, compared with the untreated control. Notably, these NETosis modulation findings were consistent with their activity as identified by the HCS. Statistical significance was identified for the inhibitory effects presented in Figure 6.7a. Celastrol treatment resulted in a non-statistically significant inhibition of NET-DNA release. This lack of statistical significance may be attributed to the donors' physiological variability. Notably, Ponatinib appeared to increase the PMA-induced NET production at higher doses (10,000nM), while Rapamycin inhibited NET release at the lowest dose (1nM) applied (Figure 6.7b). These differences were, however, not statistically significant.

a)

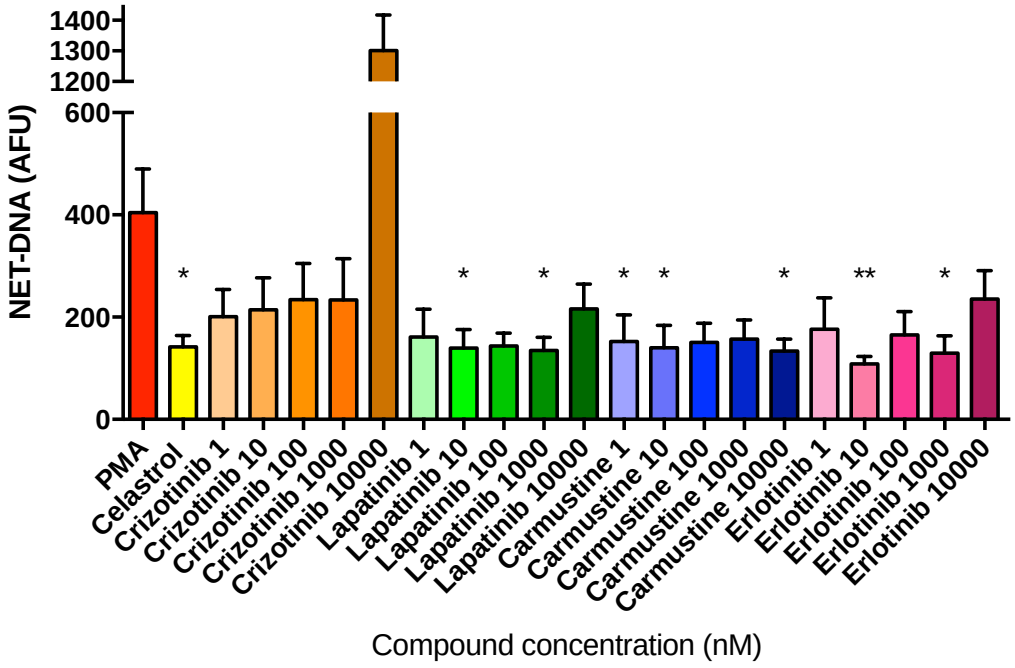

b)

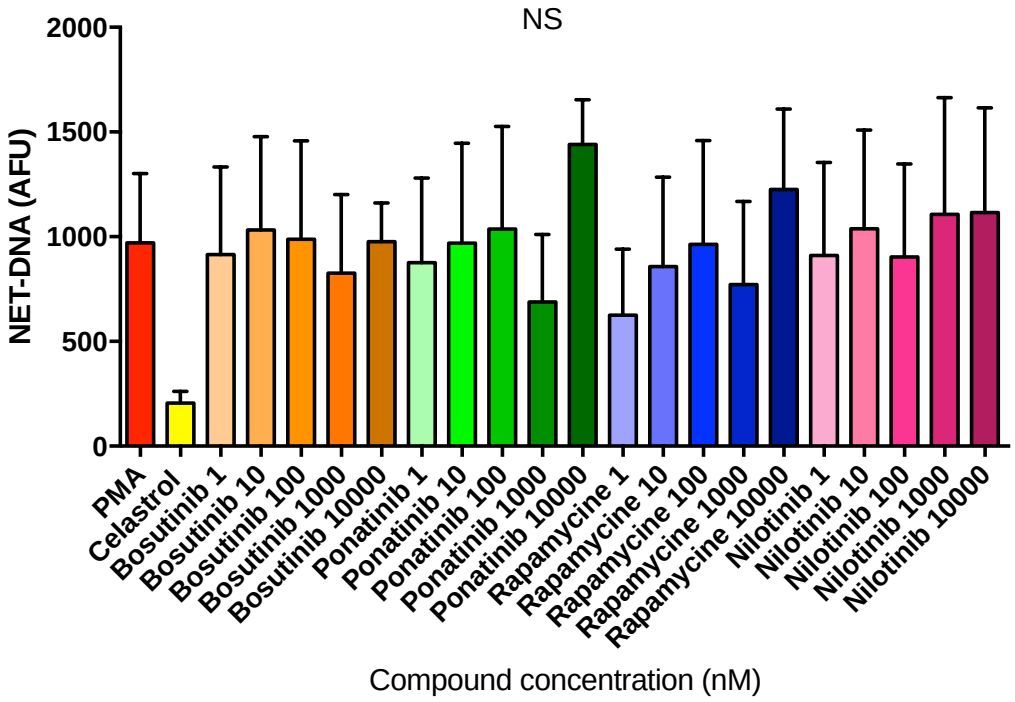

Figure 6.7: Compound inhibition of PMA-induced NETs.
NET quantification in neutrophils stimulated for 3 hours with 50nM PMA and untreated or pre-treated with 10μM celastrol and the 8 selected compounds at concentrations of between 1nM and 10,000nM. Values were normalised to the media control and expressed as arbitrary fluorescence units (AFU) and mean ± SEM. Statistical significance was calculated using the Kruskal-Wallis's multiple comparison test (n= 3; ns=non-significant, *p<0.05, **p<0.01 compared with PMA control values).

6.6 Analysis of LDH release from compound treated neutrophils

Concomitantly, with the modulation of ROS and NET production, LDH release following the use of the 8 compounds at their highest doses (10,000nM) was assessed. Neutrophils were seeded and exposed to the 8 selected compounds for 3 hours prior to LDH measurement (section 2.1.7.2). Neutrophils were unstimulated in order to determine baseline LDH activity, while the maximum LDH activity was determined following treatment with lysis buffer (as provided by the manufacturer). Results are presented in Figure 6.8 and indicated elevated percentage of LDH release were induced by Crizotinib, Bosutinib and Ponatinib treatments at their highest doses (10,000nM) while the other 5 compounds did not induce LDH release.

a)

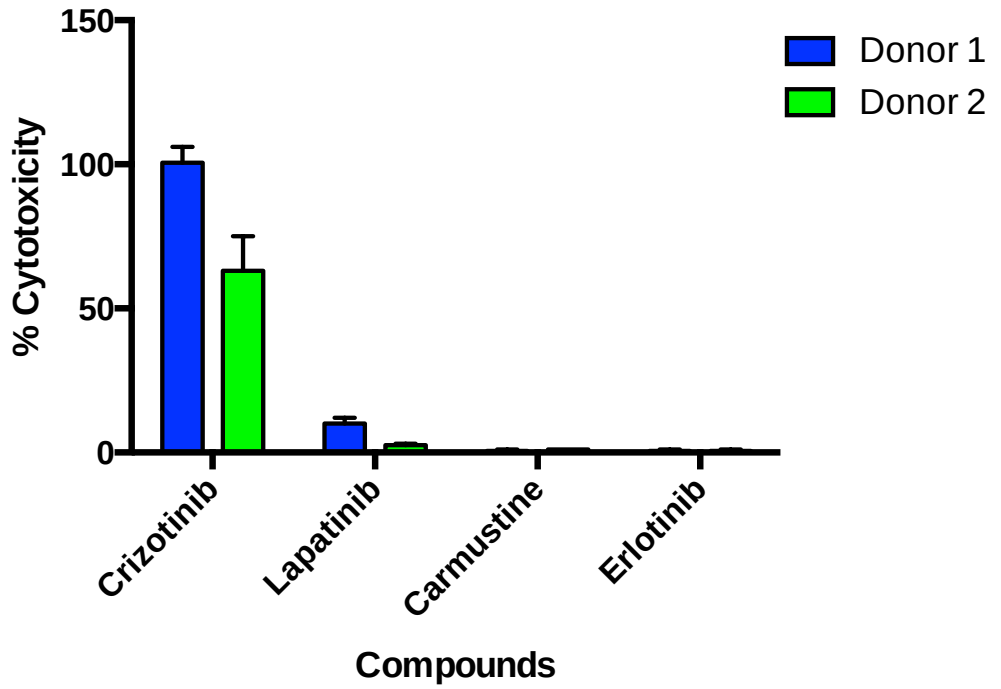

b)

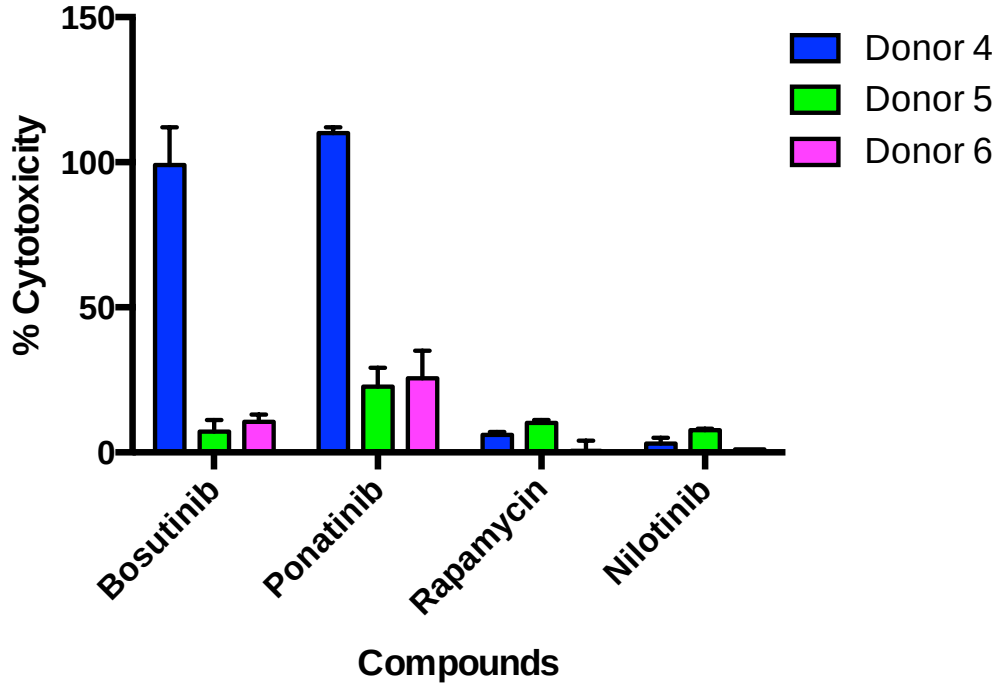

Figure 6.8: Assessment of neutrophil LDH release induced by the 8 compounds.
The 8 selected compounds were assessed at their highest concentration (10,000nM) for the percentage of LDH release in neutrophils. a) Crizotinib, Lapatinib, Carmustine and Erlotinib percentage of LDH release in two donors. b) Bosutinib, Ponatinib, Rapamycin and Nilotinib percentage of LDH release in three donors. Values are expressed as mean of two replicates (n= 2) ± SEM.

6.7 Discussion

The automated HCA approach developed and optimised for neutrophil application in the previous chapter was successfully applied in the screening of a 56-compound library for the identification of novel modulators of NETosis. The combined high-content and manual screening approaches identified 8 modulators of neutrophil activity. Subsequently, Crizotinib and Ponatinib were identified as inducers of NETosis, while Carmustine, Erlotinib and Nilotinib were identified as inhibitors. Interestingly, Lapatinib was identified as an inhibitor at a relatively low dose and acted as an inducer at higher doses, whereas Rapamycin acted as an inhibitor at low doses and Bosutinib was an inducer at low doses and an inhibitor at higher doses.

Notably the 8 compounds have been found to modulate multiple intracellular pathways in cancer cells and those relevant to neutrophil or NETosis activity are summarised in Table 6.1. Notably, several of these compounds have been previously associated with NETosing pathways. Indeed, Carmustine's inhibitory activity has been shown to target glutathione reductase (An *et al.*, 2011). This enzyme catalyzes the reduction of glutathione (GSH) from its oxidised state (GSSG), as described in section 2.1.3.1, and is responsible for maintaining a balanced redox status in neutrophils (Guerra *et al.*, 2012). Interestingly, elevated levels of GSSG have been related to the hyperactivity of neutrophils from periodontitis patients (Dias *et al.*, 2013) and, recently, Yan *et al.* (2012) demonstrated that glutathione reductase activity is essential for the production of murine NETs. Furthermore, Bosutinib is an inhibitor of the Src family kinases which have been previously identified as playing a role in regulating yeast-induced NET production (Nanì *et al.*, 2015). The compound Rapamycin has also been previously shown to regulate NETosis through the mTOR pathway and the induction of the hypoxia-inducible factor-1α (HIF-1α) (Mcinturff *et al.*, 2013).

Compound	Target of inhibition	Reference
Crizotinib	Anaplastic lymphoma kinase (ALK)/Proto-oncogene 1 receptor (ROS1) tyrosine kinase (TK)	(Ignatius Ou, 2011)
Lapatinib	Human epidermal growth factor receptor (HER)/ Epithelial growth factor receptor (EGFR) tyrosine kinase (TK)	(Davis *et al.*, 2011)
Carmustine	Glutathione reductase (GR)	(An *et al.*, 2011)
Erlotinib	Epithelial growth factor receptor (EGFR) tyrosine kinase (TK)	(Smith, 2005)
Bosutinib	Src family kinases	(Remsing Rix *et al.*, 2009)
Ponatinib	Vascular endothelial growth factor receptor (VEGFR)/Fibroblast growth factor receptor (FGFR) tyrosine kinase (TK)	(Price *et al.*, 2013)
Rapamycin	Mammalian target of rapamycin (mTOR)/Hypoxia-inducible factor 1α (HIF-1α)	(Mcinturff *et al.*, 2013)
Nilotinib	Platelet-derived growth factor receptor (PDGF-R) tyrosine kinase (TK)	(Weisberg *et al.*, 2005)

Table 6.1: Known molecular targets of the 8 selected compounds.

The 8 selected compounds were tested using relatively low-throughput techniques for further analysis of ROS production and NETosis with or without PMA stimulation. Results are summarised in Table 6.2. Notably, none of the 8 compounds induced ROS production in unstimulated neutrophils. Furthermore, Bosutinib and Ponatinib treatment resulted in significant lower levels of ROS compared with the media control. Similar results were observed in celastrol treated neutrophils, which suggests that these compounds may modulate neutrophil baseline metabolic activities. In support of this hypothesis is the fact that NF-κB, the cellular target of celastrol, has been shown to play a key role in the activation and regulation of NOX complexes in monocytes (Anrather *et al.*, 2006). Subsequently, celastrol treatment may impede the natural assembly of NADPH oxidase in resting neutrophils therefore limiting the baseline production of ROS.

Analysis of the effect of compound treatment on PMA stimulated neutrophils indicates high variability amongst the 3 donor neutrophil preparations in terms of ROS and NET production. Graphs presented in Figure 6.9 & Figure 6.10 demonstrate the trends identified for each donor individually. Graph a) in both figures represents the trends identified in experiments performed with donors 1, 2 and 3. Although minor differences were identified between donors, the 3 trends were similar and, therefore, the results were statistically significant. Conversely, experiments performed using donors 4, 5 and 6 resulted in broad and variable biological responses following compound treatment and, therefore, different trends of ROS and NET production. For instance, when analysing PMA-induced ROS formation, donor 5 presented higher values compared with the other two (Figure 6.9b). Notably, however, were the strong inhibitory effects on ROS production caused by Bosutinib and Ponatinib treatments at relatively high doses which were apparent in all 3 donor samples.

a) Set 1

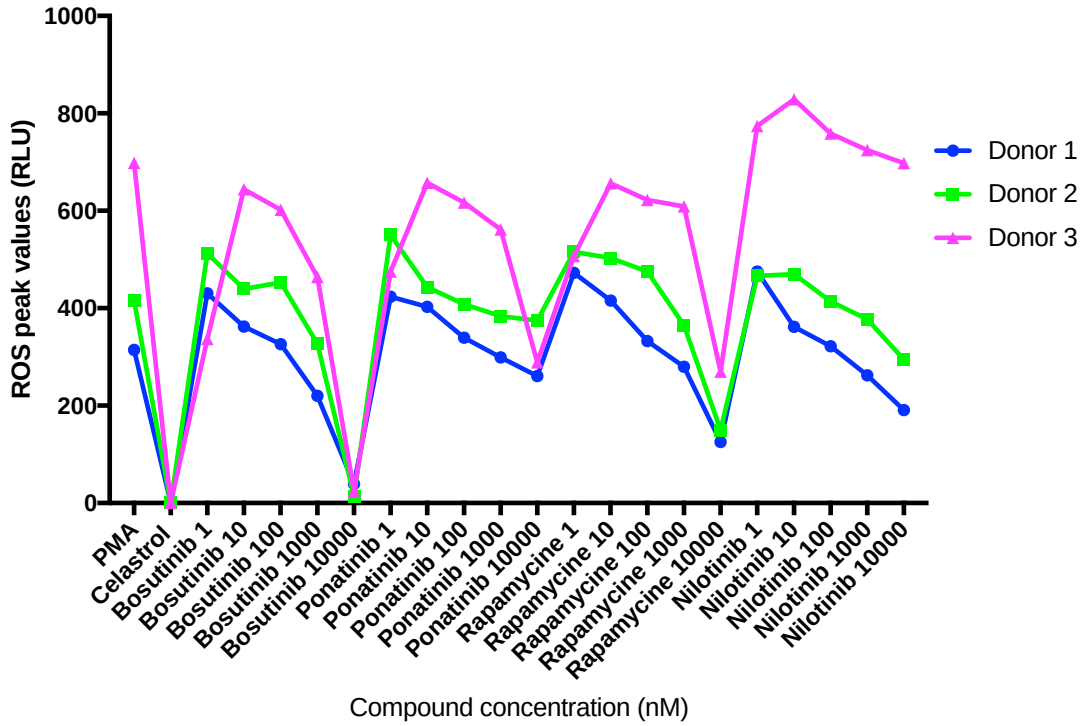

b) Set 2

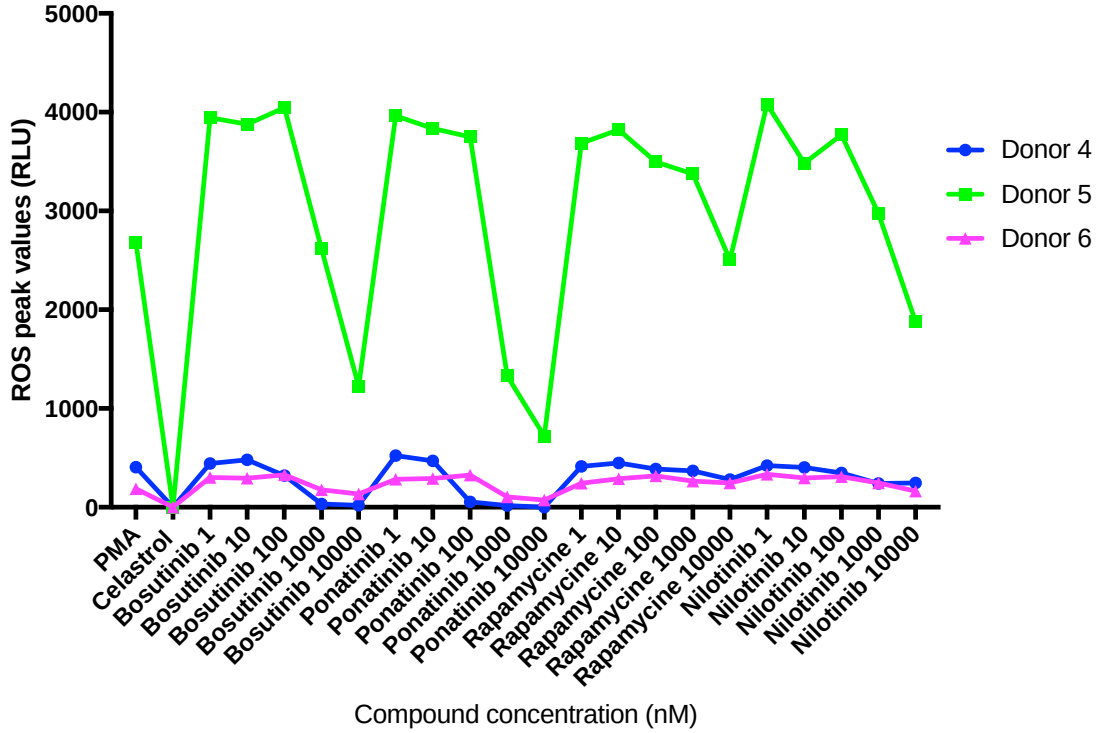

Figure 6.9: Re-plot of data presented in Figure 6.6 showing the variability in neutrophil responses from different donors.

Re-presentation of individual data points originally shown in Figure 6.6 demonstrating donor biological variability. Each individual trend (n=3) of activation is independently represented. Values are normalised to control and expressed as relative light units (RLU).

Even more variability was identified in the analysis of PMA-induced NET release (Figure 6.10b). The 3 trends of neutrophil activation showed some similarities such as in the inhibition due to treatment with celastrol, Ponatinib (1,000nM) and Rapamycin (1nM), and the increased activity due to treatment with Ponatinib (10,000nM). Notably, however, most NET-DNA values varied considerably between donors. An example of such variability was highlighted by the effect of Bosutinib treatment at the high dose (10,000nM) which resulted in inhibition in 2 donors, while induced a notable amount of NET-DNA release in the third donor. In this analysis, the absence of statistical significance for the differences presented in Figure 6.6 & Figure 6.7 is likely due to the biological variability between donors, which has been previously reported in other NET studies (Barrientos *et al.*, 2013; Brinkmann *et al.*, 2012).

a) Set 1

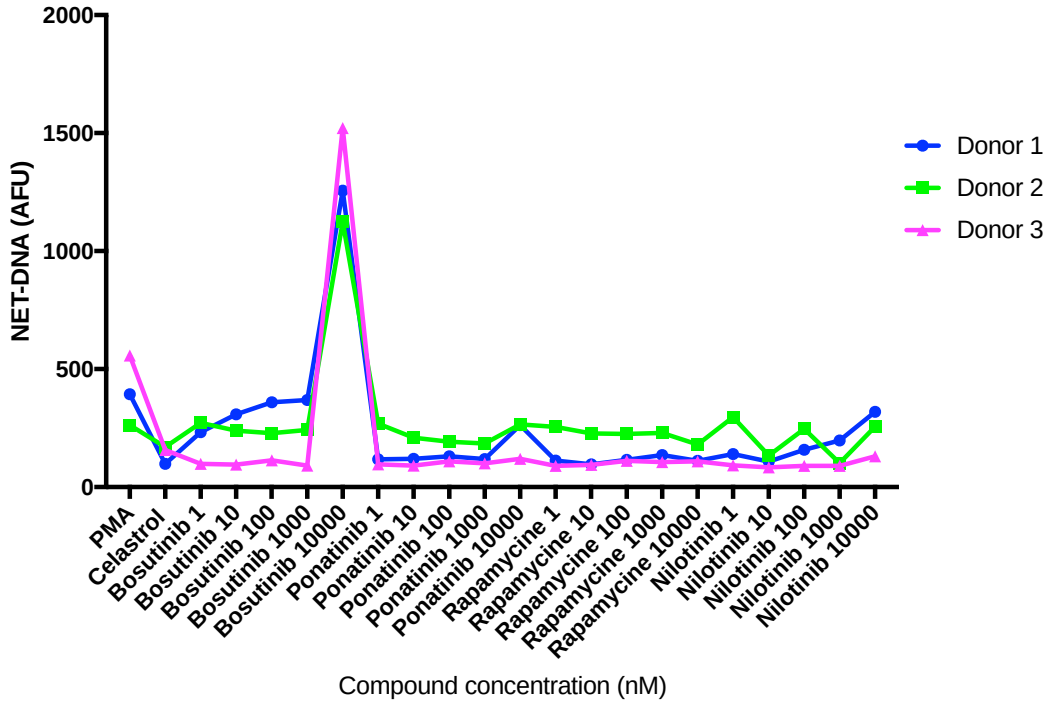

b) Set 2

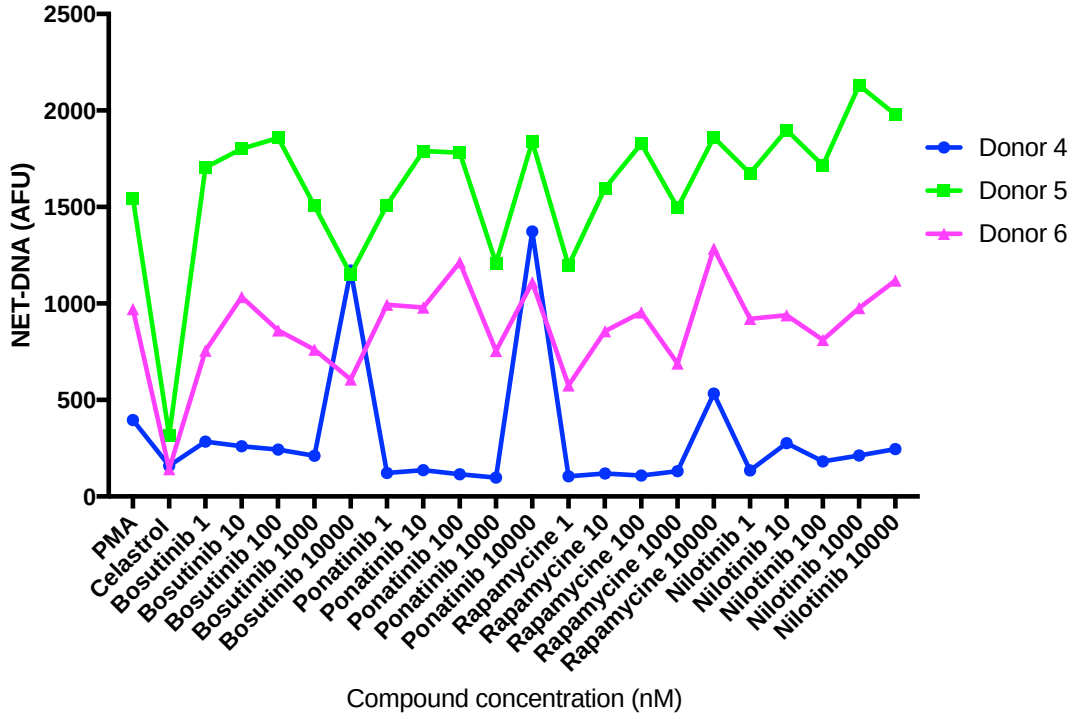

Figure 6.10: Re-plot of data presented in Figure 6.7 showing the variability in neutrophil responses from different donors.

Re-presentation of individual data points originally shown in Figure 6.7 demonstrating donor biological variability. Each individual trend (n=3) of activation is independently represented. Values are normalised to control and expressed as arbitrary fluorescence units (AFU).

Interestingly, Crizotinib treatment decreased the ROS activity induced by PMA stimulation. However, neutrophils exposed to the compound for 3 hours presented remarkably high levels of NET-DNA release, with and without additional PMA stimulation, compared with corresponding controls. Interestingly, Crizotinib, Bosutinib and Ponatinib induced DNA release but not ROS production suggesting an oxidant-independent activation of NETosis may be involved. A similar NETosis process to the aforementioned compounds has been identified with ionomycin treatment in studies which identified an alternative NADPH-independent pathway leading to NETosis and triggered by calcium influx (Parker *et al.*, 2012a). Therefore, it is possible that Crizotinib, Bosutinib and Ponatinib may target an alternative NADPH-independent pathway involved in calcium influx associated-NETosis which may overcome PMA-induced activation. However, whilst the compounds were selected based upon their induction of nuclear de-condensation, as analysed by HCS, it is not possible to exclude the possibility that data presented in this chapter that is based upon DNA staining, may also include some DNA released due to necrosis.

Data obtained for Lapatinib, Carmustine and Erlotinib treatments indicated these compounds exerted a similar effect on both unstimulated and PMA-stimulated neutrophils. In particular, ROS production was unaffected by the treatments, while PMA-induced NETosis was significantly decreased compared with the untreated control. Amongst the Lapatinib and Erlotinib targets is the phosphorylation activity of epithelial-growth-factor-receptor tyrosine kinase (EGFR-TK) which may be involved in PMA-induced NET formation. EGFR-TK regulates many intracellular activities including ROS formation and the activation of MAPKs (Purdom & Chen, 2005). However, since ROS production was not affected by the compound treatments, the modulation by theses compound may occur downstream of NOX activation. This is consistent with the findings of Keshari *et al.* (2013) which also identified the two

MAPKs, p38 and extracellular signal regulated kinase (ERK), as being involved in the regulation of PMA-induced NETosis. Interestingly, Carmustine treatment also appeared to affect NETosis downstream of the production of ROS suggesting NET formation may be modulated by the cellular redox status which, in turn, is controlled by the enzyme glutathione reductase.

Two other compounds presented similarity in their effects on unstimulated and stimulated neutrophils. Both Bosutinib and Ponatinib treatments efficiently reduced ROS production, independently of whether it was PMA-triggered or not. Their application to unstimulated neutrophils, however, induced a moderate NET-DNA release. In addition, Ponatinib treatment at high dosage was able to increase PMA-induced NET production. Since Bosutinib has among its targets the Src kinase family members, this data suggests they may be involved in NET formation (Nanì *et al.* 2015), and may regulate NET formation process by modulating MAPK activity.

Of further note was the effect of Rapamycin treatment on PMA-stimulated NETosis. Application of this compound resulted in the inhibition of the release of NET-DNA which has previously been reported by Mcinturff *et al.* (2013). Interestingly, however, no inhibition was observed with the previously published concentration of 200nM. Its effect was only detected at relatively low dose (1nM) in all three donors, while higher concentrations (100nM and above) resulted in the compound exerting no effects on NETosis, data which is in agreement with the findings of Gupta *et al.* (2014).

The LDH assay, as described in section 2.1.7.2 of Materials and Methods, provides a quantitative method for the assay of the intracellular enzyme LDH, which is released extracellularly following plasma membrane rupture in cellular death processes, such as necrosis

(Chan *et al.*, 2013). The assay is usually applied for the analysis of compound-induced or cell-mediated cytotoxicity, however, since NETs require membrane rupture for their extracellular release, in this study its application may indicate its utility as a biomarker for NETosis. Analysis of compound-induced LDH release upon treatment with Crizotinib, Bosutinib and Ponatinib at their highest dose applied (10,000nM) compared with control was assessed. These compounds induced DNA release which suggests the LDH identified in the supernatant could be released extracellularly following membrane rupture necessary for NET release. Taken together these results suggest LDH release could be applied along with other assays as a biomarker for monitoring the formation of NETs. Indeed, PMA-stimulated neutrophils presented LDH release levels above 50%, consistently with the NETotitc activity induced by this type of stimulation (Figure 6.11). Celastrol pre-treatment of PMA-stimulated neutrophils, however, decreased LDH release to minimal levels indicating that its detection is a consequence of NETosis.

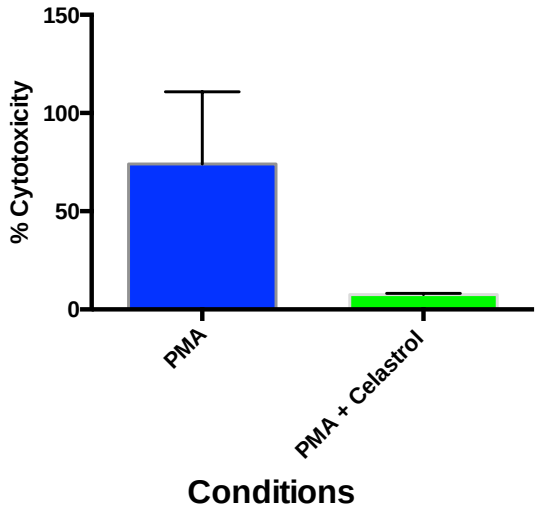

Figure 6.11: Extracellular LDH activity detected following PMA treatment of neutrophils. Percentage of LDH activity detected in PMA stimulated neutrophils with or without pre-treatment with celastrol (10μM). Values are expressed as mean of two replicates (n=2) ± SEM.

In this chapter, 8 compounds were selected for further analysis based on the initial HCS which indicated their modulatory activity for neutrophil ROS and NET production (Table 6.2). This analysis confirmed the modulatory functions of some compounds previously proposed by other

studies and, additionally, identified for the first time the involvement of other pathways or regulatory mechanisms in ROS and NET production. Subsequently, in addition to Rapamycin, the present study has now identified further 6 compounds which can modulate NETosis.

Compound	**ROS**	**NETs**
	Effect on unstimulated induction (+)/ inhibition (–)	**Effect on unstimulated induction (+)/ inhibition (–)**
Crizotinib	none	+
Lapatinib	none	none
Carmustine	none	none
Erlotinib	none	none
Bosutinib	–	$+^{ns}$
Ponatinib	–	$+^{ns}$
Rapamycin	none	none
Nilotinib	none	none
	Effect on PMA-stimulated induction (+)/ inhibition (–)	**Effect on PMA- stimulated induction (+)/ inhibition (–)**
Crizotinib	–	$+^{ns}$
Lapatinib	none	–
Carmustine	none	–
Erlotinib	none	–
Bosutinib	$-^{ns}$	none
Ponatinib	$-^{ns}$	$+^{ns}$
Rapamycin	none	$-^{ns}$
Nilotinib	none	none

Table 6.2: Summary of individual compound effects on ROS and NET activities in unstimulated and PMA-stimulated neutrophils.

(none = no effect detected; ^{ns}= non-significant)

CHAPTER 7: DISCUSSION & CONCLUSIONS

In the past decade, since Brinkmann *et al.* reported the antimicrobial properties of extracellular DNA filaments, the potential role for NETs in disease pathogenesis has attracted significant interest from researchers worldwide. NETs were originally identified as a neutrophil strategy for limiting the dissemination of microorganisms as for clearing infections in host tissues. Their antimicrobial effects were initially proposed to be fundamentally important in defending the body and maintaining a healthy host. However, numerous studies have demonstrated that an imbalance between NET production and clearance is related to tissue injury and to the development of certain diseases. Because of their components, structure and properties, these anti-microbial web-like structures have also been shown to have antigenic potential and can trigger an auto-immune/-inflammatory response in human. Subsequently, a better understanding of NET regulatory mechanisms will extend our knowledge of their role in the pathogenesis of a range of diseases enabling the development of novel therapeutic strategies.

12.1 Developing and optimising a protocol for HCA of NETs

Several automated and high-throughput techniques have previously been proposed for NET analysis, however, many of those currently exhibit a number of shortcomings including reproducibility and the limitation to single parameter analysis. In this thesis, a protocol was developed and optimised for the analysis of NETosis using HCA technology. The main advantage of this approach is the possibility of analysing a large population of neutrophils contained in the experimental sample, rather than limiting analyses to a selected proportion of that sample population. In this study experimental conditions, that were physiologically relevant to periodontitis pathogenesis as well as other inflammatory diseases involving NETs, were characterised and evaluated. Indeed, the periodontally-related pathogens, *F. nucleatum* and *P. gingivalis*, are known to induce a substantial neutrophilic response in terms of ROS and NET production and this activation reportedly contributes to the collateral tissue damage

characteristic of this disease (Delbosc *et al.*, 2011; Hirschfeld *et al.*, 2015; Matthews *et al.*, 2007b). Similar results in terms of ROS production were also observed in this thesis following stimulation with an *in vitro* multispecies biofilm of oral bacteria, developed to mimic tooth surface colonisation and which has previously been shown to induce a substantial inflammatory response in oral keratinocytes (Millhouse *et al.*, 2014). Interestingly, data from *in vitro* stimulation with oral biofilms presented in this thesis resulted in a strong response in terms of ROS production but with relatively poor levels of NET release. However, NET production was shown to be relatively high in response to challenge by a single species of heat-killed *F. nucleatum* and *P. gingivalis* but limited in response to pathogenic biofilms containing these two species, suggesting that bacterial aggregation and biofilm development may enhance bacterial mechanisms of evasion or regulation of NET release. Notably and consistently with this finding is a recent study which demonstrated that LPS from certain Gram negative bacteria is able to limit NET production (Pieterse *et al.*, 2016). It is therefore conceivable that modulatory effects upon NET release are exerted by the different components of a complex biofilm. Furthermore, DNases have been shown to be released by oral bacteria as a mechanism of enhanced virulence by degrading the NETs released and thereby evading capture by local tissue neutrophils in the periodontium (Palmer *et al.*, 2012b). Such mechanisms are likely to enable biofilm growth and bacterial spread and dissemination in tissues. Combined, data from these studies suggest that the *in vivo* developed oral biofilm at the gingival margin, although capable of inducing an inflammatory response, has evolved strategies to avoid NET capture and killing mechanisms. Potentially, therefore, neutrophils recruited to the site of infection and interacting with the pathogenic oral biofilm may employ ROS production rather than NET release to clear the biofilm-driven infection, which is supported by the *in vitro* data gathered in this thesis. In addition this could explain and be consistent with previous findings which identified *in vitro*

neutrophil hyper-responsiveness in term of ROS production (Matthews *et al.*, 2007b) but did not detect any difference in terms of NET production in periodontitis patients compared with healthy individuals (White *et al.*, 2016b). Notably, however, the *in vivo* presence of NETs in inflamed gingival tissues has been previously reported (Cooper *et al.* 2013), therefore, suggesting an alternative non-biofilm-driven mechanism *in vivo* for the NET response. Potentially, this could be underpinned by local cytokines and other immunological components present, which may contribute to disease development and its chronicity. Interestingly, inflammation chronicity in periodontitis patients is reported to be perpetuated by oral pathogens, such as *P. gingivalis*, in order for them to acquire a local source of nutrients for their growth (Scott & Krauss, 2012), subsequently, the direct or indirect triggering of NETs by virulence factors combined with bacterial evasion of NET killing may contribute to this process.

Furthermore salivary calcium, which is reportedly relatively abundant in periodontitis patients, can contribute to mineralisation of the oral biofilm providing a mechanism for its physical protection (Miller *et al.*, 2006; Sewon *et al.*, 1998; Sewón *et al.*, 1995), in addition enhanced calcium levels may contribute to the local priming of neutrophils for NETosis. Therefore, the combined process of increased biofilm protection with increased NET production in the inflamed periodontium may provide another bacterially-induced strategy for perpetuating inflammation in susceptible patients. Further studies should, therefore, explore the interaction between the oral biofilm, its composition and components, and neutrophils in order to elucidate the mechanism of NET release and its function in the pathogenesis of periodontitis.

Disease pathogenesis has been extensively investigated using murine models. In this thesis PAD4 knockout mice, which are deprived of the functional form of the enzyme, were tested for their ability to produce NETs and compared with neutrophils derived from wild-type animals and humans. PAD4 knockout mice were unable to release NETs compared with controls,

supporting previous studies claiming that PAD4 activity is fundamental for NET formation (Li *et al.*, 2010; Wang *et al.*, 2009). However, substantial differences have been identified between the NETosing activation process of murine and human neutrophils, suggesting the murine model may not be ideally suited for studying human NET biology. Further studies should better characterise the biological and molecular differences between murine and human neutrophils to determine the relevance of murine models for the investigation of human NET-related biology and disease (Gentile *et al.*, 2014).

A suitable protocol for the preparation and preservation of NET samples was developed in this study to enable the use of HCA at the laboratories of Imagen Therapeutics Ltd. Interestingly, NET production was found to be dependent upon neutrophil density when studied in a multi-well plate format, suggesting the involvement of a mechanism of cross-talk between cells in order to potentiate the NET antimicrobial response. Our previous studies have shown that following treatment with exogenous HOCl, a downstream product of the ROS cascade, relatively rapid NET release occurred (Palmer *et al.*, 2012a), and this suggests a role for ROS as an intercellular signalling factor. These findings are also supported by the infection susceptibility identified in patients affected by leukocyte adhesion disease and CGD who are ROS deficient (Bunting *et al.*, 2002; Holland, 2010) as this may in part be attributed to ineffective neutrophil cross-talk both in terms of ROS and NET production. Furthermore, potentially ineffective recruitment at the site of infection combined with aberrant neutrophil cross-talk may be involved in periodontitis pathogenesis due to the relatively low neutrophil density in tissues (Roberts *et al.*, 2015). Further studies are however necessary to better understand the mechanism of intracellular communication involved in NET regulation and determine its role in disease pathogenesis.

Particular attention in this study was paid to optimising the fixative procedures required for sample preservation and transportation since NETs are extremely fragile structures which require maintenance of their integrity for accurate analysis (Brinkmann & Zychlinsky, 2012). The majority of fixation protocols tested here were relatively aggressive and caused loss of NET filaments and alterations in NET spatial organisation. This finding raises concerns with regards to the objectivity and validity of previously published NET findings which largely employed sample preparation on glass slides and used microscopic observation for analysis. Subsequently, this supports the need for standardisation of objective analytical protocols which are automated and reproducible for NET analysis (Brinkmann *et al.*, 2012), thereby allowing meaningful comparison between studies. With the aim of robustly capturing NET structures on the well surface, poly-L-lysine pre-treatment of cultureware was assessed prior to sample preparation. However, the polymer contains cationic structures which may cause electrostatic interactions with the negatively charged extracellular DNA. This plausible interaction may retain NET filaments in the well and, therefore, may make its use unsuitable for application in fluorometric quantification assays. Indeed, the amount of NETs fluorometrically quantified in samples generated in poly-L-lysine treated wells was considerably lower than that detected in samples produced in untreated wells. Subsequently this approach was considered unsuitable for use in further studies which required validation of procedures by fluorometric NET quantification.

Once more suitable conditions for NET analysis were identified and the fixation protocol was optimised for NET preservation, HCA was performed for quantifying NETosis-associated features. Notably the HCA platform was initially developed for drug discovery and other large-scale biological applications, and has mainly been used for adherent cell analysis; indeed, there have been no previous reports using neutrophils in the HCA system. The software utilised for

HCA automated image analysis is provided with a number of built-in algorithms suitable for a wide range of biological applications. The settings of two of these algorithms, had characteristics that were thought appropriate for the features of NETosis. These were initially assessed for their ability to identify neutrophil nuclei and the quantification of NET related features. Subsequently, theses two algorithms, "Compartmental Analysis" and "Tube Formation", were tested for their accuracy and sensitivity in quantifying NETs. However, results obtained using these algorithms indicated that their application for NETosis exhibited key limitations mostly due to the inaccurate identification of the characteristic web-like morphology of NETs. Two further algorithms were, therefore, specifically developed for the analysis of NETosis-related features and these were termed "NET Detection" and "Nuclear Decondensation". These algorithms also had the advantage of being able to be applied simultaneously in order to provide multiparametric data and, therefore, were successfully utilised for the quantification of NETs and for the monitoring the activity of the PAD4 enzyme following PMA-stimulation. Notably, the Nuclear Decondensation algorithm quantified NETosing neutrophils based on changes in chromatin conformation and nuclear morphology. Data obtained using this algorithm were validated against other methods of NET quantification and supported findings that PMA induced DNA release was of a nuclear origin and subsequent NETosis involved rupture of the cell's plasma membrane (Fuchs *et al.*, 2007). These data were consistent with elevated extracellular LDH release also observed in this study. However, relevant stimuli and conditions that have been related to mitochondrial-derived NETs were not studied here (Yousefi *et al.*, 2009). Therefore, future research, undertaken using HCA and employing mitochondrial DNA tracker dyes, could focus on the identification of biomarkers for distinguishing between nuclear and mitochondrial NET release following priming of neutrophils with GM-CSF and then stimulating with LPS or complement factor 5a, as has

previously been reported by Yousefi *et al.* (2009) for mitochondrial-NET induction. Furthermore, of particular interest would be the combined HCA approach for monitoring the parameters involved in both types of NET formation pathways including, but not limited to, ROS production, histone citrullination and the extracellular release of DNA. Another result worthy of further investigation is the altered cellular morphology identified in PMA-stimulated neutrophils which is proposed to be due to cytoskeleton rearrangements. HCA has application for this analysis and provides a suitable platform for performing multiparametric measurements which may identify novel aspects of this process (Nauseef & Kubes, 2016; Yousefi & Simon, 2016).

12.2 Application of HCA for the identification of NETosis modulators

The HCA method optimised for NET analysis was applied to the screening of a compound library with the aim of identifying modulators which could increase or reduce NET formation, and subsequently, therefore, have therapeutic application. The library used was originally developed for cancer cell treatments and was composed of a wide range of pharmaceutically relevant compounds with varied targets for immune cell modulation. Following the initial HCS, further manual screening confirmed the identification of 8 modulators of NETosis among the 56 compounds tested. These 8 compounds were sub-categorised based on their effects on NET formation as being either inducers, inhibitors or biphasic modulators. Encouragingly, some of the compounds identified intracellular signalling which have been previously associated with neutrophil biology and NET formation, such as glutathione reductase, the Src and the mTOR pathways. These data supported the validity of the initial screening approach. Other potentially novel signal transduction pathways regulating NETosis were highlighted by the effects of the other compounds and identified roles for several receptor-associated tyrosine kinases. Interestingly, data presented here suggested that the MAPK pathway strongly associates with

NETosis. These data are consistent with the findings of a previous study (Keshari *et al.*, 2013), and could represent an interesting target for the treatment of NET-related diseases, since MAPK-driven phosphorylation controls a wide-range of pro-inflammatory signalling responses. The involvement of the glutathione pathway in NETosis was identified by Carmustine-induced inhibition of NET formation and was consistent with findings of a previous study showing that the activity of glutathione reductase is required for effective NET formation in murine neutrophils (Yan *et al.*, 2012). This pathway is of particular interest since it is relevant for neutrophil activation in several inflammatory diseases (Chapple, 1996), indeed, elevated levels of GSSG are associated with the hyper-responsive phenotype previously reported in neutrophils obtained from periodontitis patients (Dias *et al.*, 2013). Taken together this data suggests that periodontitis patients may be prone to aberrant glutathione reductase activity and, therefore, could exhibit decreased NET production. However this was not consistent with the finding of a recent clinical study (White, 2015), suggesting NET production in periodontitis patients may be triggered by another mechanism, such as calcium influx or increased levels of local pro-inflammatory cytokines (Ling *et al.*, 2015), which compensates for the decreased activity of glutathione reductase. Further investigation is therefore required to understand the molecular association between NETosis and the pathways identified by the HCS and these have the potential to be explored in more detail using the HCA platform. Indeed, future work could employ HCA for the screening of a larger and more targeted compound library, potentially focussing on the MAPK pathway as well as ones containing neutrophil receptor ligands. Such data would provide a better understanding of the regulation of NETosis and identify further compounds with therapeutic utility.

The effects of the 8 compounds selected by HCS were further investigated using specific low-throughput analysis of ROS and NET production. Compound treatment was assayed in

unstimulated and stimulated neutrophils. However, highly variable data were obtained using three different donors and this likely affected the statistical significance of the findings. Donor variability identified by low-throughput analysis of NETs and by previous studies (Barrientos *et al.*, 2013; Brinkmann *et al.*, 2012) may be overcome by the application of the HCA method in which levels of activation are standardised by baseline and maximum activation status using the algorithmic image analysis. Furthermore, using HCA a greater number of individual donor sample neutrophils could be simultaneously analysed adding to study power. This proposition further supports the application of HCA in the study and characterisation of NETosis.

Although the primary function of NETs is their antimicrobial effect, their structure is also reported to provide a source of autoantigens in several chronic inflammatory diseases (Hakkim *et al.*, 2010; Khandpur *et al.*, 2013). NET removal, therefore, potentially plays a fundamental role in the clearance of this antigenic material and this may be necessary in order to prevent the triggering of local and systemic autoimmune responses. Subsequently, it can be postulated that a delicate equilibrium exists between NET formation and removal in order to ensure both the adequate protection against infection and, at the same time, avoiding exposing the host tissues to injurious NET content for a prolonged time period. Indeed, when this equilibrium is lost an unbalanced immune response results in inflammation and disease progression. Notably, ineffective NET clearance has been related to the pathogenesis of inflammatory disorders such as CF (Cheng & Palaniyar, 2013), while ineffective NET formation can result in pathogen survival and infection dissemination as reported in CGD patients (Fuchs *et al.*, 2007). Anti-inflammatory drugs have previously been tested on neutrophils in order to inhibit NET formation (Lapponi *et al.*, 2013), however, interestingly, in this study, modulators with both effects, of inducing and inhibiting NETosis, were identified. The identification of compounds which exhibit a broad range of modulatory activity on NETosis provides the potential for

establishing a homeostatic balance in patients affected by NET-associated diseases. Notably, Crizotinib, Bosutinib and Ponatinib, were identified as NET inducers, and may therefore have application for treating NET-deficient patients such as those with CGD (Fuchs *et al.*, 2007); indeed, data indicates that their intracellular targets modulate NET formation downstream of the oxidative burst machinery. Furthermore, Bosutinib and Ponatinib together with Celastrol, efficiently decreased baseline and PMA-induced ROS production, suggesting treatment with these compounds may have therapeutic application for the hyper-responsiveness of neutrophils from patients affected by periodontitis (Matthews *et al.*, 2007b). Compounds identified as NET inhibitors, including Lapatinib, Carmustine and Erlotinib, may be employed for the treatment of conditions in which excess or aberrant NET production is related to disease development such as CF, SLE and RA (Cheng & Palaniyar, 2013; Hakkim *et al.*, 2010; Khandpur *et al.*, 2013). The pathways described above, however, require further investigation to identify the specific molecular mechanism behind their modulation of NET production. HCA has application for these studies, as has been demonstrated by the PAD4 analysis reported here. Indeed, the effects of compounds can be further evaluated in preclinical studies in neutrophils derived from healthy and diseased individuals as this may help understand the physiological role of NETosis in the human immune response.

12.3 Conclusions

The research described in this thesis explored analytical conditions, sample processing and protocol optimisation to develop a novel approach for the investigation of NETosis based on automated High-Content Analysis (HCA). The optimised protocol was applied for the screening of a pharmaceutically derived library of compounds for their ability to induce or inhibit the process of NETosis and successfully identified 8 modulators. The modulatory activities of the compounds selected by HCA were tested and validated by further analysis for

the induction of ROS and NET production. The analysis performed in this thesis has contributed to the understanding of previously described molecular pathways and has suggested the participation of other mechanisms involved in NETosis, which may represent new targets for feasible therapeutic approaches in treating NET-related inflammatory disorders as proposed for periodontitis.

References

Abdallah, D. S. A., Lin, C., Ball, C. J., King, M. R., Duhamel, G. E. and Denkers, E. Y. (**2012**) Toxoplasma gondii triggers release of human and mouse neutrophil extracellular traps, *Infection and Immunity*, 80 (2), pp. 768–777. DOI:10.1128/IAI.05730-11.

Abraham, V. C., Taylor, D. L. and Haskins, J. R. (**2004**) High content screening applied to large-scale cell biology, *Trends in Biotechnology*, 22 (1), pp. 15–22. DOI:10.1016/j.tibtech.2003.10.012.

Akira, S. (**2011**) Innate immunity and adjuvants., *Philosophical Transactions of the Royal Society of London. Series B, Biological Sciences*, 366 (1579), pp. 2748–55. DOI:10.1098/rstb.2011.0106.

Aleyd, E., van Hout, M. W. M., Ganzevles, S. H., Hoeben, K. a, Everts, V., Bakema, J. E. and van Egmond, M. (**2014**) IgA enhances NETosis and release of neutrophil extracellular traps by polymorphonuclear cells via Fcα receptor I., *Journal of Immunology (Baltimore, Md. : 1950)*, 192 (5), pp. 2374–83. DOI:10.4049/jimmunol.1300261.

Alteraifi, a M. and Zhelev, D. V (**1997**) Transient increase of free cytosolic calcium during neutrophil motility responses., *Journal of Cell Science*, 110 Pt 1, pp. 1967–1977.

Amulic, B., Cazalet, C., Hayes, G. L., Metzler, K. D. and Zychlinsky, A. (**2012**) Neutrophil Function: From Mechanisms to Disease, *Annu. Rev. Immunol*, 30, pp. 459–89. DOI:10.1146/annurev-immunol-020711-074942.

An, J. M., Kim, S. S., Rhie, J. H., Shin, D. M., Seo, S. R. and Seo, J. T. (**2011**) Carmustine induces ERK- and JNK-dependent cell death of neuronally-differentiated PC12 cells via generation of reactive oxygen species, *Toxicology in Vitro*, 25 (7), pp. 1359–1365. DOI:10.1016/j.tiv.2011.05.006.

Anrather, J., Racchumi, G. and Iadecola, C. (**2006**) NF-kappaB regulates phagocytic NADPH oxidase by inducing the expression of gp91phox., *The Journal of Biological Chemistry*, 281 (9), pp. 5657–67. DOI:10.1074/jbc.M506172200.

Babior, B. M., KiPNEs, R. S. and Cumvu, J. T. (**1973**) The production by leukocytes of superoxide, a potential bactericidal agent, *The Journal of Clinical Investigation*, 52, pp. 741–744.

Bardell, D. (**2004**) The Biologists' Forum: The invention of the microscope, *Bios*, 75 (2), pp. 78–84. DOI:10.1893/0005-3155(2004)75<78:TIOTM>2.0.CO;2.

Barnes, P. J. (**1997**) Nuclear factor-κB, *The International Journal of Biochemistry & Cell Biology*, 29 (6), pp. 867–870. DOI:10.1016/S1357-2725(96)00159-8.

Barrientos, L., Marin-Esteban, V., Chaisemartin, L. De, Le-Moal, V. L., Sandré, C., Bianchini, E., Nicolas, V., Pallardy, M. and Chollet-Martin, S. (**2013**) An improved strategy to recover large fragments of functional human neutrophil extracellular traps, *Frontiers in Immunology*, 4 (JUN), pp. 1–10. DOI:10.3389/fimmu.2013.00166.

Beiter, K., Wartha, F., Albiger, B., Normark, S., Zychlinsky, A. and Henriques-Normark, B. (**2006**) An endonuclease allows Streptococcus pneumoniae to escape from neutrophil extracellular traps, *Current Biology*, 16 (4), pp. 401–407. DOI:10.1016/j.cub.2006.01.056.

Bennouna, S., Bliss, S. K., Curiel, T. J. and Denkers, E. Y. (**2003**) Cross-talk in the innate immune system: neutrophils instruct recruitment and activation of dendritic cells during microbial infection., *Journal of Immunology (Baltimore, Md. : 1950)*, 171 (11), pp. 6052–8. DOI:10.4049/JIMMUNOL.171.11.6052.

Berends, E. T. M., Horswill, A. R., Haste, N. M., Monestier, M., Nizet, V. and Von Köckritz-Blickwede, M. (**2010**) Nuclease expression by Staphylococcus aureus facilitates escape from neutrophil extracellular traps, *Journal of Innate Immunity*, 2 (6), pp. 576–586. DOI:10.1159/000319909.

Berger-Achituv, S., Brinkmann, V., Abed, U. A., Kühn, L. I., Ben-Ezra, J., Elhasid, R. and Zychlinsky, A. (**2013**) A proposed role for neutrophil extracellular traps in cancer immunoediting, *Frontiers in Immunology*, 4. DOI:10.3389/fimmu.2013.00048.

Bergström, K. and Asman, B. (**1993**) Luminol enhanced Fc-receptor dependent chemiluminescence from peripheral PMN cells. A methodological study., *Scandinavian Journal of Clinical and Laboratory Investigation*, 53 (2), pp. 171–7.

Boe, D. M., Curtis, B. J., Chen, M. M., Ippolito, J. A. and Kovacs, E. J. (**2015**) Extracellular traps and macrophages: new roles for the versatile phagocyte., *Journal of Leukocyte Biology*, 97 (6), pp. 1023–35. DOI:10.1189/jlb.4RI1014-521R.

Borregaard, N. (**2010**) Neutrophils, from Marrow to Microbes, *Immunity*, 33 (5), pp. 657–670. DOI:10.1016/j.immuni.2010.11.011.

Borregaard, N. and Cowland, J. B. (**1997**) Granules of the human neutrophilic polymorphonuclear leukocyte., *Blood*, 89 (10), pp. 3503–3521.

Branzk, N. and Papayannopoulos, V. (**2013**) Molecular mechanisms regulating NETosis in infection and disease, *Seminars in Immunopathology*, 35 (4), pp. 513–530. DOI:10.1007/s00281-013-0384-6.

Bréchard, S. and Tschirhart, E. J. (**2008**) Regulation of superoxide production in neutrophils: role of calcium influx., *Journal of Leukocyte Biology*, 84 (5), pp. 1223–1237. DOI:10.1189/jlb.0807553.

Brinkmann, V., Goosmann, C., Kühn, L. I. and Zychlinsky, A. (**2012**) Automatic quantification of in vitro NET formation, *Frontiers in Immunology*, 3 (JAN), pp. 1–8.

DOI:10.3389/fimmu.2012.00413.

Brinkmann, V., Reichard, U., Goosmann, C., Fauler, B., Uhlemann, Y., Weiss, D. S., Weinrauch, Y. and Zychlinsky, A. (**2004**) Neutrophil extracellular traps kill bacteria., *Science (New York, N.Y.)*, 303 (5663), pp. 1532–1535. DOI:10.1126/science.1092385.

Brinkmann, V. and Zychlinsky, A. (**2007**) Beneficial suicide: why neutrophils die to make NETs., *Nature Reviews. Microbiology*, 5 (8), pp. 577–582. DOI:10.1038/nrmicro1710.

Brinkmann, V. and Zychlinsky, A. (**2012**) Neutrophil extracellular traps: Is immunity the second function of chromatin?, *Journal of Cell Biology*, 198 (5), pp. 773–783. DOI:10.1083/jcb.201203170.

Bruns, S., Kniemeyer, O., Hasenberg, M., Aimanianda, V., Nietzsche, S., Thywissen, A., Jeron, A., Latgé, J.-P., Brakhage, A. a and Gunzer, M. (**2010**) Production of extracellular traps against Aspergillus fumigatus in vitro and in infected lung tissue is dependent on invading neutrophils and influenced by hydrophobin RodA., *PLoS Pathogens*, 6 (4), pp. e1000873. DOI:10.1371/journal.ppat.1000873.

Buchanan, J. T., Simpson, A. J., Aziz, R. K., Liu, G. Y., Kristian, S. A., Kotb, M., Feramisco, J. and Nizet, V. (**2006**) DNase expression allows the pathogen group A Streptococcus to escape killing in neutrophil extracellular traps, *Current Biology*, 16 (4), pp. 396–400. DOI:10.1016/j.cub.2005.12.039.

Bunting, M., Harris, E. S., McIntyre, T. M., Prescott, S. M. and Zimmerman, G. A. (**2002**) Leukocyte adhesion deficiency syndromes: adhesion and tethering defects involving beta 2 integrins and selectin ligands., *Current Opinion in Hematology*, 9 (1), pp. 30–5.

Campbell, J. J., Hedrick, J., Zlotnik, A., Siani, M. A., Thompson, D. A., Butcher, E. C. and Ziotnik, A. (**1998**) Chemokines and the Arrest of Lymphocytes Rolling Under Flow Conditions, *Source: Science, New Series*, 279 (5349), pp. 381–384.

Carlin, A. F., Uchiyama, S., Chang, Y. C., Lewis, A. L., Nizet, V. and Varki, A. (**2009**) Molecular mimicry of host sialylated glycans allows a bacterial pathogen to engage neutrophil Siglec-9 and dampen the innate immune response, *Blood*, 113 (14), pp. 3333–3336. DOI:10.1182/blood-2008-11-187302.

Chan, F. K.-M., Moriwaki, K. and De Rosa, M. J. (2013) Detection of Necrosis by Release of Lactate Dehydrogenase Activity, in: pp. 65–70.

Chapple, I. L. C. (**1996**) Reviews Role of free radicals and antioxidants in the pathogenesis of the inflammatory periodontal diseases, *J Clin Pathol: Mol Pathol*, 49, pp. 247–255.

Chapple, I. L. C. and Matthews, J. B. (**2007**) The role of reactive oxygen and antioxidant species in periodontal tissue destruction, *Periodontology 2000*, 43 (1), pp. 160–232. DOI:10.1111/j.1600-0757.2006.00178.x.

Cheng, O. Z. and Palaniyar, N. (**2013**) NET balancing: A problem in inflammatory lung diseases, *Frontiers in Immunology*, 4 (JAN), pp. 1–13. DOI:10.3389/fimmu.2013.00001.

Chia, N.-Y., Chan, Y.-S., Feng, B., Lu, X., Orlov, Y. L., Moreau, D., Kumar, P., Yang, L., Jiang, J., Lau, M.-S., Huss, M., Soh, B.-S., Kraus, P., Li, P., Lufkin, T., Lim, B., Clarke, N. D., Bard, F. and Ng, H.-H. (**2010**) A genome-wide RNAi screen reveals determinants of human embryonic stem cell identity, *Nature*, 468 (7321), pp. 316–320. DOI:10.1038/nature09531.

Clark, S. R., Ma, A. C., Tavener, S. A., McDonald, B., Goodarzi, Z., Kelly, M. M., Patel, K. D., Chakrabarti, S., McAvoy, E., Sinclair, G. D., Keys, E. M., Allen-Vercoe, E., DeVinney, R., Doig, C. J., Green, F. H. Y. and Kubes, P. (**2007**) Platelet TLR4 activates neutrophil extracellular traps to ensnare bacteria in septic blood, *Nature Medicine*, 13 (4), pp. 463–469. DOI:10.1038/nm1565.

Cools-Lartigue, J., Spicer, J., McDonald, B., Gowing, S., Chow, S., Giannias, B., Bourdeau, F., Kubes, P. and Ferri, L. (**2013**) Neutrophil extracellular traps sequester circulating tumor cells and promote metastasis., *The Journal of Clinical Investigation*. DOI:10.1172/JCI67484.

Coons, A. H. and Kaplan, M. H. (**1950**) Localization of antigen in tissue cells; improvements in a method for the detection of antigen by means of fluorescent antibody., *The Journal of Experimental Medicine*, 91 (1), pp. 1–13. DOI:10.1084/jem.91.1.1.

Cooper, P. R., Palmer, L. J. and Chapple, I. L. C. (**2013**) Neutrophil extracellular traps as a new paradigm in innate immunity: friend or foe?, *Periodontology 2000*, 63 (1), pp. 165–197. DOI:10.1111/prd.12025.

Corfe, B. M., Kilner, J., Chowdry, J., Benson, R. S. P., Griffiths, G. J. and Evans, C. A. (**2013**) Application of high content biology to yield quantitative spatial proteomic information on protein acetylations., *Methods in Molecular Biology (Clifton, N.J.)*, 981, pp. 37–45. DOI:10.1007/978-1-62703-305-3_4.

Corning (**2010**) Surface Areas and Recommended Medium Volumes for Corning ® Cell Culture Vessels, l, pp. 1–4.

Dahlén, G., Manji, F., Baelum, V. and Fejerskov, O. (**1992**) Putative periodontopathogens in 'diseased' and 'non-diseased' persons exhibiting poor oral hygiene, *Journal of Clinical Periodontology*, 19 (1), pp. 35–42. DOI:10.1111/j.1600-051X.1992.tb01146.x.

Darveau, R. P. (**2010**) Periodontitis: a polymicrobial disruption of host homeostasis, *Nature Reviews Microbiology*, 8 (7), pp. 481–490. DOI:10.1038/nrmicro2337.

Darveau, R. P., Tanner, a and Page, R. C. (**1997**) The microbial challenge in periodontitis., *Periodontology 2000*, 14 (79), pp. 12–32. DOI:10.1111/j.1600-0757.1997.tb00190.x.

Daub, A., Sharma, P. and Finkbeiner, S. (**2009**) High-content screening of primary neurons:

ready for prime time, *Current Opinion in Neurobiology*, 19 (5), pp. 537–543. DOI:10.1016/j.conb.2009.10.002.

Davis, M. I., Hunt, J. P., Herrgard, S., Ciceri, P., Wodicka, L. M., Pallares, G., Hocker, M., Treiber, D. K. and Zarrinkar, P. P. (**2011**) Comprehensive analysis of kinase inhibitor selectivity, *Nature Biotechnology*, 29 (11), pp. 1046–1051. DOI:10.1038/nbt.1990.

de Buhr, N. and von Köckritz-Blickwede, M. (**2016**) How Neutrophil Extracellular Traps Become Visible., *Journal of Immunology Research*, 2016, pp. 4604713. DOI:10.1155/2016/4604713.

de Pablo, P., Chapple, I. L. C., Buckley, C. D. and Dietrich, T. (**2009**) Periodontitis in systemic rheumatic diseases., *Nature Reviews. Rheumatology*, 5 (4), pp. 218–224. DOI:10.1038/nrrheum.2009.28.

De Vos, K. J. and Sheetz, M. P. (**2007**) Visualization and Quantification of Mitochondrial Dynamics in Living Animal Cells, *Methods in Cell Biology*. DOI:10.1016/S0091-679X(06)80030-0.

DeBiasio, R., Bright, G. R., Ernst, L. A., Waggoner, A. S. and Taylor, D. L. (**1987**) Five-parameter fluorescence imaging: wound healing of living Swiss 3T3 cells., *Journal of Cell Biology*, 105 (4), pp. 1613–1622. DOI:10.1083/jcb.105.4.1613.

Delbosc, S., Alsac, J.-M., Journe, C., Louedec, L., Castier, Y., Bonnaure-Mallet, M., Ruimy, R., Rossignol, P., Bouchard, P., Michel, J.-B. and Meilhac, O. (**2011**) Porphyromonas gingivalis participates in pathogenesis of human abdominal aortic aneurysm by neutrophil activation. Proof of concept in rats., *PloS One*, 6 (4), pp. e18679. DOI:10.1371/journal.pone.0018679.

Demers, M. and Wagner, D. (**2014**) NETosis: A New Factor in Tumor Progression and Cancer-Associated Thrombosis, *Seminars in Thrombosis and Hemostasis*, 40 (3), pp. 277–283. DOI:10.1055/s-0034-1370765.

Descoteaux, A., Gabriel, C., Mcmaster, W. R. and Girard, D. (**2010**) Extracellular Traps the Antimicrobial Activity of Neutrophil Promastigotes Evade Leishmania donovani Leishmania donovani Promastigotes Evade the Antimicrobial Activity of Neutrophil Extracellular Traps, *The Journal of Immunology*, 185 (185), pp. 4319–4327. DOI:10.4049/jimmunol.1000893.

Devine, D. A., Marsh, P. D. and Meade, J. (**2015**) Modulation of host responses by oral commensal bacteria., *Journal of Oral Microbiology*, 7, pp. 26941. DOI:10.3402/jom.v7.26941.

Dewitt, S., Laffafian, I. and Hallett, M. B. (**2003**) Phagosomal oxidative activity during beta2 integrin (CR3)-mediated phagocytosis by neutrophils is triggered by a non-restricted Ca2+ signal: Ca2+ controls time not space., *Journal of Cell Science*, 116 (Pt 14), pp. 2857–2865. DOI:10.1242/jcs.00499.

Dias, I. H. K., Chapple, I. L. C., Milward, M., Grant, M. M., Hill, E., Brown, J. and

Griffiths, H. R. (**2013**) Sulforaphane Restores Cellular Glutathione Levels and Reduces Chronic Periodontitis Neutrophil Hyperactivity In Vitro, *PLoS ONE*, 8 (6), pp. 1–13. DOI:10.1371/journal.pone.0066407.

Dierickx, K., Pauwels, M., Van Eldere, J., Cassiman, J. J., van Steenberghe, D. and Quirynen, M. (**2002**) Viability of cultured periodontal pocket epithelium cells and Porphyromonas gingivalis association, *Journal of Clinical Periodontology*, 29 (11), pp. 987–996. DOI:10.1034/j.1600-051X.2002.291103.x.

Douda, D. N., Khan, M. A., Grasemann, H. and Palaniyar, N. (**2015**) SK3 channel and mitochondrial ROS mediate NADPH oxidase-independent NETosis induced by calcium influx., *Proceedings of the National Academy of Sciences of the United States of America*, 112 (9), pp. 2817–22. DOI:10.1073/pnas.1414055112.

Dragunow, M. (**2008**) High-content analysis in neuroscience., *Nature Reviews. Neuroscience*, 9 (10), pp. 779–788. DOI:10.1038/nrn2492.

Drake, P. J. M., Griffiths, G. J., Shaw, L., Benson, R. P. and Corfe, B. M. (**2009**) Application of High-Content Analysis to the Study of Post-Translational Modifications of the Cytoskeleton, *Journal of Proteome Research*, pp. 28–34. DOI:10.1021/pr8006396.

Dürr, U. H. N., Sudheendra, U. S. and Ramamoorthy, A. (**2006**) LL-37, the only human member of the cathelicidin family of antimicrobial peptides, *Biochimica et Biophysica Acta - Biomembranes*. DOI:10.1016/j.bbamem.2006.03.030.

Eash, K. J., Means, J. M., White, D. W. and Link, D. C. (**2009**) CXCR4 is a key regulator of neutrophil release from the bone marrow under basal and stress granulopoiesis conditions, *Blood*, 113 (19), pp. 4711–4719. DOI:10.1182/blood-2008.

El-Benna, J., Dang, P. M. C. and Gougerot-Pocidalo, M. A. (**2008**) Priming of the neutrophil NADPH oxidase activation: Role of p47phox phosphorylation and NOX2 mobilization to the plasma membrane, *Seminars in Immunopathology*. DOI:10.1007/s00281-008-0118-3.

Elliott, E., Dennison, C., Fortgens, P. H. and Travis, J. (**1995**) Paraformaldehyde fixation of neutrophils for immunolabeling of granule antigens in cryoultrasections., *The Journal of Histochemistry and Cytochemistry : Official Journal of the Histochemistry Society*, 43 (10), pp. 1019–25.

Ermert, D., Urban, C. F., Laube, B., Goosmann, C., Zychlinsky, A. and Brinkmann, V. (**2009**) Mouse neutrophil extracellular traps in microbial infections, *Journal of Innate Immunity*, 1 (3), pp. 181–193. DOI:10.1159/000205281.

Farrera, C. and Fadeel, B. (**2013**) Macrophage clearance of neutrophil extracellular traps is a silent process, *J Immunol*, 191 (5), pp. 2647–2656. DOI:10.4049/jimmunol.1300436.

Feng, D., Nagy, J. A., Pyne, K., Dvorak, H. F. and Dvorak, A. M. (**1998**) Neutrophils emigrate from venules by a transendothelial cell pathway in response to FMLP., *The Journal*

of Experimental Medicine, 187 (6), pp. 903–15.

Fernandez, R., Sarma, V., Younkin, E., Hirschl, R. B., Ward, P. A., Younger, J. G. and John, G. (**2013**) Exposure to perflubron is associated with decreased Syk phosphorylation in human neutrophils Exposure to perflubron is associated with decreased Syk phosphorylation in human neutrophils, *Journal of Applied Physiology*, 91 (5), pp. 1941–1947.

Friedl, P., Borgmann, S. and Bröcker, E. B. (**2001**) Amoeboid leukocyte crawling through extracellular matrix: lessons from the Dictyostelium paradigm of cell movement., *Journal of Leukocyte Biology*, 70 (4), pp. 491–509.

Fuchs, T. a., Abed, U., Goosmann, C., Hurwitz, R., Schulze, I., Wahn, V., Weinrauch, Y., Brinkmann, V. and Zychlinsky, A. (**2007**) Novel cell death program leads to neutrophil extracellular traps, *Journal of Cell Biology*, 176 (2), pp. 231–241. DOI:10.1083/jcb.200606027.

Fuchs, T. A., Brill, A., Duerschmied, D., Schatzberg, D., Monestier, M., Myers, D. D., Wrobleski, S. K., Wakefield, T. W., Hartwig, J. H. and Wagner, D. D. (**2010**) Extracellular DNA traps promote thrombosis., *Proceedings of the National Academy of Sciences of the United States of America*, 107 (36), pp. 15880–5. DOI:10.1073/pnas.1005743107.

Fuchs, T. A., Brill, A. and Wagner, D. D. (**2012**) Neutrophil extracellular trap (NET) impact on deep vein thrombosis, *Arteriosclerosis, Thrombosis, and Vascular Biology*, 32 (8), pp. 1777–1783. DOI:10.1161/ATVBAHA.111.242859.

Furze, R. C. and Rankin, S. M. (**2008**) Neutrophil mobilization and clearance in the bone marrow, *Immunology*. DOI:10.1111/j.1365-2567.2008.02950.x.

Futosi, K., Fodor, S. and Mócsai, A. (**2013**) Reprint of Neutrophil cell surface receptors and their intracellular signal transduction pathways, *International Immunopharmacology*, 17 (4), pp. 1185–1197. DOI:10.1016/j.intimp.2013.11.010.

Garippa, R. J., Hoffman, A. F., Gradl, G. and Kirsch, A. (**2006**) High-Throughput Confocal Microscopy for ??-Arrestin-Green Fluorescent Protein Translocation G Protein-Coupled Receptor Assays Using the Evotec Opera, *Methods in Enzymology*. DOI:10.1016/S0076-6879(06)14007-0.

Gavillet, M., Martinod, K., Renella, R., Harris, C., Shapiro, N. I., Wagner, D. D. and Williams, D. A. (**2015**) Flow cytometric assay for direct quantification of neutrophil extracellular traps in blood samples, *American Journal of Hematology*, 90 (12), pp. 1155–1158. DOI:10.1002/ajh.24185.

Gentile, L. F., Nacionales, D. C., Lopez, M. C., Vanzant, E., Cuenca, A., Cuenca, A. G., Ungaro, R., Baslanti, T. O., McKinley, B. a, Bihorac, A., Cuschieri, J., Maier, R. V, Moore, F. a, Leeuwenburgh, C., Baker, H. V, Moldawer, L. L. and Efron, P. a (**2014**) A better understanding of why murine models of trauma do not recapitulate the human syndrome*., *Critical Care Medicine*, 42 (6), pp. 1406–13. DOI:10.1097/CCM.0000000000000222.

Ghosh, R. N., Ph, D., Hong, S. J. and Samson, B. Multiplexed Mitosis and Apoptosis Analysis, *www.thermofisher.com*, Application Notes C-AN_MA 0513, pp. 1–3.

Girard, D., Paquin, R. and Beaulieu, A. D. (**1997**) Responsiveness of human neutrophils to interleukin-4: induction of cytoskeletal rearrangements, de novo protein synthesis and delay of apoptosis, *The Biochemical Journal*, 325, Pt 1, pp. 147–53.

Giuliano, K. A., DeBiasio, R. L., Dunlay, R. T., Gough, A., Volosky, J. M., Zock, J., Pavlakis, G. N. and Taylor, D. L. (**1997**) High-Content Screening: A New Approach to Easing Key Bottlenecks in the Drug Discovery Process, *Journal of Biomolecular Screening*, 2 (4), pp. 249–259. DOI:10.1177/108705719700200410.

Goldmann, O. and Medina, E. (**2012**) The expanding world of extracellular traps: Not only neutrophils but much more, *Frontiers in Immunology*. Frontiers Media SA. DOI:10.3389/fimmu.2012.00420.

Greabu, M., Battino, M., Mohora, M., Totan, A., Didilescu, A., Spinu, T., Totan, C., Miricescu, D. and Radulescu, R. (**2009**) Saliva--a diagnostic window to the body, both in health and in disease., *Journal of Medicine and Life*, 2 (2), pp. 124–132.

Guerra, B. A., Bolin, A. P., Morandi, A. C. and Otton, R. (**2012**) Glycolaldehyde impairs neutrophil biochemical parameters by an oxidative and calcium-dependent mechanism—Protective role of antioxidants astaxanthin and vitamin C, *Diabetes Research and Clinical Practice*, 98, pp. 108–118. DOI:10.1016/j.diabres.2012.07.004.

Guimarães-Costa, A. B., Nascimento, M. T. C., Froment, G. S., Soares, R. P. P., Morgado, F. N., Conceição-Silva, F. and Saraiva, E. M. (**2009**) Leishmania amazonensis promastigotes induce and are killed by neutrophil extracellular traps., *Proceedings of the National Academy of Sciences of the United States of America*, 106 (16), pp. 6748–6753. DOI:10.1073/pnas.0900226106.

Gupta, A. K., Giaglis, S., Hasler, P. and Hahn, S. (**2014**) Efficient neutrophil extracellular trap induction requires mobilization of both intracellular and extracellular calcium pools and is modulated by cyclosporine A, *PLoS ONE*, 9 (5), pp. 19–21. DOI:10.1371/journal.pone.0097088.

Gupta, A. K., Hasler, P., Holzgreve, W., Gebhardt, S. and Hahn, S. (**2005**) Induction of neutrophil extracellular DNA lattices by placental microparticles and IL-8 and their presence in preeclampsia., *Human Immunology*, 66 (11), pp. 1146–54. DOI:10.1016/j.humimm.2005.11.003.

Hahn, S., Giaglis, S., Chowdury, C. S., Hösli, I. and Hasler, P. (**2013**) Modulation of neutrophil NETosis: Interplay between infectious agents and underlying host physiology, *Seminars in Immunopathology*, 35 (4), pp. 439–453. DOI:10.1007/s00281-013-0380-x.

Hakkim, A., Fuchs, T. A., Martinez, N. E., Hess, S., Prinz, H., Zychlinsky, A. and

Waldmann, H. (**2011**) Activation of the Raf-MEK-ERK pathway is required for neutrophil extracellular trap formation., *Nature Chemical Biology*, 7 (2), pp. 75–77. DOI:10.1038/nchembio.496.

Hakkim, A., Fürnrohr, B. G., Amann, K., Laube, B., Abed, U. A., Brinkmann, V., Herrmann, M., Voll, R. E. and Zychlinsky, A. (**2010**) Impairment of neutrophil extracellular trap degradation is associated with lupus nephritis., *Proceedings of the National Academy of Sciences of the United States of America*, 107 (21), pp. 9813–8. DOI:10.1073/pnas.0909927107.

Hampton, M. B., Kettle, A. J. and Winterbourn, C. C. (**1998**) Inside the Neutrophil Phagosome: Oxidants, Myeloperoxidase, and Bacterial Killing, *The Journal of The American Society of Hematology*, 92 (1), pp. 3007–3017.

Hayashi, F., Means, T. K. and Luster, A. D. (**2003**) Toll-like receptors stimulate human neutrophil function, *Blood*, 102, pp. 2660–2669.

He, D., Xu, Q., Yan, M., Zhang, P., Zhou, X., Zhang, Z., Duan, W., Zhong, L., Ye, D. and Chen, W. (**2009**) The NF-kappa B inhibitor, celastrol, could enhance the anti-cancer effect of gambogic acid on oral squamous cell carcinoma, *BMC Cancer*, 9, pp. 1–9. DOI:10.1186/1471-2407-9-343.

Hirsch, J. G. (**1958**) Bactericidal action of histone., *The Journal of Experimental Medicine*, 108 (6), pp. 925–944. DOI:10.1084/jem.108.6.925.

Hirschfeld, J., Dommisch, H., Skora, P., Horvath, G., Latz, E., Hoerauf, A., Waller, T., Kawai, T., Jepsen, S., Deschner, J. and Bekeredjian-Ding, I. (**2015**) Neutrophil extracellular trap formation in supragingival biofilms, *International Journal of Medical Microbiology*, 305 (4–5), pp. 453–463. DOI:10.1016/j.ijmm.2015.04.002.

Ho-Tin-Noé, B., Carbo, C., Demers, M., Cifuni, S. M., Goerge, T. and Wagner, D. D. (**2009**) Innate immune cells induce hemorrhage in tumors during thrombocytopenia., *The American Journal of Pathology*, 175 (4), pp. 1699–708. DOI:10.2353/ajpath.2009.090460.

Holland, S. M. (**2010**) Chronic Granulomatous Disease, *Clinical Reviews in Allergy & Immunology*, 38 (1), pp. 3–10. DOI:10.1007/s12016-009-8136-z.

Honarnejad, K., Daschner, A., Giese, A., Zall, A., Schmidt, B., Szybinska, A., Kuznicki, J. and Herms, J. (**2013**) Development and implementation of a high-throughput compound screening assay for targeting disrupted ER calcium homeostasis in Alzheimer's disease, *PLoS ONE*, 8 (11), pp. e80645. DOI:10.1371/journal.pone.0080645.

Huang, H., Lindgren, A., Wu, X., Liu, N.-A. and Lin, S. (**2012**) High-throughput screening for bioactive molecules using primary cell culture of transgenic zebrafish embryos., *Cell Reports*, 2 (3), pp. 695–704. DOI:10.1016/j.celrep.2012.08.015.

Ignatius Ou, S.-H. (**2011**) Crizotinib: a novel and first-in-class multitargeted tyrosine kinase

inhibitor for the treatment of anaplastic lymphoma kinase rearranged non-small cell lung cancer and beyond, *Drug Design, Development and Therapy*, 5, pp. 471–485. DOI:10.2147/DDDT.S19045.

Insall, R. H. (**2010**) Understanding eukaryotic chemotaxis: a pseudopod-centred view, *Nature Reviews Molecular Cell Biology*, 11 (6), pp. 453–458. DOI:10.1038/nrm2905.

Jaillon, S., Galdiero, M. R., Del Prete, D., Cassatella, M. A., Garlanda, C. and Mantovani, A. (**2013**) Neutrophils in innate and adaptive immunity, *Seminars in Immunopathology*. DOI:10.1007/s00281-013-0374-8.

Jakubovics, N. S. and Grant Burgess, J. (**2015**) Extracellular DNA in oral microbial biofilms, *Microbes and Infection*, 17 (7), pp. 531–537. DOI:10.1016/j.micinf.2015.03.015.

Jesaitis, A. J., Buescher, E. S., Harrison, D., Quinn, M. T., Parkos, C. A., Livesey, S. and Linner, J. (**1990**) Ultrastructural localization of cytochrome b in the membranes of resting and phagocytosing human granulocytes., *The Journal of Clinical Investigation*, 85 (3), pp. 821–35. DOI:10.1172/JCI114509.

Kambalyal, P., Kambalyal, P. and Hungund, S. (**2015**) Comparison of salivary calcium level in smokers and non-smokers with chronic periodontitis, aggressive periodontitis, and healthy controls., *Journal of International Society of Preventive & Community Dentistry*, 5 (Suppl 2), pp. S68-73. DOI:10.4103/2231-0762.171595.

Kannaiyan, R., Shanmugam, M. K. and Sethi, G. (**2011**) Molecular targets of celastrol derived from Thunder of God Vine: Potential role in the treatment of inflammatory disorders and cancer, *Cancer Letters*, 303 (1), pp. 9–20. DOI:10.1016/j.canlet.2010.10.025.

Kaplan, M. J. and Radic, M. (**2012**) Neutrophil extracellular traps: double-edged swords of innate immunity., *Journal of Immunology (Baltimore, Md. : 1950)*, 189 (6), pp. 2689–95. DOI:10.4049/jimmunol.1201719.

Kaplan, M. J. and Radic, M. (**2013**) *NETosis: At the Intersection of Cell Biology, Microbiology, and Immunology*. DOI:10.3389/978-2-88919-158-1.

Kaufmann, S. H. E. (**2008**) Immunology's foundation: the 100-year anniversary of the Nobel Prize to Paul Ehrlich and Elie Metchnikoff., *Nature Immunology*, 9 (7), pp. 705–712. DOI:10.1038/ni0708-705.

Keshari, R. S., Jyoti, A., Dubey, M., Kothari, N., Kohli, M., Bogra, J., Barthwal, M. K. and Dikshit, M. (**2012a**) Cytokines Induced Neutrophil Extracellular Traps Formation: Implication for the Inflammatory Disease Condition, *PLoS ONE*, 7 (10). DOI:10.1371/journal.pone.0048111.

Keshari, R. S., Jyoti, A., Kumar, S., Dubey, M., Verma, A., Srinag, B. S., Krishnamurthy, H., Barthwal, M. K. and Dikshit, M. (**2012b**) Neutrophil extracellular traps contain mitochondrial as well as nuclear DNA and exhibit inflammatory potential, *Cytometry Part A*,

81 A (3), pp. 238–247. DOI:10.1002/cyto.a.21178.

Keshari, R. S., Verma, A., Barthwal, M. K. and Dikshit, M. (**2013**) Reactive oxygen species-induced activation of ERK and p38 MAPK mediates PMA-induced NETs release from human neutrophils, *Journal of Cellular Biochemistry*, 114 (3), pp. 532–540. DOI:10.1002/jcb.24391.

Kessenbrock, K., Krumbholz, M., Schönermarck, U., Back, W., Gross, W. L., Werb, Z., Gröne, H.-J., Brinkmann, V. and Jenne, D. E. (**2009**) Netting neutrophils in autoimmune small-vessel vasculitis, *Nature Medicine*, 15 (6), pp. 623–625. DOI:10.1038/nm.1959.

Khademhosseini, A., Suh, K. Y., Yang, J. M., Eng, G., Yeh, J., Levenberg, S. and Langer, R. (**2004**) Layer-by-layer deposition of hyaluronic acid and poly-l-lysine for patterned cell co-cultures, *Biomaterials*, 25 (17), pp. 3583–3592. DOI:10.1016/j.biomaterials.2003.10.033.

Khandpur, R., Carmona-Rivera, C., Vivekanandan-Giri, A., Gizinski, A., Yalavarthi, S., Knight, J. S., Friday, S., Li, S., Patel, R. M., Subramanian, V., Thompson, P., Chen, P., Fox, D. a, Pennathur, S. and Kaplan, M. J. (**2013**) NETs are a source of citrullinated autoantigens and stimulate inflammatory responses in rheumatoid arthritis., *Science Translational Medicine*, 5 (178), pp. 178ra40. DOI:10.1126/scitranslmed.3005580.

Kikkert, R., Laine, M. L., Aarden, L. A. and van Winkelhoff, A. J. (**2007**) Activation of toll-like receptors 2 and 4 by gram-negative periodontal bacteria., *Oral Microbiology and Immunology*, 22 (3), pp. 145–51. DOI:10.1111/j.1399-302X.2007.00335.x.

Knight, J. S., Subramanian, V., O'Dell, A. A., Yalavarthi, S., Zhao, W., Smith, C. K., Hodgin, J. B., Thompson, P. R. and Kaplan, M. J. (**2015**) Peptidylarginine deiminase inhibition disrupts NET formation and protects against kidney, skin and vascular disease in lupus-prone MRL/ *lpr* mice, *Annals of the Rheumatic Diseases*, 74 (12), pp. 2199–2206. DOI:10.1136/annrheumdis-2014-205365.

Koch, A. E. (**2007**) The pathogenesis of rheumatoid arthritis., *American Journal of Orthopedics (Belle Mead, N.J.)*, 36 (7 Suppl), pp. 5–8.

Köckritz-Blickwede, M. von, Chow, O., Ghochani, M. and Nizet, V. (**2010**) *Visualization and functional evaluation of phagocyte extracellular traps*, *Methods in Microbiology*. Vol. 37. DOI:10.1016/S0580-9517(10)37007-3.

Kolaczkowska, E. and Kubes, P. (**2013**) Neutrophil recruitment and function in health and inflammation, *Nature Reviews. Immunology*, 13 (3), pp. 159–75. DOI:10.1038/nri3399.

Korkmaz, B., Moreau, T. and Gauthier, F. (**2008**) Neutrophil elastase, proteinase 3 and cathepsin G: Physicochemical properties, activity and physiopathological functions, *Biochimie*, 90 (2), pp. 227–242. DOI:10.1016/j.biochi.2007.10.009.

Korn, K. and Krausz, E. (**2007**) Cell-based high-content screening of small-molecule libraries, *Current Opinion in Chemical Biology*, 11 (5), pp. 503–510. DOI:10.1016/j.cbpa.2007.08.030.

Korzeniewski, C. and Callewaert, D. M. (**1983**) An Enzyme-Release Assay for Natural Cytotoxicity 1, *Journal oflmmunologicalMethods*, 64, pp. 313–320.

Kruger, P., Saffarzadeh, M., Weber, A. N. R., Rieber, N., Radsak, M., von Bernuth, H., Benarafa, C., Roos, D., Skokowa, J. and Hartl, D. (**2015**) Neutrophils: Between host defence, immune modulation, and tissue injury., *PLoS Pathogens*, 11 (3), pp. e1004651. DOI:10.1371/journal.ppat.1004651.

Lacy, P. (**2006**) Mechanisms of Degranulation in Neutrophils, *Allergy, Asthma Adn Clinical Immunolgy*, 2 (3), pp. 98–108.

Lakowicz, J. R., Gryczynski, I., Malak, H., Schrader, M., Engelhardt, P., Kano, H. and Hell, S. W. (**1997**) Time-resolved fluorescence spectroscopy and imaging of DNA labeled with DAPI and Hoechst 33342 using three-photon excitation., *Biophysical Journal*, 72 (2 Pt 1), pp. 567–78.

Landini, B. G. (**2012**) How to correct background illumination in brightfield microscopy, *Microscopy*, pp. 1–9.

Lapponi, M. J., Carestia, A., Landoni, V. I., Rivadeneyra, L., Etulain, J., Negrotto, S., Pozner, R. G. and Schattner, M. (**2013**) Regulation of Neutrophil Extracellular Trap Formation by Anti-Inflammatory Drugs, *The Journal of Pharmaccology and Experimental Therapeutics*, 2013 (June), pp. 430–437.

Lee, W. L., Harrison, R. E. and Grinstein, S. (**2003**) Phagocytosis by neutrophils, *Microbes and Infection*, 5 (14), pp. 1299–1306. DOI:10.1016/j.micinf.2003.09.014.

Leffler, J., Martin, M., Gullstrand, B., Tyden, H., Lood, C., Truedsson, L., Bengtsson, A. A. and Blom, A. M. (**2012**) Neutrophil extracellular traps that are not degraded in systemic lupus erythematosus activate complement exacerbating the disease, *J Immunol*, 188 (7), pp. 3522–3531. DOI:10.4049/jimmunol.1102404.

Ley, K., Laudanna, C., Cybulsky, M. I. and Nourshargh, S. (**2007**) Getting to the site of inflammation: the leukocyte adhesion cascade updated., *Nature Reviews. Immunology*, 7 (9), pp. 678–89. DOI:10.1038/nri2156.

Li, P., Li, M., Lindberg, M. R., Kennett, M. J., Xiong, N. and Wang, Y. (**2010**) PAD4 is essential for antibacterial innate immunity mediated by neutrophil extracellular traps., *The Journal of Experimental Medicine*, 207 (9), pp. 1853–1862. DOI:10.1084/jem.20100239.

Lieschke, G. J., Grail, D., Hodgson, G., Metcalf, D., Stanley, E., Cheers, C., Fowler, K. J., Basu, S., Zhan, Y. F. and Dunn, A. R. (**1994**) Mice lacking granulocyte colony-stimulating factor have chronic neutropenia, granulocyte and macrophage progenitor cell deficiency, and impaired neutrophil mobilization., *Blood*, 84 (6), pp. 1737–46.

Ling, M. R., Chapple, I. L. C. and Matthews, J. B. (**2015**) Peripheral blood neutrophil cytokine hyper-reactivity in chronic periodontitis., *Innate Immunity*, 21 (7), pp. 714–25.

DOI:10.1177/1753425915589387.

Liu, G., Molas, M., Grossmann, G. A., Pasumarthy, M., Perales, J. C., Cooper, M. J. and Hanson, R. W. (**2001**) Biological properties of poly-L-lysine-DNA complexes generated by cooperative binding of the polycation., *The Journal of Biological Chemistry*, 276 (37), pp. 34379–87. DOI:10.1074/jbc.M105250200.

Liu, Y. L., Chiang, Y. H., Liu, G. Y. and Hung, H. C. (**2011**) Functional role of dimerization of human peptidylarginine deiminase 4 (PAD4), *PLoS ONE*, 6 (6). DOI:10.1371/journal.pone.0021314.

Luchi, M. and Munford, R. S. (**1993**) Binding, internalization, and deacylation of bacterial lipopolysaccharide by human neutrophils., *Journal of Immunology (Baltimore, Md. : 1950)*, 151 (2), pp. 959–69.

Lundholt, B. K., Linde, V., Loechel, F., Pedersen, H.-C., Møller, S., Praestegaard, M., Mikkelsen, I., Scudder, K., Bjørn, S. P., Heide, M., Arkhammar, P. O. G., Terry, R. and Nielsen, S. J. (**2005**) Identification of Akt pathway inhibitors using redistribution screening on the FLIPR and the IN Cell 3000 analyzer., *Journal of Biomolecular Screening : The Official Journal of the Society for Biomolecular Screening*, 10 (1), pp. 20–29. DOI:10.1177/1087057104269989.

Lundqvist, H., Kricka, L. J., Stott, R. A., Thorpe, G. H. and Dahlgren, C. (1995) Influence of different luminols on the characteristics of the chemiluminescence reaction in human neutrophils., *Journal of Bioluminescence and Chemiluminescence*, 10 (6), pp. 353–9. DOI:10.1002/bio.1170100608.

Mandavilli, B. Oxidative Stress Measurements Made Easy : CellROX Reagents with Simple Workflow for High Content Imaging, *www.thermofisher.com*, C-AN_CR0414.

Manzenreiter, R., Kienberger, F., Marcos, V., Schilcher, K., Krautgartner, W. D., Obermayer, A., Huml, M., Stoiber, W., Hector, A., Griese, M., Hannig, M., Studnicka, M., Vitkov, L. and Hartl, D. (**2012**) Ultrastructural characterization of cystic fibrosis sputum using atomic force and scanning electron microscopy, *Journal of Cystic Fibrosis*, 11 (2), pp. 84–92. DOI:10.1016/j.jcf.2011.09.008.

Martinelli, S., Urosevic, M., Baryadel, A., Oberholzer, P. A., Baumann, C., Fey, M. F., Dummer, R., Simon, H. U. and Yousefi, S. (**2004**) Induction of genes mediating interferon-dependent extracellular trap formation during neutrophil differentiation, *Journal of Biological Chemistry*, 279 (42), pp. 44123–44132. DOI:10.1074/jbc.M405883200.

Masuda, S., Nakazawa, D., Shida, H., Miyoshi, A., Kusunoki, Y., Tomaru, U. and Ishizu, A. (**2016**) NETosis markers: Quest for specific, objective, and quantitative markers, *Clinica Chimica Acta*. DOI:10.1016/j.cca.2016.05.029.

Matthews, J. B., Wright, H. J., Roberts, A., Cooper, P. R. and Chapple, I. L. C. (**2007a**)

Hyperactivity and reactivity of peripheral blood neutrophils in chronic periodontitis, *Clinical and Experimental Immunology*, 147 (2), pp. 255–264. DOI:10.1111/j.1365-2249.2006.03276.x.

Matthews, J. B., Wright, H. J., Roberts, a, Ling-Mountford, N., Cooper, P. R. and Chapple, I. L. C. (**2007b**) Neutrophil hyper-responsiveness in periodontitis., *Journal of Dental Research*, 86 (8), pp. 718–722. DOI:10.1177/154405910708600806.

Mattiazzi Usaj, M., Styles, E. B., Verster, A. J., Friesen, H., Boone, C. and Andrews, B. J. (2016) High-Content Screening for Quantitative Cell Biology, *Trends in Cell Biology*,

Mayr, L. M. and Bojanic, D. (**2009**) Novel trends in high-throughput screening, *Current Opinion in Pharmacology*, 9 (5), pp. 580–588. DOI:10.1016/j.coph.2009.08.004.

McCubbrey, A. L. and Curtis, J. L. (**2013**) Efferocytosis and lung disease, *Chest*, 143 (6), pp. 1750–1757. DOI:10.1378/chest.12-2413.

Mcinturff, A. M., Cody, M. J., Elliott, E. a, Glenn, J. W., Rowley, J. W., Matthew, T., Yost, C. C., Dc, W. and Rondina, M. T. (**2013**) formation via induction of hypoxia-inducible factor 1 α Mammalian target of rapamycin regulates neutrophil extracellular trap formation via induction of hypoxia-inducible factor 1 ⎵, *Blood*, 120 (15), pp. 3118–3125. DOI:10.1182/blood-2012-01-405993.

Metzler, K. D., Fuchs, T. a., Nauseef, W. M., Reumaux, D., Roesler, J., Schulze, I., Wahn, V., Papayannopoulos, V. and Zychlinsky, A. (**2011**) Myeloperoxidase is required for neutrophil extracellular trap formation: Implications for innate immunity, *Blood*, 117 (3), pp. 953–959. DOI:10.1182/blood-2010-06-290171.

Miller, C. S., King, C. P., Langub, M. C., Kryscio, R. J. and Thomas, M. V (**2006**) Salivary biomarkers of existing periodontal disease: a cross-sectional study., *Journal of the American Dental Association (1939)*, 137 (3), pp. 322–9.

Miller, D. M., Leonard, S. L. and Haskins, J. R. Elucidating the Mechanism of Cell Death Through the use of High Content Analysis, *www.thermofisher.com*, C-AN_CD0314.

Millhouse, E., Jose, A., Sherry, L., Lappin, D. F., Patel, N., Middleton, A. M., Pratten, J., Culshaw, S. and Ramage, G. (**2014**) Development of an in vitro periodontal biofilm model for assessing antimicrobial and host modulatory effects of bioactive molecules., *BMC Oral Health*, 14, pp. 80. DOI:10.1186/1472-6831-14-80.

Milward, M. R., Chapple, I. L. C., Wright, H. J., Millard, J. L., Matthews, J. B. and Cooper, P. R. (**2007**) Differential activation of NF-κB and gene expression in oral epithelial cells by periodontal pathogens, *Clinical & Experimental Immunology*, 148 (2), pp. 307–324. DOI:10.1111/j.1365-2249.2007.03342.x.

Milward, M. R., Chapple, I. L., Carter, K., Matthews, J. B. and Cooper, P. R. (**2013**)

Micronutrient modulation of NF-κB in oral keratinocytes exposed to periodontal bacteria., *Innate Immunity*, 19 (2), pp. 140–51. DOI:10.1177/1753425912454761.

Möllerherm, H., von Köckritz-Blickwede, M. and Branitzki-Heinemann, K. (**2016**) Antimicrobial Activity of Mast Cells: Role and Relevance of Extracellular DNA Traps., *Frontiers in Immunology*, 7, pp. 265. DOI:10.3389/fimmu.2016.00265.

Moussavi-Harami, S. F., Mladinich, K. M., Sackmann, E. K., Shelef, M. A., Starnes, T. W., Guckenberger, D. J., Huttenlocher, A., Beebe, D. J., Kolaczkowska, E., Kubes, P., Mayadas, T. N., Cullere, X., Lowell, C. A., Brinkmann, V., Reichard, U., Goosmann, C., Fauler, B., Uhlemann, Y., Weiss, D. S., *et al.* (**2016**) Microfluidic device for simultaneous analysis of neutrophil extracellular traps and production of reactive oxygen species, *Integr. Biol.*, 8 (2), pp. 243–252. DOI:10.1039/C5IB00225G.

Munoz, L. E., Gaipl, U. S., Franz, S., Sheriff, A., Voll, R. E., Kalden, J. R. and Herrmann, M. (2005) SLE - A disease of clearance deficiency?, in: *Rheumatology*.44, pp. 1101–1107.

Nanì, S., Fumagalli, L., Sinha, U., Kamen, L., Scapini, P. and Berton, G. (**2015**) Src family kinases and Syk are required for neutrophil extracellular trap formation in response to β-glucan particles., *Journal of Innate Immunity*, 7 (1), pp. 59–73. DOI:10.1159/000365249.

Narasaraju, T., Yang, E., Samy, R. P., Ng, H. H., Poh, W. P., Liew, A. A., Phoon, M. C., Van Rooijen, N. and Chow, V. T. (**2011**) Excessive neutrophils and neutrophil extracellular traps contribute to acute lung injury of influenza pneumonitis, *American Journal of Pathology*, 179 (1), pp. 199–210. DOI:10.1016/j.ajpath.2011.03.013.

Nauseef, W. M. and Borregaard, N. (**2014**) Neutrophils at work., *Nature Immunology*, 15 (7), pp. 602–11. DOI:10.1038/ni.2921.

Nauseef, W. M. and Kubes, P. (**2016**) Pondering neutrophil extracellular traps with healthy skepticism, *Cellular Microbiology*, 18 (10), pp. 1349–1357. DOI:10.1111/cmi.12652.

Neeli, I., Dwivedi, N., Khan, S. and Radic, M. (**2009**) Regulation of Extracellular Chromatin Release from Neutrophils, *J Innate Immun*, 1, pp. 194–201. DOI:10.1159/000206974.

Neeli, I., Khan, S. N. and Radic, M. (**2008**) Histone Deimination As a Response to Inflammatory Stimuli in Neutrophils, *The Journal of Immunology*, 180 (3), pp. 1895–1902. DOI:10.4049/jimmunol.180.3.1895.

Neeli, I. and Radic, M. (**2013**) Opposition between PKC isoforms regulates histone deimination and neutrophil extracellular chromatin release., *Frontiers in Immunology*, 4, pp. 38. DOI:10.3389/fimmu.2013.00038.

Németh, T., Mócsai, A. and Lowell, C. A. (**2016**) Neutrophils in animal models of autoimmune disease, *Seminars in Immunology*, 28 (2), pp. 174–186. DOI:10.1016/j.smim.2016.04.001.

Neumann, A., Völlger, L., Berends, E. T. M., Molhoek, E. M., Stapels, D. A. C., Midon, M., Friães, A., Pingoud, A., Rooijakkers, S. H. M., Gallo, R. L., Mörgelin, M., Nizet, V., Naim, H. Y. and Von Köckritz-Blickwede, M. (**2014**) Novel role of the antimicrobial peptide LL-37 in the protection of neutrophil extracellular Traps against degradation by bacterial nucleases, *Journal of Innate Immunity*, 6 (6), pp. 860–868. DOI:10.1159/000363699.

Nunes, P., Demaurex, N. and Dinauer, M. C. (**2013**) Regulation Of The NADPH Oxidase And Associated Ion Fluxes During Phagocytosis, *Traffic*, 14 (11), pp. n/a-n/a. DOI:10.1111/tra.12115.

O'Brien, P. J., Irwin, W., Diaz, D., Howard-Cofield, E., Krejsa, C. M., Slaughter, M. R., Gao, B., Kaludercic, N., Angeline, A., Bernardi, P., Brain, P. and Hougham, C. (**2006**) High concordance of drug-induced human hepatotoxicity with in vitro cytotoxicity measured in a novel cell-based model using high content screening, *Archives of Toxicology*, 80 (9), pp. 580–604. DOI:10.1007/s00204-006-0091-3.

Okshevsky, M. and Meyer, R. L. (**2015**) The role of extracellular DNA in the establishment, maintenance and perpetuation of bacterial biofilms, *Crit Rev Microbiol*, 41 (3), pp. 341–352. DOI:10.3109/1040841x.2013.841639.

Ordronneau, P., Lindström, P. B. and Petrusz, P. (**1981**) Four unlabeled antibody bridge techniques: a comparison., *The Journal of Histochemistry and Cytochemistry : Official Journal of the Histochemistry Society*, 29 (12), pp. 1397–404.

Palmer, L. J. (**2010**) Neutrophil extracellular traps in periodontitis, *PhD Thesis*.

Palmer, L. J., Chapple, I. L. C., Wright, H. J., Roberts, A. and Cooper, P. R. (**2012b**) Extracellular deoxyribonuclease production by periodontal bacteria, *Journal of Periodontal Research*, 47 (4), pp. 439–445. DOI:10.1111/j.1600-0765.2011.01451.x.

Palmer, L. J., Cooper, P. R., Ling, M. R., Wright, H. J., Huissoon, a. and Chapple, I. L. C. (**2012a**) Hypochlorous acid regulates neutrophil extracellular trap release in humans, *Clinical and Experimental Immunology*, 167 (2), pp. 261–268. DOI:10.1111/j.1365-2249.2011.04518.x.

Papayannopoulos, V., Metzler, K. D., Hakkim, A. and Zychlinsky, A. (**2010**) Neutrophil elastase and myeloperoxidase regulate the formation of neutrophil extracellular traps, *Journal of Cell Biology*, 191 (3), pp. 677–691. DOI:10.1083/jcb.201006052.

Parker, H., Albrett, A. M., Kettle, A. J. and Winterbourn, C. C. (**2012b**) Myeloperoxidase associated with neutrophil extracellular traps is active and mediates bacterial killing in the presence of hydrogen peroxide, *Journal of Leukocyte Biology*, 91 (March), pp. 369–376. DOI:10.1189/jlb.0711387.

Parker, H., Dragunow, M., Hampton, M. B., Kettle, A. J. and Winterbourn, C. C. (**2012a**) Requirements for NADPH oxidase and myeloperoxidase in neutrophil extracellular trap

formation differ depending on the stimulus., *Journal of Leukocyte Biology*, 92 (4), pp. 841–9. DOI:10.1189/jlb.1211601.

Perkins, N. D. (**2007**) Integrating cell-signalling pathways with NF-kappaB and IKK function., *Nature Reviews. Molecular Cell Biology*, 8 (1), pp. 49–62. DOI:10.1038/nrm2083.

Pertoft, H., Laurent, T. C., Låås, T. and Kågedal, L. (**1978**) Density gradients prepared from colloidal silica particles coated by polyvinylpyrrolidone (Percoll)., *Analytical Biochemistry*, 88 (1), pp. 271–82.

Peyyala, R. and Ebersole, J. L. (**2013**) Multispecies biofilms and host responses: 'discriminating the trees from the forest'., *Cytokine*, 61 (1), pp. 15–25. DOI:10.1016/j.cyto.2012.10.006.

Peyyala, R., Kirakodu, S. S., Novak, K. F. and Ebersole, J. L. (**2012**) Oral microbial biofilm stimulation of epithelial cell responses., *Cytokine*, 58 (1), pp. 65–72. DOI:10.1016/j.cyto.2011.12.016.

Phillipson, M., Heit, B., Colarusso, P., Liu, L., Ballantyne, C. M. and Kubes, P. (**2006**) Intraluminal crawling of neutrophils to emigration sites: a molecularly distinct process from adhesion in the recruitment cascade, *The Journal of Cell Biology*, 175 (5).

Pieterse, E., Rother, N., Yanginlar, C., Hilbrands, L. B. and van der Vlag, J. (**2016**) Neutrophils Discriminate between Lipopolysaccharides of Different Bacterial Sources and Selectively Release Neutrophil Extracellular Traps, *Frontiers in Immunology*, 7 (November), pp. 484. DOI:10.3389/fimmu.2016.00484.

Pilsczek, F. H., Salina, D., Poon, K. K. H., Fahey, C., Yipp, B. G., Sibley, C. D., Robbins, S. M., Green, F. H. Y., Surette, M. G., Sugai, M., Bowden, M. G., Hussain, M., Zhang, K. and Kubes, P. (**2010**) A novel mechanism of rapid nuclear neutrophil extracellular trap formation in response to Staphylococcus aureus., *Journal of Immunology (Baltimore, Md. : 1950)*, 185 (12), pp. 7413–7425. DOI:10.4049/jimmunol.1000675.

Pires, R. H., Felix, S. B. and Delcea, M. (**2016**) The architecture of neutrophil extracellular traps investigated by atomic force microscopy, *Nanoscale*. DOI:10.1039/C6NR03416K.

Price, K. E., Saleem, N., Lee, G. and Steinberg, M. (**2013**) Potential of ponatinib to treat chronic myeloid leukemia and acute lymphoblastic leukemia., *OncoTargets and Therapy*, 6, pp. 1111–8. DOI:10.2147/OTT.S36980.

Prime, S. S., Nixon, S. V, Crane, I. J., Stone, A., Matthews, J. B., Maitland, N. J., Remnant, L., Powell, S. K., Game, S. M. and Scully, C. (**1990**) The behaviour of human oral squamous cell carcinoma in cell culture., *The Journal of Pathology*, 160 (3), pp. 259–69. DOI:10.1002/path.1711600313.

Prince, L. R., Whyte, M. K., Sabroe, I. and Parker, L. C. (**2011**) The role of TLRs in neutrophil activation., *Current Opinion in Pharmacology*, 11 (4), pp. 397–403.

DOI:10.1016/j.coph.2011.06.007.

Puga, I., Cols, M., Barra, C. M., He, B., Cassis, L., Gentile, M., Comerma, L., Chorny, A., Shan, M., Xu, W., Magri, G., Knowles, D. M., Tam, W., Chiu, A., Bussel, J. B., Serrano, S., Lorente, J. A., Bellosillo, B., Lloreta, J., *et al.* (2011) B cell–helper neutrophils stimulate the diversification and production of immunoglobulin in the marginal zone of the spleen, *Nature Immunology*, 13 (2), pp. 170–180. DOI:10.1038/ni.2194.

Purdom, S. and Chen, Q. (2005) Epidermal growth factor receptor-dependent and-independent pathways in hydrogen peroxide-induced mitogen-activated protein kinase activation in cardiomyocytes, *Journal of Pharmacology and Experimental …*, 312 (3), pp. 1179–1186. DOI:10.1124/jpet.104.077057.differentiated.

Queisser, G., Wiegert, S. and Bading, H. (2011) Structural dynamics of the cell nucleus: basis for morphology modulation of nuclear calcium signaling and gene transcription., *Nucleus (Austin, Tex.)*, 2 (2), pp. 98–104. DOI:10.4161/nucl.2.2.15116.

Rada, B. K., Geiszt, M., Káldi, K., Timár, C. and Ligeti, E. (2004) Dual role of phagocytic NADPH oxidase in bacterial killing, *Blood*, 104 (9), pp. 2947–2953. DOI:10.1182/blood-2004-03-1005.

Ramachandran, V., Williams, M., Yago, T., Schmidtke, D. W., McEver, R. P., Majerus, P. W., Williamst, M. and Schmidtket, D. W. (2004) Dynamic Alterations of Membrane Tethers Stabilize Leukocyte Rolling on P-Selectin, *Source: Proceedings of the National Academy of Sciences of the United States of America*, 101 (37), pp. 13519–13524.

Remijsen, Q., Berghe, T. Vanden, Wirawan, E., Asselbergh, B., Parthoens, E., De Rycke, R., Noppen, S., Delforge, M., Willems, J. and Vandenabeele, P. (2010) Neutrophil extracellular trap cell death requires both autophagy and superoxide generation, *Nature Publishing Group*, 21 (21), pp. 290–304. DOI:10.1038/cr.2010.150.

Remsing Rix, L., Rix, U., Colinge, J., Hantschel, O., Bennett, K., Stranzl, T., Mü ller, A., Baumgartner, C., Valent, P., Augustin, M., Till, J. and Superti-Furga, G. (2009) Global target profile of the kinase inhibitor bosutinib in primary chronic myeloid leukemia cells, *Leukemia*, 23334, pp. 477–485. DOI:10.1038/leu.2008.334.

Roberts, A., Matthews, J. B., Socransky, S. S., Freestone, P. P. E., Williams, P. H. and Chapple, I. L. C. (2002) Stress and the periodontal diseases: effects of catecholamines on the growth of periodontal bacteria in vitro, *Oral Microbiology and Immunology*, 17 (5), pp. 296–303. DOI:10.1034/j.1399-302X.2002.170506.x.

Roberts, H. M., Ling, M. R., Insall, R., Kalna, G., Spengler, J., Grant, M. M. and Chapple, I. L. C. (2015) Impaired neutrophil directional chemotactic accuracy in chronic periodontitis patients, *Journal of Clinical Periodontology*, 42, pp. 1–11. DOI:10.1111/jcpe.12326.

Rohrbach, A. S., Slade, D. J., Thompson, P. R. and Mowen, K. a. (2012) Activation of

PAD4 in NET formation, *Frontiers in Immunology*, 3 (NOV), pp. 1–10. DOI:10.3389/fimmu.2012.00360.

Sadik, C. D., Kim, N. D. and Luster, A. D. (**2011**) Neutrophils cascading their way to inflammation, *Trends in Immunology*, 32 (10), pp. 452–460. DOI:10.1016/j.it.2011.06.008.

Saitoh, T., Komano, J., Saitoh, Y., Misawa, T., Takahama, M., Kozaki, T., Uehata, T., Iwasaki, H., Omori, H., Yamaoka, S., Yamamoto, N. and Akira, S. (**2012**) Neutrophil Extracellular Traps Mediate a Host Defense Response to Human Immunodeficiency Virus-1, *Cell Host & Microbe*, 12 (1), pp. 109–116. DOI:10.1016/j.chom.2012.05.015.

Schauer, C., Janko, C., Munoz, L. E., Zhao, Y., Kienhöfer, D., Frey, B., Lell, M., Manger, B., Rech, J., Naschberger, E., Holmdahl, R., Krenn, V., Harrer, T., Jeremic, I., Bilyy, R., Schett, G., Hoffmann, M. and Herrmann, M. (**2014**) Aggregated neutrophil extracellular traps limit inflammation by degrading cytokines and chemokines, *Nature Medicine*, 20 (5), pp. 511–517. DOI:10.1038/nm.3547.

Schindelin, J., Arganda-Carreras, I., Frise, E., Kaynig, V., Longair, M., Pietzsch, T., Preibisch, S., Rueden, C., Saalfeld, S., Schmid, B., Tinevez, J.-Y. J.-Y., White, D. J., Hartenstein, V., Eliceiri, K., Tomancak, P., Cardona, A., Liceiri, K., Tomancak, P. and A., C. (**2012**) Fiji: an open source platform for biological image analysis., *Nature Methods*, 9 (7), pp. 676–682. DOI:10.1038/nmeth.2019.Fiji.

Schmidt, T., Zündorf, J., Grüger, T., Brandenburg, K., Reiners, A.-L., Zinserling, J. and Schnitzler, N. (**2012**) CD66b overexpression and homotypic aggregation of human peripheral blood neutrophils after activation by a gram-positive stimulus., *Journal of Leukocyte Biology*, 91 (5), pp. 791–802. DOI:10.1189/jlb.0911483.

Schulte, J., Sepp, K. J., Wu, C., Hong, P. and Littleton, J. T. (**2011**) High-content chemical and rnai screens for suppressors of neurotoxicity in a huntington's disease model, *PLoS ONE*, 6 (8), pp. e23841. DOI:10.1371/journal.pone.0023841.

Scott, D. a. and Krauss, J. (**2012**) Neutrophils in periodontal inflammation, *Frontiers of Oral Biology*, 15, pp. 56–83. DOI:10.1159/000329672.

Seger, R. A. (**2008**) Modern management of chronic granulomatous disease, *British Journal of Haematology*, 140 (3), pp. 255–266. DOI:10.1111/j.1365-2141.2007.06880.x.

Selvatici, R., Falzarano, S., Mollica, A. and Spisani, S. (**2006**) Signal transduction pathways triggered by selective formylpeptide analogues in human neutrophils, *European Journal of Pharmacology*, 534 (1), pp. 1–11. DOI:10.1016/j.ejphar.2006.01.034.

Serhan, C. N., Chiang, N. and Van Dyke, T. E. (**2008**) Resolving inflammation: dual anti-inflammatory and pro-resolution lipid mediators., *Nature Reviews. Immunology*, 8 (5), pp. 349–61. DOI:10.1038/nri2294.

Sewon, L. A., Karjalainen, S. M., Soderling, E., Lapinleimu, H. and Simell, O. (**1998**)

Associations between salivary calcium and oral health, *Journal of Clinical Periodontology*, 25 (11), pp. 915–919. DOI:10.1111/j.1600-051X.1998.tb02390.x.

Sewón, L. a, Karjalainen, S. M., Sainio, M. and Seppä, O. (**1995**) Calcium and other salivary factors in periodontitis-affected subjects prior to treatment., *Journal of Clinical Periodontology*, 22 (4), pp. 267–270.

Seymour, G. J., Ford, P. J., Cullinan, M. P., Leishman, S. and Yamazaki, K. (**2007**) Relationship between periodontal infections and systemic disease, *Clinical Microbiology and Infection*, 13 (SUPPL. 4), pp. 3–10. DOI:10.1111/j.1469-0691.2007.01798.x.

Shariff, A., Kangas, J., Coelho, L. P., Quinn, S. and Murphy, R. F. (**2010**) Automated image analysis for high-content screening and analysis., *Journal of Biomolecular Screening : The Official Journal of the Society for Biomolecular Screening*, 15 (7), pp. 726–734. DOI:10.1177/1087057110370894.

Smith, J. (**2005**) Erlotinib: small-molecule targeted therapy in the treatment of non-small-cell lung cancer., *Clinical Therapeutics*, 27 (10), pp. 1513–34. DOI:10.1016/j.clinthera.2005.10.014.

Socransky, S. S., Haffajee, a D., Cugini, M. a, Smith, C. and Kent, R. L. (**1998**) Microbial complexes in subgingival plaque., *Journal of Clinical Periodontology*, 25 (2), pp. 134–144. DOI:10.1111/j.1600-051X.1998.tb02419.x.

Soehnlein, O., Zernecke, A. and Weber, C. (**2009**) Neutrophils launch monocyte extravasation by release of granule proteins, *Thrombosis and Haemostasis*, 102 (2), pp. 198–205. DOI:10.1160/TH08-11-0720.

Spengler, J., Lugonja, B., Ytterberg, A. J., Zubarev, R. A., Creese, A. J., Pearson, M. J., Grant, M. M., Milward, M., Lundberg, K., Buckley, C. D., Filer, A., Raza, K., Cooper, P. R., Chapple, I. L. and Scheel-Toellner, D. (**2015**) Release of active peptidyl arginine deiminases by neutrophils can explain production of extracellular citrullinated autoantigens in RA synovial fluid., *Arthritis & Rheumatology (Hoboken, N.J.)*. DOI:10.1002/art.39313.

Sperandio, M., Walzog Sascha Jakob, B. M., Frommhold, D., Sixt, M., Ingrid Hepper, M., Schymeinsky, J., Weckbach, L. T., Hepper, I., rgen Schymeinsky, J., Jakob, S. M., Laschinger, M. and Walzog, B. (**2012**) Conditions Crawling of Neutrophils under Flow Critical for Spreading and Intraluminal The Mammalian Actin-Binding Protein 1 Is The Mammalian Actin-Binding Protein 1 Is Critical for Spreading and Intraluminal Crawling of Neutrophils under Flow Conditions, *J Immunol Material SupplementaryDC2.html The Journal of Immunology at University of Birmingham on The Journal of Immunology*, 188 (8), pp. 4590–4601. DOI:10.4049/jimmunol.1100878.

Stark, M. A., Huo, Y., Burcin, T. L., Morris, M. A., Olson, T. S. and Ley, K. (**2005**) Phagocytosis of Apoptotic Neutrophils Regulates Granulopoiesis via IL-23 and IL-17,

Immunity, 22 (3), pp. 285–294. DOI:10.1016/j.immuni.2005.01.011.

Strydom, N. and Rankin, S. M. (**2013**) Regulation of Circulating Neutrophil Numbers under Homeostasis and in Disease, *J Innate Immun*, 5, pp. 304–314. DOI:10.1159/000350282.

Sullivan, J. F., Blotcky, a J., Jetton, M. M., Hahn, H. K. and Burch, R. E. (**1979**) Serum levels of selenium, calcium, copper magnesium, manganese and zinc in various human diseases., *The Journal of Nutrition*, 109 (8), pp. 1432–1437.

Sullivan, R. (**1992**) Biochemical effects of human granulocyte-macrophage colony-stimulating factor (GM-CSF) on the human neutrophil., *Immunology Series*, 57, pp. 485–98.

Suzuki, T., Matsuzaki, T. and Takata, K. (**1998**) Fluorescence Counter-Staining of Cell Nuclear DNA for Multi-Color Laser Confocal Microscopy, *Acta. Histochem. Cytochem*, 31 (4), pp. 297–301.

Swaminathan, R. (**2000**) Disorders of magnesium metabolism, *CPD Bulletin Clinical Biochemistry*, 2 (1), pp. 3–12. DOI:10.1016/B978-0-323-04883-5.50036-2.

Tan, A. S., Ahmed, N. and Berridge, M. V (**1998**) Acute regulation of glucose transport after activation of human peripheral blood neutrophils by phorbol myristate acetate, fMLP, and granulocyte-macrophage colony-stimulating factor., *Blood*, 91 (2), pp. 649–55.

Taylor, D. L. (**2007**) Past, present, and future of high content screening and the field of cellomics., *Methods in Molecular Biology*, 356, pp. 3–18. DOI:10.1385/1-59745-217-3:3.

Thornton, R. B., Wiertsema, S. P., Kirkham, L. A. S., Rigby, P. J., Vijayasekaran, S., Coates, H. L. and Richmond, P. C. (**2013**) Neutrophil Extracellular Traps and Bacterial Biofilms in Middle Ear Effusion of Children with Recurrent Acute Otitis Media - A Potential Treatment Target, *PLoS ONE*, 8 (2). DOI:10.1371/journal.pone.0053837.

Tillack, K., Breiden, P., Martin, R. and Sospedra, M. (**2012**) T Lymphocyte Priming by Neutrophil Extracellular Traps Links Innate and Adaptive Immune Responses, *The Journal of Immunology*, 188 (7), pp. 3150–3159. DOI:10.4049/jimmunol.1103414.

Tintinger, G., Steel, H. C. and Anderson, R. (**2005**) Taming the neutrophil: Calcium clearance and influx mechanisms as novel targets for pharmacological control, *Clinical and Experimental Immunology*, 141 (2), pp. 191–200. DOI:10.1111/j.1365-2249.2005.02800.x.

Underhill, D. and Ozinsky, A. (**2002**) Phagocytosis of Microbes: Complexity in Action, *Annual Review of Immunology*, 20 (1), pp. 825–852. DOI:10.1146/annurev.immunol.20.103001.114744.

Urban, C. F., Ermert, D., Schmid, M., Abu-Abed, U., Goosmann, C., Nacken, W., Brinkmann, V., Jungblut, P. R. and Zychlinsky, A. (**2009**) Neutrophil extracellular traps contain calprotectin, a cytosolic protein complex involved in host defense against Candida albicans, *PLoS Pathogens*, 5 (10). DOI:10.1371/journal.ppat.1000639.

Urban, C. F., Reichard, U., Brinkmann, V. and Zychlinsky, A. (**2006**) Neutrophil extracellular traps capture and kill Candida albicans and hyphal forms, *Cellular Microbiology*, 8 (4), pp. 668–676. DOI:10.1111/j.1462-5822.2005.00659.x.

Vitkov, L., Klappacher, M., Hannig, M. and Krautgartner, W. D. (**2009**) Extracellular neutrophil traps in periodontitis, *Journal of Periodontal Research*, 44 (5), pp. 664–672. DOI:10.1111/j.1600-0765.2008.01175.x.

Vossenaar, E. R., Zendman, a. J. W., Van Venrooij, W. J. and Pruijn, G. J. M. (**2003**) PAD, a growing family of citrullinating enzymes: Genes, features and involvement in disease, *BioEssays*, 25 (11), pp. 1106–1118. DOI:10.1002/bies.10357.

Wang, Y., Li, M., Stadler, S., Correll, S., Li, P., Wang, D., Hayama, R., Leonelli, L., Han, H., Grigoryev, S. a., Allis, C. D. and Coonrod, S. a. (**2009**) Histone hypercitrullination mediates chromatin decondensation and neutrophil extracellular trap formation, *Journal of Cell Biology*, 184 (2), pp. 205–213. DOI:10.1083/jcb.200806072.

Weinberg, E. D. (**1975**) Nutritional Immunity, *Jama*, 231 (1), pp. 39. DOI:10.1001/jama.1975.03240130021018.

Weisberg, E., Manley, P. W., Breitenstein, W., Brüggen, J., Cowan-Jacob, S. W., Ray, A., Huntly, B., Fabbro, D., Fendrich, G., Hall-Meyers, E., Kung, A. L., Mestan, J., Daley, G. Q., Callahan, L., Catley, L., Cavazza, C., Mohammed, A., Neuberg, D., Wright, R. D., *et al.* (**2005**) Characterization of AMN107, a selective inhibitor of native and mutant Bcr-Abl, *Cancer Cell*, 7 (2), pp. 129–141. DOI:10.1016/j.ccr.2005.01.007.

White, P. (**2015**) The role of neutrophil extracellular traps in the pathogenesis of periodontal diseases, *PhD thesis*.

White, P. C., Chicca, I. J., Cooper, P. R., Milward, M. R. and Chapple, I. L. (**2016a**) Neutrophil Extracellular Traps in Periodontitis: A Web of Intrigue, *J Dent Res*, 95 (1), pp. 26–34. DOI:10.1177/0022034515609097.

White, P., Sakellari, D., Roberts, H., Risafi, I., Ling, M., Cooper, P., Milward, M. and Chapple, I. (**2016b**) Peripheral blood neutrophil extracellular trap production and degradation in chronic periodontitis, *Journal of Clinical Periodontology*, 43(12) (14945), pp. 1041–1049. DOI:10.1111/jcpe.12628.

Willis, V. C., Gizinski, A. M., Banda, N. K., Causey, C. P., Knuckley, B., Cordova, K. N., Luo, Y., Levitt, B., Glogowska, M., Chandra, P., Kulik, L., Robinson, W. H., Arend, W. P., Thompson, P. R. and Holers, V. M. (**2011**) N- -Benzoyl-N5-(2-Chloro-1-Iminoethyl)-L-Ornithine Amide, a Protein Arginine Deiminase Inhibitor, Reduces the Severity of Murine Collagen-Induced Arthritis, *The Journal of Immunology*, 186 (7), pp. 4396–4404. DOI:10.4049/jimmunol.1001620.

Wolff, M., Haasen, D., Merk, S., Kroner, M., Maier, U., Bordel, S., Wiedenmann, J.,

Nienhaus, G. U., Valler, M. and Heilker, R. (**2006**) Automated high content screening for phosphoinositide 3 kinase inhibition using an AKT 1 redistribution assay., *Combinatorial Chemistry & High Throughput Screening*, 9 (5), pp. 339–50.

Woodfin, A., Voisin, M. B. and Nourshargh, S. (**2010**) Recent developments and complexities in neutrophil transmigration, *Curr Opin Hematol*, 17 (1), pp. 9–17. DOI:10.1097/MOH.0b013e3283333930.

Wu, F., Han, M. and Wilson, J. X. (**2009**) Tripterine prevents endothelial barrier dysfunction by inhibiting endogenous peroxynitrite formation, *British Journal of Pharmacology*, 157 (6), pp. 1014–1023. DOI:10.1111/j.1476-5381.2009.00292.x.

Xiao, C., Ran, S., Huang, Z. and Liang, J. (**2016**) Bacterial diversity and community structure of supragingival plaques in adults with dental health or caries revealed by 16S pyrosequencing, *Frontiers in Microbiology*, 7 (JUL). DOI:10.3389/fmicb.2016.01145.

Yan, J., Meng, X., Wancket, L. M., Lintner, K., Nelin, L. D., Chen, B., Francis, K. P., Smith, C. V, Rogers, L. K. and Liu, Y. (**2012**) Glutathione reductase facilitates host defense by sustaining phagocytic oxidative burst and promoting the development of neutrophil extracellular traps., *Journal of Immunology (Baltimore, Md. : 1950)*, 188 (5), pp. 2316–27. DOI:10.4049/jimmunol.1102683.

Yipp, B. G. and Kubes, P. (**2013**) NETosis: how vital is it?, *Blood*, 122 (16), pp. 2784–94. DOI:10.1182/blood-2013-04-457671.

Yousefi, S., Gold, J. a, Andina, N., Lee, J. J., Kelly, A. M., Kozlowski, E., Schmid, I., Straumann, A., Reichenbach, J., Gleich, G. J. and Simon, H.-U. (**2008**) Catapult-like release of mitochondrial DNA by eosinophils contributes to antibacterial defense., *Nature Medicine*, 14 (9), pp. 949–953. DOI:10.1038/nm.1855.

Yousefi, S., Mihalache, C., Kozlowski, E., Schmid, I. and Simon, H. U. (**2009**) Viable neutrophils release mitochondrial DNA to form neutrophil extracellular traps., *Cell Death and Differentiation*, 16 (11), pp. 1438–1444. DOI:10.1038/cdd.2009.96.

Yousefi, S., Morshed, M., Amini, P., Stojkov, D., Simon, D., von Gunten, S., Kaufmann, T. and Simon, H.-U. (**2015**) Basophils exhibit antibacterial activity through extracellular trap formation, *Allergy*, 70 (9), pp. 1184–1188. DOI:10.1111/all.12662.

Yousefi, S., Simon, D. and Simon, H. U. (**2012**) Eosinophil extracellular DNA traps: Molecular mechanisms and potential roles in disease, *Current Opinion in Immunology*, 24 (6), pp. 736–737. DOI:10.1016/j.coi.2012.08.010.

Yousefi, S. and Simon, H.-U. (**2016**) NETosis – Does It Really Represent Nature's 'Suicide Bomber'?, *Frontiers in Immunology*, 7, pp. 328. DOI:10.3389/fimmu.2016.00328.

Yu, Y., Koehn, C. D., Yue, Y., Li, S., Thiele, G. M., Hearth-Holmes, M. P., Mikuls, T. R., O'Dell, J. R., Klassen, L. W., Zhang, Z. and Su, K. (**2015**) Celastrol inhibits inflammatory

stimuli-induced neutrophil extracellular trap formation., *Current Molecular Medicine*, 15 (4), pp. 401–10.

Zhao, W., Fogg, D. K. and Kaplan, M. J. (**2015**) A novel image-based quantitative method for the characterization of NETosis, *Journal of Immunological Methods*, 423, pp. 104–110. DOI:10.1016/j.jim.2015.04.027.

Appendix I

Ilaria detect NET s II [Version 20]

Last Modified on 27/10/2016 13:43:25

NOTE: The information here represents data that is saved in the database with an Assay Protocol. This data does not include scan settings like Field Offset, Form Factor , Scan Area, Store Imag es or Show Composite Image.

Comments

Event1=(None) Event2=(None) Event3=(None)

Image Acquisition

Objective	20x
Camera Name	ORCA-ER;1.00
Acquisition Camera Mode	HiRes (1024x1024;1x1)
AutoFocus Camera Mode	HiRes (1024x1024;1x1)
AutoFocus Field Interval	0

AutoFocus Parameters

Fine Focus Step Size	9.9
Fine Focus Plane Count	9
Coarse Focus Step Size	39.6
Coarse Focus Plane Count	16
Smart Focus Plane Count	21
Use Extended Range Focusing	False
Apply Backlash Correction	False
AutoFocus Method	STANDARD
Laser AutoFocus Method	
How To Focus During Scan	2
Use Relaxed Pass/Fail Criteria	False
Focus Edge Threshhold	5
Focus Adjustment	0
Focus Score Min Ratio	0.25
Focus Score Mid Ratio	0.4
Focus Score Max Ratio	0.5
Focus Exposure Time for AutoExpose (seconds)	0.1

Scan Limits

Max Fields for Well	20
Min Objects for Well	No Limit
Max Sparse Fields for Well	No Limit
Min Objects for Field	N/A
Max Sparse Wells for Plate	N/A

Channel 1: Channel1

Dye	BGRFR_485_20
Apply Illumination Correction	False
Apply Background Correction	True
Gain	3
Z Offset	6.00
Step Size	3.86
Number of Steps	10
Projection Method	
Projection Direction	None
Detection Mode	Widefield
Grid Type	
Pin Hole Size	
Intensity Percent	100

Exposure Parameters

Method	Fixed
Exposure Time (seconds)	0.005

Object Identification

Method	FixedThreshold
Value	1033

Object Selection Parameter	Min	Max
ObjectAreaCh1	1501.66	73143
ObjectShapeP2ACh1	0	1000
ObjectShapeLWRCh1	0	1000
ObjectAvgIntenCh1	0	65535
ObjectVarIntenCh1	0	65535
ObjectTotalIntenCh1	0	1000000000000

Display Options

Composite Color (Hex)	#0000FF
SelectedObject	#0000FF
RejectedObject	#FF8040

Channel 2: Channel2

Dye	BGRFR_386_23
Apply Illumination Correction	False
Apply Background Correction	True
Gain	3
Z Offset	6.60
Step Size	0.00
Number of Steps	0
Projection Method	
Projection Direction	None
Detection Mode	Widefield
Grid Type	
Pin Hole Size	
Intensity Percent	100

Exposure Parameters

Method	Fixed
Exposure Time (seconds)	0.33388

Object Identification

Method	FixedThreshold
Value	1488

Object Selection Parameter	Min	Max

Channel 2:	**Channel2**	
RingAvgIntenCh2	0	32767
CircAvgIntenCh2	0	32767
CircRingAvgIntenDiffCh2	-32767	32767
CircRingAvgIntenRatioCh2	0	1000000000000
RingSpotTotalAreaCh2	0	250000000000
RingSpotAvgIntenCh2	0	32767
CircSpotTotalAreaCh2	0	250000000000
CircSpotAvgIntenCh2	0	32767
AvgIntenCh2	0	32767
TotalIntenCh2	0	250000000000

Display Options

Composite Color (Hex)	#00FF00
Circ	#008080
CircSpot	#FF0000

Assay

Assay Algorithm	CompartmentalAnalysis.V4
Assay V ersion	6.0 (Locally Installed V ersion: 6.0.3.4021)
Focus Channel	1
#Channels	2

Assay Parameters

PixelSize	0.3225
Type_1_EventDefinition	0
Type_2_EventDefinition	0
Type_3_EventDefinition	0
CircAvgIntenCh2LevelHigh	1159.87
CircAvgIntenCh2LevelHigh_CC	1
CircAvgIntenCh2LevelLow	25
CircAvgIntenCh2LevelLow_CC	1
CircAvgIntenRatioCh2Ch1LevelHigh	0.05
CircAvgIntenRatioCh2Ch1LevelHigh_CC	1
CircAvgIntenRatioCh2Ch1LevelLow	0.03
CircAvgIntenRatioCh2Ch1LevelLow_CC	1
CircRingAvgIntenDiffCh2LevelHigh	50
CircRingAvgIntenDiffCh2LevelHigh_CC	1
CircRingAvgIntenDiffCh2LevelLow	15
CircRingAvgIntenDiffCh2LevelLow_CC	1
CircRingAvgIntenRatioCh2LevelHigh	7.5
CircRingAvgIntenRatioCh2LevelHigh_CC	1
CircRingAvgIntenRatioCh2LevelLow	2
CircRingAvgIntenRatioCh2LevelLow_CC	1
CircSpotAvgAreaCh2LevelHigh	21.28
CircSpotAvgAreaCh2LevelHigh_CC	1
CircSpotAvgAreaCh2LevelLow	0
CircSpotAvgAreaCh2LevelLow_CC	1
CircSpotAvgIntenCh2LevelHigh	80
CircSpotAvgIntenCh2LevelHigh_CC	1
CircSpotAvgIntenCh2LevelLow	30
CircSpotAvgIntenCh2LevelLow_CC	1
CircSpotCountCh2LevelHigh	0
CircSpotCountCh2LevelHigh_CC	1
CircSpotCountCh2LevelLow	0
CircSpotCountCh2LevelLow_CC	1
CircSpotTotalAreaCh2LevelHigh	2.56
CircSpotTotalAreaCh2LevelHigh_CC	1
CircSpotTotalAreaCh2LevelLow	0.16
CircSpotTotalAreaCh2LevelLow_CC	1
CircSpotTotalIntenCh2LevelHigh	6864
CircSpotTotalIntenCh2LevelHigh_CC	1
CircSpotTotalIntenCh2LevelLow	0
CircSpotTotalIntenCh2LevelLow_CC	1
CircTotalIntenCh2LevelHigh	10640

11/8/2016 Ilaria detect NETs II

Assay	
CircTotalInternCh2LevelHigh_CC	1
CircTotalInternCh2LevelLow	2496
CircTotalInternCh2LevelLow_CC	1
MinRadAvgObjectCountPerField	1
ObjectAreaCh1LevelHigh	87536
ObjectAreaCh1LevelHigh_CC	1
ObjectAreaCh1LevelLow	73881.44
ObjectAreaCh1LevelLow_CC	1
ObjectAvgIntenCh1LevelHigh	1226.08
ObjectAvgIntenCh1LevelHigh_CC	1
ObjectAvgIntenCh1LevelLow	59.88
ObjectAvgIntenCh1LevelLow_CC	1
ObjectShapeLWRCh1LevelHigh	1.7
ObjectShapeLWRCh1LevelHigh_CC	1
ObjectShapeLWRCh1LevelLow	1.2
ObjectShapeLWRCh1LevelLow_CC	1
ObjectShapeP2ACh1LevelHigh	15.33
ObjectShapeP2ACh1LevelHigh_CC	1
ObjectShapeP2ACh1LevelLow	13.41
ObjectShapeP2ACh1LevelLow_CC	1
ObjectSizeCh1LevelHigh	13.76
ObjectSizeCh1LevelHigh_CC	1
ObjectSizeCh1LevelLow	10
ObjectSizeCh1LevelLow_CC	1
ObjectTotalIntenCh1LevelHigh	150000
ObjectTotalIntenCh1LevelHigh_CC	1
ObjectTotalIntenCh1LevelLow	75008
ObjectTotalIntenCh1LevelLow_CC	1
ObjectVarIntenCh1LevelHigh	32767
ObjectVarIntenCh1LevelHigh_CC	1
ObjectVarIntenCh1LevelLow	0
ObjectVarIntenCh1LevelLow_CC	1
RingAvgIntenCh2LevelHigh	14
RingAvgIntenCh2LevelHigh_CC	1
RingAvgIntenCh2LevelLow	5
RingAvgIntenCh2LevelLow_CC	1
RingSpotAvgAreaCh2LevelHigh	1.12
RingSpotAvgAreaCh2LevelHigh_CC	1
RingSpotAvgAreaCh2LevelLow	0.32
RingSpotAvgAreaCh2LevelLow_CC	1
RingSpotAvgIntenCh2LevelHigh	50
RingSpotAvgIntenCh2LevelHigh_CC	1
RingSpotAvgIntenCh2LevelLow	10
RingSpotAvgIntenCh2LevelLow_CC	1
RingSpotCountCh2LevelHigh	95
RingSpotCountCh2LevelHigh_CC	1
RingSpotCountCh2LevelLow	50
RingSpotCountCh2LevelLow_CC	1
RingSpotTotalAreaCh2LevelHigh	60
RingSpotTotalAreaCh2LevelHigh_CC	1
RingSpotTotalAreaCh2LevelLow	37.6
RingSpotTotalAreaCh2LevelLow_CC	1
RingSpotTotalIntenCh2LevelHigh	2128
RingSpotTotalIntenCh2LevelHigh_CC	1
RingSpotTotalIntenCh2LevelLow	624
RingSpotTotalIntenCh2LevelLow_CC	1
RingTotalIntenCh2LevelHigh	2496
RingTotalIntenCh2LevelHigh_CC	1
RingTotalIntenCh2LevelLow	992
RingTotalIntenCh2LevelLow_CC	1
UseMicrometers	0
BackgroundCorrectionCh1	0
BackgroundCorrectionCh2	-88
ChannelToDeriveCircOverlay	2

Assay	
ChannelToDeriveCircSpotOverlay	3
ChannelToDeriveRingOverlay	2
ChannelToDeriveRingSpotOverlay	3
CircModifierCh2	0
MaskModifierCh2	0
ObjectCleanUpCh1	1
ObjectSegmentationCh1	-65535
ObjectSmoothFactorCh1	0
ObjectTypeCh1	0
RejectBorderObjectsCh1	0
RingDistanceCh2	-4
RingWidthCh2	4
SpotDetectRadiusCh2	24
SpotTypeCh2	0
UseReferenceWells	0

Well Feature Extents		
Feature Name	Lower Extent	Upper Extent
ValidObjectCount	1	100
SelectedObjectCount	1	100
MEAN_ObjectSizeCh1	0.527131782945735	52.7131782945735
ValidFieldCount	1	100
MEAN_ObjectAreaCh1	0	25
MEAN_ObjectShapeP2ACh1	0	100
MEAN_ObjectShapeLWRCh1	0	100
MEAN_ObjectTotalIntenCh1	0.277687916591 55	27.7687916591 55
MEAN_ObjectAvgIntenCh1	1	100
MEAN_ObjectVarIntenCh1	1	100
%SelectedObjects	1	100
SelectedObjectCountPerValidField	3.59883217993 08	359.883217993 08
%HIGH_ObjectAreaCh1	0	100
%HIGH_ObjectShapeP2ACh1	0	100
%HIGH_ObjectShapeLWRCh1	0	100
%HIGH_ObjectTotalIntenCh1	1	100
%HIGH_ObjectAvgIntenCh1	1	100
%HIGH_ObjectVarIntenCh1	1	100
%HIGH_ObjectSizeCh1	1	100

* Indicates the default well feature for the Assay Protocol
** Indicates feature extents are dependant upon system reference well settings

Selected Well Features to Store
CompartmentalAnalysis/4Well/%HIGH_ObjectAreaCh1
CompartmentalAnalysis/4Well/%HIGH_ObjectAvgIntenCh1
CompartmentalAnalysis/4Well/%HIGH_ObjectShapeLWRCh1
CompartmentalAnalysis/4Well/%HIGH_ObjectShapeP2ACh1
CompartmentalAnalysis/4Well/%HIGH_ObjectSizeCh1
CompartmentalAnalysis/4Well/%HIGH_ObjectTotalIntenCh1
CompartmentalAnalysis/4Well/%HIGH_ObjectVarIntenCh1
CompartmentalAnalysis/4Well/%SelectedObjects
CompartmentalAnalysis/4Well/MEAN_ObjectAreaCh1
CompartmentalAnalysis/4Well/MEAN_ObjectAvgIntenCh1
CompartmentalAnalysis/4Well/MEAN_ObjectShapeLWRCh1
CompartmentalAnalysis/4Well/MEAN_ObjectShapeP2ACh1
CompartmentalAnalysis/4Well/MEAN_ObjectSizeCh1
CompartmentalAnalysis/4Well/MEAN_ObjectTotalIntenCh1
CompartmentalAnalysis/4Well/MEAN_ObjectVarIntenCh1
CompartmentalAnalysis/4Well/SelectedObjectCount
CompartmentalAnalysis/4Well/SelectedObjectCountPerValidField
CompartmentalAnalysis/4Well/ValidFieldCount
CompartmentalAnalysis/4Well/ValidObjectCount

Selected Cell Features to Store
CompartmentalAnalysis/4Cell/Cell#
CompartmentalAnalysis/4Cell/Height
CompartmentalAnalysis/4Cell/Left
CompartmentalAnalysis/4Cell/Top
CompartmentalAnalysis/4Cell/Width

Figure I: Settings of the NET Detection algorithm employed in this thesis.
Full description of the parameters of the NET Detection algorithms applied in this thesis for the quantification of NET by HCA.

Appendix II

Ilaria nuclear decondensation [Version 9]

Last Modified on 27/10/2016 13:43:37

NOTE: The information here represents data that is saved in the database with an Assay Protocol. This data does not include scan settings like Field Offset, Form Factor , Scan Area, Store Images or Show Composite Image.

Comments

Event1=((ObjectAreaCh1 AND ObjectAvgIntenCh1)) Event2=((ObjectAreaCh1 AND ObjectTotalIntenCh1)) Event3=(None)

Image Acquisition	
Objective	20x
Camera Name	ORCA-ER;1.00
Acquisition Camera Mode	HiRes (1024x1024;1x1)
AutoFocus Camera Mode	HiRes (1024x1024;1x1)
AutoFocus Field Interval	0

AutoFocus Parameters	
Fine Focus Step Size	9.9
Fine Focus Plane Count	9
Coarse Focus Step Size	39.6
Coarse Focus Plane Count	16
Smart Focus Plane Count	21
Use Extended Range Focusing	False
Apply Backlash Correction	False
AutoFocus Method	STANDARD
Laser AutoFocus Method	LASER
How To Focus During Scan	2
Use Relaxed Pass/Fail Criteria	False
Focus Edge Threshhold	5
Focus Adjustment	0
Focus Score Min Ratio	0.25
Focus Score Mid Ratio	0.4
Focus Score Max Ratio	0.5
Focus Exposure Time for AutoExpose (seconds)	0.1

Scan Limits	
Max Fields for Well	30
Min Objects for Well	No Limit
Max Sparse Fields for Well	No Limit
Min Objects for Field	N/A
Max Sparse Wells for Plate	N/A

Channel 1: Nuclei	
Dye	BGRFR_485_20
Apply Illumination Correction	False
Apply Background Correction	True
Gain	25
Z Offset	0.00
Step Size	6.56
Number of Steps	1
Projection Method	
Projection Direction	None
Detection Mode	Widefield
Grid Type	
Pin Hole Size	
Intensity Percent	100

Exposure Parameters

Method	Fixed
Exposure Time (seconds)	0.12

Object Identification

Method	IsodataThreshold
Value	-0.462

Object Selection Parameter	Min	Max
ObjectAreaCh1	200	3000
ObjectShapeP2ACh1	0	1000
ObjectShapeLWRCh1	0	1000
ObjectAvgIntenCh1	0	50000
ObjectVarIntenCh1	0	65535
ObjectTotalIntenCh1	0	1000000000000

Display Options

Composite Color (Hex)	#0000FF
SelectedObject	#0000FF
RejectedObject	#FF7F00

Assay

Assay Algorithm	TargetActivation.V4
Assay Version	6.0 (Locally Installed Version: 6.0.1.4021)
Focus Channel	1
#Channels	1

Assay Parameters

PixelSize	0.3225
Type_1_EventDefinition	912.22
Type_2_EventDefinition	912.218
Type_3_EventDefinition	0
MinRefAvgObjectCountPerField	2
ObjectAreaCh1LevelHigh	629.01
ObjectAreaCh1LevelHigh_CC	1
ObjectAreaCh1LevelLow	100
ObjectAreaCh1LevelLow_CC	1
ObjectAvgIntenCh1LevelHigh	5000
ObjectAvgIntenCh1LevelHigh_CC	1

Assay

ObjectAvgIntenCh1LevelLow	1206.18
ObjectAvgIntenCh1LevelLow_CC	1
ObjectShapeLWRCh1LevelHigh	0.99
ObjectShapeLWRCh1LevelHigh_CC	1
ObjectShapeLWRCh1LevelLow	0.99
ObjectShapeLWRCh1LevelLow_CC	1
ObjectShapeP2ACh1LevelHigh	1.06
ObjectShapeP2ACh1LevelHigh_CC	1
ObjectShapeP2ACh1LevelLow	1.05
ObjectShapeP2ACh1LevelLow_CC	1
ObjectTotalIntenCh1LevelHigh	1039807
ObjectTotalIntenCh1LevelHigh_CC	1
ObjectTotalIntenCh1LevelLow	13392
ObjectTotalIntenCh1LevelLow_CC	1
ObjectVarIntenCh1LevelHigh	55
ObjectVarIntenCh1LevelHigh_CC	1
ObjectVarIntenCh1LevelLow	55
ObjectVarIntenCh1LevelLow_CC	1
UseMicrometers	0
BackgroundCorrectionCh1	148
NucCleanupCh1	1
ObjectSegmentationCh1	15
ObjectSmoothFactorCh1	2
ObjectTypeCh1	0
RejectBorderObjectsCh1	1
UseReferenceWells	0

Well Feature Extents

Feature Name	Lower Extent	Upper Extent
%EventType1Objects	1	100
%EventType2Objects	1	100
%EventType3Objects	1	100
%RESPONDER_ObjectAreaCh1	1	100
%RESPONDER_ObjectAvgIntenCh1	1	100
%RESPONDER_ObjectShapeLWRCh1	1	100
%RESPONDER_ObjectShapeP2ACh1	1	100
%RESPONDER_ObjectTotalIntenCh1	1	100
%RESPONDER_ObjectVarIntenCh1	1	100
%SelectedObjects	1	100
CV_ObjectAreaCh1	1	100
CV_ObjectAvgIntenCh1	1	100
CV_ObjectShapeLWRCh1	1	100
CV_ObjectShapeP2ACh1	1	100
CV_ObjectTotalIntenCh1	1	100
CV_ObjectVarIntenCh1	1	100
EventType1ObjectCount	1	100
EventType2ObjectCount	1	100
EventType3ObjectCount	1	100
MEAN_ObjectAreaCh1	0	40000000
MEAN_ObjectAvgIntenCh1	0	4095
MEAN_ObjectShapeLWRCh1	0	100
MEAN_ObjectShapeP2ACh1	0	100
MEAN_ObjectTotalIntenCh1	0	40000000000
MEAN_ObjectVarIntenCh1	0	10000000
SD_ObjectAreaCh1	16	1600
SD_ObjectAvgIntenCh1	1	100
SD_ObjectShapeLWRCh1	1	100
SD_ObjectShapeP2ACh1	1	100
SD_ObjectTotalIntenCh1	16	1600
SD_ObjectVarIntenCh1	1	100
SE_ObjectAreaCh1	16	1600
SE_ObjectAvgIntenCh1	1	100
SE_ObjectShapeLWRCh1	1	100

11/8/2016 Ilaria nuclear decondensation

Well Feature Extents

SE_ObjectShapeP2ACh1	1	100
SE_ObjectTotalIntenCh1	16	1600
SE_ObjectVarIntenCh1	1	100
SelectedObjectCount	20	750
SelectedObjectCountPerValidField	0.0625	6.25
ValidFieldCount	0	111
ValidObjectCount*	0	100

* Indicates the default well feature for the Assay Protocol
** Indicates feature extents are dependent upon system reference well settings

Selected W ell Features to Store

TargetActivation/4W ell %EventType1Objects
TargetActivation/4W ell %EventType2Objects
TargetActivation/4W ell %RESPONDER_ObjectAreaCh
TargetActivation/4W ell %RESPONDER_ObjectAlgIntenCh1
TargetActivation/4W ell %RESPONDER_ObjectShapeBACh1
TargetActivation/4W ell %RESPONDER_ObjectTotalIntenCh1
TargetActivation/4W ell %RESPONDER_ObjectVarIntenCh1
TargetActivation/4W ell %SelectedObjects
TargetActivation/4W ell EventType1ObjectCount
TargetActivation/4W ell EventType2ObjectCount
TargetActivation/4W ell MEAN_ObjectAreaCh1
TargetActivation/4W ell MEAN_ObjectAlgIntenCh1
TargetActivation/4W ell MEAN_ObjectShapeUVRCh1
TargetActivation/4W ell MEAN_ObjectShapeP2ACh1
TargetActivation/4W ell MEAN_ObjectTotalIntenCh1
TargetActivation/4W ell MEAN_ObjectVarIntenCh1
TargetActivation/4W ell SelectedObjectCount
TargetActivation/4W ell ValidFieldCount
TargetActivation/4W ell ValidObjectCount

Selected Cell Features to Store

TargetActivation/4Cell Cell#
TargetActivation/4Cell Height
TargetActivation/4Cell Left
TargetActivation/4Cell Top
TargetActivation/4Cell Width

Figure II: Settings of the Nuclear Decondensation algorithm employed in this thesis.
Full description of the parameters of the Nuclear Decondensation algorithm applied in this thesis for the quantification of NET by HCA.

Ilaria H400 nfkb [Version 5]

Last Modified on 27/10/2016 13:43:26

NOTE: The information here represents data that is saved in the database with an Assay Protocol. This data does not include scan settings like Field Offset, Form Factor , Scan Area, Store Images or Show Composite Image.

Comments

Event1=(None) Event2=(None) Event3=(None)

Image Acquisition	
Objective	20x
Camera Name	ORCA-ER;1.00
Acquisition Camera Mode	HiRes (1024x1024;1x1)
AutoFocus Camera Mode	HiRes (1024x1024;1x1)
AutoFocus Field Interval	0

AutoFocus Parameters	
Fine Focus Step Size	9.9
Fine Focus Plane Count	9
Coarse Focus Step Size	39.6
Coarse Focus Plane Count	16
Smart Focus Plane Count	21
Use Extended Range Focusing	False
Apply Backlash Correction	False
AutoFocus Method	STANDARD
Laser AutoFocus Method	LASER
How To Focus During Scan	2
Use Relaxed Pass/Fail Criteria	False
Focus Edge Threshhold	5
Focus Adjustment	0
Focus Score Min Ratio	0.25
Focus Score Mid Ratio	0.4
Focus Score Max Ratio	0.5
Focus Exposure Time for AutoExpose (seconds)	0.1

Scan Limits	
Max Fields for Well	25
Min Objects for Well	No Limit
Max Sparse Fields for Well	No Limit
Min Objects for Field	N/A
Max Sparse Wells for Plate	N/A

Channel 1:	Channel1
Dye	BGRFR_386_23
Apply Illumination Correction	False
Apply Background Correction	True
Gain	25
Z Offset	6.00
Step Size	6.56
Number of Steps	10
Projection Method	Maximum
Projection Direction	None
Detection Mode	Widefield
Grid Type	
Pin Hole Size	
Intensity Percent	100
Exposure Parameters	
Method	Fixed
Exposure Time (seconds)	0.05
Object Identification	
Method	FixedThreshold
Value	99

Object Selection Parameter	Min	Max
ObjectAreaCh1	105	8337
ObjectShapeP2ACh1	0	1000
ObjectShapeLWRCh1	0	1000
ObjectAvgIntenCh1	0	65535
ObjectVarIntenCh1	0	65535
ObjectTotalIntenCh1	0	1000000000000

Display Options	
Composite Color (Hex)	#00FFFF
SelectedObject	#0000FF
RejectedObject	#FF7F00

Channel 2:	Channel2
Dye	BGRFR_485_20
Apply Illumination Correction	False
Apply Background Correction	True
Gain	25
Z Offset	6.60
Step Size	0.00
Number of Steps	0
Projection Method	
Projection Direction	None
Detection Mode	Widefield
Grid Type	
Pin Hole Size	
Intensity Percent	100
Exposure Parameters	
Method	Fixed
Exposure Time (seconds)	2
Object Identification	
Method	FixedThreshold
Value	193

Object Selection Parameter	Min	Max
RingAvgIntenCh2	0	65535
CircAvgIntenCh2	0	65535
CircRingAvgIntenDiffCh2	-65535	65535
CircRingAvgIntenRatioCh2	0	1000000000000
RingSpotTotalAreaCh2	0	1000000000000
RingSpotAvgIntenCh2	0	65535
CircSpotTotalAreaCh2	0	1000000000000
CircSpotAvgIntenCh2	0	65535
AvgIntenCh2	0	65535
TotalIntenCh2	0	1000000000000

Display Options	
Composite Color (Hex)	#80FF00
CircSpot	#FF0000

Assay	
Assay Algorithm	CompartmentalAnalysis.V4
Assay Version	6.0 (Locally Installed Version: 6.0.3.4021)
Focus Channel	1
#Channels	2
Assay Parameters	
PixelSize	0.3225
Type_1_EventDefinition	0
Type_2_EventDefinition	0
Type_3_EventDefinition	0
CircAvgIntenCh2LevelHigh	375.67
CircAvgIntenCh2LevelHigh_CC	1
CircAvgIntenCh2LevelLow	25
CircAvgIntenCh2LevelLow_CC	1
CircAvgIntenRatioCh2Ch1LevelHigh	0.05
CircAvgIntenRatioCh2Ch1LevelHigh_CC	1
CircAvgIntenRatioCh2Ch1LevelLow	0.03
CircAvgIntenRatioCh2Ch1LevelLow_CC	1
CircRingAvgIntenDiffCh2LevelHigh	50
CircRingAvgIntenDiffCh2LevelHigh_CC	1
CircRingAvgIntenDiffCh2LevelLow	15
CircRingAvgIntenDiffCh2LevelLow_CC	1
CircRingAvgIntenRatioCh2LevelHigh	7.5
CircRingAvgIntenRatioCh2LevelHigh_CC	1
CircRingAvgIntenRatioCh2LevelLow	2
CircRingAvgIntenRatioCh2LevelLow_CC	1
CircSpotAvgAreaCh2LevelHigh	85
CircSpotAvgAreaCh2LevelHigh_CC	1
CircSpotAvgAreaCh2LevelLow	0
CircSpotAvgAreaCh2LevelLow_CC	1
CircSpotAvgIntenCh2LevelHigh	80
CircSpotAvgIntenCh2LevelHigh_CC	1
CircSpotAvgIntenCh2LevelLow	30
CircSpotAvgIntenCh2LevelLow_CC	1
CircSpotCountCh2LevelHigh	0
CircSpotCountCh2LevelHigh_CC	1
CircSpotCountCh2LevelLow	0
CircSpotCountCh2LevelLow_CC	1
CircSpotTotalAreaCh2LevelHigh	269.48
CircSpotTotalAreaCh2LevelHigh_CC	1
CircSpotTotalAreaCh2LevelLow	137.4
CircSpotTotalAreaCh2LevelLow_CC	1
CircSpotTotalIntenCh2LevelHigh	506736
CircSpotTotalIntenCh2LevelHigh_CC	1
CircSpotTotalIntenCh2LevelLow	109484
CircSpotTotalIntenCh2LevelLow_CC	1
CircTotalIntenCh2LevelHigh	516096
CircTotalIntenCh2LevelHigh_CC	1

Assay	
CircTotalIntenCh2LevelLow	0
CircTotalIntenCh2LevelLow_CC	1
MinRefAvgObjectCountPerField	1
ObjectAreaCh1LevelHigh	184.8
ObjectAreaCh1LevelHigh_CC	1
ObjectAreaCh1LevelLow	7.4
ObjectAreaCh1LevelLow_CC	1
ObjectAvgIntenCh1LevelHigh	1314.11
ObjectAvgIntenCh1LevelHigh_CC	1
ObjectAvgIntenCh1LevelLow	423.65
ObjectAvgIntenCh1LevelLow_CC	1
ObjectShapeLWRCh1LevelHigh	1.59
ObjectShapeLWRCh1LevelHigh_CC	1
ObjectShapeLWRCh1LevelLow	1
ObjectShapeLWRCh1LevelLow_CC	1
ObjectShapeP2ACh1LevelHigh	1.39
ObjectShapeP2ACh1LevelHigh_CC	1
ObjectShapeP2ACh1LevelLow	1.06
ObjectShapeP2ACh1LevelLow_CC	1
ObjectSizeCh1LevelHigh	27.5
ObjectSizeCh1LevelHigh_CC	1
ObjectSizeCh1LevelLow	20
ObjectSizeCh1LevelLow_CC	1
ObjectTotalIntenCh1LevelHigh	280228
ObjectTotalIntenCh1LevelHigh_CC	1
ObjectTotalIntenCh1LevelLow	5376
ObjectTotalIntenCh1LevelLow_CC	1
ObjectVarIntenCh1LevelHigh	32767
ObjectVarIntenCh1LevelHigh_CC	1
ObjectVarIntenCh1LevelLow	17.38
ObjectVarIntenCh1LevelLow_CC	1
RingAvgIntenCh2LevelHigh	14
RingAvgIntenCh2LevelHigh_CC	1
RingAvgIntenCh2LevelLow	5
RingAvgIntenCh2LevelLow_CC	1
RingSpotAvgAreaCh2LevelHigh	4.6
RingSpotAvgAreaCh2LevelHigh_CC	1
RingSpotAvgAreaCh2LevelLow	1.2
RingSpotAvgAreaCh2LevelLow_CC	1
RingSpotAvgIntenCh2LevelHigh	50
RingSpotAvgIntenCh2LevelHigh_CC	1
RingSpotAvgIntenCh2LevelLow	10
RingSpotAvgIntenCh2LevelLow_CC	1
RingSpotCountCh2LevelHigh	95
RingSpotCountCh2LevelHigh_CC	1
RingSpotCountCh2LevelLow	50
RingSpotCountCh2LevelLow_CC	1
RingSpotTotalAreaCh2LevelHigh	125.52
RingSpotTotalAreaCh2LevelHigh_CC	1
RingSpotTotalAreaCh2LevelLow	25.04
RingSpotTotalAreaCh2LevelLow_CC	1
RingSpotTotalIntenCh2LevelHigh	63428
RingSpotTotalIntenCh2LevelHigh_CC	1
RingSpotTotalIntenCh2LevelLow	0
RingSpotTotalIntenCh2LevelLow_CC	1
RingTotalIntenCh2LevelHigh	29292
RingTotalIntenCh2LevelHigh_CC	1
RingTotalIntenCh2LevelLow	24
RingTotalIntenCh2LevelLow_CC	1
UseMicrometers	0
BackgroundCorrectionCh1	220
BackgroundCorrectionCh2	48
ChannelToDeriveCircOverlay	2
ChannelToDeriveCircSpotOverlay	2

Assay	
ChannelToDeriveRingOverlay	2
ChannelToDeriveRingSpotOverlay	2
CircModifierCh2	-2
MaskModifierCh2	0
ObjectCleanUpCh1	1
ObjectSegmentationCh1	25
ObjectSmoothFactorCh1	2
ObjectTypeCh1	0
RejectBorderObjectsCh1	1
RingDistanceCh2	4
RingWidthCh2	34
SpotDetectRadiusCh2	0
SpotTypeCh2	0
UseReferenceWells	0

Well Feature Extents

Feature Name	Lower Extent	Upper Extent
#HIGH_CircRingAvgIntenDiffCh2	1	100
#HIGH_CircRingAvgIntenRatioCh2	1	100
#LOW_CircRingAvgIntenDiffCh2	1	100
#LOW_CircRingAvgIntenRatioCh2	1	100
%EventType1Objects	1	100
%EventType2Objects	1	100
%EventType3Objects	1	100
%HIGH_CircAvgIntenCh2	1	100
%HIGH_CircAvgIntenRatioCh2Ch1	1	100
%HIGH_CircRingAvgIntenDiffCh2	1	100
%HIGH_CircRingAvgIntenRatioCh2	1	100
%HIGH_CircSpotAvgAreaCh2	1	100
%HIGH_CircSpotAvgIntenCh2	1	100
%HIGH_CircSpotCountCh2*	1	100
%HIGH_CircSpotTotalAreaCh2	1	100
%HIGH_CircSpotTotalIntenCh2	1	100
%HIGH_CircTotalIntenCh2	1	100
%HIGH_ObjectAreaCh1	1	100
%HIGH_ObjectAvgIntenCh1	1	100
%HIGH_ObjectShapeLWRCh1	1	100
%HIGH_ObjectShapeP2ACh1	1	100
%HIGH_ObjectSizeCh1	1	100
%HIGH_ObjectTotalIntenCh1	1	100
%HIGH_ObjectVarIntenCh1	1	100
%HIGH_RingAvgIntenCh2	1	100
%HIGH_RingSpotAvgAreaCh2	1	100
%HIGH_RingSpotAvgIntenCh2	1	100
%HIGH_RingSpotCountCh2	1	100
%HIGH_RingSpotTotalAreaCh2	1	100
%HIGH_RingSpotTotalIntenCh2	1	100
%HIGH_RingTotalIntenCh2	1	100
%LOW_CircAvgIntenCh2	1	100
%LOW_CircAvgIntenRatioCh2Ch1	1	100
%LOW_CircRingAvgIntenDiffCh2	1	100
%LOW_CircRingAvgIntenRatioCh2	1	100
%LOW_CircSpotAvgAreaCh2	1	100
%LOW_CircSpotAvgIntenCh2	1	100
%LOW_CircSpotCountCh2	1	100
%LOW_CircSpotTotalAreaCh2	1	100
%LOW_CircSpotTotalIntenCh2	1	100
%LOW_CircTotalIntenCh2	1	100
%LOW_ObjectAreaCh1	1	100
%LOW_ObjectAvgIntenCh1	1	100
%LOW_ObjectShapeLWRCh1	1	100
%LOW_ObjectShapeP2ACh1	1	100
%LOW_ObjectSizeCh1	1	100

Well Feature Extents		
%LOW_ObjectTotalIntenCh1	1	100
%LOW_ObjectVarIntenCh1	1	100
%LOW_RingAvgIntenCh2	1	100
%LOW_RingSpotAvgAreaCh2	1	100
%LOW_RingSpotAvgIntenCh2	1	100
%LOW_RingSpotCountCh2	1	100
%LOW_RingSpotTotalAreaCh2	1	100
%LOW_RingSpotTotalIntenCh2	1	100
%LOW_RingTotalIntenCh2	1	100
%SelectedObjects	1	100
CV_CircAvgIntenCh2	1	100
CV_CircAvgIntenRatioCh2Ch1	1	100
CV_CircRingAvgIntenDiffCh2	1	100
CV_CircRingAvgIntenRatioCh2	1	100
CV_CircSpotAvgAreaCh2	1	100
CV_CircSpotAvgIntenCh2	1	100
CV_CircSpotCountCh2	1	100
CV_CircSpotTotalAreaCh2	1	100
CV_CircSpotTotalIntenCh2	1	100
CV_CircTotalIntenCh2	1	100
CV_ObjectAreaCh1	1	100
CV_ObjectAvgIntenCh1	1	100
CV_ObjectShapeLWRCh1	1	100
CV_ObjectShapeP2ACh1	1	100
CV_ObjectSizeCh1	1	100
CV_ObjectTotalIntenCh1	1	100
CV_ObjectVarIntenCh1	1	100
CV_RingAvgIntenCh2	1	100
CV_RingSpotAvgAreaCh2	1	100
CV_RingSpotAvgIntenCh2	1	100
CV_RingSpotCountCh2	1	100
CV_RingSpotTotalAreaCh2	1	100
CV_RingSpotTotalIntenCh2	1	100
CV_RingTotalIntenCh2	1	100
EventType1ObjectCount	1	100
EventType2ObjectCount	1	100
EventType3ObjectCount	1	100
MEAN_CircAvgIntenCh2	1	100
MEAN_CircAvgIntenRatioCh2Ch1	1	100
MEAN_CircRingAvgIntenDiffCh2	1	100
MEAN_CircRingAvgIntenRatioCh2	1	100
MEAN_CircSpotAvgAreaCh2	1	100
MEAN_CircSpotAvgIntenCh2	1	100
MEAN_CircSpotCountCh2	1	100
MEAN_CircSpotTotalAreaCh2	1.11147166636662	111.14716636662
MEAN_CircSpotTotalIntenCh2	1.11147166636662	111.14716636662
MEAN_CircTotalIntenCh2	1.11147166636662	111.14716636662
MEAN_ObjectAreaCh1	0	100
MEAN_ObjectAvgIntenCh1	1	100
MEAN_ObjectShapeLWRCh1	0	100
MEAN_ObjectShapeP2ACh1	0	100
MEAN_ObjectSizeCh1	1.05426356589147	105.426356589147
MEAN_ObjectTotalIntenCh1	1.11147166636662	111.14716636662
MEAN_ObjectVarIntenCh1	1	100
MEAN_RingAvgIntenCh2	1	100
MEAN_RingSpotAvgAreaCh2	1	100
MEAN_RingSpotAvgIntenCh2	1	100
MEAN_RingSpotCountCh2	1	100
MEAN_RingSpotTotalAreaCh2	1.11147166636662	111.14716636662
MEAN_RingSpotTotalIntenCh2	1.11147166636662	111.14716636662
MEAN_RingTotalIntenCh2	1.11147166636662	111.14716636662
SD_CircAvgIntenCh2	1	100
SD_CircAvgIntenRatioCh2Ch1	1	100
SD_CircRingAvgIntenDiffCh2	1	100

Well Feature Extents		
SD_CircRingAvgIntenRatioCh2	1	100
SD_CircSpotAvgAreaCh2	1	100
SD_CircSpotAvgIntenCh2	1	100
SD_CircSpotCountCh2	1	100
SD_CircSpotTotalAreaCh2	1	100
SD_CircSpotTotalIntenCh2	1	100
SD_CircTotalIntenCh2	1	100
SD_ObjectAreaCh1	1	100
SD_ObjectAvgIntenCh1	1	100
SD_ObjectShapeLWRCh1	1	100
SD_ObjectShapeP2ACh1	1	100
SD_ObjectSizeCh1	1	100
SD_ObjectTotalIntenCh1	1	100
SD_ObjectVarIntenCh1	1	100
SD_RingAvgIntenCh2	1	100
SD_RingSpotAvgAreaCh2	1	100
SD_RingSpotAvgIntenCh2	1	100
SD_RingSpotCountCh2	1	100
SD_RingSpotTotalAreaCh2	1	100
SD_RingSpotTotalIntenCh2	1	100
SD_RingTotalIntenCh2	1	100
SE_CircAvgIntenCh2	1	100
SE_CircAvgIntenRatioCh2Ch1	1	100
SE_CircRingAvgIntenDiffCh2	1	100
SE_CircRingAvgIntenRatioCh2	1	100
SE_CircSpotAvgAreaCh2	1	100
SE_CircSpotAvgIntenCh2	1	100
SE_CircSpotCountCh2	1	100
SE_CircSpotTotalAreaCh2	1	100
SE_CircSpotTotalIntenCh2	1	100
SE_CircTotalIntenCh2	1	100
SE_ObjectAreaCh1	1	100
SE_ObjectAvgIntenCh1	1	100
SE_ObjectShapeLWRCh1	1	100
SE_ObjectShapeP2ACh1	1	100
SE_ObjectSizeCh1	1	100
SE_ObjectTotalIntenCh1	1	100
SE_ObjectVarIntenCh1	1	100
SE_RingAvgIntenCh2	1	100
SE_RingSpotAvgAreaCh2	1	100
SE_RingSpotAvgIntenCh2	1	100
SE_RingSpotCountCh2	1	100
SE_RingSpotTotalAreaCh2	1	100
SE_RingSpotTotalIntenCh2	1	100
SE_RingTotalIntenCh2	1	100
SelectedObjectCount	1	100
SelectedObjectCountPerValidField	0.899708044982699	89.9708044982699
ValidFieldCount	1	100
ValidObjectCount	1	100

* Indicates the default well feature for the Assay Protocol
** Indicates feature extents are dependent upon system reference well settings

Selected W ell Features to Store	Selected Cell Features to Store
CompartmentalAnalysisV4Well:%SelectedObjects	CompartmentalAnalysisV4Cell:Cell#
CompartmentalAnalysisV4Well:MEAN_CircAvgIntenCh2	CompartmentalAnalysisV4Cell:Height
CompartmentalAnalysisV4Well:MEAN_CircAvgIntenRatioCh2Ch1	CompartmentalAnalysisV4Cell:Left
CompartmentalAnalysisV4Well:MEAN_CircRingAvgIntenDiffCh2	CompartmentalAnalysisV4Cell:Top
CompartmentalAnalysisV4Well:MEAN_CircRingAvgIntenRatioCh2	CompartmentalAnalysisV4Cell:Width
CompartmentalAnalysisV4Well:MEAN_CircSpotAvgAreaCh2	
CompartmentalAnalysisV4Well:MEAN_CircSpotAvgIntenCh2	
CompartmentalAnalysisV4Well:MEAN_CircSpotCountCh2	
CompartmentalAnalysisV4Well:MEAN_CircSpotTotalAreaCh2	
CompartmentalAnalysisV4Well:MEAN_CircSpotTotalIntenCh2	

Figure III: Settings of the Compartmental Analysis algorithm employed for the assessment of NF-κB nuclear translocation in H400 in this thesis.
Full description of the parameters of the Compartmental Analysis algorithm applied in this thesis for H400 cells and for tracking the translocation of NF-κB.

Ilaria_elastase_ [Version 16]

Last Modified on 01/05/2015 10:50:52

NOTE: The information here represents data that is saved in the database with an Assay Protocol. This data does not include scan settings like Field Offset, Form Factor , Scan Area, Store Imag es or Show Composite Image.

Comments

Event1=(None) Event2=(None) Event3=(None)

Image Acquisition	
Objective	20x
Camera Name	ORCA-ER;1.00
Acquisition Camera Mode	HiRes (1024x1024;1x1)
AutoFocus Camera Mode	AutoFocus (1024x1024;4x4)
AutoFocus Field Interval	0

AutoFocus Parameters	
Fine Focus Step Size	9.9
Fine Focus Plane Count	9
Coarse Focus Step Size	39.6
Coarse Focus Plane Count	16
Smart Focus Plane Count	21
Use Extended Range Focusing	False
Apply Backlash Correction	False
AutoFocus Method	STANDARD
Laser AutoFocus Method	
How To Focus During Scan	2
Use Relaxed Pass/Fail Criteria	False
Focus Edge Threshhold	5
Focus Adjustment	0
Focus Score Min Ratio	0.25
Focus Score Mid Ratio	0.4
Focus Score Max Ratio	0.5
Focus Exposure Time for AutoExpose (seconds)	0.1

Scan Limits	
Max Fields for Well	10
Min Objects for Well	No Limit
Max Sparse Fields for Well	No Limit
Min Objects for Field	N/A
Max Sparse Wells for Plate	N/A

Channel 1: Channel1	
Dye	BGRFR_386_23
Apply Illumination Correction	False
Apply Background Correction	True
Gain	25
Z Offset	6.00
Step Size	3.86
Number of Steps	10
Projection Method	Maximum
Projection Direction	None
Detection Mode	Widefield
Grid Type	
Pin Hole Size	
Intensity Percent	100
Exposure Parameters	
Method	Fixed
Exposure Time (seconds)	0.05
Object Identification	
Method	FixedThreshold
Value	224

Object Selection Parameter	**Min**	**Max**
ObjectAreaCh1	105	3382.624
ObjectShapeP2ACh1	0	1000
ObjectShapeLWRCh1	0	1000
ObjectAvgIntenCh1	0	32767
ObjectVarIntenCh1	0	32767
ObjectTotalIntenCh1	0	1000000000000

Display Options	
Composite Color (Hex)	#00FFFF
SelectedObject	#0000FF
RejectedObject	#FF8040

Channel 2: Channel2	
Dye	BGRFR_549_15
Apply Illumination Correction	False
Apply Background Correction	True
Gain	25
Z Offset	6.60
Step Size	0.00
Number of Steps	0
Projection Method	
Projection Direction	None
Detection Mode	Widefield
Grid Type	
Pin Hole Size	
Intensity Percent	100
Exposure Parameters	
Method	Fixed
Exposure Time (seconds)	2
Object Identification	
Method	FixedThreshold
Value	350

Object Selection Parameter	**Min**	**Max**

Channel 2: Channel2		
RingAvgIntenCh2	0	32767
CircAvgIntenCh2	0	32767
CircRingAvgIntenDiffCh2	-27186	30954
CircRingAvgIntenRatioCh2	0	1000000000000
RingSpotTotalAreaCh2	0	1000000000000
RingSpotAvgIntenCh2	0	32767
CircSpotTotalAreaCh2	0	1000000000000
CircSpotAvgIntenCh2	0	32767
AvgIntenCh2	0	32767
TotalIntenCh2	0	1000000000000
Display Options		
Composite Color (Hex)	#FF0000	
Ring	#960096	

Channel 3: Channel3	
Dye	BGRFR_650_13
Apply Illumination Correction	False
Apply Background Correction	True
Gain	25
Z Offset	0.00
Step Size	0.00
Number of Steps	0
Projection Method	
Projection Direction	none
Detection Mode	widefield
Grid Type	
Pin Hole Size	
Intensity Percent	100
Exposure Parameters	
Method	Fixed
Exposure Time (seconds)	1
Object Identification	
Method	FixedThreshold
Value	545

Object Selection Parameter	**Min**	**Max**
RingAvgIntenCh3	0	32767
CircAvgIntenCh3	0	32767
CircRingAvgIntenDiffCh3	-32767	32767
CircRingAvgIntenRatioCh3	0	1000000000000
RingSpotTotalAreaCh3	0	1000000000000
RingSpotAvgIntenCh3	0	32767
CircSpotTotalAreaCh3	0	1000000000000
CircSpotAvgIntenCh3	0	32767
AvgIntenCh3	0	32767
TotalIntenCh3	0	1000000000000

Display Options	

Assay	
Assay Algorithm	CompartmentalAnalysis.V4
Assay V ersion	6.0 (Locally Installed V ersion: 6.0.3.4021)
Focus Channel	1
#Channels	3
Assay Parameters	
PixelSize	0.3225
Type_1_EventDefinition	0
Type_2_EventDefinition	0
Type_3_EventDefinition	0
CircAvgIntenCh2LevelHigh	375.668
CircAvgIntenCh2LevelHigh_CC	1
CircAvgIntenCh2LevelLow	25
CircAvgIntenCh2LevelLow_CC	1
CircAvgIntenCh3LevelHigh	32767

Assay	
CircAvgIntenCh3LevelHigh_CC	1
CircAvgIntenCh3LevelLow	0
CircAvgIntenCh3LevelLow_CC	1
CircAvgIntenRatioCh2Ch1LevelHigh	0.05
CircAvgIntenRatioCh2Ch1LevelHigh_CC	1
CircAvgIntenRatioCh2Ch1LevelLow	0.03
CircAvgIntenRatioCh2Ch1LevelLow_CC	1
CircAvgIntenRatioCh3Ch1LevelHigh	1000000000000
CircAvgIntenRatioCh3Ch1LevelHigh_CC	1
CircAvgIntenRatioCh3Ch1LevelLow	0
CircAvgIntenRatioCh3Ch1LevelLow_CC	1
CircAvgIntenRatioCh3Ch2LevelHigh	1000000000000
CircAvgIntenRatioCh3Ch2LevelHigh_CC	1
CircAvgIntenRatioCh3Ch2LevelLow	0
CircAvgIntenRatioCh3Ch2LevelLow_CC	1
CircRingAvgIntenDiffCh2LevelHigh	50
CircRingAvgIntenDiffCh2LevelHigh_CC	1
CircRingAvgIntenDiffCh2LevelLow	15
CircRingAvgIntenDiffCh2LevelLow_CC	1
CircRingAvgIntenDiffCh3LevelHigh	32767
CircRingAvgIntenDiffCh3LevelHigh_CC	1
CircRingAvgIntenDiffCh3LevelLow	-32767
CircRingAvgIntenDiffCh3LevelLow_CC	1
CircRingAvgIntenRatioCh2LevelHigh	7.5
CircRingAvgIntenRatioCh2LevelHigh_CC	1
CircRingAvgIntenRatioCh2LevelLow	2
CircRingAvgIntenRatioCh2LevelLow_CC	1
CircRingAvgIntenRatioCh3LevelHigh	1000000000000
CircRingAvgIntenRatioCh3LevelHigh_CC	1
CircRingAvgIntenRatioCh3LevelLow	0
CircRingAvgIntenRatioCh3LevelLow_CC	1
CircSpotAvgAreaCh2LevelHigh	85
CircSpotAvgAreaCh2LevelHigh_CC	1
CircSpotAvgAreaCh2LevelLow	0
CircSpotAvgAreaCh2LevelLow_CC	1
CircSpotAvgAreaCh3LevelHigh	1000000000000
CircSpotAvgAreaCh3LevelHigh_CC	1
CircSpotAvgAreaCh3LevelLow	0
CircSpotAvgAreaCh3LevelLow_CC	1
CircSpotAvgIntenCh2LevelHigh	80
CircSpotAvgIntenCh2LevelHigh_CC	1
CircSpotAvgIntenCh2LevelLow	30
CircSpotAvgIntenCh2LevelLow_CC	1
CircSpotAvgIntenCh3LevelHigh	32767
CircSpotAvgIntenCh3LevelHigh_CC	1
CircSpotAvgIntenCh3LevelLow	0
CircSpotAvgIntenCh3LevelLow_CC	1
CircSpotAvgIntenRatioCh3Ch2LevelHigh	1000000000000
CircSpotAvgIntenRatioCh3Ch2LevelHigh_CC	1
CircSpotAvgIntenRatioCh3Ch2LevelLow	0
CircSpotAvgIntenRatioCh3Ch2LevelLow_CC	1
CircSpotCountCh2LevelHigh	0
CircSpotCountCh2LevelHigh_CC	1
CircSpotCountCh2LevelLow	0
CircSpotCountCh2LevelLow_CC	1
CircSpotCountCh3LevelHigh	32767
CircSpotCountCh3LevelHigh_CC	1
CircSpotCountCh3LevelLow	0
CircSpotCountCh3LevelLow_CC	1
CircSpotCountRatioCh3Ch2LevelHigh	1000000000000
CircSpotCountRatioCh3Ch2LevelHigh_CC	1
CircSpotCountRatioCh3Ch2LevelLow	0
CircSpotCountRatioCh3Ch2LevelLow_CC	1
CircSpotTotalAreaCh2LevelHigh	269.482

Assay	
CircSpotTotalAreaCh2LevelHigh_CC	1
CircSpotTotalAreaCh2LevelLow	137.392
CircSpotTotalAreaCh2LevelLow_CC	1
CircSpotTotalAreaCh3LevelHigh	1000000000000
CircSpotTotalAreaCh3LevelHigh_CC	1
CircSpotTotalAreaCh3LevelLow	0
CircSpotTotalAreaCh3LevelLow_CC	1
CircSpotTotalIntenCh2LevelHigh	506735.756
CircSpotTotalIntenCh2LevelHigh_CC	1
CircSpotTotalIntenCh2LevelLow	109485.399
CircSpotTotalIntenCh2LevelLow_CC	1
CircSpotTotalIntenCh3LevelHigh	1000000000000
CircSpotTotalIntenCh3LevelHigh_CC	1
CircSpotTotalIntenCh3LevelLow	0
CircSpotTotalIntenCh3LevelLow_CC	1
CircTotalIntenCh2LevelHigh	516097.599
CircTotalIntenCh2LevelHigh_CC	1
CircTotalIntenCh2LevelLow	0
CircTotalIntenCh2LevelLow_CC	1
CircTotalIntenCh3LevelHigh	1000000000000
CircTotalIntenCh3LevelHigh_CC	1
CircTotalIntenCh3LevelLow	0
CircTotalIntenCh3LevelLow_CC	1
MinRefAvgObjectCountPerField	1
ObjectAreaCh1LevelHigh	184.82
ObjectAreaCh1LevelHigh_CC	1
ObjectAreaCh1LevelLow	7.404
ObjectAreaCh1LevelLow_CC	1
ObjectAvgIntenCh1LevelHigh	1314.11
ObjectAvgIntenCh1LevelHigh_CC	1
ObjectAvgIntenCh1LevelLow	423.648
ObjectAvgIntenCh1LevelLow_CC	1
ObjectShapeLWRCh1LevelHigh	1.594
ObjectShapeLWRCh1LevelHigh_CC	1
ObjectShapeLWRCh1LevelLow	0.997
ObjectShapeLWRCh1LevelLow_CC	1
ObjectShapeP2ACh1LevelHigh	1.393
ObjectShapeP2ACh1LevelHigh_CC	1
ObjectShapeP2ACh1LevelLow	1.062
ObjectShapeP2ACh1LevelLow_CC	1
ObjectSizeCh1LevelHigh	27.5
ObjectSizeCh1LevelHigh_CC	1
ObjectSizeCh1LevelLow	20
ObjectSizeCh1LevelLow_CC	1
ObjectTotalIntenCh1LevelHigh	280227.016
ObjectTotalIntenCh1LevelHigh_CC	1
ObjectTotalIntenCh1LevelLow	5377.701
ObjectTotalIntenCh1LevelLow_CC	1
ObjectVarIntenCh1LevelHigh	32767
ObjectVarIntenCh1LevelHigh_CC	1
ObjectVarIntenCh1LevelLow	17.379
ObjectVarIntenCh1LevelLow_CC	1
RingAvgIntenCh2LevelHigh	14
RingAvgIntenCh2LevelHigh_CC	1
RingAvgIntenCh2LevelLow	5
RingAvgIntenCh2LevelLow_CC	1
RingAvgIntenCh3LevelHigh	32767
RingAvgIntenCh3LevelHigh_CC	1
RingAvgIntenCh3LevelLow	0
RingAvgIntenCh3LevelLow_CC	1
RingAvgIntenRatioCh3Ch2LevelHigh	1000000000000
RingAvgIntenRatioCh3Ch2LevelHigh_CC	1
RingAvgIntenRatioCh3Ch2LevelLow	0
RingAvgIntenRatioCh3Ch2LevelLow_CC	1

Assay	
RingSpotAvgAreaCh2LevelHigh	4.6
RingSpotAvgAreaCh2LevelHigh_CC	1
RingSpotAvgAreaCh2LevelLow	1.2
RingSpotAvgAreaCh2LevelLow_CC	1
RingSpotAvgAreaCh3LevelHigh	1000000000000
RingSpotAvgAreaCh3LevelHigh_CC	1
RingSpotAvgAreaCh3LevelLow	0
RingSpotAvgAreaCh3LevelLow_CC	1
RingSpotAvgIntenCh2LevelHigh	50
RingSpotAvgIntenCh2LevelHigh_CC	1
RingSpotAvgIntenCh2LevelLow	10
RingSpotAvgIntenCh2LevelLow_CC	1
RingSpotAvgIntenCh3LevelHigh	32767
RingSpotAvgIntenCh3LevelHigh_CC	1
RingSpotAvgIntenCh3LevelLow	0
RingSpotAvgIntenCh3LevelLow_CC	1
RingSpotAvgIntenRatioCh3Ch2LevelHigh	1000000000000
RingSpotAvgIntenRatioCh3Ch2LevelHigh_CC	1
RingSpotAvgIntenRatioCh3Ch2LevelLow	0
RingSpotAvgIntenRatioCh3Ch2LevelLow_CC	1
RingSpotCountCh2LevelHigh	95
RingSpotCountCh2LevelHigh_CC	1
RingSpotCountCh2LevelLow	50
RingSpotCountCh2LevelLow_CC	1
RingSpotCountCh3LevelHigh	32767
RingSpotCountCh3LevelHigh_CC	1
RingSpotCountCh3LevelLow	0
RingSpotCountCh3LevelLow_CC	1
RingSpotCountRatioCh3Ch2LevelHigh	1000000000000
RingSpotCountRatioCh3Ch2LevelHigh_CC	1
RingSpotCountRatioCh3Ch2LevelLow	0
RingSpotCountRatioCh3Ch2LevelLow_CC	1
RingSpotTotalAreaCh2LevelHigh	125.543
RingSpotTotalAreaCh2LevelHigh_CC	1
RingSpotTotalAreaCh2LevelLow	25.063
RingSpotTotalAreaCh2LevelLow_CC	1
RingSpotTotalAreaCh3LevelHigh	1000000000000
RingSpotTotalAreaCh3LevelHigh_CC	1
RingSpotTotalAreaCh3LevelLow	0
RingSpotTotalAreaCh3LevelLow_CC	1
RingSpotTotalIntenCh2LevelHigh	63429.184
RingSpotTotalIntenCh2LevelHigh_CC	1
RingSpotTotalIntenCh2LevelLow	0
RingSpotTotalIntenCh2LevelLow_CC	1
RingSpotTotalIntenCh3LevelHigh	1000000000000
RingSpotTotalIntenCh3LevelHigh_CC	1
RingSpotTotalIntenCh3LevelLow	0
RingSpotTotalIntenCh3LevelLow_CC	1
RingTotalIntenCh2LevelHigh	29292.73
RingTotalIntenCh2LevelHigh_CC	1
RingTotalIntenCh2LevelLow	25.984
RingTotalIntenCh2LevelLow_CC	1
RingTotalIntenCh3LevelHigh	1000000000000
RingTotalIntenCh3LevelHigh_CC	1
RingTotalIntenCh3LevelLow	0
RingTotalIntenCh3LevelLow_CC	1
UseMicrometers	0
BackgroundCorrectionCh1	220
BackgroundCorrectionCh2	49
BackgroundCorrectionCh3	0
ChannelToDeriveCircOverlay	2
ChannelToDeriveCircSpotOverlay	2
ChannelToDeriveRingOverlay	2
ChannelToDeriveRingSpotOverlay	2

Assay	
CircModifierCh2	-2
CircModifierCh3	0
MaskModifierCh2	-3
MaskModifierCh3	-3
ObjectCleanUpCh1	1
ObjectSegmentationCh1	-87
ObjectSmoothFactorCh1	1
ObjectTypeCh1	0
RejectBorderObjectsCh1	1
RingDistanceCh2	0
RingDistanceCh3	-2
RingWidthCh2	60
RingWidthCh3	60
SpotDetectRadiusCh2	55
SpotDetectRadiusCh3	55
SpotTypeCh2	0
SpotTypeCh3	0
UseReferenceWells	0

Well Feature Extents

Feature Name	Lower Extent	Upper Extent
#HIGH_CircRingAvgIntenDiffCh2	0	100
#HIGH_CircRingAvgIntenDiffCh3	1	100
#HIGH_CircRingAvgIntenRatioCh2	0	100
#HIGH_CircRingAvgIntenRatioCh3	1	100
#LOW_CircRingAvgIntenDiffCh2	0	100
#LOW_CircRingAvgIntenDiffCh3	1	100
#LOW_CircRingAvgIntenRatioCh2	0	100
#LOW_CircRingAvgIntenRatioCh3	1	100
%EventType1Objects	0	100
%EventType2Objects	0	100
%EventType3Objects	0	100
%HIGH_CircAvgIntenCh2	1	100
%HIGH_CircAvgIntenCh3	1	100
%HIGH_CircAvgIntenRatioCh2Ch1	1	100
%HIGH_CircAvgIntenRatioCh3Ch1	1	100
%HIGH_CircAvgIntenRatioCh3Ch2	1	100
%HIGH_CircRingAvgIntenDiffCh2	1	100
%HIGH_CircRingAvgIntenDiffCh3	1	100
%HIGH_CircRingAvgIntenRatioCh2	1	100
%HIGH_CircRingAvgIntenRatioCh3	1	100
%HIGH_CircSpotAvgAreaCh2	1	100
%HIGH_CircSpotAvgAreaCh3	1	100
%HIGH_CircSpotAvgIntenCh2	1	100
%HIGH_CircSpotAvgIntenCh3	1	100
%HIGH_CircSpotAvgIntenRatioCh3Ch2	1	100
%HIGH_CircSpotCountCh2*	4	100
%HIGH_CircSpotCountCh3	1	100
%HIGH_CircSpotCountRatioCh3Ch2	1	100
%HIGH_CircSpotTotalAreaCh2	0	100
%HIGH_CircSpotTotalAreaCh3	1	100
%HIGH_CircSpotTotalIntenCh2	0	100
%HIGH_CircSpotTotalIntenCh3	1	100
%HIGH_CircTotalIntenCh2	0	100
%HIGH_CircTotalIntenCh3	1	100
%HIGH_ObjectAreaCh1	0	100
%HIGH_ObjectAvgIntenCh1	1	100
%HIGH_ObjectShapeLWRCh1	0	100
%HIGH_ObjectShapeP2ACh1	0	100
%HIGH_ObjectSizeCh1	1	100
%HIGH_ObjectTotalIntenCh1	1	100
%HIGH_ObjectVarIntenCh1	1	100
%HIGH_RingAvgIntenCh2	1	100

Well Feature Extents		
%HIGH_RingAvgIntenCh3	1	100
%HIGH_RingAvgIntenRatioCh3Ch2	1	100
%HIGH_RingSpotAvgAreaCh2	1	100
%HIGH_RingSpotAvgAreaCh3	1	100
%HIGH_RingSpotAvgIntenCh2	1	100
%HIGH_RingSpotAvgIntenCh3	1	100
%HIGH_RingSpotAvgIntenRatioCh3Ch2	1	100
%HIGH_RingSpotCountCh2	1	100
%HIGH_RingSpotCountCh3	1	100
%HIGH_RingSpotCountRatioCh3Ch2	1	100
%HIGH_RingSpotTotalAreaCh2	0	100
%HIGH_RingSpotTotalAreaCh3	1	100
%HIGH_RingSpotTotalIntenCh2	0	100
%HIGH_RingSpotTotalIntenCh3	1	100
%HIGH_RingTotalIntenCh2	0	100
%HIGH_RingTotalIntenCh3	1	100
%LOW_CircAvgIntenCh2	1	100
%LOW_CircAvgIntenCh3	1	100
%LOW_CircAvgIntenRatioCh2Ch1	1	100
%LOW_CircAvgIntenRatioCh3Ch1	1	100
%LOW_CircAvgIntenRatioCh3Ch2	1	100
%LOW_CircRingAvgIntenDiffCh2	1	100
%LOW_CircRingAvgIntenDiffCh3	1	100
%LOW_CircRingAvgIntenRatioCh2	1	100
%LOW_CircRingAvgIntenRatioCh3	1	100
%LOW_CircSpotAvgAreaCh2	1	100
%LOW_CircSpotAvgAreaCh3	1	100
%LOW_CircSpotAvgIntenCh2	1	100
%LOW_CircSpotAvgIntenCh3	1	100
%LOW_CircSpotAvgIntenRatioCh3Ch2	1	100
%LOW_CircSpotCountCh2	3	100
%LOW_CircSpotCountCh3	1	100
%LOW_CircSpotCountRatioCh3Ch2	1	100
%LOW_CircSpotTotalAreaCh2	0	100
%LOW_CircSpotTotalAreaCh3	1	100
%LOW_CircSpotTotalIntenCh2	0	100
%LOW_CircSpotTotalIntenCh3	1	100
%LOW_CircTotalIntenCh2	0	100
%LOW_CircTotalIntenCh3	1	100
%LOW_ObjectAreaCh1	0	100
%LOW_ObjectAvgIntenCh1	1	100
%LOW_ObjectShapeLWRCh1	0	100
%LOW_ObjectShapeP2ACh1	0	100
%LOW_ObjectSizeCh1	1	100
%LOW_ObjectTotalIntenCh1	1	100
%LOW_ObjectVarIntenCh1	1	100
%LOW_RingAvgIntenCh2	1	100
%LOW_RingAvgIntenCh3	1	100
%LOW_RingAvgIntenRatioCh3Ch2	1	100
%LOW_RingSpotAvgAreaCh2	1	100
%LOW_RingSpotAvgAreaCh3	1	100
%LOW_RingSpotAvgIntenCh2	1	100
%LOW_RingSpotAvgIntenCh3	1	100
%LOW_RingSpotAvgIntenRatioCh3Ch2	1	100
%LOW_RingSpotCountCh2	1	100
%LOW_RingSpotCountCh3	1	100
%LOW_RingSpotCountRatioCh3Ch2	1	100
%LOW_RingSpotTotalAreaCh2	0	100
%LOW_RingSpotTotalAreaCh3	1	100
%LOW_RingSpotTotalIntenCh2	0	100
%LOW_RingSpotTotalIntenCh3	1	100
%LOW_RingTotalIntenCh2	0	100
%LOW_RingTotalIntenCh3	1	100
%SelectedObjects	1	100

Well Feature Extents		
CV_CircAvgIntenCh2	1	100
CV_CircAvgIntenCh3	1	100
CV_CircAvgIntenRatioCh2Ch1	1	100
CV_CircAvgIntenRatioCh3Ch1	1	100
CV_CircAvgIntenRatioCh3Ch2	1	100
CV_CircRingAvgIntenDiffCh2	1	100
CV_CircRingAvgIntenDiffCh3	1	100
CV_CircRingAvgIntenRatioCh2	1	100
CV_CircRingAvgIntenRatioCh3	1	100
CV_CircSpotAvgAreaCh2	1	100
CV_CircSpotAvgAreaCh3	1	100
CV_CircSpotAvgIntenCh2	1	100
CV_CircSpotAvgIntenCh3	1	100
CV_CircSpotAvgIntenRatioCh3Ch2	1	100
CV_CircSpotCountCh2	1	100
CV_CircSpotCountCh3	1	100
CV_CircSpotCountRatioCh3Ch2	1	100
CV_CircSpotTotalAreaCh2	1	100
CV_CircSpotTotalAreaCh3	1	100
CV_CircSpotTotalIntenCh2	1	100
CV_CircSpotTotalIntenCh3	1	100
CV_CircTotalIntenCh2	1	100
CV_CircTotalIntenCh3	1	100
CV_ObjectAreaCh1	0	100
CV_ObjectAvgIntenCh1	1	100
CV_ObjectShapeLWRCh1	0	100
CV_ObjectShapeP2ACh1	0	100
CV_ObjectSizeCh1	1	100
CV_ObjectTotalIntenCh1	1	100
CV_ObjectVarIntenCh1	1	100
CV_RingAvgIntenCh2	1	100
CV_RingAvgIntenCh3	1	100
CV_RingAvgIntenRatioCh3Ch2	1	100
CV_RingSpotAvgAreaCh2	1	100
CV_RingSpotAvgAreaCh3	1	100
CV_RingSpotAvgIntenCh2	1	100
CV_RingSpotAvgIntenCh3	1	100
CV_RingSpotAvgIntenRatioCh3Ch2	1	100
CV_RingSpotCountCh2	1	100
CV_RingSpotCountCh3	1	100
CV_RingSpotCountRatioCh3Ch2	1	100
CV_RingSpotTotalAreaCh2	1	100
CV_RingSpotTotalAreaCh3	1	100
CV_RingSpotTotalIntenCh2	1	100
CV_RingSpotTotalIntenCh3	1	100
CV_RingTotalIntenCh2	1	100
CV_RingTotalIntenCh3	1	100
EventType1ObjectCount	0	100
EventType2ObjectCount	0	100
EventType3ObjectCount	0	100
MEAN_CircAvgIntenCh2	1	100
MEAN_CircAvgIntenCh3	1	100
MEAN_CircAvgIntenRatioCh2Ch1	1	100
MEAN_CircAvgIntenRatioCh3Ch1	1	100
MEAN_CircAvgIntenRatioCh3Ch2	1	100
MEAN_CircRingAvgIntenDiffCh2	1	100
MEAN_CircRingAvgIntenDiffCh3	1	100
MEAN_CircRingAvgIntenRatioCh2	1	100
MEAN_CircRingAvgIntenRatioCh3	1	100
MEAN_CircSpotAvgAreaCh2	1	100
MEAN_CircSpotAvgAreaCh3	1	100
MEAN_CircSpotAvgIntenCh2	1	100
MEAN_CircSpotAvgIntenCh3	1	100
MEAN_CircSpotAvgIntenRatioCh3Ch2	1	100

Well Feature Extents

MEAN_CircSpotCountCh2	1	100
MEAN_CircSpotCountCh3	1	100
MEAN_CircSpotCountRatioCh3Ch2	1	100
MEAN_CircSpotTotalAreaCh2	1.1114716663662	111.14716663662
MEAN_CircSpotTotalAreaCh3	1	100
MEAN_CircSpotTotalIntenCh2	1.1114716663662	111.14716663662
MEAN_CircSpotTotalIntenCh3	1	100
MEAN_CircTotalIntenCh2	1.1114716663662	111.14716663662
MEAN_CircTotalIntenCh3	1	100
MEAN_ObjectAreaCh1	0	100
MEAN_ObjectAvgIntenCh1	1	100
MEAN_ObjectShapeLWRCh1	0	100
MEAN_ObjectShapeP2ACh1	0	100
MEAN_ObjectSizeCh1	1.05426356589147	105.426356589147
MEAN_ObjectTotalIntenCh1	1.1114716663662	111.14716663662
MEAN_ObjectVarIntenCh1	1	100
MEAN_RingAvgIntenCh2	1	100
MEAN_RingAvgIntenCh3	1	100
MEAN_RingAvgIntenRatioCh3Ch2	1	100
MEAN_RingSpotAvgAreaCh2	1	100
MEAN_RingSpotAvgAreaCh3	1	100
MEAN_RingSpotAvgIntenCh2	1	100
MEAN_RingSpotAvgIntenCh3	1	100
MEAN_RingSpotAvgIntenRatioCh3Ch2	1	100
MEAN_RingSpotCountCh2	1	100
MEAN_RingSpotCountCh3	1	100
MEAN_RingSpotCountRatioCh3Ch2	1	100
MEAN_RingSpotTotalAreaCh2	1.1114716663662	111.14716663662
MEAN_RingSpotTotalAreaCh3	1	100
MEAN_RingSpotTotalIntenCh2	1.1114716663662	111.14716663662
MEAN_RingSpotTotalIntenCh3	1	100
MEAN_RingTotalIntenCh2	1.1114716663662	111.14716663662
MEAN_RingTotalIntenCh3	1	100
SD_CircAvgIntenCh2	1	100
SD_CircAvgIntenCh3	1	100
SD_CircAvgIntenRatioCh2Ch1	1	100
SD_CircAvgIntenRatioCh3Ch1	1	100
SD_CircAvgIntenRatioCh3Ch2	1	100
SD_CircRingAvgIntenDiffCh2	1	100
SD_CircRingAvgIntenDiffCh3	1	100
SD_CircRingAvgIntenRatioCh2	1	100
SD_CircRingAvgIntenRatioCh3	1	100
SD_CircSpotAvgAreaCh2	1	100
SD_CircSpotAvgAreaCh3	1	100
SD_CircSpotAvgIntenCh2	1	100
SD_CircSpotAvgIntenCh3	1	100
SD_CircSpotAvgIntenRatioCh3Ch2	1	100
SD_CircSpotCountCh2	1	100
SD_CircSpotCountCh3	1	100
SD_CircSpotCountRatioCh3Ch2	1	100
SD_CircSpotTotalAreaCh2	1.1114716663662	111.14716663662
SD_CircSpotTotalAreaCh3	1	100
SD_CircSpotTotalIntenCh2	1.1114716663662	111.14716663662
SD_CircSpotTotalIntenCh3	1	100
SD_CircTotalIntenCh2	1.1114716663662	111.14716663662
SD_CircTotalIntenCh3	1	100
SD_ObjectAreaCh1	0	100
SD_ObjectAvgIntenCh1	1	100
SD_ObjectShapeLWRCh1	0	100
SD_ObjectShapeP2ACh1	0	100
SD_ObjectSizeCh1	1.05426356589147	105.426356589147
SD_ObjectTotalIntenCh1	1.1114716663662	111.14716663662
SD_ObjectVarIntenCh1	1	100
SD_RingAvgIntenCh2	1	100

Well Feature Extents

SD_RingAvgIntenCh3	1	100
SD_RingAvgIntenRatioCh3Ch2	1	100
SD_RingSpotAvgAreaCh2	1	100
SD_RingSpotAvgAreaCh3	1	100
SD_RingSpotAvgIntenCh2	1	100
SD_RingSpotAvgIntenCh3	1	100
SD_RingSpotAvgIntenRatioCh3Ch2	1	100
SD_RingSpotCountCh2	1	100
SD_RingSpotCountCh3	1	100
SD_RingSpotCountRatioCh3Ch2	1	100
SD_RingSpotTotalAreaCh2	1.1114716663662	111.14716663662
SD_RingSpotTotalAreaCh3	1	100
SD_RingSpotTotalIntenCh2	1.1114716663662	111.14716663662
SD_RingSpotTotalIntenCh3	1	100
SD_RingTotalIntenCh2	1.1114716663662	111.14716663662
SD_RingTotalIntenCh3	1	100
SE_CircAvgIntenCh2	1	100
SE_CircAvgIntenCh3	1	100
SE_CircAvgIntenRatioCh2Ch1	1	100
SE_CircAvgIntenRatioCh3Ch1	1	100
SE_CircAvgIntenRatioCh3Ch2	1	100
SE_CircRingAvgIntenDiffCh2	1	100
SE_CircRingAvgIntenDiffCh3	1	100
SE_CircRingAvgIntenRatioCh2	1	100
SE_CircRingAvgIntenRatioCh3	1	100
SE_CircSpotAvgAreaCh2	1	100
SE_CircSpotAvgAreaCh3	1	100
SE_CircSpotAvgIntenCh2	1	100
SE_CircSpotAvgIntenCh3	1	100
SE_CircSpotAvgIntenRatioCh3Ch2	1	100
SE_CircSpotCountCh2	1	100
SE_CircSpotCountCh3	1	100
SE_CircSpotCountRatioCh3Ch2	1	100
SE_CircSpotTotalAreaCh2	1.1114716663662	111.14716663662
SE_CircSpotTotalAreaCh3	1	100
SE_CircSpotTotalIntenCh2	1.1114716663662	111.14716663662
SE_CircSpotTotalIntenCh3	1	100
SE_CircTotalIntenCh2	1.1114716663662	111.14716663662
SE_CircTotalIntenCh3	1	100
SE_ObjectAreaCh1	0	100
SE_ObjectAvgIntenCh1	1	100
SE_ObjectShapeLWRCh1	0	100
SE_ObjectShapeP2ACh1	0	100
SE_ObjectSizeCh1	1.05426356589147	105.426356589147
SE_ObjectTotalIntenCh1	1.1114716663662	111.14716663662
SE_ObjectVarIntenCh1	1	100
SE_RingAvgIntenCh2	1	100
SE_RingAvgIntenCh3	1	100
SE_RingAvgIntenRatioCh3Ch2	1	100
SE_RingSpotAvgAreaCh2	1	100
SE_RingSpotAvgAreaCh3	1	100
SE_RingSpotAvgIntenCh2	1	100
SE_RingSpotAvgIntenCh3	1	100
SE_RingSpotAvgIntenRatioCh3Ch2	1	100
SE_RingSpotCountCh2	1	100
SE_RingSpotCountCh3	1	100
SE_RingSpotCountRatioCh3Ch2	1	100
SE_RingSpotTotalAreaCh2	1.1114716663662	111.14716663662
SE_RingSpotTotalAreaCh3	1	100
SE_RingSpotTotalIntenCh2	1.1114716663662	111.14716663662
SE_RingSpotTotalIntenCh3	1	100
SE_RingTotalIntenCh2	1.1114716663662	111.14716663662
SE_RingTotalIntenCh3	1	100
SelectedObjectCount	1	100

Well Feature Extents

SelectedObjectCountPerValidField	0.899708044982699	89.9708044982699
ValidFieldCount	1	100
ValidObjectCount	1	100

* Indicates the default well feature for the Assay Protocol
** Indicates feature extents are dependent upon system reference well settings

Selected W ell Features to Store

CompartmentalAnalysisV4Well:#HIGH_CircRingAvgIntenDiffCh2
CompartmentalAnalysisV4Well:#HIGH_CircRingAvgIntenDiffCh3
CompartmentalAnalysisV4Well:#HIGH_CircRingAvgIntenRatioCh2
CompartmentalAnalysisV4Well:#HIGH_CircRingAvgIntenRatioCh3
CompartmentalAnalysisV4Well:#LOW_CircRingAvgIntenDiffCh2
CompartmentalAnalysisV4Well:#LOW_CircRingAvgIntenDiffCh3
CompartmentalAnalysisV4Well:#LOW_CircRingAvgIntenRatioCh2
CompartmentalAnalysisV4Well:#LOW_CircRingAvgIntenRatioCh3
CompartmentalAnalysisV4Well:%EventType1Objects
CompartmentalAnalysisV4Well:%EventType2Objects
CompartmentalAnalysisV4Well:%EventType3Objects
CompartmentalAnalysisV4Well:%HIGH_CircAvgIntenCh2
CompartmentalAnalysisV4Well:%HIGH_CircAvgIntenCh3
CompartmentalAnalysisV4Well:%HIGH_CircAvgIntenRatioCh2Ch1
CompartmentalAnalysisV4Well:%HIGH_CircAvgIntenRatioCh3Ch1
CompartmentalAnalysisV4Well:%HIGH_CircAvgIntenRatioCh3Ch2
CompartmentalAnalysisV4Well:%HIGH_CircRingAvgIntenDiffCh2
CompartmentalAnalysisV4Well:%HIGH_CircRingAvgIntenDiffCh3
CompartmentalAnalysisV4Well:%HIGH_CircRingAvgIntenRatioCh2
CompartmentalAnalysisV4Well:%HIGH_CircRingAvgIntenRatioCh3
CompartmentalAnalysisV4Well:%HIGH_CircSpotAvgAreaCh2
CompartmentalAnalysisV4Well:%HIGH_CircSpotAvgAreaCh3
CompartmentalAnalysisV4Well:%HIGH_CircSpotAvgIntenCh2
CompartmentalAnalysisV4Well:%HIGH_CircSpotAvgIntenCh3
CompartmentalAnalysisV4Well:%HIGH_CircSpotAvgIntenRatioCh3Ch2
CompartmentalAnalysisV4Well:%HIGH_CircSpotCountCh2
CompartmentalAnalysisV4Well:%HIGH_CircSpotCountCh3
CompartmentalAnalysisV4Well:%HIGH_CircSpotCountRatioCh3Ch2
CompartmentalAnalysisV4Well:%HIGH_CircSpotTotalAreaCh2
CompartmentalAnalysisV4Well:%HIGH_CircSpotTotalAreaCh3
CompartmentalAnalysisV4Well:%HIGH_CircSpotTotalIntenCh2
CompartmentalAnalysisV4Well:%HIGH_CircSpotTotalIntenCh3
CompartmentalAnalysisV4Well:%HIGH_CircTotalIntenCh2
CompartmentalAnalysisV4Well:%HIGH_CircTotalIntenCh3
CompartmentalAnalysisV4Well:%HIGH_ObjectAreaCh1
CompartmentalAnalysisV4Well:%HIGH_ObjectAvgIntenCh1
CompartmentalAnalysisV4Well:%HIGH_ObjectShapeLWRCh1
CompartmentalAnalysisV4Well:%HIGH_ObjectShapeP2ACh1
CompartmentalAnalysisV4Well:%HIGH_ObjectSizeCh1
CompartmentalAnalysisV4Well:%HIGH_ObjectTotalIntenCh1
CompartmentalAnalysisV4Well:%HIGH_ObjectVarIntenCh1
CompartmentalAnalysisV4Well:%HIGH_RingAvgIntenCh2
CompartmentalAnalysisV4Well:%HIGH_RingAvgIntenCh3
CompartmentalAnalysisV4Well:%HIGH_RingAvgIntenRatioCh3Ch2
CompartmentalAnalysisV4Well:%HIGH_RingSpotAvgAreaCh2
CompartmentalAnalysisV4Well:%HIGH_RingSpotAvgAreaCh3
CompartmentalAnalysisV4Well:%HIGH_RingSpotAvgIntenCh2
CompartmentalAnalysisV4Well:%HIGH_RingSpotAvgIntenCh3
CompartmentalAnalysisV4Well:%HIGH_RingSpotAvgIntenRatioCh3Ch2
CompartmentalAnalysisV4Well:%HIGH_RingSpotCountCh2
CompartmentalAnalysisV4Well:%HIGH_RingSpotCountCh3
CompartmentalAnalysisV4Well:%HIGH_RingSpotCountRatioCh3Ch2
CompartmentalAnalysisV4Well:%HIGH_RingSpotTotalAreaCh2
CompartmentalAnalysisV4Well:%HIGH_RingSpotTotalAreaCh3
CompartmentalAnalysisV4Well:%HIGH_RingSpotTotalIntenCh2
CompartmentalAnalysisV4Well:%HIGH_RingSpotTotalIntenCh3

Selected Cell Features to Store

CompartmentalAnalysisV4Cell:Cell#
CompartmentalAnalysisV4Cell:Height
CompartmentalAnalysisV4Cell:Left
CompartmentalAnalysisV4Cell:Top
CompartmentalAnalysisV4Cell:Width

Selected W ell Features to Store

CompartmentalAnalysisV4Well:%HIGH_RingTotalIntenCh2
CompartmentalAnalysisV4Well:%HIGH_RingTotalIntenCh3
CompartmentalAnalysisV4Well:%LOW_CircAvgIntenCh2
CompartmentalAnalysisV4Well:%LOW_CircAvgIntenCh3
CompartmentalAnalysisV4Well:%LOW_CircAvgIntenRatioCh2Ch1
CompartmentalAnalysisV4Well:%LOW_CircAvgIntenRatioCh3Ch1
CompartmentalAnalysisV4Well:%LOW_CircAvgIntenRatioCh3Ch2
CompartmentalAnalysisV4Well:%LOW_CircRingAvgIntenDiffCh2
CompartmentalAnalysisV4Well:%LOW_CircRingAvgIntenDiffCh3
CompartmentalAnalysisV4Well:%LOW_CircRingAvgIntenRatioCh2
CompartmentalAnalysisV4Well:%LOW_CircRingAvgIntenRatioCh3
CompartmentalAnalysisV4Well:%LOW_CircSpotAvgAreaCh2
CompartmentalAnalysisV4Well:%LOW_CircSpotAvgAreaCh3
CompartmentalAnalysisV4Well:%LOW_CircSpotAvgIntenCh2
CompartmentalAnalysisV4Well:%LOW_CircSpotAvgIntenCh3
CompartmentalAnalysisV4Well:%LOW_CircSpotAvgIntenRatioCh3Ch2
CompartmentalAnalysisV4Well:%LOW_CircSpotCountCh2
CompartmentalAnalysisV4Well:%LOW_CircSpotCountCh3
CompartmentalAnalysisV4Well:%LOW_CircSpotCountRatioCh3Ch2
CompartmentalAnalysisV4Well:%LOW_CircSpotTotalAreaCh2
CompartmentalAnalysisV4Well:%LOW_CircSpotTotalAreaCh3
CompartmentalAnalysisV4Well:%LOW_CircSpotTotalIntenCh2
CompartmentalAnalysisV4Well:%LOW_CircSpotTotalIntenCh3
CompartmentalAnalysisV4Well:%LOW_CircTotalIntenCh2
CompartmentalAnalysisV4Well:%LOW_CircTotalIntenCh3
CompartmentalAnalysisV4Well:%LOW_ObjectAreaCh1
CompartmentalAnalysisV4Well:%LOW_ObjectAvgIntenCh1
CompartmentalAnalysisV4Well:%LOW_ObjectShapeLWRCh1
CompartmentalAnalysisV4Well:%LOW_ObjectShapeP2ACh1
CompartmentalAnalysisV4Well:%LOW_ObjectSizeCh1
CompartmentalAnalysisV4Well:%LOW_ObjectTotalIntenCh1
CompartmentalAnalysisV4Well:%LOW_ObjectVarIntenCh1
CompartmentalAnalysisV4Well:%LOW_RingAvgIntenCh2
CompartmentalAnalysisV4Well:%LOW_RingAvgIntenCh3
CompartmentalAnalysisV4Well:%LOW_RingAvgIntenRatioCh3Ch2
CompartmentalAnalysisV4Well:%LOW_RingSpotAvgAreaCh2
CompartmentalAnalysisV4Well:%LOW_RingSpotAvgAreaCh3
CompartmentalAnalysisV4Well:%LOW_RingSpotAvgIntenCh2
CompartmentalAnalysisV4Well:%LOW_RingSpotAvgIntenCh3
CompartmentalAnalysisV4Well:%LOW_RingSpotAvgIntenRatioCh3Ch2
CompartmentalAnalysisV4Well:%LOW_RingSpotCountCh2
CompartmentalAnalysisV4Well:%LOW_RingSpotCountCh3
CompartmentalAnalysisV4Well:%LOW_RingSpotCountRatioCh3Ch2
CompartmentalAnalysisV4Well:%LOW_RingSpotTotalAreaCh2
CompartmentalAnalysisV4Well:%LOW_RingSpotTotalAreaCh3
CompartmentalAnalysisV4Well:%LOW_RingSpotTotalIntenCh2
CompartmentalAnalysisV4Well:%LOW_RingSpotTotalIntenCh3
CompartmentalAnalysisV4Well:%LOW_RingTotalIntenCh2
CompartmentalAnalysisV4Well:%LOW_RingTotalIntenCh3
CompartmentalAnalysisV4Well:%SelectedObjects
CompartmentalAnalysisV4Well:CV_CircAvgIntenCh2
CompartmentalAnalysisV4Well:CV_CircAvgIntenCh3
CompartmentalAnalysisV4Well:CV_CircAvgIntenRatioCh2Ch1
CompartmentalAnalysisV4Well:CV_CircAvgIntenRatioCh3Ch1
CompartmentalAnalysisV4Well:CV_CircAvgIntenRatioCh3Ch2
CompartmentalAnalysisV4Well:CV_CircRingAvgIntenDiffCh2
CompartmentalAnalysisV4Well:CV_CircRingAvgIntenDiffCh3
CompartmentalAnalysisV4Well:CV_CircRingAvgIntenRatioCh2
CompartmentalAnalysisV4Well:CV_CircRingAvgIntenRatioCh3
CompartmentalAnalysisV4Well:CV_CircSpotAvgAreaCh2
CompartmentalAnalysisV4Well:CV_CircSpotAvgAreaCh3
CompartmentalAnalysisV4Well:CV_CircSpotAvgIntenCh2
CompartmentalAnalysisV4Well:CV_CircSpotAvgIntenCh3
CompartmentalAnalysisV4Well:CV_CircSpotAvgIntenRatioCh3Ch2

Selected W ell Features to Store

CompartmentalAnalysisV4Well:CV_CircSpotCountCh2
CompartmentalAnalysisV4Well:CV_CircSpotCountCh3
CompartmentalAnalysisV4Well:CV_CircSpotCountRatioCh3Ch2
CompartmentalAnalysisV4Well:CV_CircSpotTotalAreaCh2
CompartmentalAnalysisV4Well:CV_CircSpotTotalAreaCh3
CompartmentalAnalysisV4Well:CV_CircSpotTotalIntenCh2
CompartmentalAnalysisV4Well:CV_CircSpotTotalIntenCh3
CompartmentalAnalysisV4Well:CV_CircTotalIntenCh2
CompartmentalAnalysisV4Well:CV_CircTotalIntenCh3
CompartmentalAnalysisV4Well:CV_ObjectAreaCh1
CompartmentalAnalysisV4Well:CV_ObjectAvgIntenCh1
CompartmentalAnalysisV4Well:CV_ObjectShapeLWRCh1
CompartmentalAnalysisV4Well:CV_ObjectShapeP2ACh1
CompartmentalAnalysisV4Well:CV_ObjectSizeCh1
CompartmentalAnalysisV4Well:CV_ObjectTotalIntenCh1
CompartmentalAnalysisV4Well:CV_ObjectVarIntenCh1
CompartmentalAnalysisV4Well:CV_RingAvgIntenCh2
CompartmentalAnalysisV4Well:CV_RingAvgIntenCh3
CompartmentalAnalysisV4Well:CV_RingAvgIntenRatioCh3Ch2
CompartmentalAnalysisV4Well:CV_RingSpotAvgAreaCh2
CompartmentalAnalysisV4Well:CV_RingSpotAvgAreaCh3
CompartmentalAnalysisV4Well:CV_RingSpotAvgIntenCh2
CompartmentalAnalysisV4Well:CV_RingSpotAvgIntenCh3
CompartmentalAnalysisV4Well:CV_RingSpotAvgIntenRatioCh3Ch2
CompartmentalAnalysisV4Well:CV_RingSpotCountCh2
CompartmentalAnalysisV4Well:CV_RingSpotCountCh3
CompartmentalAnalysisV4Well:CV_RingSpotCountRatioCh3Ch2
CompartmentalAnalysisV4Well:CV_RingSpotTotalAreaCh2
CompartmentalAnalysisV4Well:CV_RingSpotTotalAreaCh3
CompartmentalAnalysisV4Well:CV_RingSpotTotalIntenCh2
CompartmentalAnalysisV4Well:CV_RingSpotTotalIntenCh3
CompartmentalAnalysisV4Well:CV_RingTotalIntenCh2
CompartmentalAnalysisV4Well:CV_RingTotalIntenCh3
CompartmentalAnalysisV4Well:EventType1ObjectCount
CompartmentalAnalysisV4Well:EventType2ObjectCount
CompartmentalAnalysisV4Well:EventType3ObjectCount
CompartmentalAnalysisV4Well:MEAN_CircAvgIntenCh2
CompartmentalAnalysisV4Well:MEAN_CircAvgIntenCh3
CompartmentalAnalysisV4Well:MEAN_CircAvgIntenRatioCh2Ch1
CompartmentalAnalysisV4Well:MEAN_CircAvgIntenRatioCh3Ch1
CompartmentalAnalysisV4Well:MEAN_CircAvgIntenRatioCh3Ch2
CompartmentalAnalysisV4Well:MEAN_CircRingAvgIntenDiffCh2
CompartmentalAnalysisV4Well:MEAN_CircRingAvgIntenDiffCh3
CompartmentalAnalysisV4Well:MEAN_CircRingAvgIntenRatioCh2
CompartmentalAnalysisV4Well:MEAN_CircRingAvgIntenRatioCh3
CompartmentalAnalysisV4Well:MEAN_CircSpotAvgAreaCh2
CompartmentalAnalysisV4Well:MEAN_CircSpotAvgAreaCh3
CompartmentalAnalysisV4Well:MEAN_CircSpotAvgIntenCh2
CompartmentalAnalysisV4Well:MEAN_CircSpotAvgIntenCh3
CompartmentalAnalysisV4Well:MEAN_CircSpotAvgIntenRatioCh3Ch2
CompartmentalAnalysisV4Well:MEAN_CircSpotCountCh2
CompartmentalAnalysisV4Well:MEAN_CircSpotCountCh3
CompartmentalAnalysisV4Well:MEAN_CircSpotCountRatioCh3Ch2
CompartmentalAnalysisV4Well:MEAN_CircSpotTotalAreaCh2
CompartmentalAnalysisV4Well:MEAN_CircSpotTotalAreaCh3
CompartmentalAnalysisV4Well:MEAN_CircSpotTotalIntenCh2
CompartmentalAnalysisV4Well:MEAN_CircSpotTotalIntenCh3
CompartmentalAnalysisV4Well:MEAN_CircTotalIntenCh2
CompartmentalAnalysisV4Well:MEAN_CircTotalIntenCh3
CompartmentalAnalysisV4Well:MEAN_ObjectAreaCh1
CompartmentalAnalysisV4Well:MEAN_ObjectAvgIntenCh1
CompartmentalAnalysisV4Well:MEAN_ObjectShapeLWRCh1
CompartmentalAnalysisV4Well:MEAN_ObjectShapeP2ACh1
CompartmentalAnalysisV4Well:MEAN_ObjectSizeCh1

Selected W ell Features to Store

CompartmentalAnalysisV4Well:MEAN_ObjectTotalIntenCh1
CompartmentalAnalysisV4Well:MEAN_ObjectVarIntenCh1
CompartmentalAnalysisV4Well:MEAN_RingAvgIntenCh2
CompartmentalAnalysisV4Well:MEAN_RingAvgIntenCh3
CompartmentalAnalysisV4Well:MEAN_RingAvgIntenRatioCh3Ch2
CompartmentalAnalysisV4Well:MEAN_RingSpotAvgAreaCh2
CompartmentalAnalysisV4Well:MEAN_RingSpotAvgAreaCh3
CompartmentalAnalysisV4Well:MEAN_RingSpotAvgIntenCh2
CompartmentalAnalysisV4Well:MEAN_RingSpotAvgIntenCh3
CompartmentalAnalysisV4Well:MEAN_RingSpotAvgIntenRatioCh3Ch2
CompartmentalAnalysisV4Well:MEAN_RingSpotCountCh2
CompartmentalAnalysisV4Well:MEAN_RingSpotCountCh3
CompartmentalAnalysisV4Well:MEAN_RingSpotCountRatioCh3Ch2
CompartmentalAnalysisV4Well:MEAN_RingSpotTotalAreaCh2
CompartmentalAnalysisV4Well:MEAN_RingSpotTotalAreaCh3
CompartmentalAnalysisV4Well:MEAN_RingSpotTotalIntenCh2
CompartmentalAnalysisV4Well:MEAN_RingSpotTotalIntenCh3
CompartmentalAnalysisV4Well:MEAN_RingTotalIntenCh2
CompartmentalAnalysisV4Well:MEAN_RingTotalIntenCh3
CompartmentalAnalysisV4Well:SD_CircAvgIntenCh2
CompartmentalAnalysisV4Well:SD_CircAvgIntenCh3
CompartmentalAnalysisV4Well:SD_CircAvgIntenRatioCh2Ch1
CompartmentalAnalysisV4Well:SD_CircAvgIntenRatioCh3Ch1
CompartmentalAnalysisV4Well:SD_CircAvgIntenRatioCh3Ch2
CompartmentalAnalysisV4Well:SD_CircRingAvgIntenDiffCh2
CompartmentalAnalysisV4Well:SD_CircRingAvgIntenDiffCh3
CompartmentalAnalysisV4Well:SD_CircRingAvgIntenRatioCh2
CompartmentalAnalysisV4Well:SD_CircRingAvgIntenRatioCh3
CompartmentalAnalysisV4Well:SD_CircSpotAvgAreaCh2
CompartmentalAnalysisV4Well:SD_CircSpotAvgAreaCh3
CompartmentalAnalysisV4Well:SD_CircSpotAvgIntenCh2
CompartmentalAnalysisV4Well:SD_CircSpotAvgIntenCh3
CompartmentalAnalysisV4Well:SD_CircSpotAvgIntenRatioCh3Ch2
CompartmentalAnalysisV4Well:SD_CircSpotCountCh2
CompartmentalAnalysisV4Well:SD_CircSpotCountCh3
CompartmentalAnalysisV4Well:SD_CircSpotCountRatioCh3Ch2
CompartmentalAnalysisV4Well:SD_CircSpotTotalAreaCh2
CompartmentalAnalysisV4Well:SD_CircSpotTotalAreaCh3
CompartmentalAnalysisV4Well:SD_CircSpotTotalIntenCh2
CompartmentalAnalysisV4Well:SD_CircSpotTotalIntenCh3
CompartmentalAnalysisV4Well:SD_CircTotalIntenCh2
CompartmentalAnalysisV4Well:SD_CircTotalIntenCh3
CompartmentalAnalysisV4Well:SD_ObjectAreaCh1
CompartmentalAnalysisV4Well:SD_ObjectAvgIntenCh1
CompartmentalAnalysisV4Well:SD_ObjectShapeLWRCh1
CompartmentalAnalysisV4Well:SD_ObjectShapeP2ACh1
CompartmentalAnalysisV4Well:SD_ObjectSizeCh1
CompartmentalAnalysisV4Well:SD_ObjectTotalIntenCh1
CompartmentalAnalysisV4Well:SD_ObjectVarIntenCh1
CompartmentalAnalysisV4Well:SD_RingAvgIntenCh2
CompartmentalAnalysisV4Well:SD_RingAvgIntenCh3
CompartmentalAnalysisV4Well:SD_RingAvgIntenRatioCh3Ch2
CompartmentalAnalysisV4Well:SD_RingSpotAvgAreaCh2
CompartmentalAnalysisV4Well:SD_RingSpotAvgAreaCh3
CompartmentalAnalysisV4Well:SD_RingSpotAvgIntenCh2
CompartmentalAnalysisV4Well:SD_RingSpotAvgIntenCh3
CompartmentalAnalysisV4Well:SD_RingSpotAvgIntenRatioCh3Ch2
CompartmentalAnalysisV4Well:SD_RingSpotCountCh2
CompartmentalAnalysisV4Well:SD_RingSpotCountCh3
CompartmentalAnalysisV4Well:SD_RingSpotCountRatioCh3Ch2
CompartmentalAnalysisV4Well:SD_RingSpotTotalAreaCh2
CompartmentalAnalysisV4Well:SD_RingSpotTotalAreaCh3
CompartmentalAnalysisV4Well:SD_RingSpotTotalIntenCh2
CompartmentalAnalysisV4Well:SD_RingSpotTotalIntenCh3

Figure IV: Settings of the Compartmental Analysis algorithm employed in this thesis for the analysis of PAD4 and citrullinated-H3 distribution in neutrophils.

Full description of the parameters of the Compartmental Analysis algorithm applied in this thesis for neutrophils and for tracking PAD4 and citrullinated-H3 distribution.

Appendix V

Ilaria nuclear decondensation II [Version 2]

Last Modified on 27/10/2016 13:43:36

NOTE: The information here represents data that is saved in the database with an Assay Protocol. This data does not include scan settings like Field Offset, Form Factor , Scan Area, Store Imag es or Show Composite Image.

Comments

Event1=((ObjectAreaCh1 AND ObjectAvgIntenCh1)) Event2=((ObjectAreaCh1 AND ObjectTotalIntenCh1)) Event3=(None)

Image Acquisition	
Objective	20x
Camera Name	ORCA-ER;1.00
Acquisition Camera Mode	HiRes (1024x1024;1x1)
AutoFocus Camera Mode	HiRes (1024x1024;1x1)
AutoFocus Field Interval	0

AutoFocus Parameters	
Fine Focus Step Size	9.9
Fine Focus Plane Count	9
Coarse Focus Step Size	39.6
Coarse Focus Plane Count	16
Smart Focus Plane Count	21
Use Extended Range Focusing	False
Apply Backlash Correction	False
AutoFocus Method	STANDARD
Laser AutoFocus Method	LASER
How To Focus During Scan	2
Use Relaxed Pass/Fail Criteria	False
Focus Edge Threshhold	5
Focus Adjustment	0
Focus Score Min Ratio	0.25
Focus Score Mid Ratio	0.4
Focus Score Max Ratio	0.5
Focus Exposure Time for AutoExpose (seconds)	0.1

Scan Limits	
Max Fields for Well	20
Min Objects for Well	No Limit
Max Sparse Fields for Well	No Limit
Min Objects for Field	N/A
Max Sparse Wells for Plate	N/A

Channel 1: Nuclei	
Dye	BGRFR_485_20
Apply Illumination Correction	False
Apply Background Correction	True
Gain	25
Z Offset	0.00
Step Size	6.56
Number of Steps	1
Projection Method	
Projection Direction	None
Detection Mode	Widefield
Grid Type	
Pin Hole Size	
Intensity Percent	100
Exposure Parameters	
Method	Fixed
Exposure Time (seconds)	0.12
Object Identification	
Method	IsodataThreshold
Value	-0.462

Object Selection Parameter	Min	Max
ObjectAreaCh1	21.9	4391.38
ObjectShapeP2ACh1	0	1000
ObjectShapeLWRCh1	0	1000
ObjectAvgIntenCh1	0	50000
ObjectVarIntenCh1	0	65535
ObjectTotalIntenCh1	0	1000000000000

Display Options	
Composite Color (Hex)	#0000FF
SelectedObject	#0000FF
RejectedObject	#FF7F00

Assay	
Assay Algorithm	TargetActivation.V4
Assay V ersion	6.0 (Locally Installed V ersion: 6.0.1.4021)
Focus Channel	1
#Channels	1

Assay Parameters	
PixelSize	0.3225
Type_1_EventDefinition	912.22
Type_2_EventDefinition	912.218
Type_3_EventDefinition	0
MinRefAvgObjectCountPerField	2
ObjectAreaCh1LevelHigh	765.12
ObjectAreaCh1LevelHigh_CC	1
ObjectAreaCh1LevelLow	100
ObjectAreaCh1LevelLow_CC	1
ObjectAvgIntenCh1LevelHigh	5000
ObjectAvgIntenCh1LevelHigh_CC	1

Assay	
ObjectAvgIntenCh1LevelLow	954.55
ObjectAvgIntenCh1LevelLow_CC	1
ObjectShapeLWRCh1LevelHigh	0.99
ObjectShapeLWRCh1LevelHigh_CC	1
ObjectShapeLWRCh1LevelLow	0.99
ObjectShapeLWRCh1LevelLow_CC	1
ObjectShapeP2ACh1LevelHigh	1.06
ObjectShapeP2ACh1LevelHigh_CC	1
ObjectShapeP2ACh1LevelLow	1.05
ObjectShapeP2ACh1LevelLow_CC	1
ObjectTotalIntenCh1LevelHigh	1271412
ObjectTotalIntenCh1LevelHigh_CC	1
ObjectTotalIntenCh1LevelLow	13392
ObjectTotalIntenCh1LevelLow_CC	1
ObjectVarIntenCh1LevelHigh	55
ObjectVarIntenCh1LevelHigh_CC	1
ObjectVarIntenCh1LevelLow	55
ObjectVarIntenCh1LevelLow_CC	1
UseMicrometers	0
BackgroundCorrectionCh1	148
NucCleanupCh1	1
ObjectSegmentationCh1	15
ObjectSmoothFactorCh1	2
ObjectTypeCh1	0
RejectBorderObjectsCh1	1
UseReferenceWells	0

Well Feature Extents

Feature Name	Lower Extent	Upper Extent
ValidObjectCount*	0	100
SelectedObjectCount	20	750
ValidFieldCount	0	111
MEAN_ObjectAreaCh1	0	40000000
MEAN_ObjectShapeP2ACh1	0	100
MEAN_ObjectShapeLWRCh1	0	100
MEAN_ObjectTotalIntenCh1	0	40000000000
MEAN_ObjectAvgIntenCh1	0	4095
MEAN_ObjectVarIntenCh1	0	10000000
SelectedObjectCountPerValidField	0.0625	6.25
%EventType1Objects	1	100
%EventType2Objects	1	100
%EventType3Objects	1	100
%RESPONDER_ObjectAreaCh1	1	100
%RESPONDER_ObjectAvgIntenCh1	1	100
%RESPONDER_ObjectShapeLWRCh1	1	100
%RESPONDER_ObjectShapeP2ACh1	1	100
%RESPONDER_ObjectTotalIntenCh1	1	100
%RESPONDER_ObjectVarIntenCh1	1	100
%SelectedObjects	1	100
CV_ObjectAreaCh1	1	100
CV_ObjectAvgIntenCh1	1	100
CV_ObjectShapeLWRCh1	1	100
CV_ObjectShapeP2ACh1	1	100
CV_ObjectTotalIntenCh1	1	100
CV_ObjectVarIntenCh1	1	100
EventType1ObjectCount	1	100
EventType2ObjectCount	1	100
EventType3ObjectCount	1	100
SD_ObjectAreaCh1	16	1600
SD_ObjectAvgIntenCh1	1	100
SD_ObjectShapeLWRCh1	1	100
SD_ObjectShapeP2ACh1	1	100
SD_ObjectTotalIntenCh1	16	1600

11/8/2016 Ilaria nuclear decondensation II

Well Feature Extents

SD_ObjectVarInternCh1	1	100
SE_ObjectAreaCh1	16	1600
SE_ObjectAvgInternCh1	1	100
SE_ObjectShapeLWRCh1	1	100
SE_ObjectShapeP2ACh1	1	100
SE_ObjectTotalInternCh1	16	1600
SE_ObjectVarInternCh1	1	100

* Indicates the default well feature for the Assay Protocol
** Indicates feature extents are dependent upon system reference well settings

Selected W ell Features to Store	Selected Cell Features to Store
TargetActivation\4W ell %EventType1Objects	TargetActivation\4Cell Cell#
TargetActivation\4W ell %EventType2Objects	TargetActivation\4Cell EventType1Status
TargetActivation\4W ell %RESPONDER_ObjectAreaCh	TargetActivation\4Cell EventType2Status
TargetActivation\4W ell %RESPONDER_ObjectAvgInternCh1	TargetActivation\4Cell EventType3Status
TargetActivation\4W ell %RESPONDER_ObjectShapeLWRCh1	TargetActivation\4Cell EventTypeProfile
TargetActivation\4W ell %RESPONDER_ObjectShapeP2ACh1	TargetActivation\4Cell Height
TargetActivation\4W ell %RESPONDER_ObjectTotalInternCh1	TargetActivation\4Cell Left
TargetActivation\4W ell %RESPONDER_ObjectVarInternCh1	TargetActivation\4Cell ObjectAreaCh1
TargetActivation\4W ell %SelectedObjects	TargetActivation\4Cell ObjectAreaCh1Status
TargetActivation\4W ell EventType1ObjectCount	TargetActivation\4Cell ObjectA vgInternCh1
TargetActivation\4W ell EventType2ObjectCount	TargetActivation\4Cell ObjectA vgInternCh1Status
TargetActivation\4W ell MEAN_ObjectAreaCh1	TargetActivation\4Cell ObjectShapeL WRCh1
TargetActivation\4W ell MEAN_ObjectAvgInternCh1	TargetActivation\4Cell ObjectShapeL WRCh1Status
TargetActivation\4W ell MEAN_ObjectShapeLWRCh1	TargetActivation\4Cell ObjectShapeP2ACh1
TargetActivation\4W ell MEAN_ObjectShapeP2ACh1	TargetActivation\4Cell ObjectShapeP2ACh1Status
TargetActivation\4W ell MEAN_ObjectTotalInternCh1	TargetActivation\4Cell ObjectT otalInternCh1
TargetActivation\4W ell MEAN_ObjectVarInternCh1	TargetActivation\4Cell ObjectT otalInternCh1Status
TargetActivation\4W ell SelectedObjectCount	TargetActivation\4Cell ObjectV arInternCh1
TargetActivation\4W ell ValidFieldCount	TargetActivation\4Cell ObjectV arInternCh1Status
TargetActivation\4W ell ValidObjectCount	TargetActivation\4Cell Top
	TargetActivation\4Cell Width
	TargetActivation\4Cell XCentroid
	TargetActivation\4Cell YCentroid

Figure V: Settings of the Nuclear Decondensation algorithm employed in this thesis for the HCS of a compound library on neutrophils.
Full description of the parameters of the Nuclear Decondensation algorithm applied in this thesis for screening of a compound library for the modulation of NETosis.

Conference presentations

High-Throughput screening method for studying NETosis.
Chicca IJ, Milward MR, Chapple IL, Griffiths G, Benson R, Cooper PR. April 2016, College of Medical and Dental Sciences Festival of Graduate Research, University of Birmingham, Birmingham, UK.

Automated Image Analysis for Studying NET Production in Periodontitis.
Chicca IJ, Milward MR, Chapple IL, Griffiths G, Benson R, Cooper PR. March 2015, International Association for Dental Research International Meeting, Boston, MA, USA.

High-Throughput screening method for studying NETosis.
Chicca IJ, Milward MR, Chapple IL, Griffiths G, Benson R, Cooper PR. April 2016, Midlands Academy of Medical Sciences Research Festival, University of Leicester, UK.

High Content Analysis for studying neutrophil extracellular traps in inflammatory diseases.
Chicca IJ, Milward MR, Chapple IL, Griffiths G, Benson R, Cooper PR. June 2015, Research Poster Conference, University of Birmingham, Birmingham, UK.

Development of a High Content Analysis approach for the study of NETs in Periodontitis. **Chicca IJ**, Milward MR, Chapple IL, Griffiths G, Benson R, Cooper PR. September 2014, British Society of Periodontology meeting, Birmingham, UK.

Development of a High Content Analysis approach for the study of NETs in Periodontitis. **Chicca IJ**, Milward MR, Chapple IL, Griffiths G, Benson R, Cooper PR. March 2014, Oral Microbiology and Immunology Group meeting, Gregynog Hall, UK.

Potential application of High Content Analysis for the study of NETs in chronic disease. **Chicca IJ**, Milward MR, Chapple IL, Griffiths G, Benson R, Cooper PR. March 2014, The Gums & Joints Consortium conference, Ustron, Poland.

Paper publications

***Chicca IJ**, White PC, Cooper PR, Milward MR, Chapple ILC* (2015). Neutrophil extracellular traps in periodontitis: A web of intrigue. *Journal of Dental Research 1-9.* Joint first authorship.

*White PC, **Chicca IJ**, Ling MR, Wright HJ, Cooper PR, Milward MR, Chapple ILC* (2017). Characterization, Quantification, and Visualisation of Neutrophil Extracellular traps. *Methods in Molecular Biology.*

*Cooper PR, **Chicca IJ**, Holder MJ, Milward MR*. Inflammation and regeneration in dentin-pulp complex, NET gain of loss? Submitted to the *Journal of Endodontics*.

Journal of Dental Research
1–9
© International & American Associations for Dental Research 2015
Reprints and permissions:
sagepub.com/journalsPermissions.nav
DOI: 10.1177/0022034515609097
jdr.sagepub.com

Neutrophil Extracellular Traps in Periodontitis: A Web of Intrigue

P.C. White[1*], I.J. Chicca[1,2*], P.R. Cooper[1], M.R. Milward[1], and I.L.C. Chapple[1]

Abstract

Neutrophil extracellular traps (NETs) represent a novel paradigm in neutrophil-mediated immunity. NETs are believed to constitute a highly conserved antimicrobial strategy comprising decondensed nuclear DNA and associated histones that are extruded into the extracellular space. Associated with the web-like strands of DNA is an array of antimicrobial peptides (AMPs), which facilitate the extracellular destruction of microorganisms that become entrapped within the NETs. NETs can be released by cells that remain viable or following a unique form of programmed cell death known as NETosis, which is dependent on the production of reactive oxygen species (ROS) and the decondensing of the nuclear DNA catalyzed by peptidyl arginine deiminase-4. NETs are produced in response to a range of pathogens, including bacteria, viruses, fungi, and protozoa, as well as host-derived mediators. NET release is, however, not without cost, as the concomitant release of cytotoxic molecules can also cause host tissue damage. This is evidenced by a number of immune-mediated diseases, in which excess or dysfunctional NET production, bacterial NET evasion, and decreased NET removal are associated with disease pathogenesis. Periodontitis is the most prevalent infectious-inflammatory disease of humans, characterized by a dysregulated neutrophilic response to specific bacterial species within the subgingival plaque biofilm. Neutrophils are the predominant inflammatory cell involved in periodontitis and have previously been found to exhibit hyperactivity and hyperreactivity in terms of ROS production in chronic periodontitis patients. However, the contribution of ROS-dependent NET formation to periodontal health or disease remains unclear. In this focused review, we discuss the mechanisms, stimuli, and requirements for NET production; the ability of NET-DNA and NET-associated AMPs to entrap and kill pathogens; and the potential immunogenicity of NETs in disease. We also speculate on the potential role of NETs in the pathogenesis of periodontitis.

Keywords: innate immunity, periodontal disease(s), inflammation, neutrophil biology, bacteria, host pathogen interactions

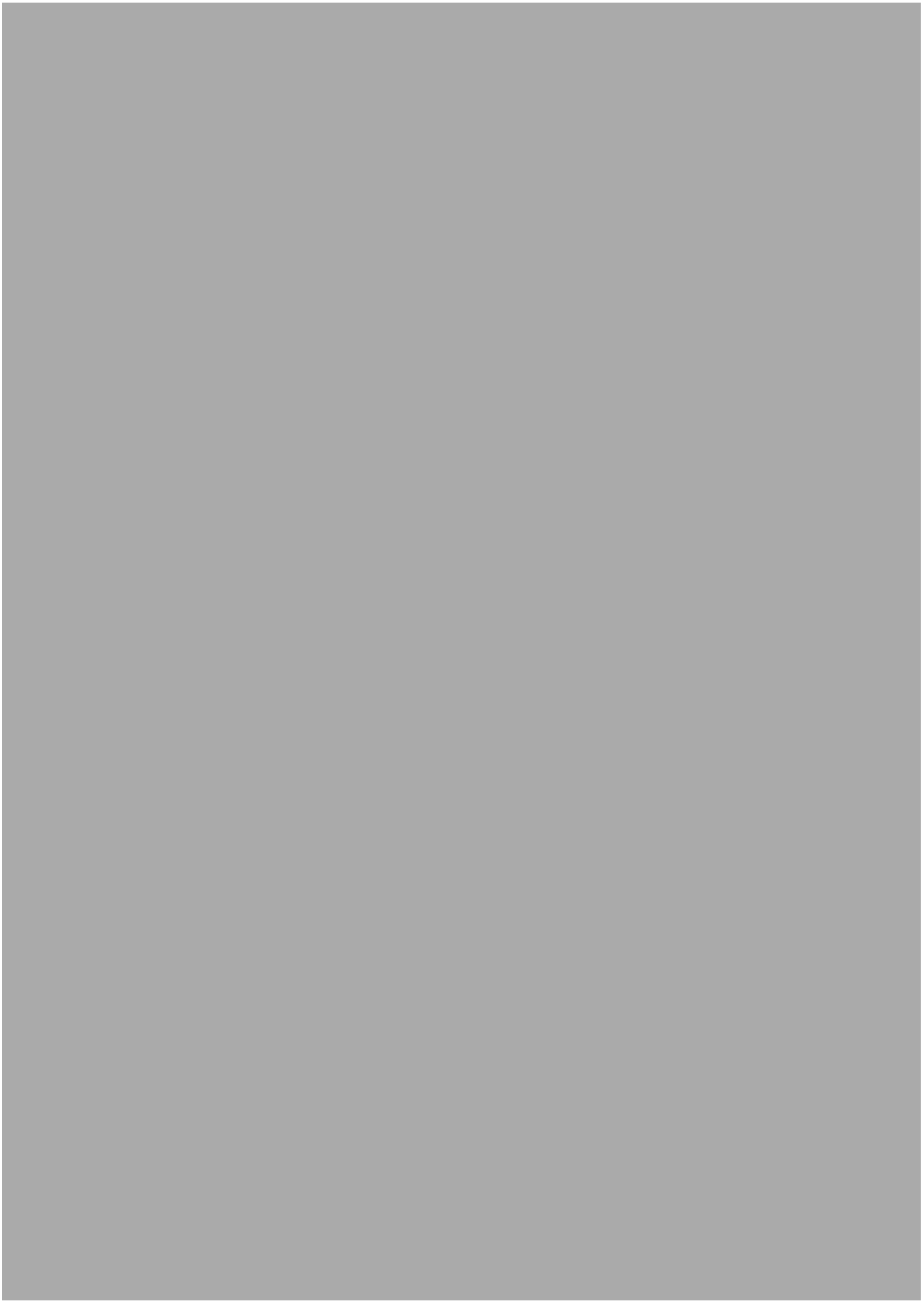

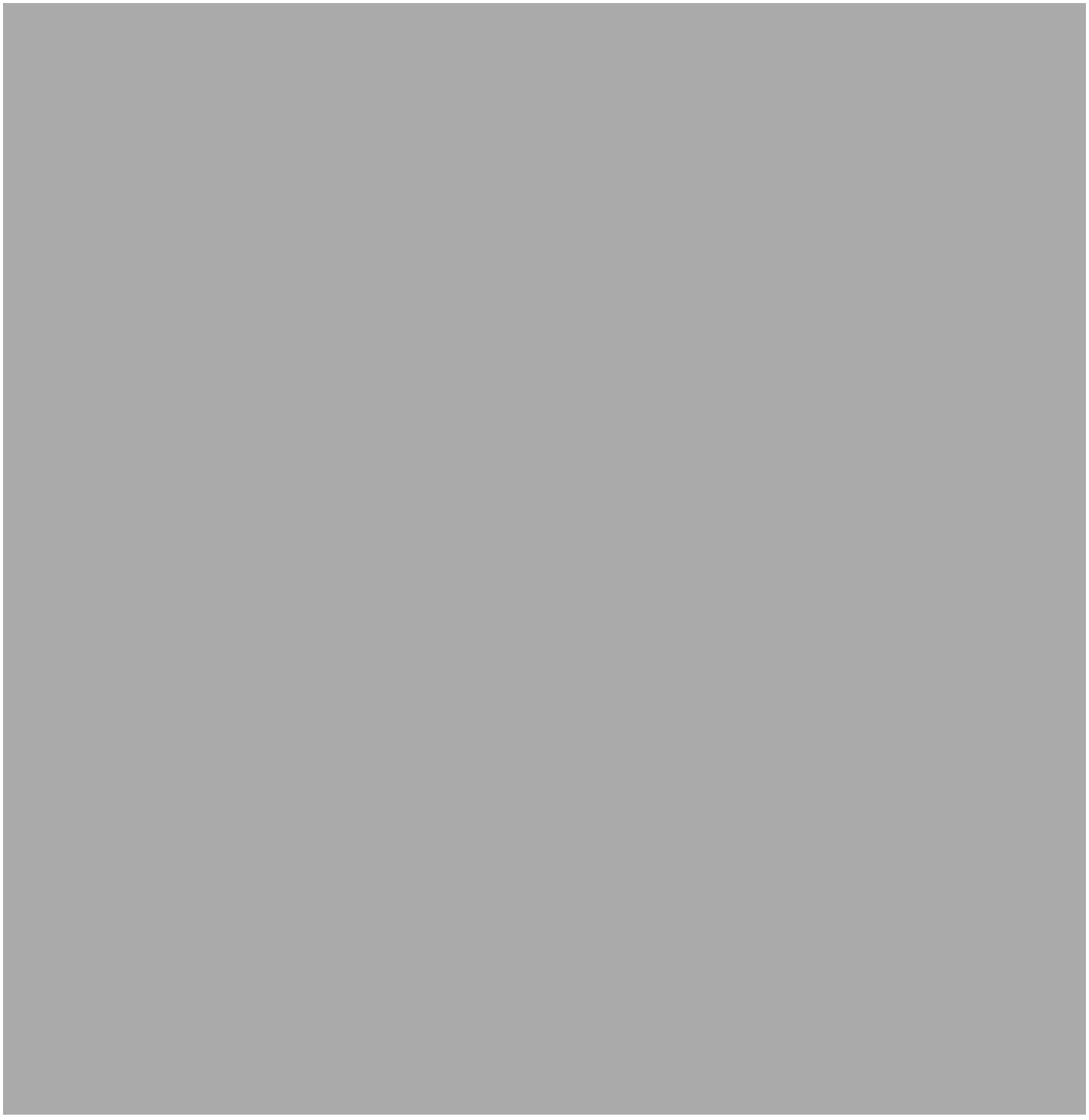

Chapter 29

Characterization, Quantification, and Visualization of Neutrophil Extracellular Traps

Phillipa C. White, Ilaria J. Chicca, Martin R. Ling, Helen J. Wright, Paul R. Cooper, Mike R. Milward, and Iain L.C. Chapple

Abstract

Following the discovery of neutrophil extracellular traps (NETs) in 2004 by Brinkmann and colleagues, there has been extensive research into the role of NETs in a number of inflammatory diseases, including periodontitis. This chapter describes the current methods for the isolation of peripheral blood neutrophils for subsequent NET experiments, including approaches to quantify and visualize NET production, the ability of NETs to entrap and kill bacteria, and the removal of NETs by nuclease-containing plasma.

Key words Neutrophil extracellular traps, Reactive oxygen species, Fluorescence microscopy, SEM, Chemiluminescence, DNA, Elastase, Myeloperoxidase, Cathepsin G, Immunostaining

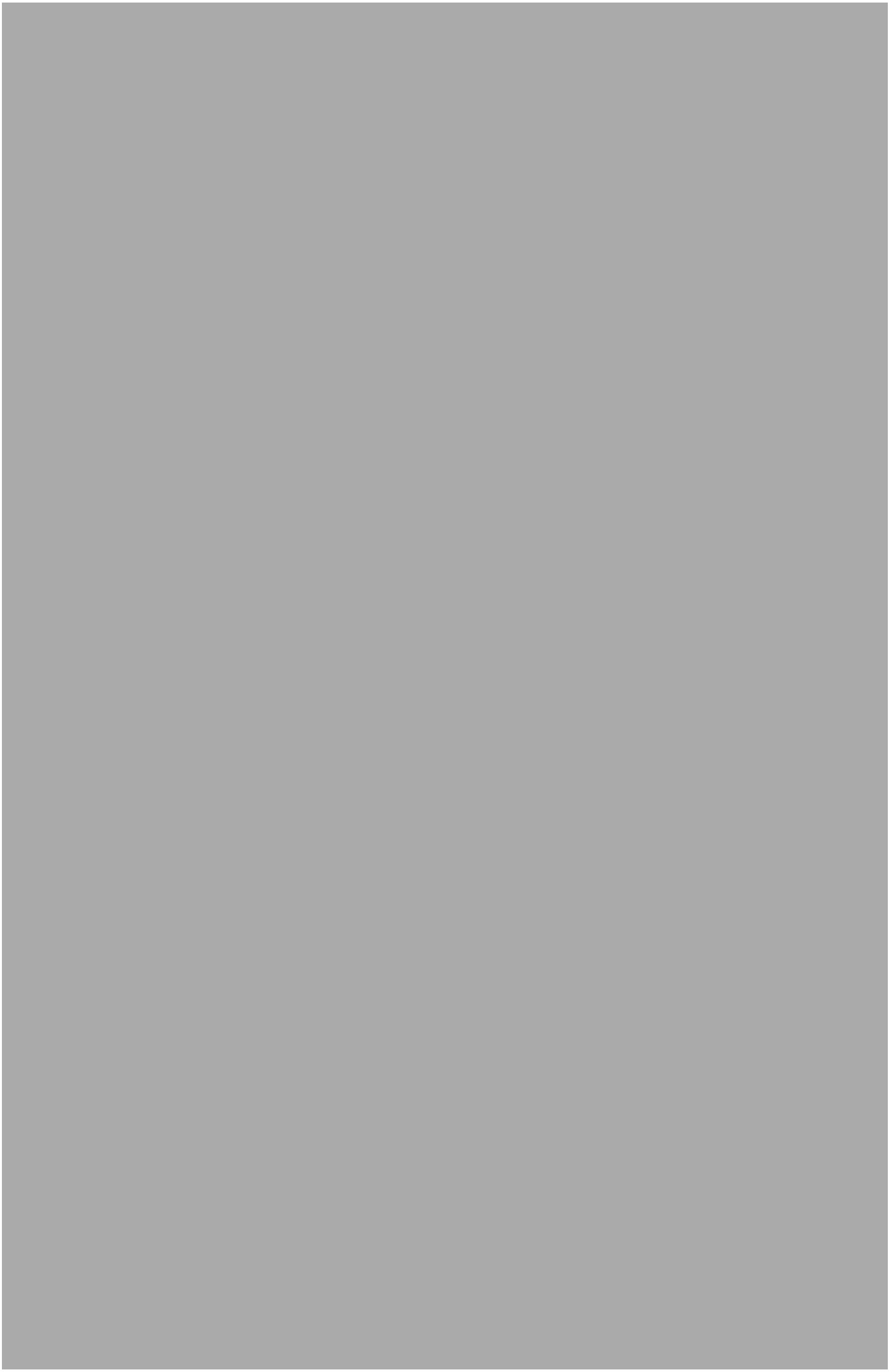

INFLAMMATION AND REGENERATION IN THE DENTIN-PULP COMPLEX, NET GAIN OR LOSS?

PR Cooper*, IJ Chicca, MJ Holder & MR Milward

Oral Biology, School of Dentistry, College of Medical and Dental Sciences, 5 Mill Pool Way, Edgbaston, Birmingham B5 7EG, UK.

Key words: Pulp, dentine, neutrophil extracellular traps, Polymorphonuclear leukocytes, reactive oxygen species, granulocytes

Corresponding author:

*Paul R. Cooper

Oral Biology,

School of Dentistry,

The University of Birmingham,

5 Mill Pool Way,

Edgbaston,

Birmingham,

UK

B5 7EG

Direct Dial: +44 (0) 121 466 5526

Secretary: +44 (0) 121 466 5073

ABSTRACT

The balance between the immune/inflammatory and regenerative responses in the diseased pulp is central to clinical outcome and this response is unique within the body due to its environmental context. Cariogenic bacteria invade the dental hard and soft tissues triggering molecular and cellular events dependent on the disease stage. Initially odontoblasts respond to bacterial components in an attempt to protect the tooth's hard and soft tissues and limit disease progression. However as disease advances the odontoblasts die and cells central to the pulp core, including resident immune cells, pulpal fibroblasts, endothelial cells and stem cells, respond to the infection via their expression of a range of pattern recognition receptors which identify pathogen associated molecular patterns. Subsequently there is recruitment and activation of a range of immune cell types, including neutrophils, macrophages, T- and B-cells, which are attracted to the diseased site by cytokine/chemokine chemotactic gradients initially generated by resident pulpal cells. While these cells aim to disinfect the tooth their extravasation, migration and antibacterial activity [eg release of reactive oxygen species (ROS)] along with the bacterial toxins cause pulp damage and impede tissue regeneration processes. Recently a novel bacterial killing mechanism termed Neutrophil Extracellular Traps (NETs) has been described which utilises ROS signalling and results in cellular DNA extrusion. The NETs are decorated with antimicrobial peptides (AMPs) and their interaction with bacteria results in microbial entrapment and death. Recent data demonstrates that NETs can be stimulated by bacteria associated with endodontic infections and they may be present in inflamed pulps. Interestingly some bacteria associated with pulpal infections express DNase enzymes which may enable their evasion of NETs. Furthermore, while NETs aim to localize and kill invading bacteria using AMPs and histones, limiting the spread of the infection, data also indicates that NETs can exacerbate inflammation and that their components are cytotoxic. This review considers the potential role of NETs within pulpal infections and how these structures may influence the pulp's vitality and regenerative responses.

[redacted]

[redacted]

[redacted]

[redacted]

[redacted].